ENGINEERING BEHAVIOR OF FINE-GRAINED SOILS MODIFIED WITH A CONTROLLED ORGANIC PHASE

A Thesis
Presented to
The Academic Faculty

by

Bate Bate

In Partial Fulfillment
of the Requirements for the Degree
Doctor of Philosophy in the
School of Civil Engineering

Georgia Institute of Technology
December 2010

ENGINEERING BEHAVIOR OF FINE-GRAINED SOILS MODIFIED WITH A CONTROLLED ORGANIC PHASE

Approved by:

Dr. Susan E. Burns, Advisor
School of Civil and Environmental Engineering
Georgia Institute of Technology

Dr. J.David Frost
School of Civil and Environmental Engineering
Georgia Institute of Technology

Dr. Haiying Huang
School of Civil and Environmental Engineering
Georgia Institute of Technology

Dr. E. Michael Perdue
School of Earth and Atmospheric Sciences
Georgia Institute of Technology

Dr. J. Carlos Santamarina
School of Civil and Environmental Engineering
Georgia Institute of Technology

Date Approved: July 28, 2010

To my parents, my wife, and my friends

ACKNOWLEDGEMENTS

I would like to thank my advisor, Dr. Susan E. Burns, for her brilliant research ideas, patient guidance, and financial support throughout my Ph.D. study. Also I would like to express my great appreciations to Dr. J. Carlos Santamarina who allowed me to use his electrical permittivity testing system, and gave valuable opinions on the results, and also served as a committee member; and to Dr. J. David Frost, Dr. Haiying Huang, and Dr. E. Michael Perdue who served on my Ph.D. defense committee, and gave me valuable guidance throughout my Ph.D. study, and to Dr. Glenn J. Rix who allowed me to use his resonant column test apparatus, and gave valuable suggestions about the RC results. My thanks also go to Dr. Guangxuan Zhu and Mr. Andy Udell of the School of Civil and Environmental Engineering who provided valuable suggestions on my experimental setup.

I want to thank my graduate student colleagues, Hyunwook Choo helped me set up the bender element test, and collaborated in BE testing results analysis, and Aditya Bhatt, who helped me set up the thermal conductivity test, and gave me valuable suggestions on the experiments, and Junbong Jang helped me with RC test. Also, two undergraduate student researchers, Joseph Thomas and James McNash, helped collect data on the characterization of organobentonites. Their help was invaluable and is very much appreciated.

I want to thank the following people in Georgia Tech, Quanwang Li, Ruiting Wu, Xuan Yang, Hyunki Kim, Alec and Catherine McGullivray, Andrew Fuggle, and Wei Li who helped me fit in at Tech and life in the U.S. in my first few years of Ph.D. study.

I also want to thank my wife, Di Yang, and our parents, who supported me mentally during my study at Tech; their support was selfless and priceless.

TABLE OF CONTENTS

LIST OF TABLES

LIST OF FIGURES

SUMMARY

Organic materials are ubiquitous in the geologic environment, and can exert significant influence over the interfacial properties of minerals. However, due to the complexity in their structure and interaction with soil solids, their impact has remained relatively unquantified. This study investigated the engineering behaviors of organoclays, which were synthesized in the laboratory using naturally occurring clay minerals and quaternary ammonium compounds of controlled structure and density of loading. Organic cations were chosen to study the effects of functional group structure and size.

The laboratory investigation showed that the presence of the organic cations on the mineral surfaces led to increased hydrophobicity of all clays tested. Conduction studies on the electrical, hydraulic, and thermal properties of the organoclay composites suggested that increasing the total organic carbon content resulted in decreased electrical and thermal conductivity, but increased hydraulic conductivity, due to the reduced swelling of the base clay mineral phase. Electrokinetic properties of the organoclays illustrated that compared with the clay's naturally occurring inorganic cations, exchanged quaternary ammonium cations were more likely bound within a particle's shear plane. Consequently, organoclays had less negative zeta potential than that of unmodified bentonite. Increasing the length of one carbon tail was more effective at binding organic cations within the shear plane than increasing the size of the cation, when compared on the basis of total organic carbon content.

In terms of large strain strength, the modified organic clays exhibited increased shear strength, in part owing to the reduction in water content caused by the presence of the

hydrophobic organic layering. Shear strength increased with single carbon tail length or with cation size, although the latter effect tended to reach a plateau as the length of the four short cation tails increased from 2 to 4. In terms of small strain behavior, the shear modulus was shown to be a function of the total organic carbon content. It is believed that number of particle contacts increased as the organic carbon content increased. Stiffness increased as either the size of the cation or the total organic carbon content was increased. Damping also increased as the organic loading was increased, with the organic phase acting as an energy dissipation mechanism.

Chapter 1 Properties and Behavior of Engineered Organic Phases on Soil

Organoclays are composites of organic matter and clay minerals that have had their naturally occurring inorganic cations exchanged with organic cations. Bentonite is a naturally occurring mixed mineral soil that is composed primarily of montmorillonite, a commonly occurring aluminosilicate clay mineral. Due to isomorphous substitution, montmorillonite exhibits a permanent structural surface charge that attracts weakly bonded interlayer cations to neutralize that charge (van Olphen, 1977). Typically, interlayer cations are inorganic (e.g. Na^{+}, Ca^{2+}). However, organic-clay complexes can be made by exchanging the clay's naturally occurring inorganic cations with a variety of organic cations. Quaternary alkylammonium cations (QACs), with a nitrogen head group and four positions for functional groups, have been extensively studied as exchange cations in montmorillonite (Figure 1-1). The organic phase sorbs on the mineral surface through electrostatic attraction with the nitrogen head group. As the sorbed organic content is increased, the clay surfaces change from hydrophilic to hydrophobic. The cation exchange generates an organic-enriched phase on the mineral surface that is highly sorbent for nonpolar organic compounds, which have potential applications as wastewater and groundwater sorbents (Bartelt-Hunt et al., 2005a).

Quaternary ammonium organic cations belong to a class of surfactants known as self-assembling monolayers (SAMS), which have been studied extensively as model lubricants in nanoscale and microscale electronic components (Chen et al., 2005; Gao et

al., 2004; Lin et al., 2005; Ruths et al., 2003), and as sorptive additives in environmental containment and remediation systems (Bartelt-Hunt et al., 2003; Bartelt-Hunt et al., 2005a; Bartelt-Hunt et al., 2005b; Lorenzetti et al., 2005; Redding et al., 2002; Smith et al., 2003). The formation of self-assembled monolayers can be controlled by manipulating the surfactant type and concentration, as well as the mineral solid surface. Because they can act as lubricants, SAMS are attractive model compounds for the study of friction and adhesion at the molecular and nanoscale levels. A variety of surfactants can be chosen, with properties manipulated to optimize the robustness of the layer, the lubrication of the interface, or the contaminant sorptive capacity of the engineered organic phase.

a) $\left[\begin{array}{ccc} & \textit{exchangeable} & \\ & | & \\ \textit{exchangeable} & -N- & \textit{exchangeable} \\ & | & \\ & \textit{exchangeable} & \end{array}\right]^{+}$ *Counterion*

b) $\left[\begin{array}{ccc} & CH_3 & \\ & | & \\ H_3C & -N- & CH_3 \\ & | & \\ & CH_3 & \end{array}\right]^{+} Cl^{-}$

Figure 1-1. Sturcture of quaternary ammonium cations: a) nitrogen head group, with four locations for exchangeable functional groups; replacement can occur at each location, with either singular, or multiple replacements occurring by a variety of functional groups with specifcied structure; b) tetramethylammoniumchloride, with ammonium (*N*) center and four methyl (*CH_3*) functional groups.

In aluminosilicate minerals, the organic cations penetrate the interlamellar space, replacing the naturally occurring inorganic cations like Na^{+} or Ca^{2+}. These engineered clays have been synthesized from a variety of clay minerals including montmorillonite, kaolinite (Jaynes and Boyd, 1991; Xu and Boyd, 1995), and illite (Jaynes and Boyd, 1991;

Polubesova and Nir, 1999). However, montmorillonite, or bentonite, is the most commonly used mineral. The organic cations can be chosen so that the tail length of the cation is longer than the interlamellar spacing of the substrate mineral, which will result in the expansion of the mineral. Sample x-ray diffraction data, gathered for two quaternary ammonium organic cations, hexadecyltrimethlyammonium (HDTMA) and benzyltriethlyammonium (BTEA), are given in Table 1-1 (Burns et al., 2006a). The cations were added to montmorillonite at increasing percentages of the montmorillonite's cation exchange capacity (CEC). As the percent CEC exchanged with HDTMA organic cations was increased, the dry basal spacing of the montmorillonite increased, up to a maximum of approximately 21-22 Å, which is the approximate tail length of the HDTMA cation. In contrast, the smaller BTEA cation with a tail length of approximately 10 Å, which is somewhat smaller than the interlamellar spacing of the unmodified montmorillonite, did not significantly expand the interlayer spacing of montmorillonite (Table 1-1).

Previous studies on adsorption of organic compounds and surfactants onto solid surfaces demonstrated that there were multiple driving forces for adsorption, including electrostatic or coulombic interaction, covalent bonding, hydrogen bonding (in systems containing hydroxyl, phenolic, carboxylic and amine groups on the surfactants), hydrophobic lateral interactions (transferring the hydrocarbon chains from the aqueous environment into the hydrophobic interior of the aggregates, when hemi-micelles formed), hydrophobic interaction between the hydrocarbon chains and hydrophobic sites on the solid like talc or graphite, solvation (due to dissolution or solvation of the adsorbate species or any species displaced from the interface due to adsorption), and desolvation

(when a hydrated head group of the surfactant transfers from the bulk to the mineral-solution interfacial region, water from the secondary solvation shell around the surfactants head groups may be partially removed) (Fuerstenau, 1971; Fuerstenau and Pradip, 2005; Zhang and Somasundaran, 2006).

Table 1-1. Basal Spacings of Two Organically Modified Clays (Burns et al., 2006a)

Clay	Basal Spacing (Å)	Clay	Basal Spacing (Å)
Unmodified Montmorillonite	15.0		
HDTMA 30	14.7	BTEA 30	14.8
HDTMA 50	16.3	BTEA 50	14.9
HDTMA 70	20.2	BTEA 70	14.8
HDTMA 90	21.9	BTEA 90	undetermined
HDTMA 120	20.9	BTEA 120	14.9

The theoretical structure of alkylammonium ions arrangement on the clay surface was proposed as (Lagaly et al., 2006): alkylammonium ions with short-chain(s) usually form monolayers, while alkylammonium ions with a single long chain can form monolyers, bilayers (pseudo-trilayers on highly-charged phyllosilocates), or paraffin structures, which tend to form on the alkylammonium ions with two or more long carbon chains (Table 1-2). This structure has been studied experimentally and by molecular simulations, and provides a consistently reliable explanation for the behavior of organoglays (Liu et al., 2007). In the monolayer structure, the hydrophilic head group (N^+) orients toward the clay surface with the hydrophobic alkyl chains either lying flat, inclined, or perpendicular to the clay surface, depending on their amount of loading on

the clay surface. In a bilayer structure, excess alkylammonium ions with a single long chain can arrange with their long chain towards the clay surface, while their head group points towards the bulk solution.

Quaternary ammonium cations can be chosen with different structures to optimize the chemical or mechanical behavior. Additionally, the amount of organic cation exchanged onto the surface of a clay can also be varied. By targeting a percentage of a clay's cation exchange capacity (CEC) for replacement, the total organic carbon content, or the amount of cation on the clay surface, can be carefully controlled. In terms of surface coverage, the following simplified analysis yields a conceptual model for the amount of surface coverage for five of the quaternary ammonium cations that were chosen for study in this work (Table 1-3). The analysis assumed that all the available exchange sites (i.e., cation exchange capacity) on a clay mineral were uniformly distributed across the clay surface and the clay mineral had one exchange site spaced every 2.4 nm, which is equivalent to a CEC = 69.1 meq/100 g. This would result in an exchange site area of influence of 1.44 nm^2. The quaternary ammonium cations tetramethylammonium (TMA, denoted: $4C_1$) chloride , tetraethylammonium (TEA, denoted: $4C_2$) bromide, tetrapropylammonium (TPA, denoted: $4C_3$) bromide, tetrabutylammonium (TBA, denoted: C_4) bromide, would cover 26%, 35%, 44%, and 53% of the clay surface area, respectively, assuming that the cations were distributed in a circular area on the surface with a diameter of 0.694 nm for TMA, 0.80 nm for TEA, 0.904 nm for TPA, and 0.998 nm for TBA (Robinson and Stokes, 1965). Similarly, the QACs with long C-chains, such as hexadecyltrimethylammonium (HDTMA, denoted: $1C_{16}$) bromide, have the same percent area coverage as that of TMA because the head

groups occupy the same area. However, the long tail length (2.5 nm for HDTMA), could cover as much as 100% of the surface, depending on orientation.

This research investigated the properties of quaternary ammonium cations and quantified their engineering effects on clays as functions of the molecular structures and cation loadings. Effects of two structures was studied: the branch effect examined the influence of increasing the cation size by increasing the size of the functional groups in all four quaternary positions on the cation (TMA, TEA, TPA, and TBA, Table 1-3), while the tail length effect examined the influence of increasing the cation size by increasing the length of the functional group in only one position (i.e., cation had three methyl groups CH_3 and one functional group with increasing number of carbons in the chain, for example, HDTMA in Table 1-3). Then electrokinetic, electromagnetic, and geotechnical tests were carried out to analyze the effect of cation loading, or total organic carbon content, on the behavior of the organoclays made with the quaternary ammonium cations. Tests were also conducted to characterize the organic cations in the dissolved state, as well as when sorbed to clay surfaces. The following chapters present the results of the organoclay study. Chapter 2 focused on characterization. Chapter 3 presented the electrical, hydraulic, and thermal conductivities. Chapter 4 gave results of zeta potential. The large strain strength and dynamic properties were reported in Chapter 5 and 6, respectively. Chapter 7 summarized the behavior of the organoclay composites.

Table 1-2. Theoretical Structure of Organoclay Complexes with Increasing Organic Loading (Inferred from XRD data, (Polubesova and Nir, 1999))

Structure	Layering
Single Layer	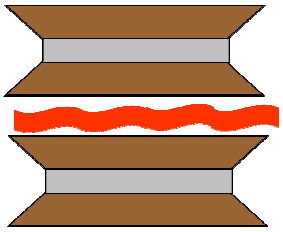
Double Layer	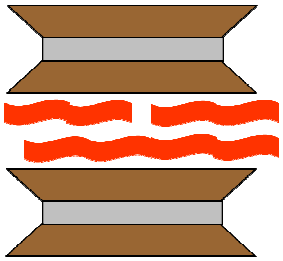
Pseudo Triple Layer	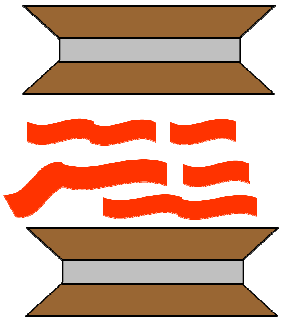
Paraffin Complex	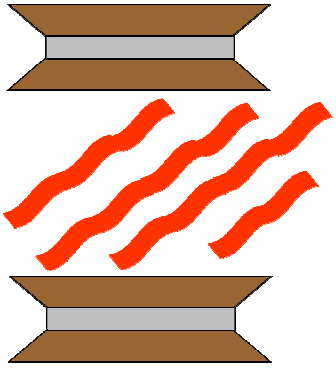

Table 1-3. Structure of Selected Quaternary Ammonium Cations

QAC	Structure
a) TMA [$4C_1$] Tetramethyl-ammonium	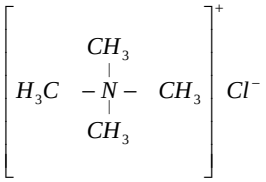
b) TEA [$4C_2$] Tetraethyl-ammonium	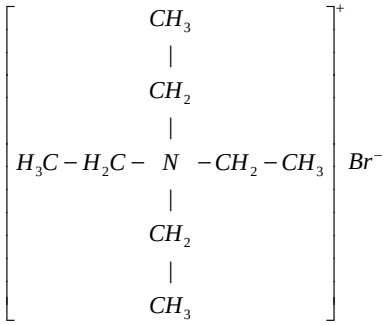
c) TPA [$4C_3$] Tetrapropyl-ammonium	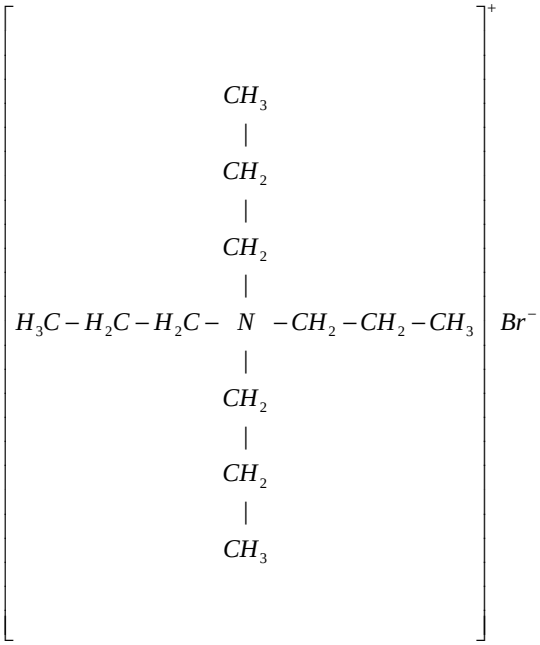

Table 1—3 continued. Structure of Selected Quaternary Ammonium Cations

QAC	Structure
d) TBA [*4C*$_4$] Tetrambutyl-ammonium	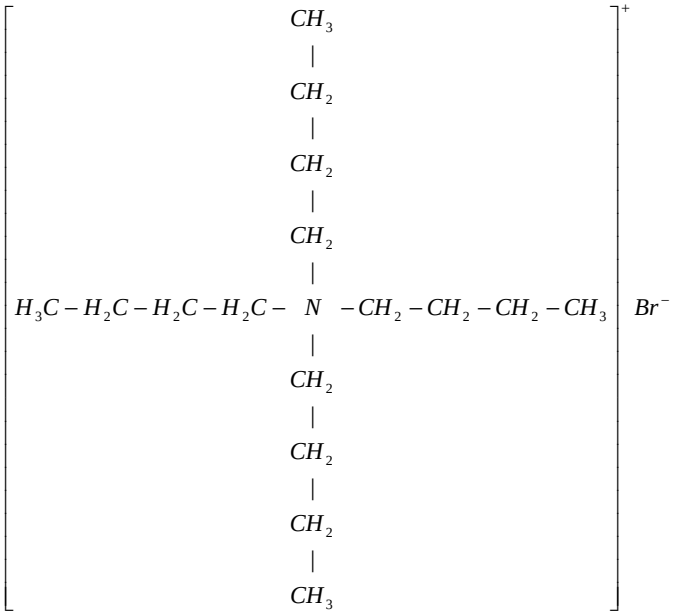
e) HDTMA [*1* C_{16}] Hexadecyltrimethly-ammonium	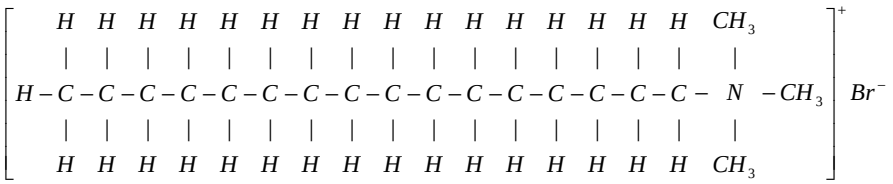

Chapter 2 Preparation and Characterization of Organobentonites

Introduction

The organic cations studied in this work were surfactants (surface active agents) that contain hydrophobic functional groups (akyl) and a hydrophilic head group (amine). Quaternary ammonium cations (QACs) consist of an ammonium center with four branches for attachment of functional groups (Figure 1-1). The ammonium center is hydrophilic, with an excess of positive charge, while the branched functional groups are hydrophobic with a neutral charge. Due to the large hydrophobic driving force from the neutrally charged functional groups, the affinity of QACs to the clay mineral surface is very high. Once exposed to the clay surface, QACs displace naturally occurring inorganic cations (e.g., Na^+) and are very easily adsorbed onto the mineral surface, forming organoclays. When exchanged at percentages below the cation exchange capacity (CEC) of clay minerals such as montmorillonite, the adsorption is primarily due to electrostatic attraction. The hydrophilic nitrogen-head groups bond to the clay surface at sites of excess negative charge, while the hydrophobic alkyl groups can coat the mineral surface, or extend to the bulk solution, depending on their concentration. The cation arrangement on the particle surfaces result in an organic layer on the mineral surfaces which alter the interfacial behaviors of the resulting organoclay, leading to changes in adsorption behavior, friction, contact angles, and wettability.

This chapter performs characterization of five organoclays (TMA, TEA, TBA, DTMA, and HDTMA) made from quaternary ammonium cations and a sixth cation, dodecyltrimethylammonium (DDTMA) which was also studied for its behavior in aqueous solution. The organic cations were such chosen as to study the effect of increasing cation tail length (i.e., increasing chain length in one functional position, TMA→DTMA→DDTMA→HDTMA), and of increasing the branch length (i.e., increasing the chain length in all four positions, TMA→TEA→TBA). Additionally, the effect of organic concentration on the particle surface was also examined for the TMA and HDTMA cations by increasing the percentage of cations exchanged on the surface at 30%, 60% and 100% of CEC replacement. The organoclays were tested for total organic carbon content, Atterberg limits, specific gravity, specific surface area, and surface tension of the aqueous surfactants solutions (Table 2-1).

Table 2-1. Test Matrix for Study of Organobentonites: Atterberg Limits and Specific Surface

Organic Cation	**Amount of organic cations exchanged (% CEC of bentonite)**		
	30%	**60%**	**100%**
TMA	×	×	√
TEA	×	×	√
TBA	×	×	√
DTMA	×	×	√
HDTMA	√	√	√

Note: √: tested; ×: not tested

Materials and Methods

Wyoming bentonite (CG-50, CETCO), composed primarily of sodium montmorillonite, was the base clay for the study and was used as received. The natural-organic carbon content of the material was 0.2% (Huffman Laboratories, Inc., Golden, CO), and its cation exchange capacity (CEC) was 69.1 meq/100g (Hazen Research Inc., Golden, CO). Five quaternary ammonium cations were chosen for study: tetramethylammonium (TMA, denoted: *4 C_1*) chloride [$(CH_3)_4NCl$], tetraethylammonium (TEA, denoted: *4 C_2*) bromide [$(CH_2CH_3)_4NBr$], tetrabutylammonium (TBA, denoted: *4 C_4*) bromide [$((CH_2)_3(CH_3))_4NBr$], decyltrimethylammonium (DTMA, denoted: *1 C_{10}*) bromide [$(CH_3)_3NC_{10}H_{21}Br$], and hexadecyltrimethylammonium (HDTMA, denoted: *1 C_{16}*) bromide [$(CH_3)_3NC_{16}H_{33}Br$] (Figure 2-1). The properties of the aqueous solution of a sixth organic cation dodecyltrimethylammonium (DDTMA, denoted: *1 C_{12}*) bromide [$(CH_3)_3NC_{12}H_{25}Br$] were also studied. All cations were obtained from Fisher Scientific, and were used as received. The water used in all experimentation was deionized (Barnstead E-pure).

a) TMA [*4 C_1*]	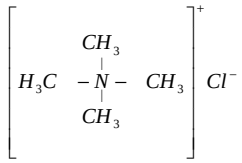
b) TEA [*4 C_2*]	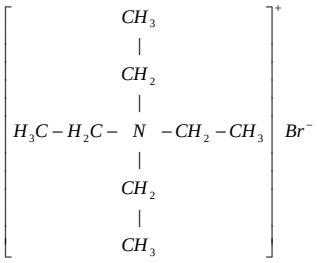
c) TBA [*4 C_4*]	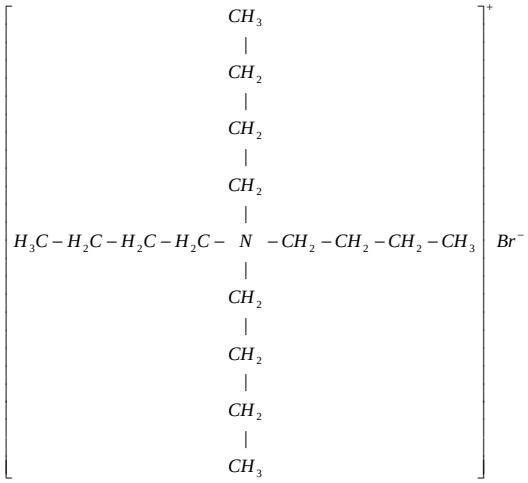
d) DTMA [*1 C_{10}*]	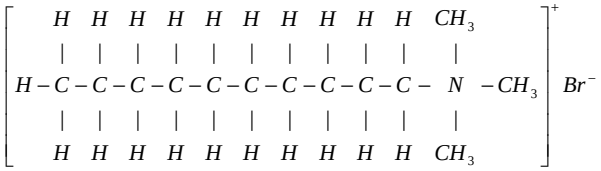
e) HDTMA [*1 C_{16}*]	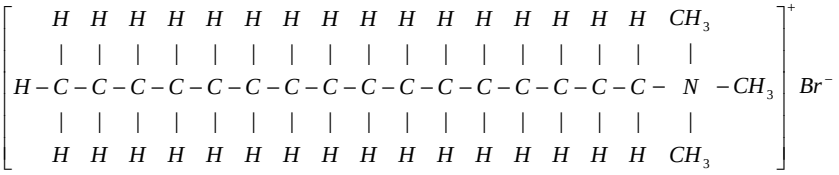

Figure 2-1. Structure of the quaternary ammonium cations tested in this study: a) tetramethylammonium (TMA, denoted: *4 C_1*) chloride [$(CH_3)_4NCl$], b) tetraethylammonium (TEA, denoted: *4 C_2*) bromide [$(CH_2CH_3)_4NBr$], c) tetrabutylammonium (TBA, denoted: *4 C_4*) bromide [$((CH_2)_3(CH_3))_4NBr$], d) decyltrimethylammonium (DTMA, denoted: *1 C_{10}*) bromide [$(CH_3)_3NC_{10}H_{21}Br$], and e) hexadecyltrimethylammonium (HDTMA, denoted: *1 C_{16}*) bromide [$(CH_3)_3NC_{16}H_{33}Br$].

The organobentonites were synthesized in the laboratory by exposing the particle surfaces of the bentonite to an aqueous solution containing the quaternary ammonium cation TMA and HDTMA at 30%, 60%, and 100% of the cation exchange capacity of the clay, while TEA, TBA, and DTMA were exchanged at 100% of the cation exchange capacity of the clay. The chosen organic compound was dissolved in 40 liters of deionized water, and 2 kg of the clay were added to the aqueous solution. The resulting suspension was mechanically stirred for 1 hour and allowed to gravity settle for a minimum of 24 hours. The supernatant was then siphoned off, and the deposits were rinsed with deionized water to remove any salts or loosely bound cations. The process was repeated until the conductivity of the supernatant was below 600 μS/cm. Mineralogical impurities were separated by gravity separation.

Total organic carbon (TOC) was measured for each organobentonite using an organic carbon analyzer and a solid sample module (TOC-$V_{CPH/CPN}$, SSM-5000A, Shimadzu Co. Kyoto, Japan). The sample was combusted at 680 ^{o}C in the presence of an oxidation catalyst, and the resulting CO_2 was measured using a non-dispersive infrared (NDIR) gas analyzer. A known reference material, anhydrous dextrose powder (C% = 40% in mass, Fisher Scientific), was used as the calibration source. Calibrations were performed daily during measurements. The measured total organic carbon content in each organoclay agreed well with the calculated values of sorbed carbon (Table 2-2 and Figure 2-2). TOC data were plotted for both zeta potential tests (Chapter 4) and for all other tests using organobentonite throughout this thesis.

Table 2-2. Theoretical Total Organic Carbon Content Versus Experimentally Determined Values (from Zeta Potential Test)

Organoclay	Amount of organic cations exchanged (%CEC)	Theoretical organic carbon content (%)	Measured organic carbon content (%)
TMA-bentonite	100	3.2	2.2
	60	1.9	2.0
	30	1.0	0.8
TEA-bentonite	100	6.1	5.3
	60	3.8	3.8
	30	1.9	1.5
TBA-bentonite	100	11.4	8.6
	60	7.2	6.3
	30	3.8	4.2
DTMA-bentonite	100	9.5	8.5
	60	5.9	6.8
	30	3.1	3.6
DDTMA-bentonite	100	10.8	10.3
	60	6.8	7.6
	30	3.5	4.3
HDTMA-bentonite	100	13.2	13.9
	60	8.4	9.1
	30	4.4	5.9

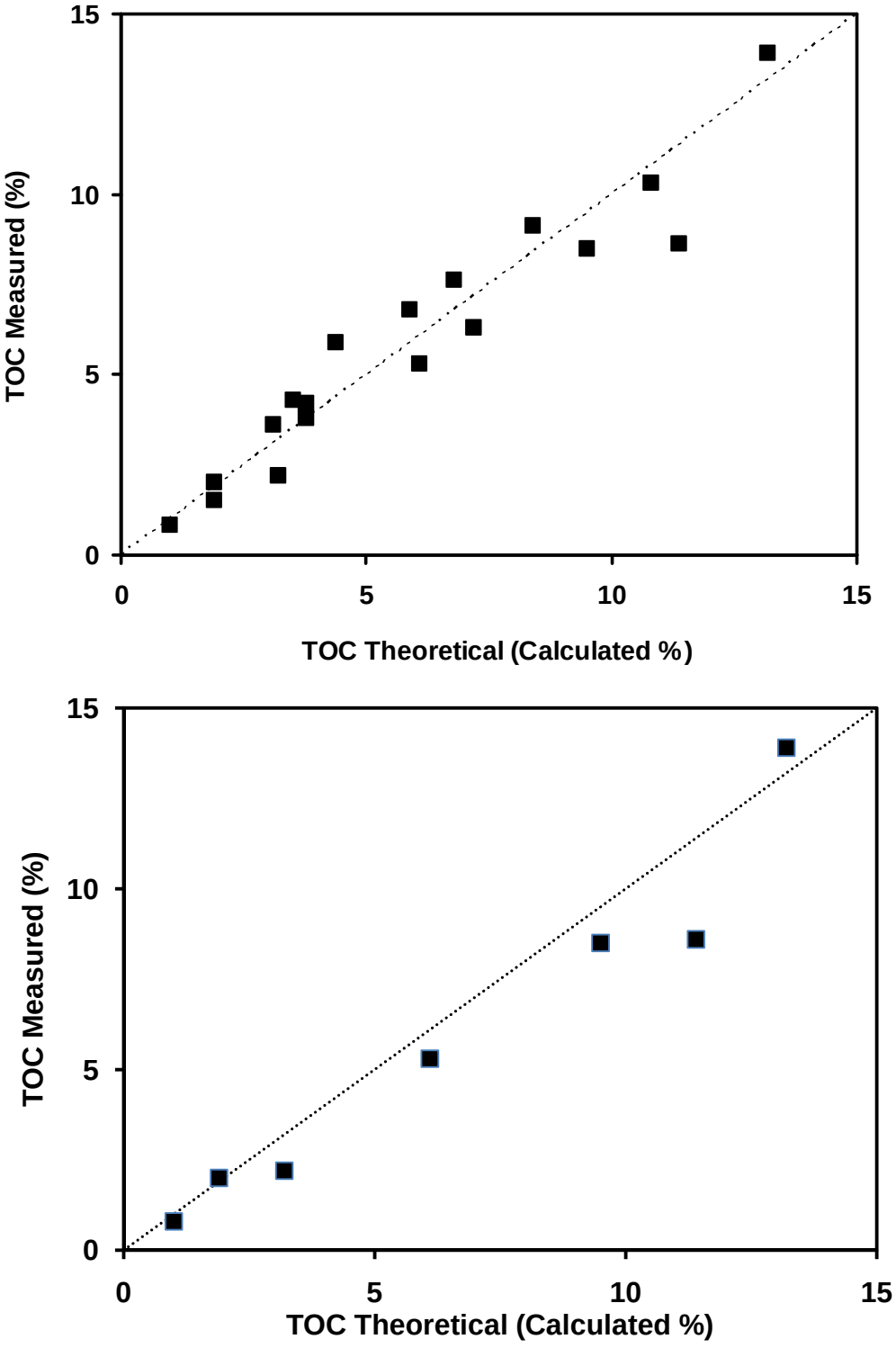

Figure 2-2. Theoretical total organic carbon content versus experimentally determined values from (a) zeta potential test, and (b) all other tests using organobentonite

The liquid limits of unmodified bentonite and nine organoclay soils were tested using the fall cone apparatus (Wykeham Farrance Engineering Ltd, Slough, England) in accordance with British Standard 1377 (1990) according to the experimental matrix outlined in Table 2-1. The tests were started from the dry side, and deionized water was added to the soil to increase the water content. In the case of high initial water content, the organobentonite was left to air dry for several hours to reduce the water content before the start of testing. The plastic limits of the soils were determined according to the procedures outlined in ASTM D 4318 - 05. Nitrile powder-free gloves (Fisher Scientific) were worn during the test. For both the plastic and liquid limit tests, the water content of the soil paste was measured by using the Precision economy oven (Thermo Electron Corporation) at 104^{o}C and balance (Accu – 4102, Fisher Scientific).

Specific gravity tests on the unmodified soil and the modified clays were performed according to ASTM D854-92, using the liquid pycnometer (Method B). The volume of the volumetric flask (pycnometer) was 500 mL, and the mass of soil used ranged from 6 to 19 grams. De-aired water was used in all measurements. Vacuum up to 27 in Hg was produced by a vacuum pump, which was the sole method of de-airing, and was applied for 2 hours for de-airing of the soil-water mixture.

The specific surface area of the soils was measured using the methylene blue (MB) spot test procedure, according to the methods outlined in Kandhal and Parker (1998) and Santamarina et al. (2002). The methylene blue procedure consisted of the following steps: 200 mL of methylene blue solution was prepared by adding 1 gram of methylene blue powder ($C_{16}H_{18}ClN_3S \cdot 3H_2O$, molecular weight = 373.87, Fisher Scientific) to 200 mL de-ionized water (Barnstead E-pure) and followed by thorough

mixing. Soil suspensions with solids concentration between 0.006 to 0.04 g/mL were prepared, with concentrations chosen to prevent making a paste or gel (likely in the case of bentonite). Next, the methylene blue solution was added to the soil suspension in 0.5 mL increments, while being mixed with a mechanical stirrer (Thermix Stirrer Model 120S, Fisher Scientific) for 1 minute. A small drop of the suspension was removed, and placed on filter paper (P5 grade, Fisher Scientific). For samples that were below the sorption capacity, no methylene blue halo appeared. As soon as a light blue halo formed around the soil suspension, it was assumed that the sorption capacity was reached and the sample was used to calculated surface area. An additional 2 – 3 increments of MB were added to the soil suspension to confirm the consistent formation of the halo. The specific surface area was then calculated according to:

$$S_s = \frac{1}{MW}\frac{1}{V}(0.5N)A_V A_{MB}\frac{1}{M_s} \qquad \textbf{Equation 2-1}$$

where MW is the molecular weight of the MB powder, MW = 373.87, V is the volume of de-ionized water used to dissolve 1 gram of MB, V = 200 mL, N is the number of MB increments added to the soil suspension, A_V is Avogadro's number, $6.02 \times 10^{23} / mol$, A_{MB} is the area covered by one MB molecule, typically assumed to be 1.30 nm^2, and M_s is the total mass of soil in the soil suspension. Each methylene blue test was repeated two times.

For each of the organic cations tested, the surface tension of an aqueous surfactant solution was measured using the du Noüy ring method (Tensiomat* Model 21 tensiometer, Fisher Scientific) with a platinum-iridium ring of 5.983 cm in the mean circumference and the ratio between ring radius and ring-wire radius of 53.59. The surface tension was measured according to ASTM D1131 – 89 (reapproved 2001) at the

air water interface, and experiments were performed at the room temperature. A minimum of three repetitions were performed for each experiment, and the average value for surface tension was reported.

Table 2-3. Atterberg Limits of Unmodified Bentonite and Organobentonites

Clay	Liquid limit (%)	Plastic Limit (%)	Plasticity Index (%)
Unmodified Na-bentonite	274	53	221
100TMA bentonite	266	82	184
100TEA bentonite	140	66	74
100TBA bentonite	118	73	46
100DT bentonite	205	107	98
30HD bentonite	215	70	145
60HD bentonite	202	112	89
100HD bentonite	219	89	130
Na-montmorillonite[1],*	1140	-	-
Ca-montmorillonite[1],**	207-220	33-35	172 – 187
Na-Montmorillonite[2]	710	54	656
Ca-montmorillonite[2]	510	81	429

*: Concentration is 0.001 N, pH = 7.

** Concentration is 0.001 N, pH = 5 and 9.

[1] Mesri and Olson (1970).

[2] Lambe and Whitman (1969).

Results and Discussion

Liquid and plastic limits

The liquid limit for fine-grained soils corresponds to a dynamic shear resistance of approximately 1.7 to 2.0 kPa and a pore water suction of about 6 kPa (Mitchell and Soga, 2005). Liquid limit, plastic limit, and their derived indices are widely used throughout the world because they provided excellent bases for the classification and identification of fine-grained soils (Lambe, 1951). The unmodified bentonite exhibited the highest plasticity, with a liquid limit of 274% and a plasticity index of 221% (Table 2-3). In all cases, the addition of the organic cation to the clay surface resulted in decreases in the liquid limits, when compared to the unmodified clay. The plastic limits were generally higher than that observed in the unmodified clay. The liquid limit for the bentonite used in this study was lower than values reported for pure montmorillonite. This was because bentonite soil represents a mixed mineral soil with a higher percentage of large grained particles than would be found in pure montmorillonite.

In terms of the branch effect of the exchanged organic cations, as the size, or the carbon chain length of all four branches increased from 1 to 2 and 4 (TMA, TEA, and TBA), the liquid limit decreased (from 266% to 140% and 108%) (Figure 2-3). The same trend was observed for the case of tail length increase as well. As the length of one carbon chain was increased (TMA, DTMA, and HDTMA), the liquid limit decreased (Figure 2-4). Increasing the size of the organic cation by either branch effect or tail effect, increased the total organic carbon content of the clay, which in turn yielded a more hydrophobic soil with strongly bound cations, and reduced the net charge of the organoclay particles as compared to unmodified clay (Bate and Burns, 2010).

Subsequently, the electrical repulsive force between clay particles was decreased, and the clay particles maintained a closer spacing in the presence of organic cations when compared to the free swell conditions observed for unmodified bentonite. Consequently, less water was retained in the hydrophobic organoclays, and the liquid limit was reduced. Additionally, the organoclays illustrated a higher plastic limit than unmodified bentonite (in the range of 66 – 82% for the branched organoclays and 89%-107% for the organoclays with single long tail; in comparison, plastic limit of unmodified clay was 53%), indicating a tendency to crack at a higher water content, as would be anticipated due to the increased hydrophobicity.

In addition to the branch and tail length effect, the effect of the density of organic loading, or surface coverage, was tested for HDTMA-organoclay. Interestingly, the liquid limit of HDTMA remained fairly constant as the organic loading was increased (range of 202%-219%) (Figure 2-5). The results were also presented as a function of measured total organic carbon (Figure 2-6). Examination of the liquid limit behavior of HDTMA organoclays evidenced that the long chain HDTMA molecules excluded water from the clay surface, even at low organic contents. At low concentrations, the hydrophobic tails of the HDTMA molecules lay parallel to the clay surface and are attracted to the clay through hydrophobic expulsion from the polar water phase, resulting in exclusion of water from the surface even at low organic cation concentrations; Thus, increasing the organic loading has little effect on the water sorption and the resulting liquid limit. The measured plastic limits were mildly sensitive to organic loading, with relatively small variations observed (Figure 2-5 and Figure 2-6).

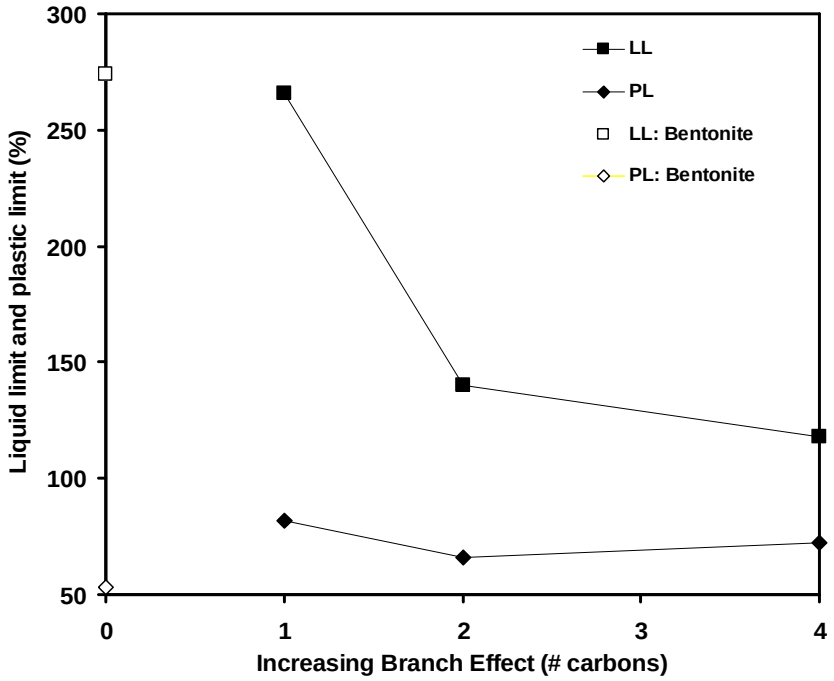

Figure 2-3. Liquid and plastic limits versus the size of organic cations, increasing branch effect (chain length in all four alkyl positions increased).

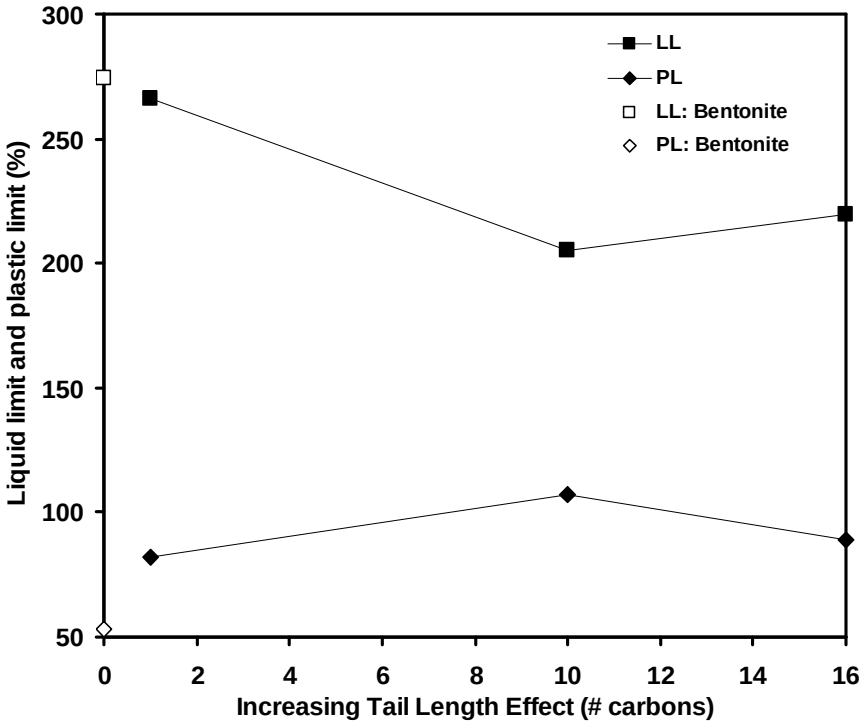

Figure 2-4. Liquid and plastic limits versus the size of organic cations, increasing tail length effect (chain length in only one alkyl position increased).

The trends measured in the Atterberg limits data were consistent with those reported for other organoclays by Burns et al. (2006). However, the liquid limits for the organoclays tested in that study were between 51% and 74%, which were significantly lower than the results in this study. It was believed that the difference is attributable to the different base clay used in the studies and the sample preparation methods. The soils in Burns et al. (2006) were oven dried before testing, whereas the soils in the current study were not dehydrated before testing.

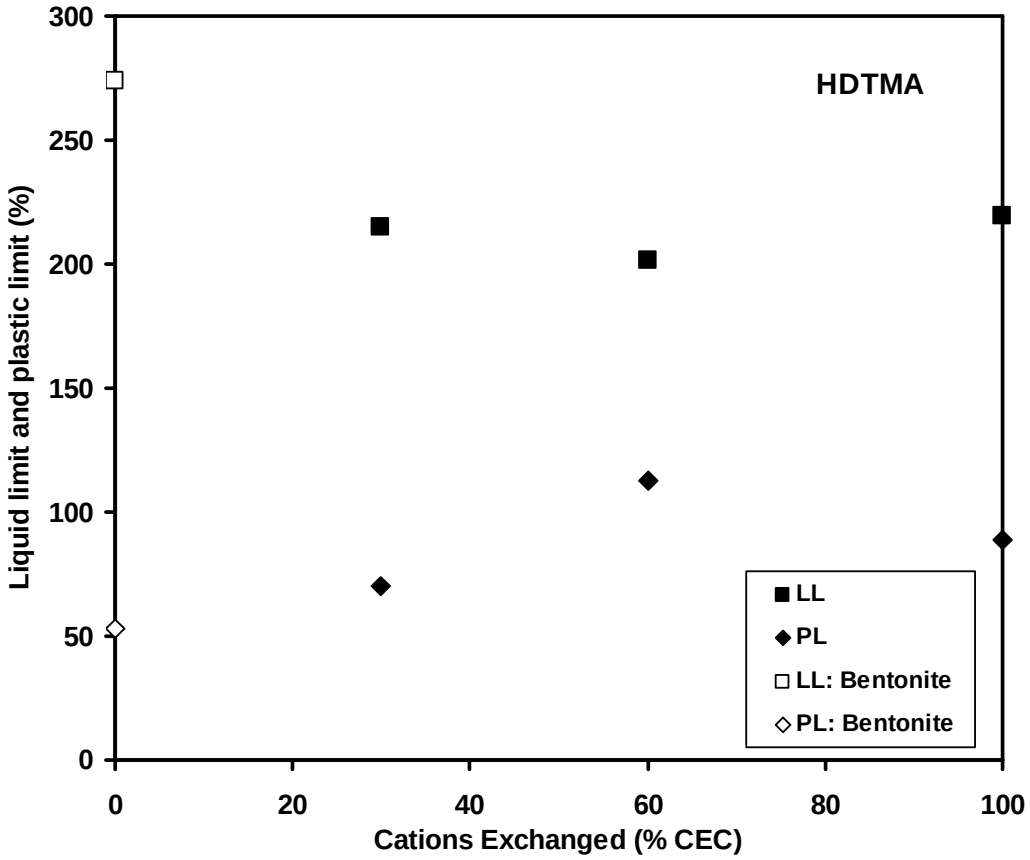

Figure 2-5. Liquid and plastic limits versus density of organic loading for HDTMA-bentonites

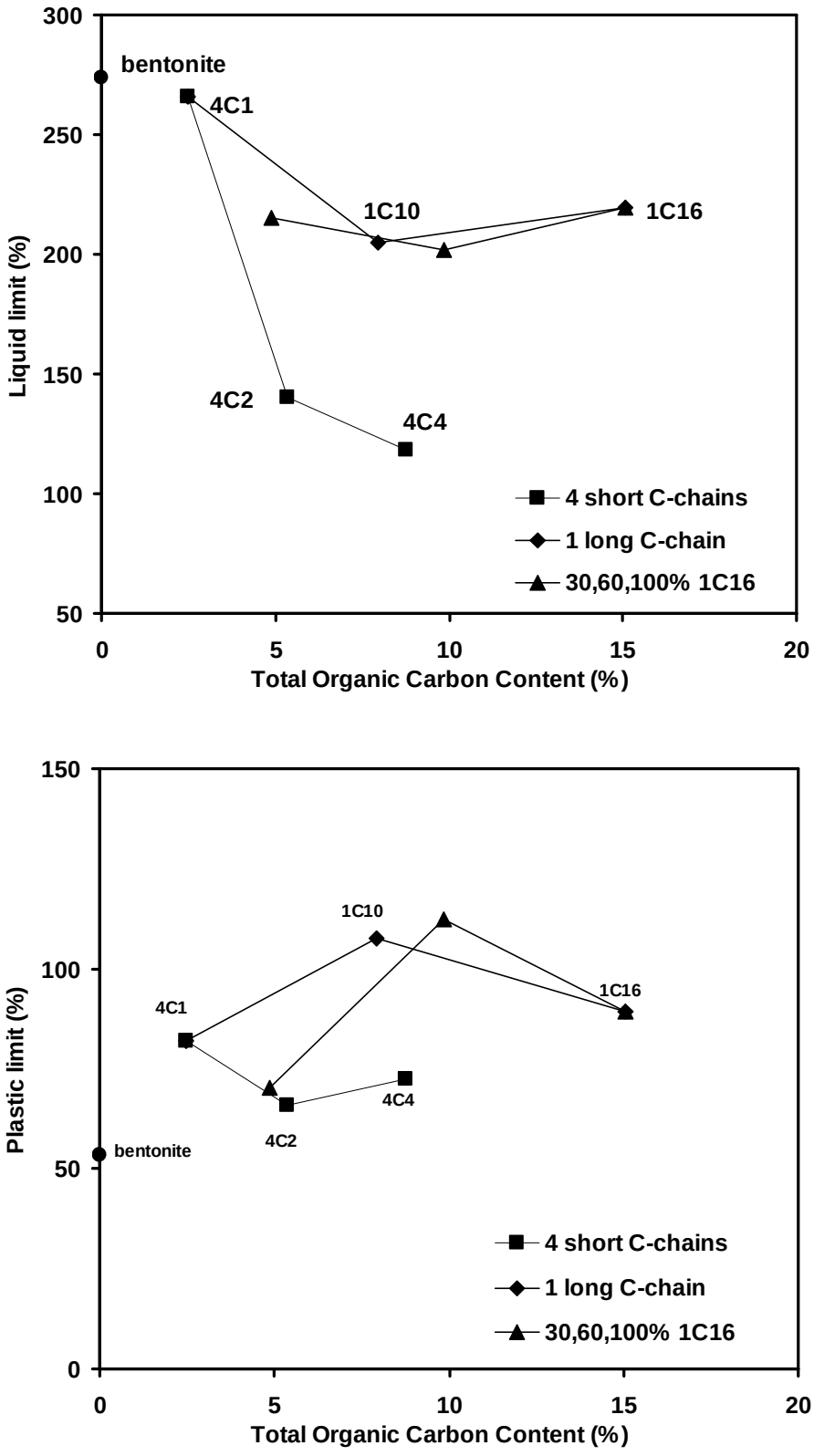

Figure 2-6. (a) Liquid limit and (b) plastic limit versus organic carbon content.

Specific gravity

The specific gravities of seven organobentonites (TMA, TEA, TBA, DTMA, and HDTMA at 100% CEC, and HDTMA at 30% and 60% CEC) were tested. The results showed that specific gravity decreased as the total organic carbon content or the total cation exchange percentage increased (Table 2-4, Figure 2-7 and Figure 2-8). The test results produced a specific gravity that was lower than expected based on a mixture of organic carbon and clay at ratios equal to the amounts exchanged in this study. The dashed line in Figure 2-7 was calculated for a hypothetical mixture of mineral solids (assuming G_s = 2.74) and organic solids (assuming G_s = 1.0). It was believed that the hydrophobic interlayer created by the presence of the organic cations excluded a disproportionate quantity of water during the specific gravity tests. Because the specific gravity method relies on the measurement of the volume of displaced water, the results of organoclays will appear artificially low (Burns et al., 2006). The measured values of specific gravity were lower than those reported in Burns et al. (2006), but the trend was consistent.

Table 2-4. Specific Gravity of Organoclays

Clay	G_s
Bentonite	2.74
100TMA-bentonite	2.80
100TEA-bentonite	2.23
100TBA-bentonite	2.20
100DTMA-bentonite	2.26
30HDTMA-bentonite	2.29
60HDTMA-bentonite	2.07
100HDTMA-bentonite	1.75

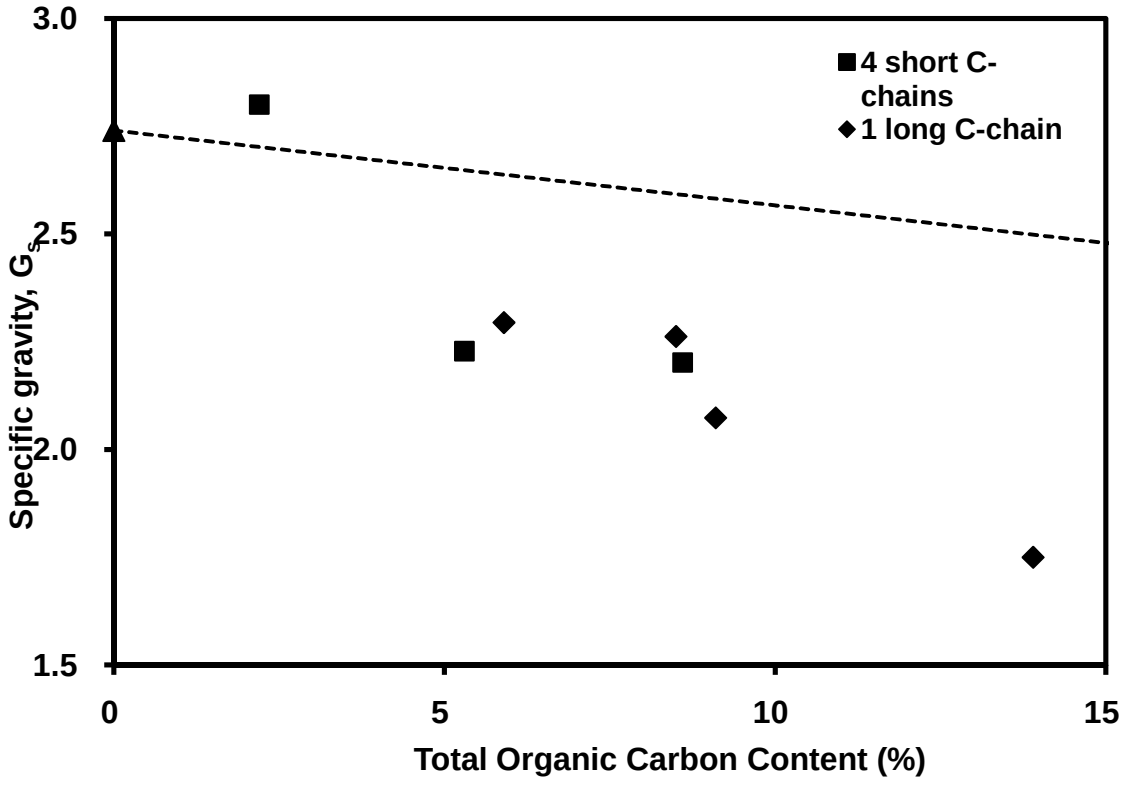

Figure 2-7. Specific gravity of organobentonites as a function of total organic carbon content. Dashed line represents theoretical specific gravity, calculated assuming mixture of mineral solids (G_s = 2.74) with organic solids (G_s = 1.0).

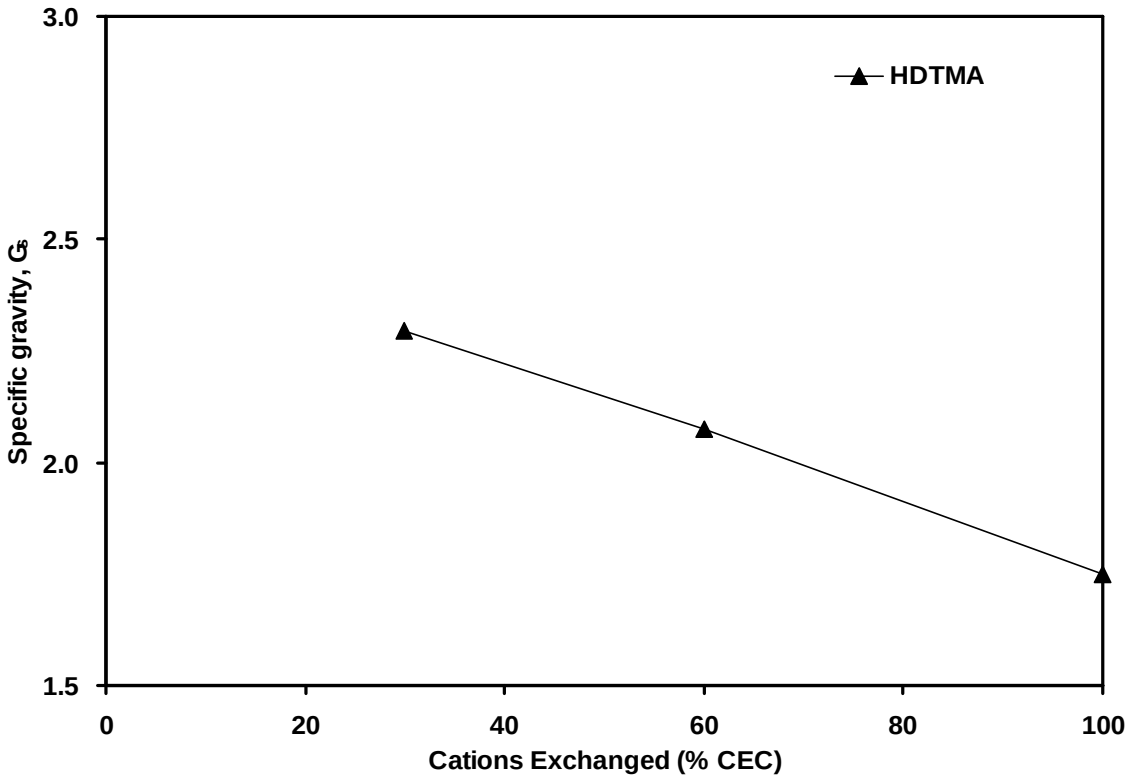

Figure 2-8. Specific gravity of HDTMA-bentonite at increasing percentages of cationexchange capacity.

Specific surface area

The specific surface areas of nine clays (TMA and HDTMA at 30%, 60%, and 100% CEC, and TEA, TBA, and DTMA at 100% CEC) were measured using the methylene blue test method. Unmodified bentonite possessed the highest specific surface area of 628 m^2/g (Table 2-5, Figure 2-9), which is consistent with values in the literature, i.e., 50 – 120 m^2/g for primary surface area and 700 – 840 m^2/g when the secondary surface area is included in the measurement (Mitchell and Soga, 2005). Based on the measured surface area, it was clear that the methylene blue was able to penetrate the interlayer surface areas of the unmodified bentonite, resulting in the high values of measured surface area. On the

contrary, the measured specific surface area of organobentonites was significantly lower than that of unmodified bentonite, ranging from 56 – 167 m^2/g for the modified clays. Note that it appears that sorption of methylene blue to the quaternary ammonium cations does not appear to have occurred, because in the case of sorption, the surface area would indicate higher than expected values of uptake of methylene blue.

Table 2-5. Soil Concentrations and Specific Surface Area of Organoclays

Clay	Soil concentration (g/mL)		Specific Surface Area (m^2/g)
	trial 1	trial 2	
Bentonite	0.015	-	628
30TMA-bentonite	0.034	0.035	234
60TMA-bentonite	0.034	0.036	189
100TMA-bentonite	0.009	0.010	149
100TEA-bentonite	0.033	0.032	82
100TBA-bentonite	0.011	0.006	104
100DTMA-bentonite	0.015	0.015	65
30HDTMA-bentonite	0.039	0.039	87
60HDTMA-bentonite	0.029	0.040	58
100HDTMA-bentonite	0.036	0.030	56

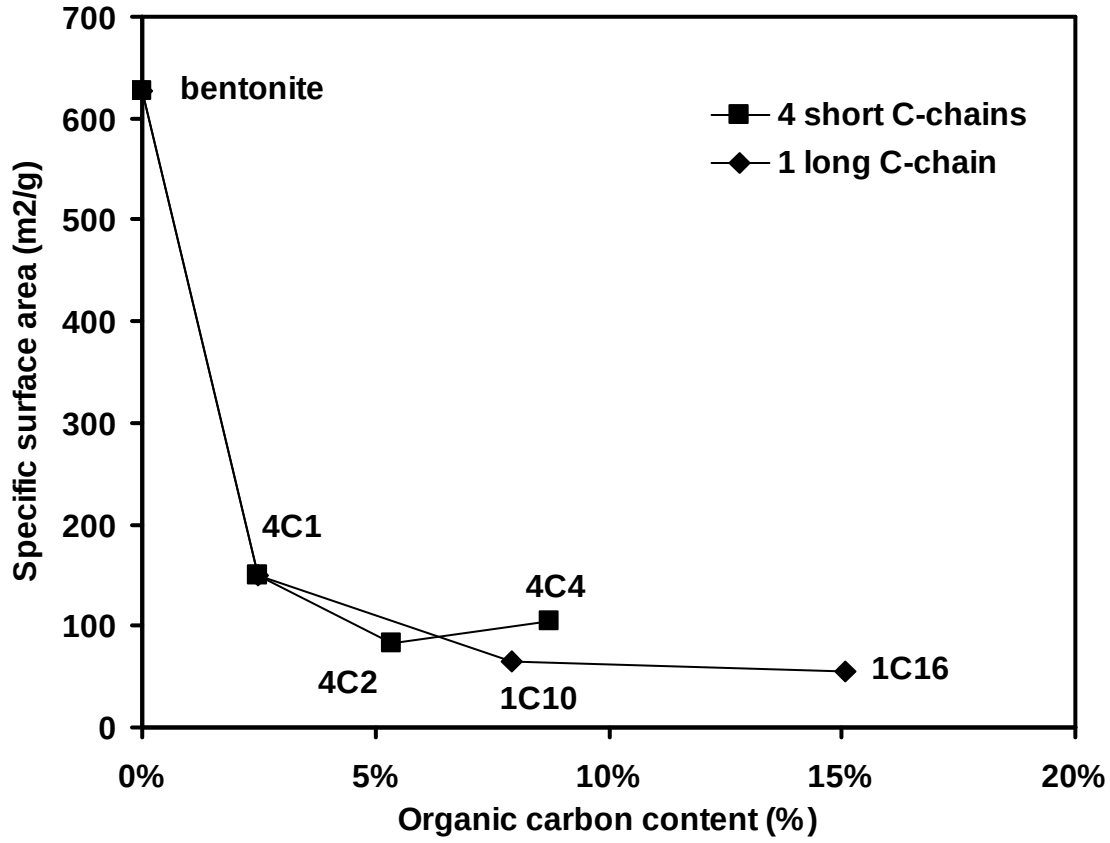

Figure 2-9. Specific surface area versus carbon chain length

Examination of the effect of the total organic carbon content illustrated that increasing the length of a single C-chain on the cation (*$4C_1$* to *$1C_{10}$* to *$1C_{16}$*, TMA→DTMA→HDTMA at 100% CEC) reduced the surface area from 149 m^2/g to 65 and 56 m^2/g (Figure 2-9). Similarly, increasing the size of the all four branches on the organic cation (*$4C_1$* to *$4C_2$* to *$4C_4$*, TMA→TEA→TBA at 100% CEC) altered the measured surface area, from 149 m^2/g to 82 and 104 m^2/g, respectively. Organic cations with longer single C-chain or with larger size bound to clay surface more tightly, therefore the net surface charge of clay particles were further reduced. As a result, larger clay aggregates tended to form, which in turn would blocked the methelene blue from

adsorption within clay aggregates. As a result the measured specific surface areas of organoclays were lower. Furthermore, it is very difficult to displace the organic cations from the particle surfaces energetically. For QACs with a long C-chain (number of C ≥ 10), the energy required to move one $-CH_2$ from the adsorbed bentonite site to the bulk solution is about 2.5 kJ/mol (Stumm and Morgan, 1996). As the length of the C-chain increases, the required energy to displace the cations also increases. Hence it was believed that the presence of the organic cations physically obstructed the access of the methylene blue molecules to the particle surface, which in turn reduced the measured specific surface area.

Comparison of the surface area measured for TMA and HDTMA at 30%, 60%, and 100% CEC (equivalent percentages of exchange sites occupied, as opposed to total organic carbon), suggested that increasing the percentage of exchange sites occupied by organic cations reduced the surface area (Figure 2-10). In addition, replacement of the same number of exchange sites with a small molecule (TMA) versus a long molecule (HDTMA) resulted in a reduction in the measured specific surface area as the size of the molecule increased (Figure 2-10). TMA surface area decreased from 234 m^2/g to 189 m^2/g to 149 m^2/g, as exchange percentage was increased; HDTMA surface area decreased from 87 m^2/g to 58 m^2/g to 56 m^2/g, as exchange percentage was increased. Organic cations with more organic coatings bound to clay surface more tightly, therefore the net surface charge of organobentonite particles were further reduced. As a result, larger organobentonite aggregates tended to form, which in turn would blocked the methelene blue from adsorption within clay aggregates. As a result the measured specific surface areas of organobentonites were lower. In addition, at low concentrations (e.g., 30%

CEC), the longer HDTMA molecule conformed to the particle surfaces, lying close to parallel to the particle surfaces, further limiting the access of the methylene blue to the surface area of the bentonite. TMA, which is a much smaller molecule than HDTMA, leaves a much larger portion of the mineral surface accessible to additional molecules, resulting in a higher measured surface area. Comparison of the surface areas as a function of total organic content for all nine clays tested, as opposed to % CEC exchanged, displayed that the measured surface areas for the organoclays were very similar when compared on a % organic carbon basis, indicating that the presence of the organic material is a primary driver in the exclusion of the methylene blue molecule, as opposed to only the number of exchange sites (Figure 2-11).

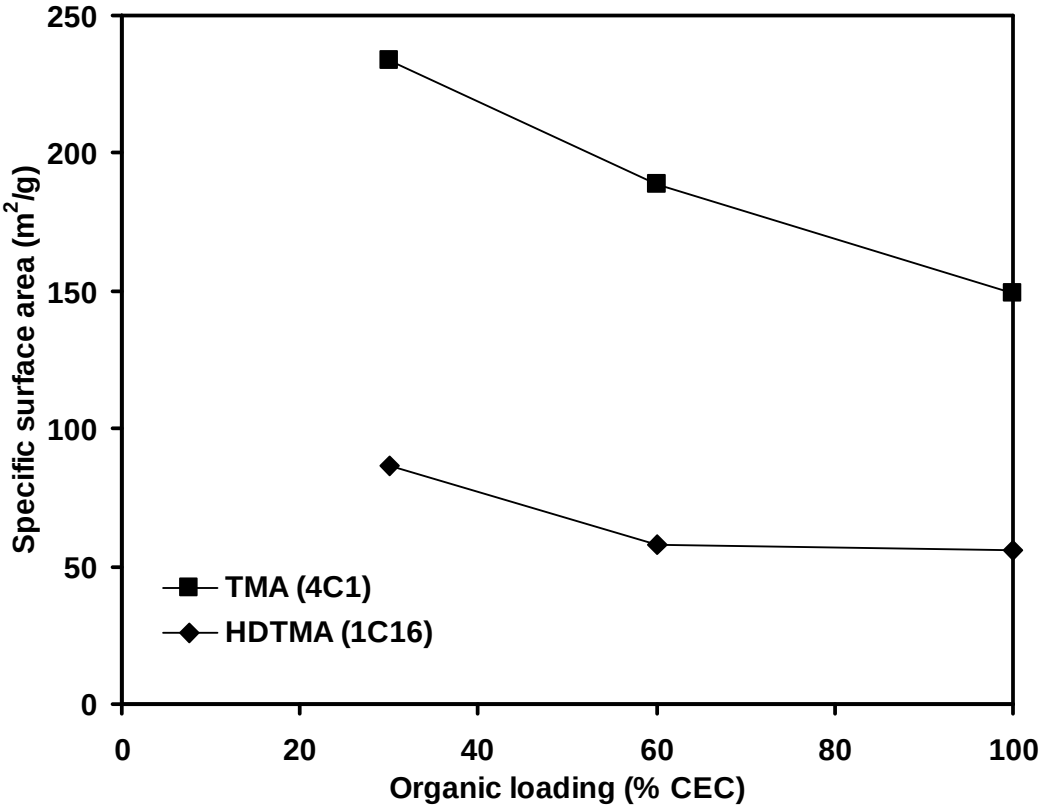

Figure 2-10. Specific surface area versus organic loading for TMA- and HDTMA-bentonite

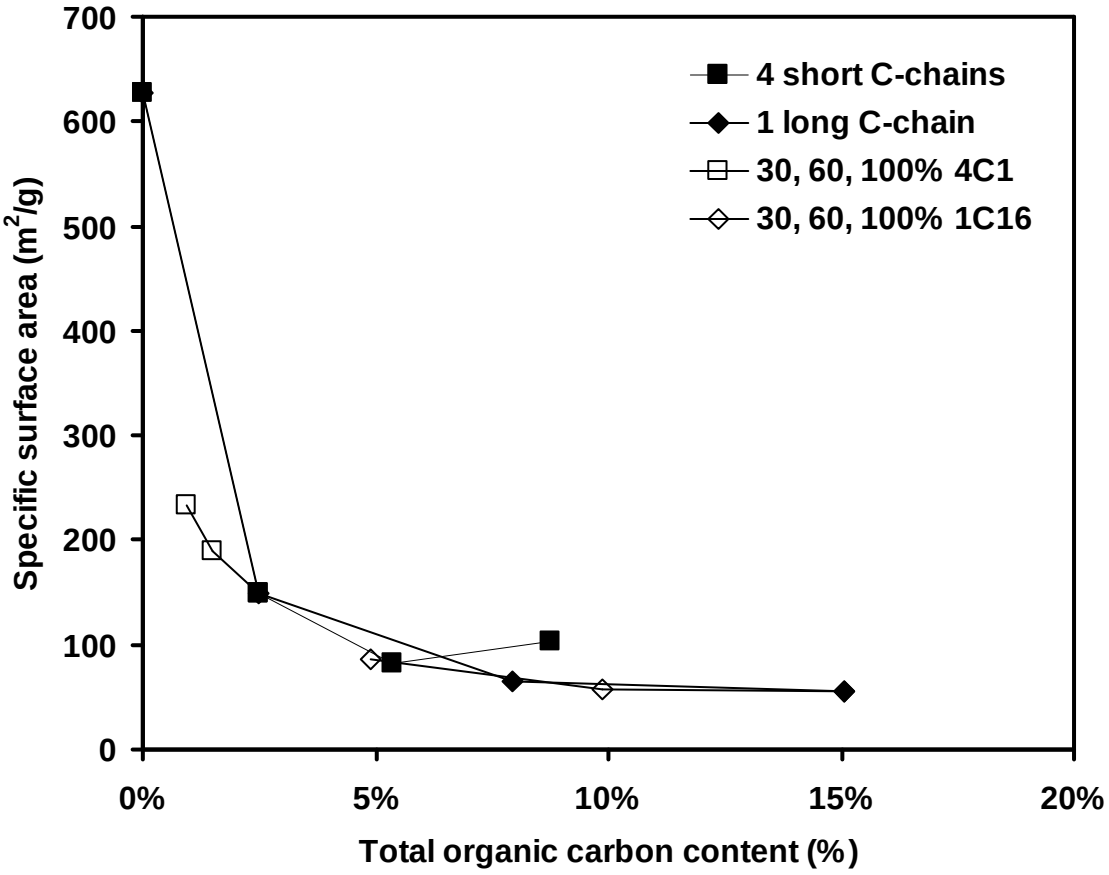

Figure 2-11. Specific surface area versus organic carbon content

Properties of aqueous solutions of quaternary ammonium cations: surface tension, hydrophobicity, and micelle formation

In addition to the characterization tests performed on the quaternary ammonium cations while sorbed to the clay surfaces, the surface tension of aqueous solutions of the cations, in the absence of clay particles, were also measured. The surface tension of surfactant solutions was an indication of the hydrophobicity of the quaternary ammonimum cation solutions, with lower surface tension representing higher hydrophobicity (Rosen, 2004). Because the value of the surface tension was also a

function of the concentration of the surfactant solutions, the measurement can be used to identify the critical surface tension and the critical micelle concentration. At low concentrations (typically less than 10^{-5} mol/L), surfactants such as the quaternary ammonium cations in this study will distort the structure of the water and therefore increase the free energy of the system due to the presence of the hydrophobic group in the cation structure. Consequently, the cations concentrate at the surface, orienting their hydrophobic groups away from the solvent, minimizing the free energy of the solutions (Rosen, 2004). Solubility data for the surfactants used in this investigation are given in Table 2-6.

Table 2-6. Aqueous Solubility of Quaternary Ammonium Cations

Chemical name	Solubility (mol/L)	Temp (ºC)
Sodium chloride, NaCl	6.16[1]	20
Tetramethylammonium chloride, TMA Cl	5.47[1] 6.00[2]	20 20
Tetraethylammonium bromide, TEA Br	13.30[1]	25
Tetrabutylammonium bromide, TBA Br	1.86[1]	20
Decyltrimethylammonium bromide, DTMA Br	Not found	
Dodecyltrimethylammonium bromide, DDTMA Br	0.10	20
Hexadecyltrimethylammonium bromide, HDTMA Br	0.10[1] 0.04[1]	20 20

[1] www.chemblink.com (2010)

[2] www.sigma-aldrich.com (2010)

As the concentration of a surfactant in water is increased, the hydrophobicity increases, and surface tension decreases. Upon reaching a critical concentration, some surfactants, especially those with long carbon chains, start to form micelles, which are aggregates of surfactant. Micelles orient with their hydrophobic groups gathered together in an interior cluster, while their hydrophilic groups point away from the aggregate, towards the bulk solution. Thermodynamically, the micelles are formed at the point of minimum free energy of the solutions. Once the micelles form, further increase in surfactant concentration does not decrease the surface tension of the solution, and this concentration is called the critical micelle concentration, or CMC. The CMC is an important parameter because it is related to substantial changes in many physical properties of surfactant solutions, such as adsorption, conductivity, density, osmotic pressure, and detergency (Adamson and Gast, 1997). The minimum surface tension of a surfactant solution is also known as the critical surface tension of that surfactant.

The surface tension of quaternary ammonium cations was compared when increasing the length of one carbon chain, (TMA ($4C_1$), DTMA ($1C_{10}$), DDTMA ($1C_{12}$), and HDTMA ($1C_{16}$)) and increasing branch size (TMA ($4C_1$), TEA ($4C_2$), and TBA ($4C_4$)). In all cases, the surface tension decreased as the concentration of surfactant in solution increased (Figure 2-12). At the same concentration, surface tension decreased as the chain length increased and/or as the branch size increased, indicating that hydrophobicity was higher as cation size increased. It follows that the hydrophobicity of the solution increased with the size of the cation.

Surfactant concentrations in this study were also large enough to identify the critical micelle concentrations (CMC) and critical surface tension for DTMA, DDTMA,

and HDTMA (Table 2-7). As the length of a single carbon chain was increased, the critical micelle concentration and the critical surface tension decreased (Figure 2-12). The measured CMC and critical surface tension values for DDTMA and HDTMA cations agreed with those reported in the literature (Menger and Littau, 1993; Wong et al., 1989). At the concentrations tested (up to 1 M), CMC was not reached for the organic cations tested for increasing branch effect (TMA, TEA, and TBA).

Table 2-7. Critical Micelle Concentration and Critical Surface Tension of Organoclays

Chemical name	Critical micelle concentration, CMC, (mol/L)	Critical surface tension (dynes/cm)
Decyltrimethylammonium bromide, DTMA Br	0.05[1]	43[1]
	0.065[3]	
Dodecyltrimethylammonium bromide, DDTMA Br	0.0125[1]	41[1]
	0.02[2]	38[2]
	0.015[3]	
Hexadecyltrimethylammonium bromide, HDTMA Br	0.001[1]	38[1]
	0.0009[3]	

[1]This study

[2]Menger and Littau (1993).

[3]Wong et al. (1989).

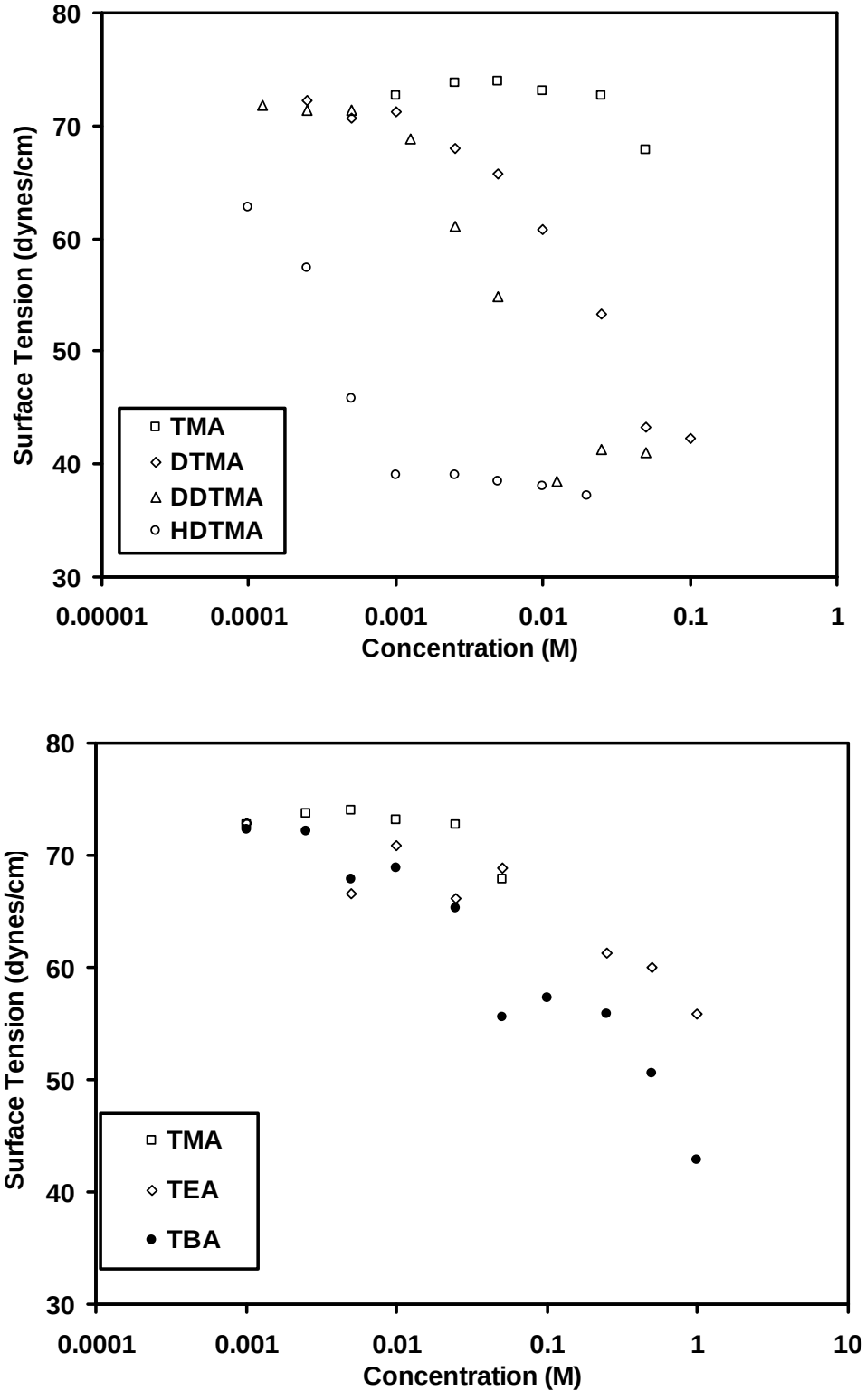

Figure 2-12. Surface tension vs. concentration for quaternary ammonium cations with (a) single long C-chain and (b) four short C-chains

Chapter 3 Conductivity of Organoclays: Hydraulic, Thermal, and Electrical

Introduction

Four types of conduction behavior are of general interest in the study of geomaterials: electrical, hydraulic, thermal, and chemical. For each case, flow through a soil results from a gradient, or concentration difference, and occurs from areas of higher concentration to areas of lower concentration. In each conduction case, the rate of flow, or the flux, will be linearly related to the driving force, given a cross sectional area A (Mitchell and Soga, 2005):

Electrical	$I = \sigma_e i_e A$	**Ohm's law**	**Equation 3-1**
Hydraulic	$q_h = k_h i_h A$	**Darcy's law**	**Equation 3-2**
Thermal	$q_t = k_t i_t A$	**Fourier's law**	**Equation 3-3**
Chemical	$J_D = D i_c A$	**Fick's law**	**Equation 3-4**

where I, q_h, q_t, and J_D are the flowrates (or flux) for electricity, water, heat, and chemicals; σ_e, k_h, k_t, and D represent the conductivities, and i represents the gradient for flow in each condition.

In this study, the electrical, hydraulic, and thermal conductivities of organobentonites were measured. The hydraulic and chemical conductivity of organobentonites has been studied extensively in the past (Bartelt-Hunt et al., 2005a; Bartelt-Hunt et al., 2006; Lorenzetti et al., 2005; Smith and Jaffe, 1994; Smith and Galan, 1995; Smith et al., 1995; Smith et al., 2003); consequently, no diffusion tests were

performed, and only limited hydraulic conductivity tests were performed. Electrical conductivity and permittivity tests were performed to quantify the branch effect for increasing the size of organic cations (TMA ($4C_1$), TEA ($4C_2$), TPA ($4C_3$), and TBA ($4C_4$)), as well as the tail length effect (DTMA ($1C_{10}$), DDTMA ($1C_{12}$), and HDTMA ($1C_{16}$)) in the aqueous phase. Electrical permittivity tests were performed on organoclays made from TMA ($4C_1$), TEA ($4C_2$), and TBA ($4C_4$)) to study the branch effect, as well as (DTMA ($1C_{10}$), and HDTMA ($1C_{16}$)) to study the tail length effect; tests were also performed to evaluate the effect of organic cation surface coverage (30% and 60% cation exchange capacity for TMA and HDTMA). Hydraulic and thermal conductivity tests were performed on TMA, TEA, TBA, DTMA and HDTMA at 100% CEC, to quantify branch and tail length effects, and tests were also performed to assess the effect of organic cation surface coverage (30% and 60% cation exchange capacity for TMA and HDTMA) on the hydraulic and thermal conductivity of organobentonites. The experimental matrix allowed comparison of the effects of organic structure and loading on the conduction phenomena.

Electrical conductivity and high frequency permittivity

Literature review

Investigation of the electromagnetic parameters of water, electrolytes, and moist soil can provide useful information about their molecular structures. Because the organic cations used in this study dissolve/dissociate in water, the response of both the aqueous organic cation and the sorbed organic cations (organobentonites) in the presence of an applied electric field were studied to give more insights into the behavior of the clays.

The organic cations tested in this study are salts that fully ionize in aqueous solution, which categorizes them as strong electrolytes; depending on size and structure, the cations may hydrate to varying degrees. Typically, the larger the cation, the lower the conductivity, due to the drag forces that act on the large cation; however, smaller ions will hydrate strongly, creating a large hydrodynamic radius, which also makes them vulnerable to large drag forces. By definition, ions are not electrically neutral and move in the presence of an applied electric field. Electric conductivity is a measurement of charge mobility in response to the applied electric field; as the mobility of the dissolved ions increases, the conductivity of the solution will increase. Consequently, increasing cation size and solution viscosity result in decreased conductivity due to increased drag forces.

In the presence of an applied electric field, cations will accelerate toward the cathode, while anions will accelerate toward the anode until a terminal velocity was reached due to Stokes drag force. The charged ion will be subjected to the following force (Atkins, 1998):

$$F = \frac{ze_o \Delta\phi}{l} = ze_o E \qquad \textbf{Equation 3-5}$$

where ze_o = ion charge, $\Delta\phi$ = electric field, and l = electrode spacing. The ion will also experience drag as it moves through the solvent, and assuming Stokes law is applicable, and that particles are spherical, the drag can be calculated according to (Atkins, 1998)

$$F' = 6\pi\eta as \qquad \textbf{Equation 3-6}$$

where η = viscosity, a = radius, and s = drift speed. Equating the two forces allows determination of the terminal velocity. Drift speed will be proportional to the strength of the electric field which is applied to the solution:

$$s = uE \qquad \textbf{Equation 3-7}$$

where u = mobility ($m^2V^{-1}s^{-1}$), which is the terminal velocity of an ion subject to a unit electric field, $u \equiv \frac{v_{ion}}{E}$. It follows that the mobility can be determined as (Atkins, 1998):

$$u = \frac{ze_0}{6\pi\eta r_h} \qquad \textbf{Equation 3-8}$$

where E is the strength of the electric field (V/m); z is valence; $e_0 = 1.602\times10^{-19}C$ is electronic charge; η is viscosity of the solution ($Pa\cdot s$); $\eta = 8.90\times10^{-4}(Pa\cdot s)$ for water at 25 ^{o}C; and r_h is the radii of the hydrated ion; typical values of the radii of hydrated ions r_h given in Table 3-1 and Table 3-2. Equation 3-8 assumes that Stoke's law is applicable at the microscopic scale.

Table 3-1. Radii of Hydrated Ions and Mobility of Ions

Ion	r_h **[1], (nm)**	**Mobility[2]*, (** $m^2V^{-1}s^{-1}$ **)**
Na^+	0.358	5.2×10^{-8}
NH_4^+	0.331	
Cl^-	0.332	7.9×10^{-8}
Br^-	0.330	8.1×10^{-8}

[1] Nightingale (1959)

[2] Santamarina et al. (2001)

* 25°C and low concentration

Table 3-2. Radii of Hydrated Tetraalkylammonium Ions

TMA+	TEA+	TPA+	TBA+	Reference
Ion Radius (nm)				
0.347	0.400	0.452	0.494	(Robinson and Stokes, 1965)
0.285	0.348	0.398	0.437	(Conway et al., 1966)
0.256	0.306	0.343	0.375	(Ramanathan et al., 1972)
0.235	0.176	--	0.367	Calculated at 0.00195 M
0.247	0.229	--	0.498	Calculated at 0.00391 M
0.269	0.279	--	0.557	Calculated at 0.00781 M

In cases where the electrolyte is completely ionized and the concentration is low, such that ion-ion interactions are negligible, the conductivity can be derived by (Santamarina et al., 2001):

$$\sigma = F\sum_i c_i z_i u_i \qquad \textbf{Equation 3-9}$$

where *c*, *z*, and *u* were the concentration, valence and mobility of the ion, respectively, and F = 96,485 *C/mol* which is Faraday's constant. At high concentrations, the decrease in mobility may prevail over the increase in ion availability, and the conductivity of the electrolyte may decrease (Santamarina et al., 2001). The macroscopic conductivity σ can be measured by a conductivity cell, which allows the mobility *u* of the hydrated organic ions to be calculated from Equation 3-9; determination of mobility in turn allows calculation of the radius of hydrated ions.

While conductivity represents the ability of ions to move in the presence of an applied electric field, polarization is the displacement of constrained charges from an

equilibrium position in the presence of an applied electric field (Santamarina et al., 2001). The polarizability of a molecule proportionally relates the dipole moment which is induced in the presence of an electric field to the strength of the electric field (Atkins, 1998):

$$\mu_d = \alpha E \qquad \textbf{Equation 3-10}$$

where μ_d = dipole moment, α = polarizability, and E = electric field. From a macroscopic view, the polarizability of a material is effectively the permittivity, or the measure of the material's ability to transmit an electric field. Because the displacement is not instantaneous, and occurs after the application of the electric field, polarization will be proportional to the electric field, but the amplitude and phase will be a function of frequency. Consequently, the complex permittivity can be separated into real and imaginary parts (Santamarina et al., 2001):

$$\kappa^* = \kappa' - j\kappa'' \qquad \textbf{Equation 3-11}$$

where κ^* = relative complex permittivity, κ' = real portion of relative permittivity, κ'' = imaginary portion of the relative permittivity, and j represents an imaginary quantity. The real relative permittivity is related to energy stored within the medium, while the imaginary portion is related to energy dissipation within the medium. At high frequencies (MHz and GHz), the real relative permittivity decreases with increasing ionic concentration due to the reduced mobility of the molecules involved in hydrating ions (Santamarina et al., 2001).

When measuring losses due to polarization and conduction simultaneously, the 'effective' imaginary permittivity can be determined by (Santamarina et al., 2001):

$$\kappa_{\mathbf{eff}}'' = \kappa'' + \frac{\sigma}{\varepsilon_0 \omega} \qquad \textbf{Equation 3-12}$$

where $\varepsilon_0 = 8.85 \times 10^{-12} C^2 / \left(N \cdot m^2\right) = 8.85 \times 10^{-12} F / m$, and ω = frequency. Clearly, as the frequency increases, the conduction losses become less significant. Consequently, it is possible to define an effective AC conductivity (non-zero frequency), which includes DC conductivity and the dynamic effects of polarization (Santamarina et al., 2001):

$$\sigma_{\mathbf{eff}} = \sigma + \kappa'' \varepsilon_0 \omega \qquad \textbf{Equation 3-13}$$

Polarization mechanisms can display one of two characteristic spectra: resonance or relaxation. Typically within water or water solutions, molecular, spatial, and double layer polarization will occur, which results in the relaxation spectrum as the dominant mode (Santamarina et al., 2001). When the applied electric field is alternating, the molecules will rotate in order to align with the direction of the applied field. In the relaxation spectrum, the molecules cannot rotate quickly enough to align with the alternating direction of the field and damping can dominate over the inertial forces. Consequently, polarization of larger amplitude can occur at lower frequencies because enough time is given during each cycle for the dipoles to achieve complete alignment; however, as the frequency is increased, the polarization amplitude will decrease because the dipoles do not have enough time to completely align (Hayt and Buck, 2006).

The objective of this section was to investigate the electrical conductivity and the polarizability of the aqueous quaternary ammonium cations and their corresponding organobentonite forms from the microscopic viewpoint, as well as permittivity from the macroscopic viewpoint. Three experiments were performed: (1) Electrical conductivity tests of quaternary ammonium salts, which were measured as a function of salt

concentration; (2) Electrical permittivity tests on quaternary ammonium salts, which were measured as a function of salt concentration in the frequency range of 0.1 GHz – 1.3 GHz (radio to microwave range); (3) Electrical permittivity tests on organobentonites, which were performed as a function of water content.

Materials and experimental methods

Stock solutions were prepared using the method of serial dilutions: ammonium salts were dissolved in de-ionized water with concentration at either 0.1 mol/L (DTMA, DDTMA, and HDTMA) or 1 mol/L (NaCl, TMA, TEA, TBA, and NH_4), depending on the cation's aqueous solubility (Table 3-3). Next, the organic cations solutions were serially diluted to make a total of ten solutions (Table 3-4). High concentration solutions (> 1M) of highly soluble salts (e.g. NaCl, TMA Cl, TEA Br, and TBA Br) were prepared for permittivity tests (Table 3-4).

Electrical conductivity measurements of salt solutions with different concentrations were obtained by testing with an Accumet Excel XL60 conductivity meter and Accumet temperature-compensated two-cell conductivity probe (Accumet). AC voltage was used to minimize the effect of polarization. The conductivity probe was rinsed with deionized water between measurements.

Table 3-3. Solubility of Ammonium Salts

Chemical Name	Molecular Weight (g/mol)	Aqueous Solubility (g/L)	Aqueous Solubility (M)	Temp (°C)
Sodium chloride, NaCl	58.44	360	6.16	20[1]
Ammonium chloride, NH_4Cl	53.49	soluble		n/a[1]
Ammonium bromide, NH_4Br	97.94	970	9.90	25[1]
Tetramethylammonium chloride, TMA Cl	109.6	10%		n/a[2]
	109.6	600	5.47	20[1]
	109.6		6.00	20[3]
Tetramethylammonium bromide, TMA Br				
Tetraethylammonium bromide, TEA Br	210.16	2795	13.30	25[1]
Tetrapropylammonium bromide, TPA Br	266.26	100	0.38	n/a[1]
Tetrabutylammonium bromide, TBA Br	322.37	600	1.86	20[1]
Decyltrimethylammonium bromide, DTMA Br				
Dodecyltrimethylammonium bromide, DDTMA Br	308.34		0.10	20[1]
Tetradecyltrimethylammonium bromide, TDTMA Br	336.4	200	0.59	n/a
Hexadecyltrimethylammonium bromide, HDTMA Br	364.45		0.10	20[3]
	364.45	13	0.04	20[1]

[1] www.chemblink.com (2010)

[2] www.usbweb.com (2010)

[3] www.sigma-aldrich.com (2010)

Table 3-4. Tested Concentrations of Aqueous Ammonium Cation Solutions

Cation	Solution Concentration for Conductivity Tests (M)	Additional Solution Concentration for Permittivity Tests (M)
NaCl	1, 0.5, 0.25, 0.125, 0.0625, 0.0313, 0.0156, 0.00781, 0.00391, 0.00195	5, 3, 1.8, 1.08
NH_4 Br	1, 0.5, 0.25, 0.125, 0.0625, 0.0313, 0.0156, 0.00781, 0.00391, 0.00195	4.95, 2.48, 1.24
TMA Cl	1, 0.5, 0.25, 0.125, 0.0625, 0.0313, 0.0156, 0.00781, 0.00391, 0.00195	2, 2.4, 1.44
TEA Br	1, 0.5, 0.25, 0.125, 0.0625, 0.0313, 0.0156, 0.00781, 0.00391, 0.00195	2
TBA Br	1, 0.5, 0.25, 0.125, 0.0625, 0.0313, 0.0156, 0.00781, 0.00391, 0.00195	1.2
DTMA Br	0.1, 0.05, 0.025, 0.0125, 0.00625, 0.00313, 0.00156, 0.000781, 0.000391, 0.000195	--
DDTMA Br	0.1, 0.05, 0.025, 0.0125, 0.00625, 0.00313, 0.00156, 0.000781, 0.000391, 0.000195	--
HDTMA Br	0.1, 0.05, 0.025, 0.0125, 0.00625, 0.00313, 0.00156, 0.000781, 0.000391, 0.000195	--

An HP-8752A network analyzer in conjunction with an HP-85070A coaxial termination probe (frequency = 0.1 GHz ~ 1.3 GHz) was used for the measurement of electric permittivity of all salt solutions. Because the geometry of the coaxial cable is very critical to the results, the coaxial cable was fixed to prevent any distortion or geometric shape change during measurement, and calibration was performed at the beginning of each measurement session. Tests were performed on approximately 5 mL of solution, and three measurements were performed for each sample. The solution

container for measurement was cleaned twice with deionized water and once with ethanol between measurements, and then wiped with Kimwipe lint-free tissues, and the probe was wiped clean between measurements. In the cases of high concentration solutions, the probe was both rinsed and wiped. The solutions were tested in the order from low to high concentrations.

Results and Discussion

Electrical conductivities of sodium chloride and the quaternary ammonium salts displayed that the conductivity of sodium chloride was higher than all quaternary ammonium salts at all tested concentration range (Figure 3-1). As the size of quaternary ammonium cations increased from TMA ($4C_1$) to TEA ($4C_2$) to TBA ($4C_4$), the conductivity decreased. Additionally, as the length of long C-chain increased from TMA ($4C_1$) to DTMA ($1C_{10}$), to DDTMA ($1C_{12}$), and to HDTMA ($1C_{16}$), the conductivity decreased. As was anticipated, the conductivity results indicated that as the size of the cation or the length of long C-chain increased, the mobilities decreased due to increased drag forces being exerted on the molecule. When evaluated on the basis of approximately equivalent total organic carbon contents, the conductivity measurements indicated that the drag force exerted by lengthening the cation tail in one of the four quaternary positions led to a similar level of drag on the molecule as when the carbon was divided equally between the four quaternary positions (compare TBA and DTMA).

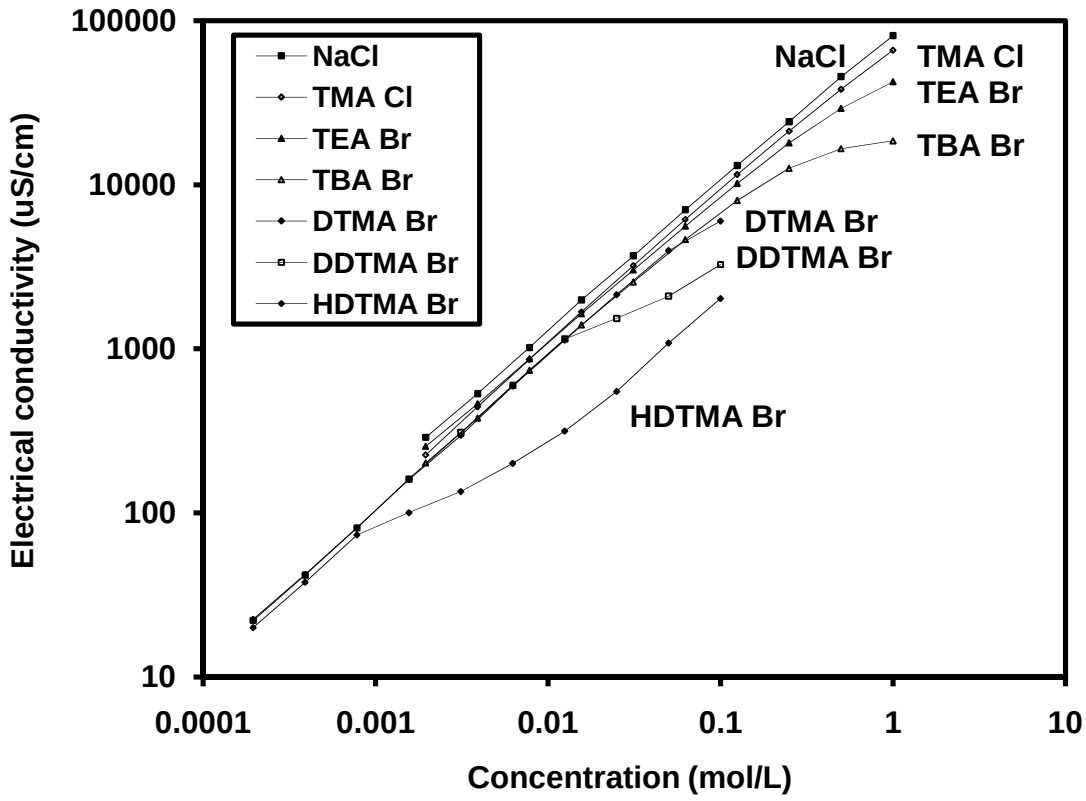

Figure 3-1. Electrical conductivity versus concentration for quaternary ammonium salts.

It was also observed that at low concentrations, the conductivity increased linearly with concentration for all the quaternary ammonium salts. However, upon reaching a threshold concentration, the relation between conductivity and concentration became non-linear. This indicated that the ion-ion interaction came into play after this threshold concentration, which decreased as the length of long C-chain increased, or as the size of the QACs increased. Comparison to results of the surface tension measurements (Chapter 2) unveiled that the threshold concentration corresponded to the critical micelle concentration for the long chain cations tested. Micelles, which result from ion-ion interaction, are clusters of cations with their hydrophobic tail portions preferentially

oriented toward each other, and their hydrophilic head groups oriented toward the bulk solution. Clearly, the agglomeration of ions and formation of micelles resulted in decreased mobility of the quaternary ammonium cations, as reflected in the decreased conductivity measurements. From the measured conductivity and known mobility of chloride and bromide ions (Table 3 – 1), the radii of hydrated organic ions at low concentrations (simulating infinite dilution) were calculated by Equations 3–8 and 3–9. The calculated radii of hydrated ions were in agreement with those in the literature (Table 3-2). At high concentrations, calculated radii of hydrated organic ions were not reliable, indicating that the ion-ion interaction came into play.

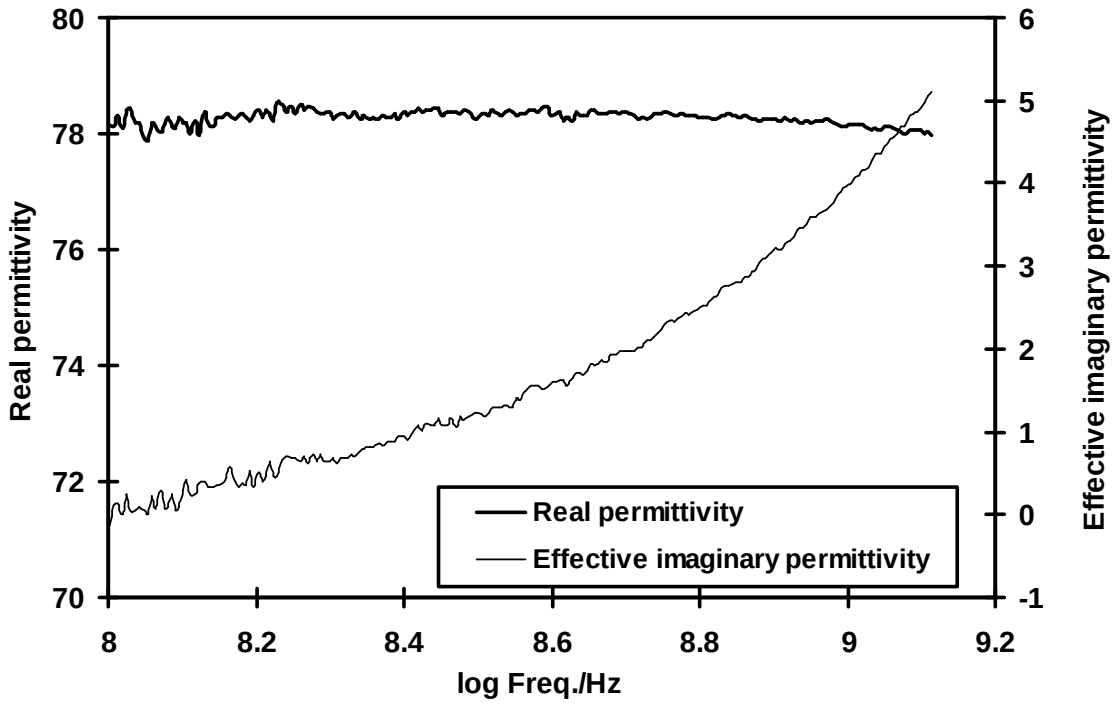

Figure 3-2. Real and effective imaginary permittivity of de-ionized water.

The real (κ') and effective imaginary (κ_{eff}'') relative permittivities of deionized water measured between 0.1 to 1.3 GHz showed that κ' decreased as the frequency was increased (Figure 3-2). As was anticipated, free water experienced relaxation at microwave frequencies, which can be attributed to the orientational polarization of free water, and the out of phase component of water polarization led to an increase in κ_{eff}''. When electrolytes, such as NaCl, TMA Cl, TEA Br, DTMA Br, DDTMA Br, and HDTMA Br were added to the water, their real and effective imaginary relative permittivities exhibited three clear features (Figure 3-3 through Figure 3-9): (1) As frequency increased, κ' decreased. This observation agreed with that of water, indicating orientational polarization also took effect in salt solutions. (2) Except for solutions at very low concentrations where orientational polarization of free water dominated, κ_{eff}'' decreased as the frequency increased. This is due to the DC conduction loss as the frequency increased (Equation 3-12). (3) Except for organic solutions with a single long C-chain (DTMA Br, DDTMA Br, and HDTMA Br) at lower frequency (< 0.6 GHz) (discussed later), as the concentration increased, κ' decreased due to the reduced mobility of molecules involved in hydrating ions.

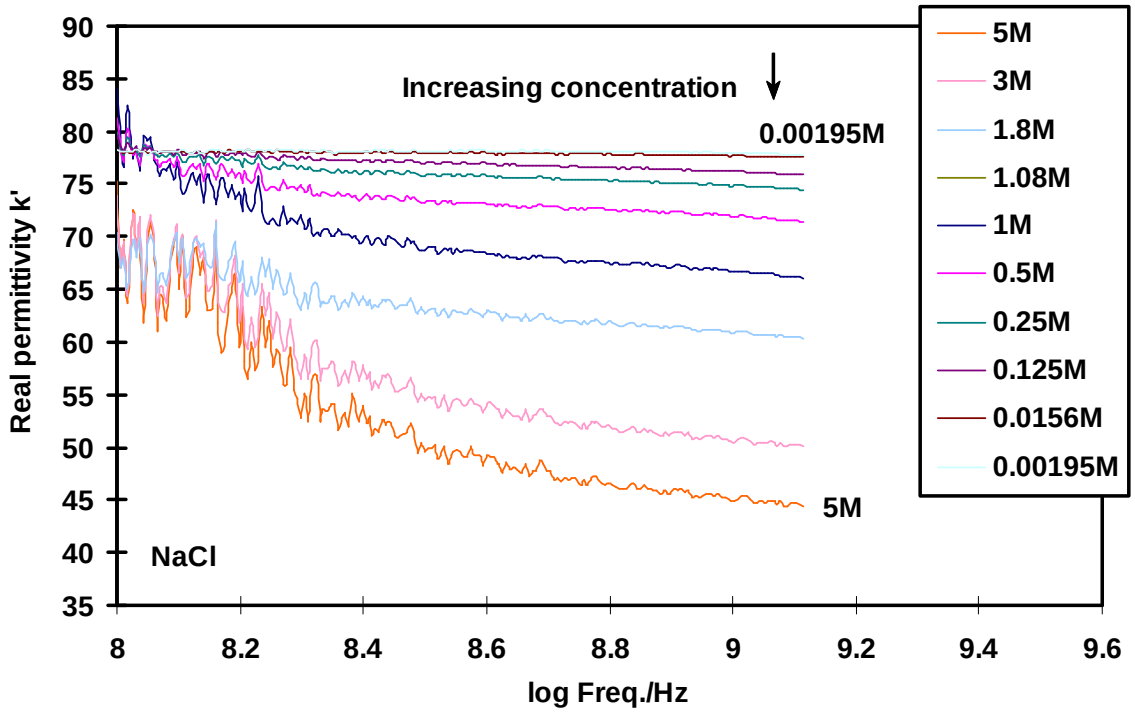

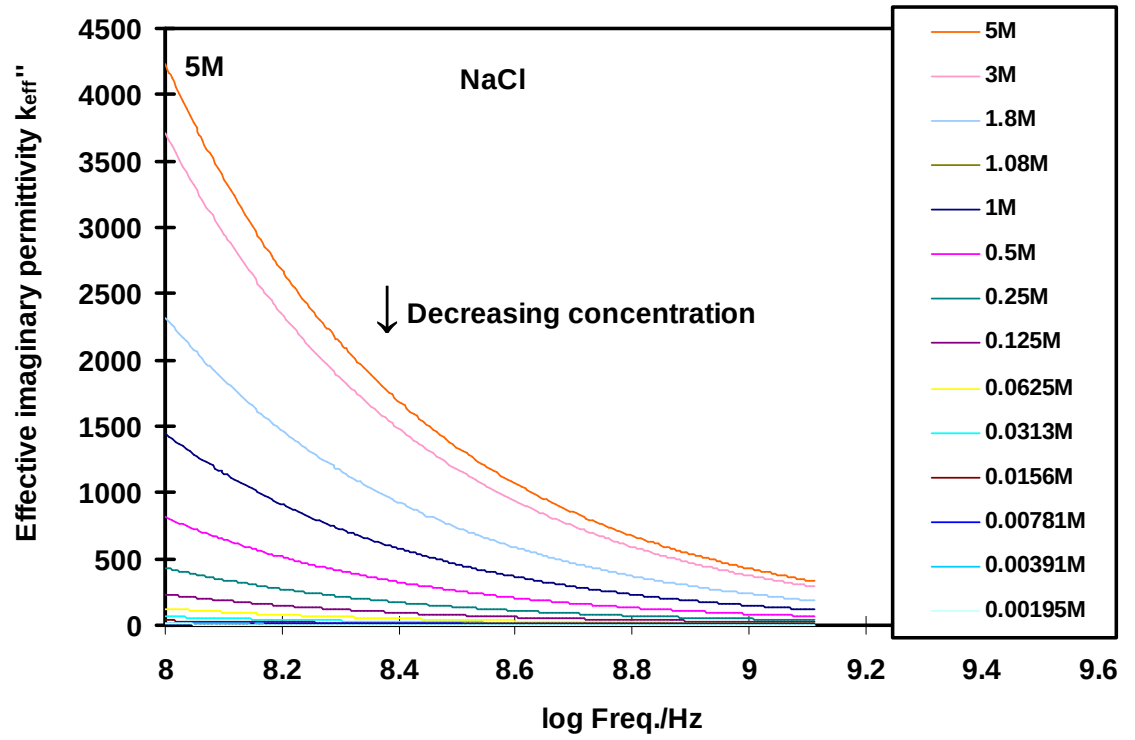

Figure 3-3. Real and effective imaginary permittivity of NaCl solutions.

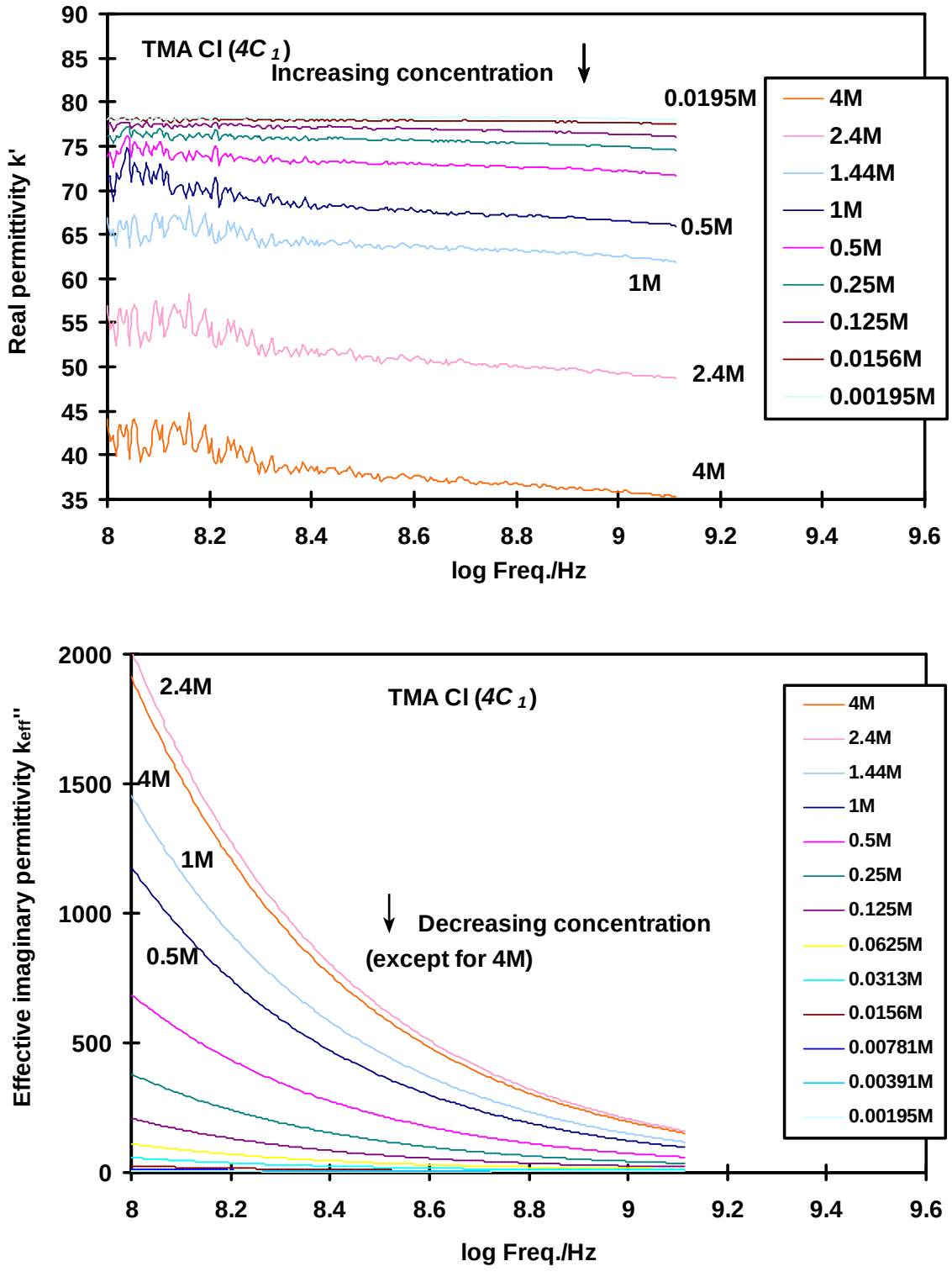

Figure 3-4. Real and effective imaginary permittivity of TMA Cl solutions.

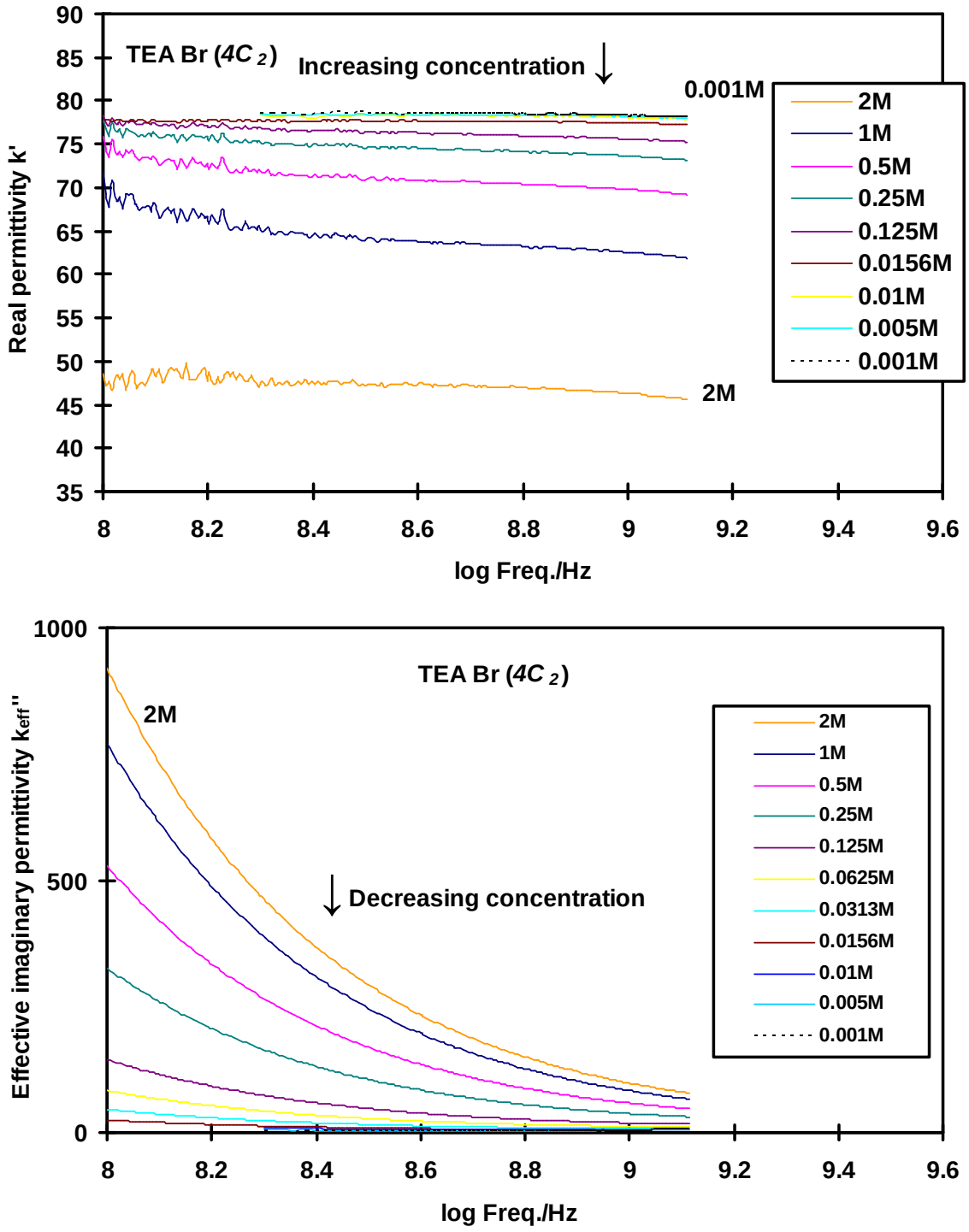

Figure 3-5. Real and effective imaginary permittivity of TEA Cl solutions.

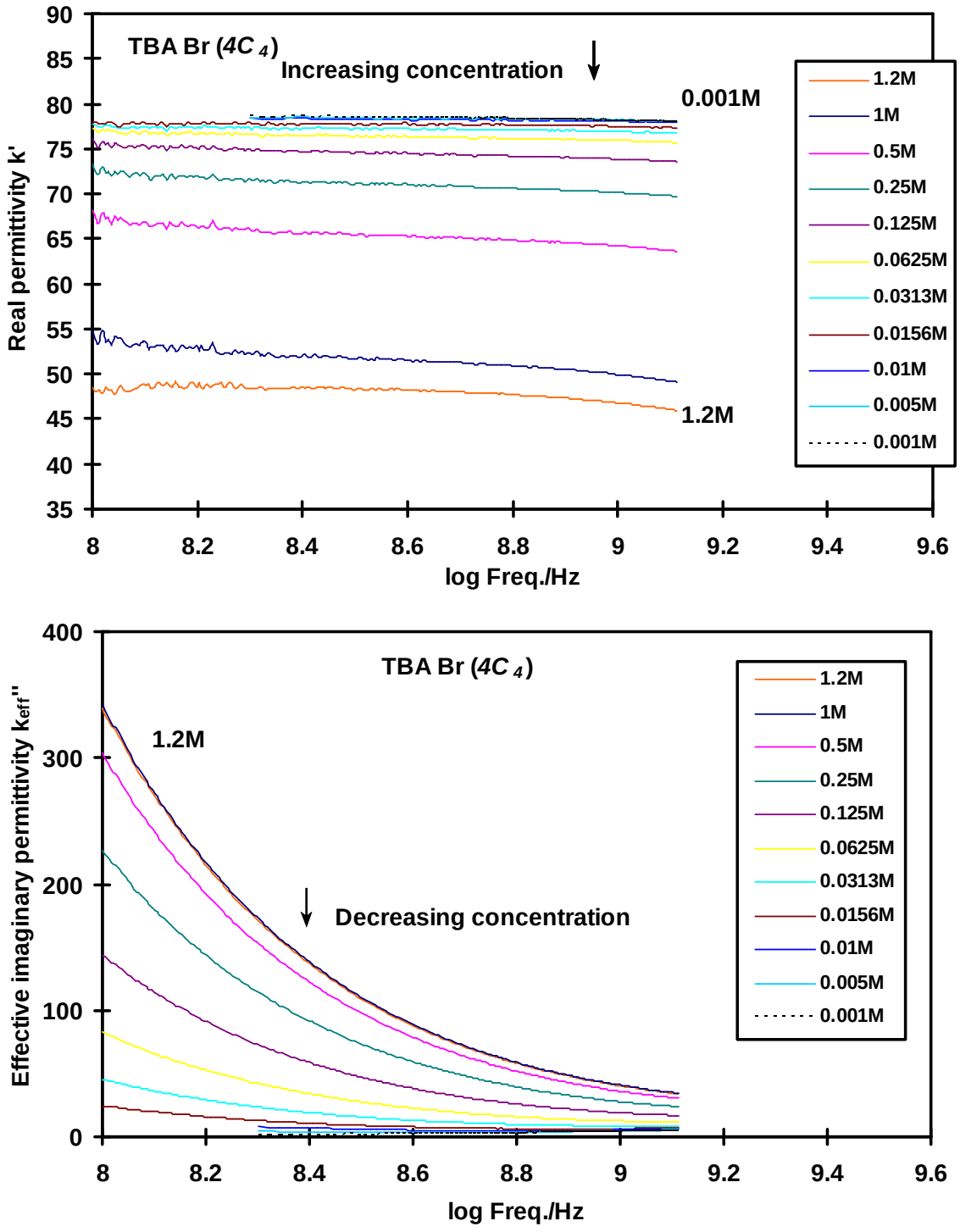

Figure 3-6. Real and effective imaginary permittivity of TBA Cl solutions.

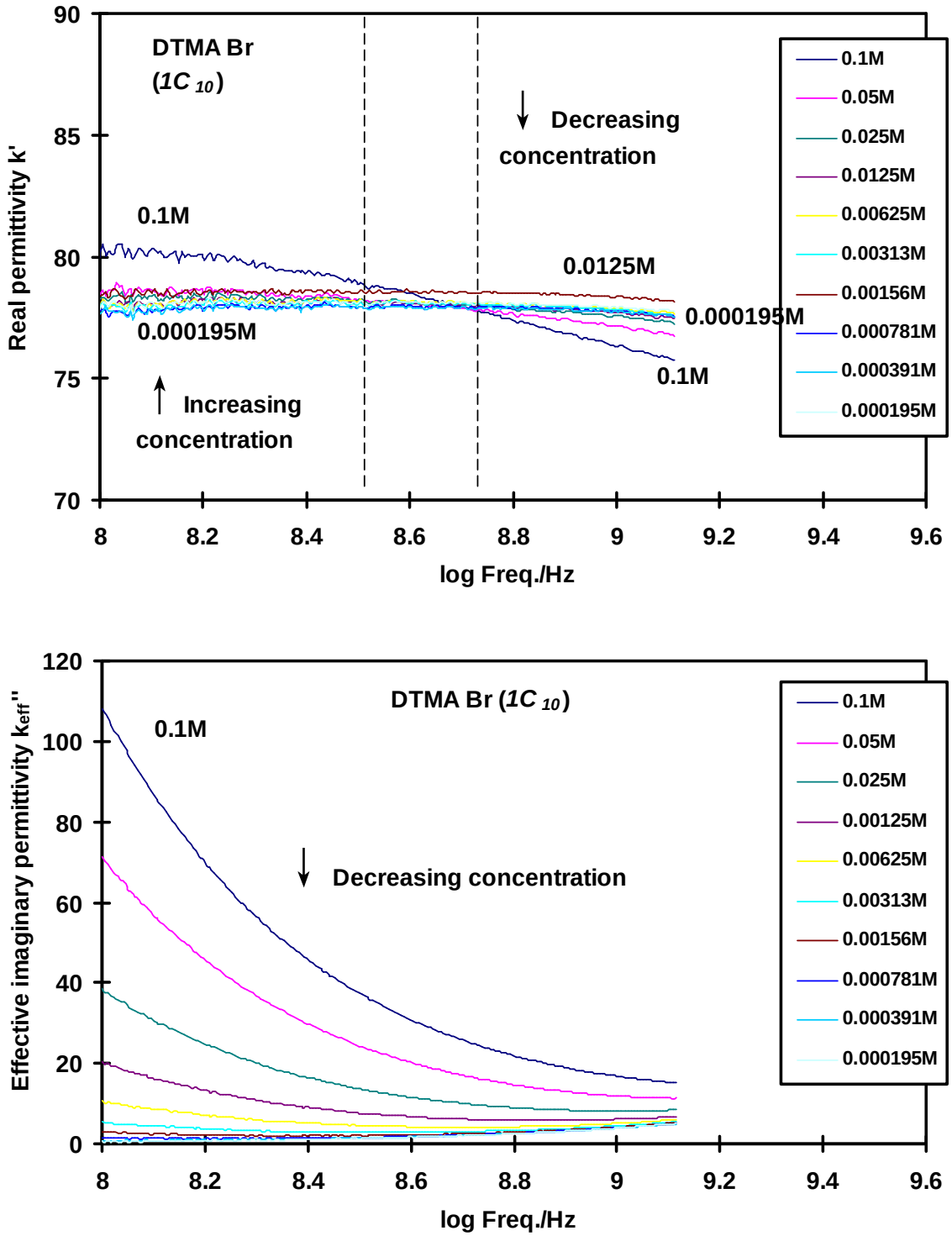

Figure 3-7. Real and effective imaginary permittivity of DTMA Cl solutions.

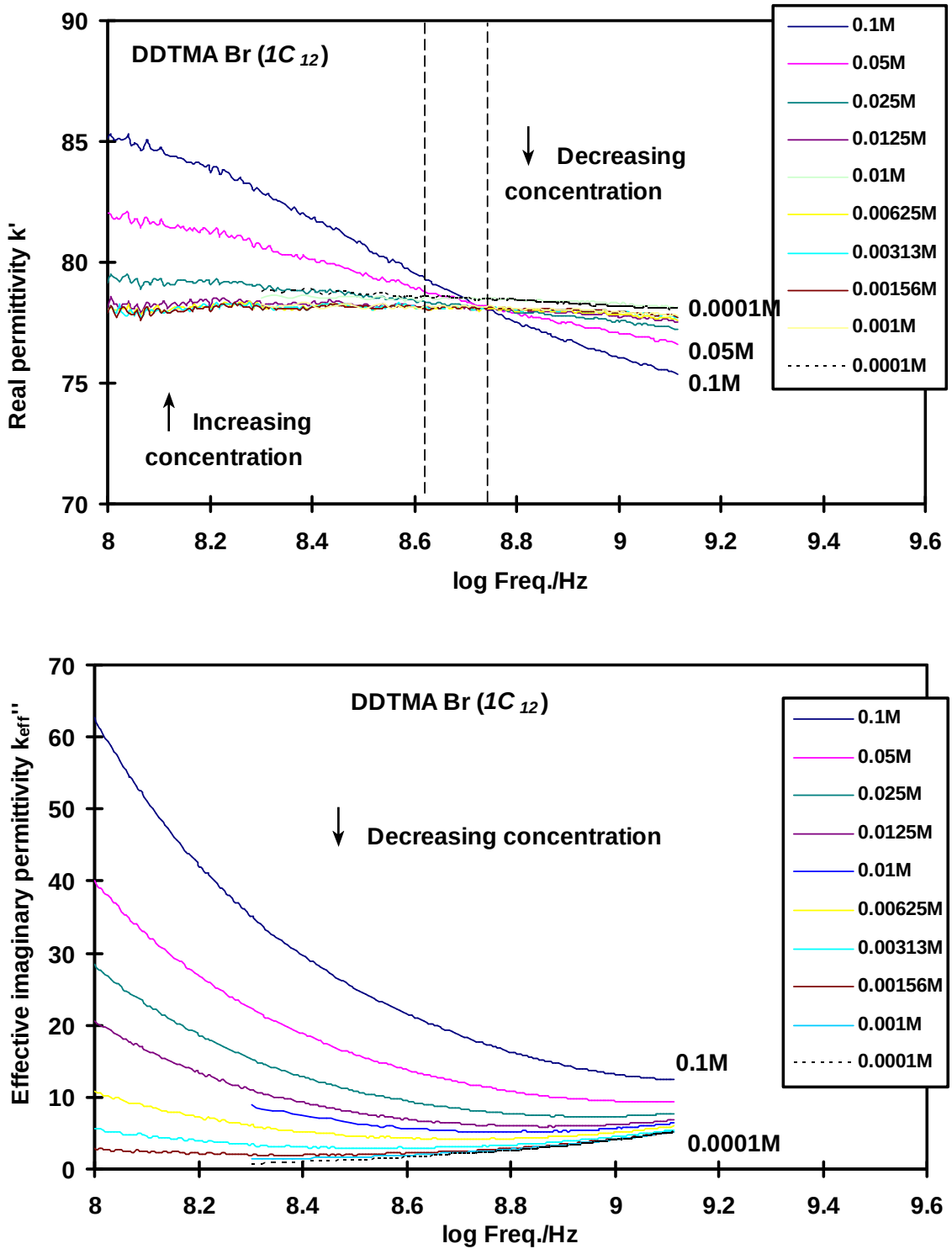

Figure 3-8. Real and effective imaginary permittivity of DDTMA Cl solutions.

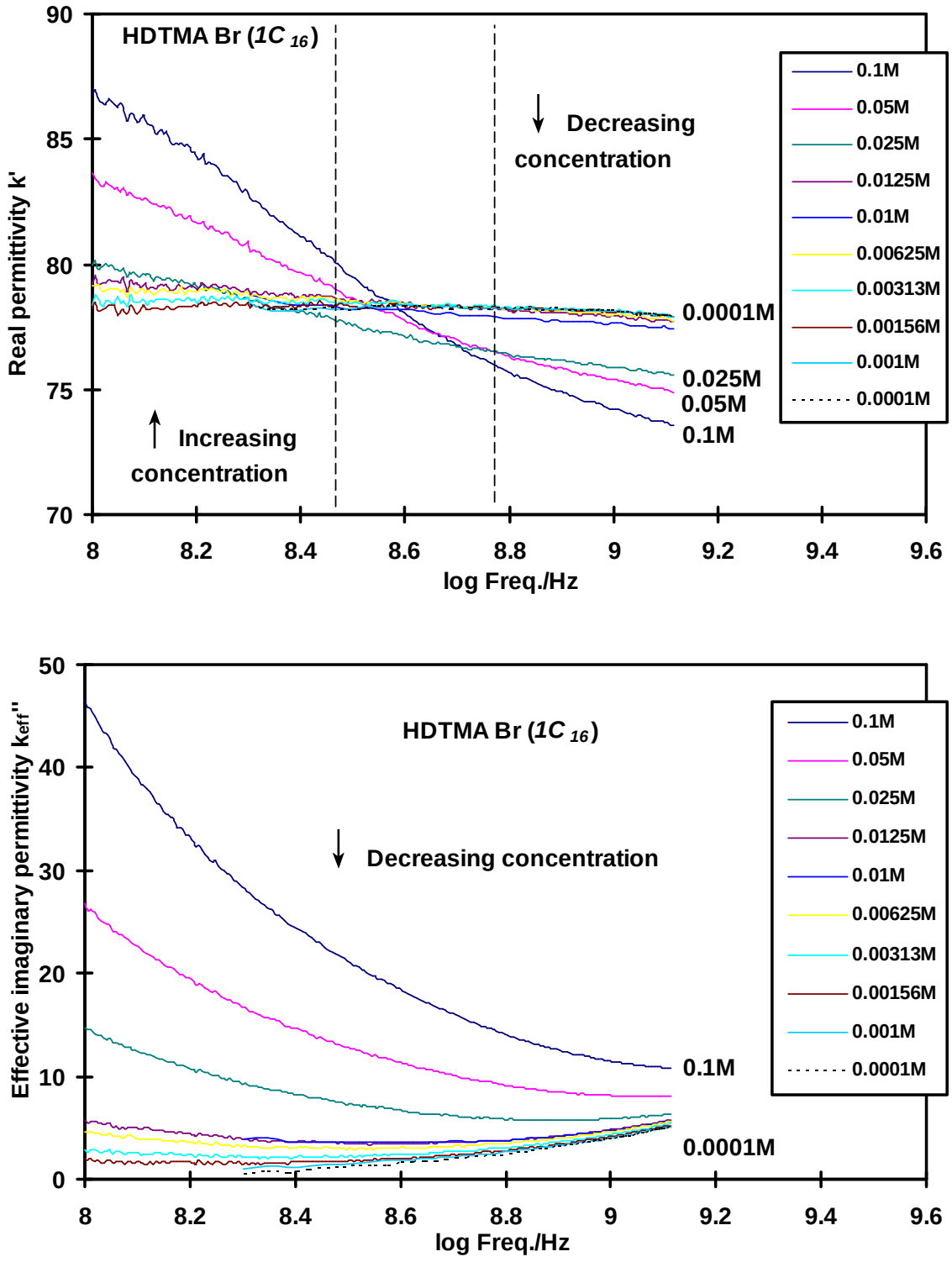

Figure 3-9. Real and effective imaginary permittivity of HDTMA Cl solutions.

The effective conductivities, σ_{eff}'' (measured at the same frequency (1.3 GHz)) of NaCl, TMA Cl, TEA Br, TBA Br, DTMA Br, DDTMA Br, and HDTMA Br presented that σ_{eff}'' for each solution was higher than its corresponding DC (zero frequency) conductivity (Figure 3-10). The orientational polarization of free water, κ'', contributed to the differences, which was more significant at low concentrations. At concentrations lower than 0.01 M, σ_{eff}'' for all the tested solutions was approximately the same, and equaled to that of deionized water (approximately 3700 uS/cm). The DC conductivity contribution to σ_{eff}'' was secondary comparing to κ''. At higher concentrations (> 0.01 M), for different electrolyte solutions, the higher the corresponding DC conductivity, the higher the σ_{eff}'' values. That is, as the size, or the length of the long C-chain, of organic cations increased, the DC conductivity decreased, and σ_{eff}'' decreased. It seems that DC conductivity played a more important role than κ''.

To further examine its weight in overall effective permittivity, κ'' was calculated as the difference between σ_{eff}'' and σ (Equation 3-13) (Figure 3-11). It was observed that at concentrations lower than 0.01 M, κ'' was almost identical for every salt solutions, at approximately 5. No bias towards the size or the length of long C-chain increment was observed. At higher concentrations, κ'' ranged from 3 to 8. The variation of κ'' could be the results of the limited precision of DC conductivity measurement at high concentrations. Nonetheless, at concentrations higher than 0.01M, κ'' values were less significant than the DC conduction-induced permittivities, which were normally 2 or 3 orders of magnitude larger (Figure 3-3 through Figure 3-9). Therefore κ'' was only

important at low concentration (< 0.01 M) and at high frequency excitation, where DC conduction loss – induced polarization was minimum.

Real permittivities of NaCl, TMA Cl, TEA Br, TBA Br, DTMA Br, DDTMA Br, and HDTMA Br solutions decreased as concentration increased (Figure 3-12 κ' versus concentration plots at 1.3 GHz excitement), which held true at all frequencies from 0.1 to 1.3 GHz in most cases. Real permittivity decreased because the mobility of water molecules involved in hydrating ions was decreased due to the increased presence of electrolyte ions; however, there were exceptions: at frequencies lower than 0.6 GHz, organic cations with a long C-chain (DTMA, DDTMA, and HDTMA) and concentration higher than approximately 0.02 M, higher concentration led to an increased real permittivity value. The values of real relative permittivities at these conditions were even higher than that of deionized water (~78); consequently, polarization of water molecules alone was not enough to generate such high values of real permittivities. It is postulated that the orientational relaxation mechanism prevailed at the frequency range from 0.1 to about 0.6 GHz due to the presence of micelles, which would occur at high concentration solutions of organic cations with a long C-chain (DTMA, DDTMA, and HDTMA). The relation between micelles and the relaxation mechanism was not clear.

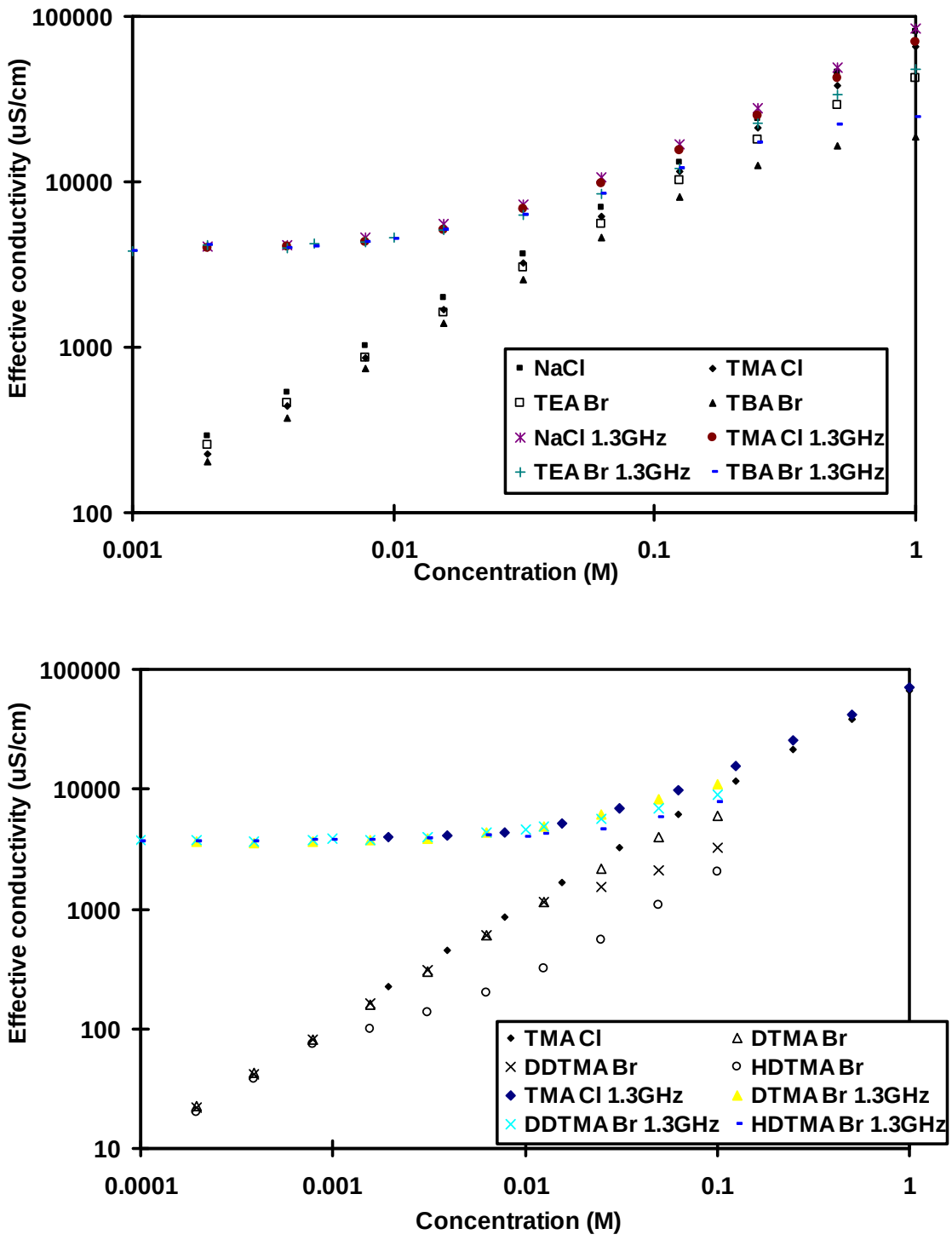

Figure 3-10. Effective conductiviy of organic cations as a function of concentration: a) branch effect; b) tail effect

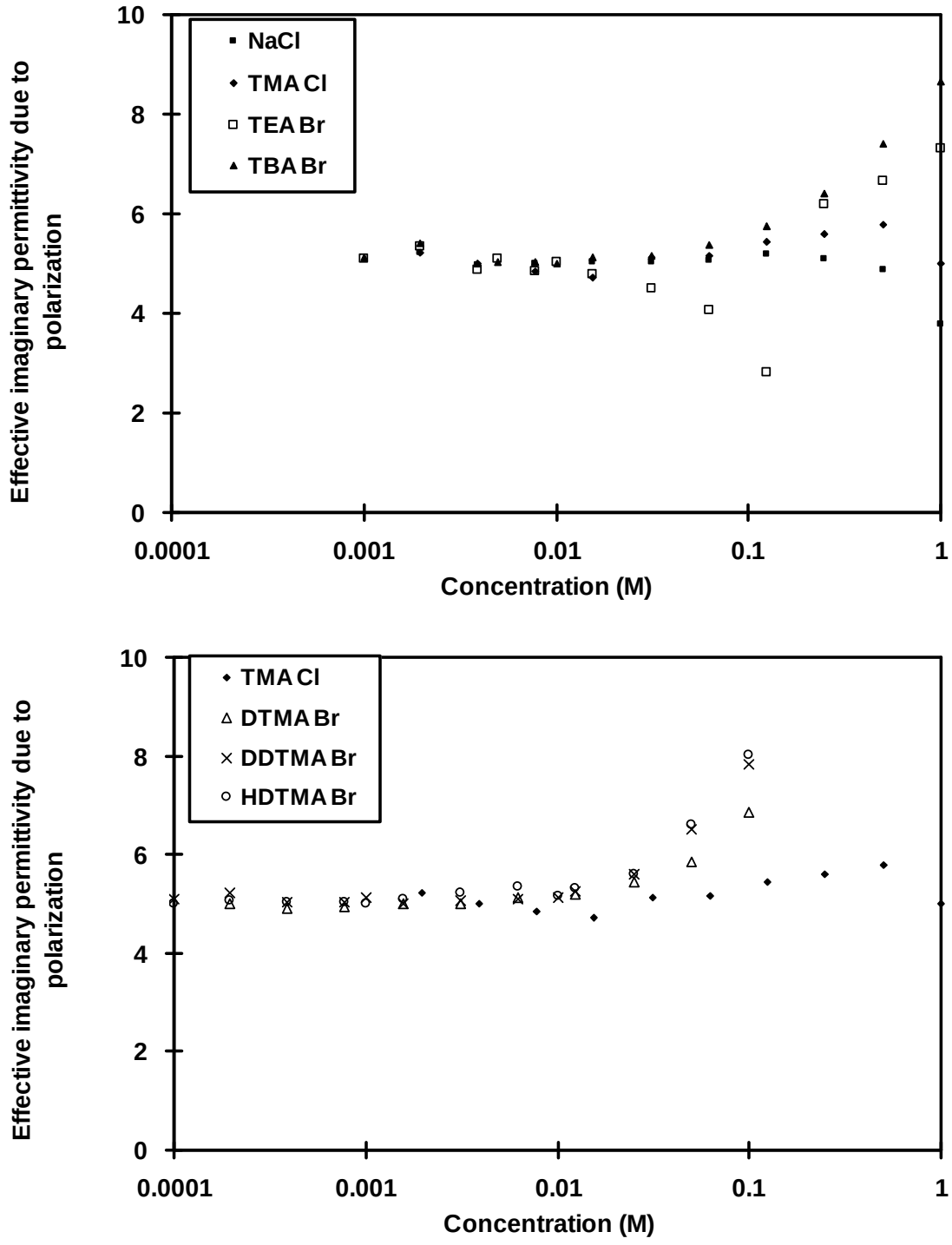

Figure 3-11. Effective imaginary permittivity due to polarization as a function of concentration: 1) branch effect; b) tail effect.

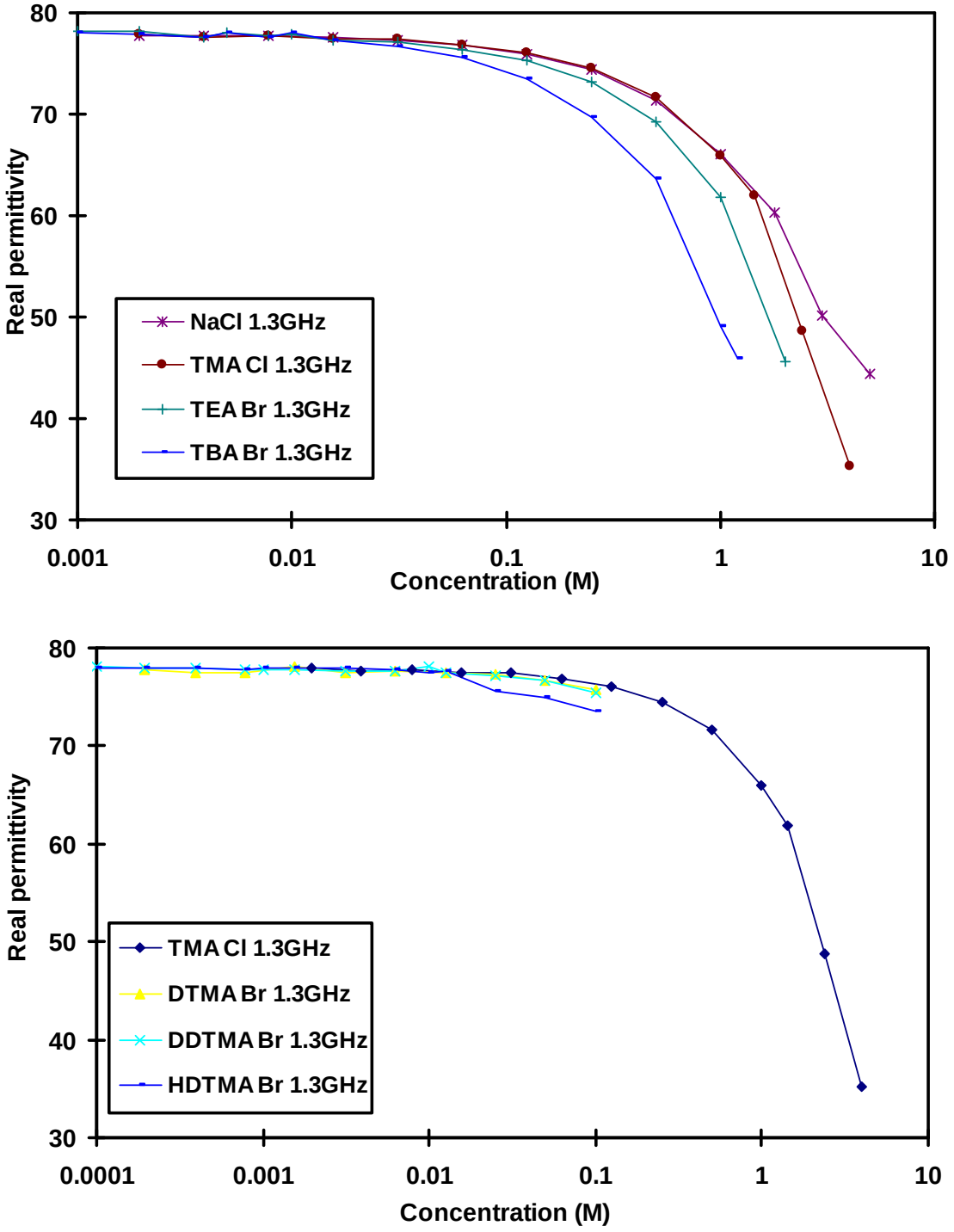

Figure 3-12. Real permittivity as a function of concentration: a) branch effect; b) tail length effect.

The real and imaginary permittivity of 9 organobentonites, i.e. 30TMA, 60TMA, 100TMA, 100TEA, 100TBA, 100DTMA, 30HDTMA, 60HDTMA, and 100HDTMA bentonites, at frequency ranges of 0.2 GHz to 1.3 GHz were also determined (Figure 3-13 through Figure 3-21). Observations on the measured permittivity of the organoclays were: (1) As water content increased, real permittivity increased. The real permittivity of wet soil at microwave frequencies is determined by the polarizability of the free water (Santamarina et al., 2001), therefore κ' of wet organobentonites increased continuously with water content. On the other hand, water content increase led to the effective permittivity decrease in most scenarios (except for those where orientational polarization relaxation occurred – discussed later). (2) As frequency increased, due to the orientational polarization of free water, the real permittivity decreased, and effective permittivity increased.

Permittivity and conductivity depended on the volume fraction of pore fluid and soil phase. Archie's law (Archie, 1942) captured this relationship. The simple form of Archie's law can be expressed as (Santamarina et al., 2001):

$$\kappa^* = \kappa^*_{fluid} \cdot n \qquad \textbf{Equation 3-14}$$

and

$$\sigma_{eff}'' = \sigma_{fluid}'' \cdot n \qquad \textbf{Equation 3-15}$$

where n is porosity, κ^*_{fluid} is the complex permittivity of the pore fluid, and σ_{fluid}'' is the effective conductivity of the pore fluid. A linear relationship between κ' and porosity was obtained due to κ' is relatively unchanged as the water was added to the suspensions [Figure 3-22(a)]. However, in the method of this study de-ionized water was added to the soil suspension, which changed σ_{fluid}''. Therefore the trend between σ_{eff}'' and porosity

was not specified [Figure 3-22(b)]. To characterize the relationship between σ_{eff}'' and volume properties, Equation 3-15 was rewritten as

$$\sigma_{eff}'' = \frac{\mathrm{C}\cdot \text{number of charges in pore fluid}}{\mathrm{V}_{\text{fluid}}} \cdot \frac{\frac{\rho_{\text{fluid}}\mathrm{V}_{\text{fluid}}}{\mathrm{M}_{\text{soil}}}}{\omega + \frac{1}{G_s}}$$

$$= \frac{\mathrm{C}\cdot \text{number of charges in pore fluid} \cdot \frac{\rho_{\text{fluid}}}{\mathrm{M}_{\text{soil}}}}{\omega + \frac{1}{G_s}} \qquad \textbf{Equation 3-16}$$

$$= \frac{C_2}{\omega + \frac{1}{G_s}}$$

where C is a constant relating pore fluid concentration to conductivity at diluted condition, V is volume, subscripts fluid and soil is for the pore fluid and soil in the suspension, ρ_{fluid} is the density of pore fluid, M_{soil} is the mass of soil in the suspension, and $\mathrm{G_s}$ is the specific gravity of the soil. C, number of charges in pore fluid, ρ_{fluid}, and M_{soil} were constants, the product of which can be represented by a new constant, C_2. Therefore from Equation 3-16 we found that there was a simple hyperbolic relation between water content and effective conductivity. In the following discussion water content was used to present the results of effective conductivity. Permittivity was also presented versus water content for consistency.

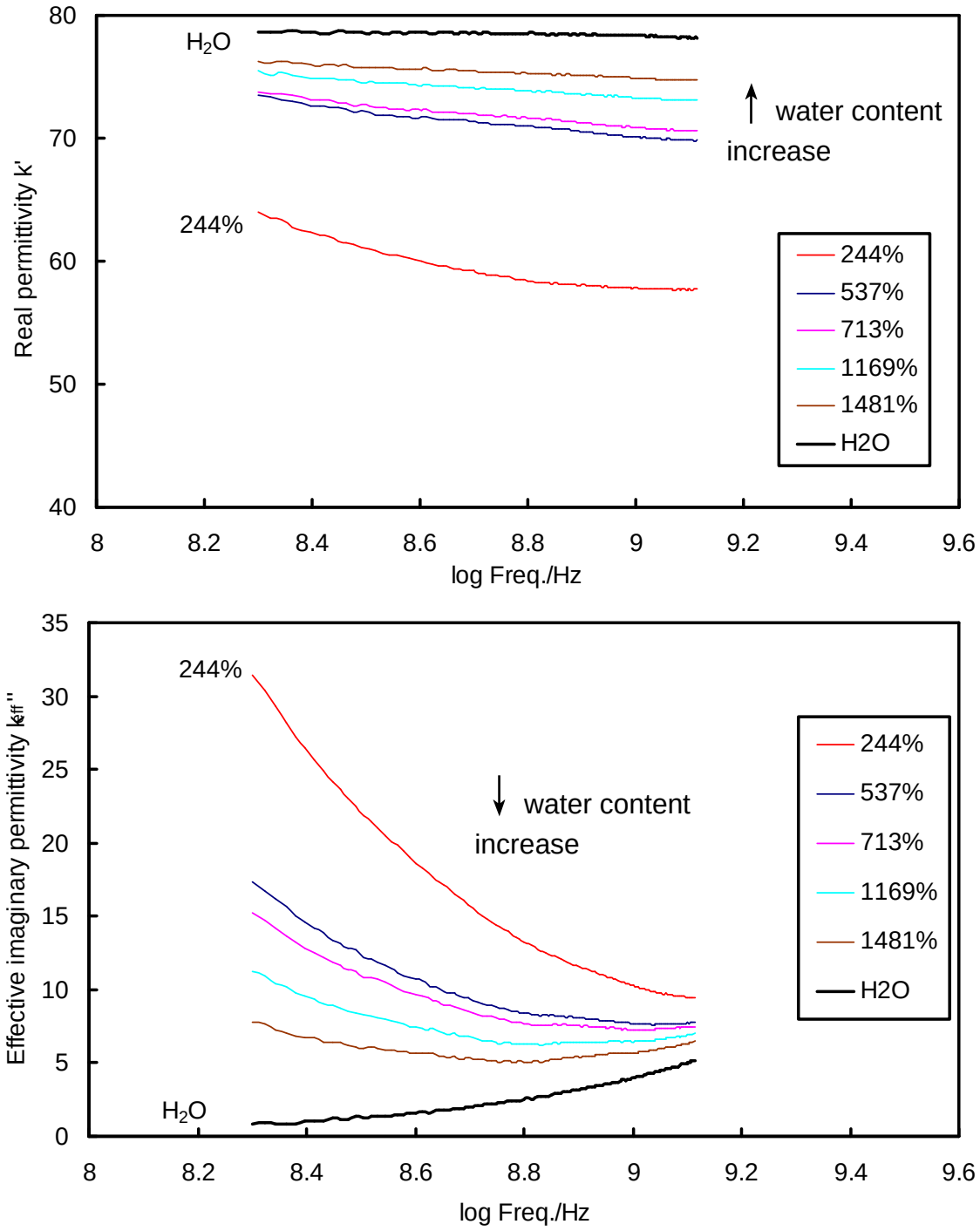

Figure 3-13. Real and effective imaginary permittivity of 30% TMA bentonite.

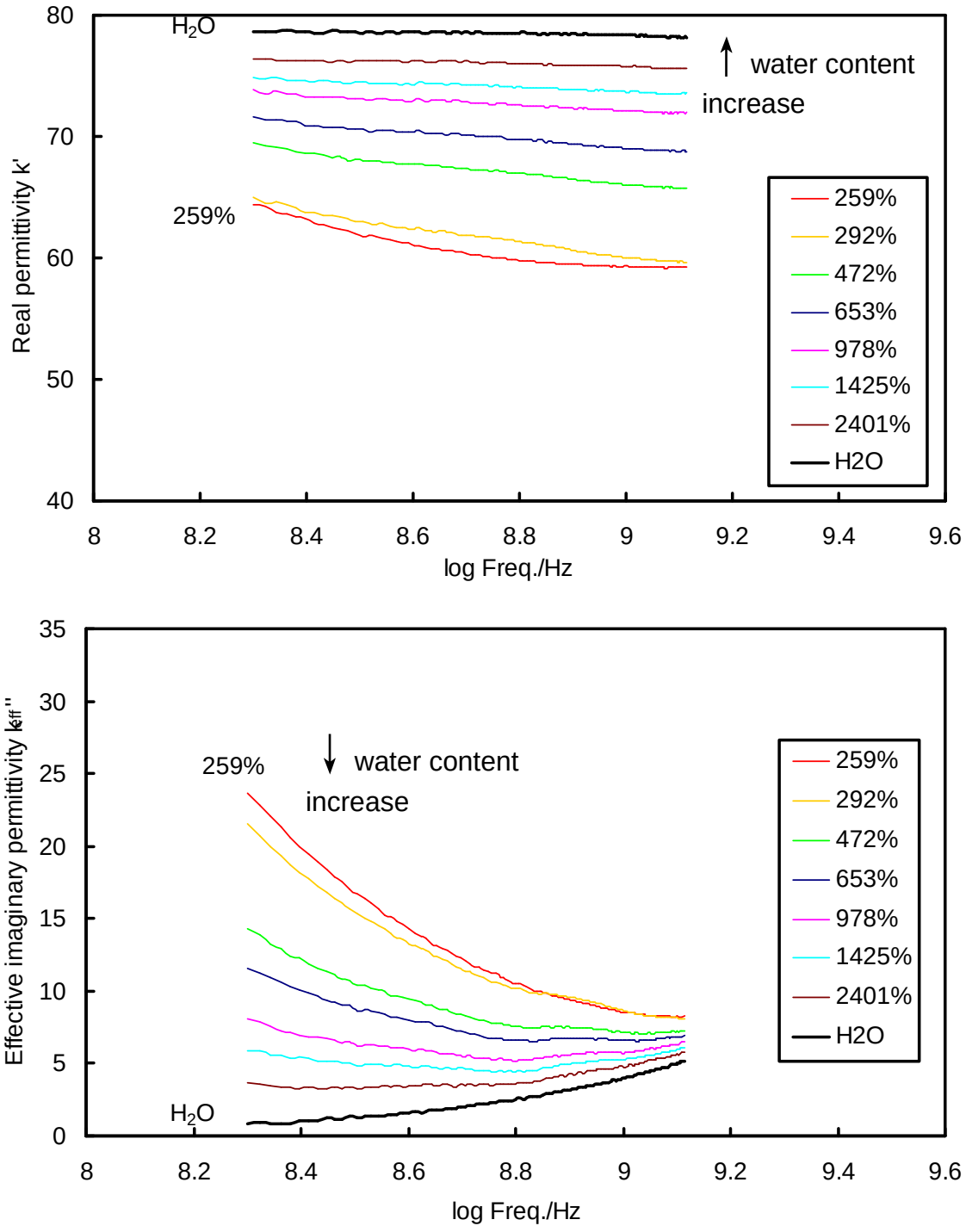

Figure 3-14. Real and effective imaginary permittivity of 60% TMA bentonite.

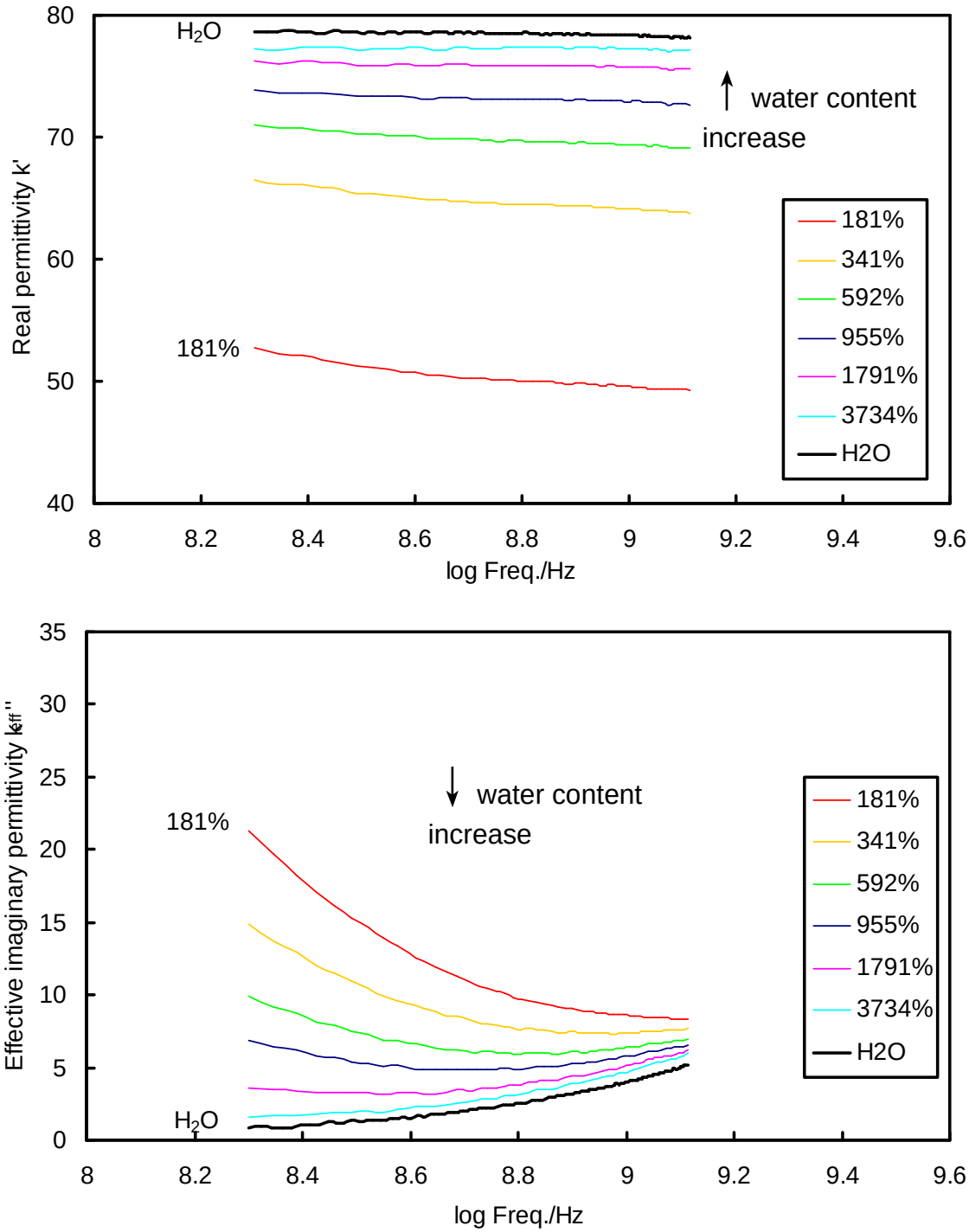

Figure 3-15. Real and effective imaginary permittivity of 100% TMA bentonite.

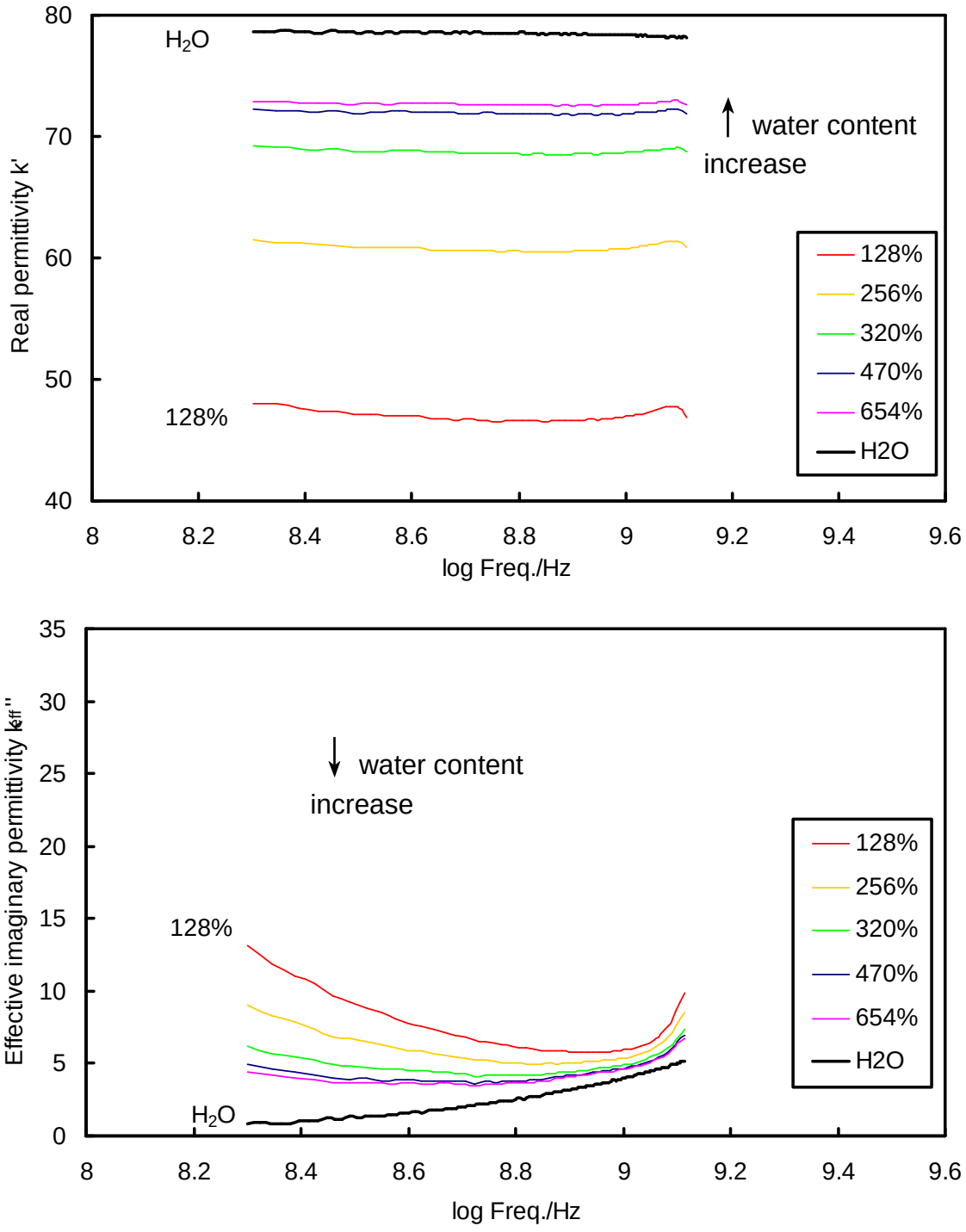

Figure 3-16. Real and effective imaginary permittivity of 100% TEA bentonite.

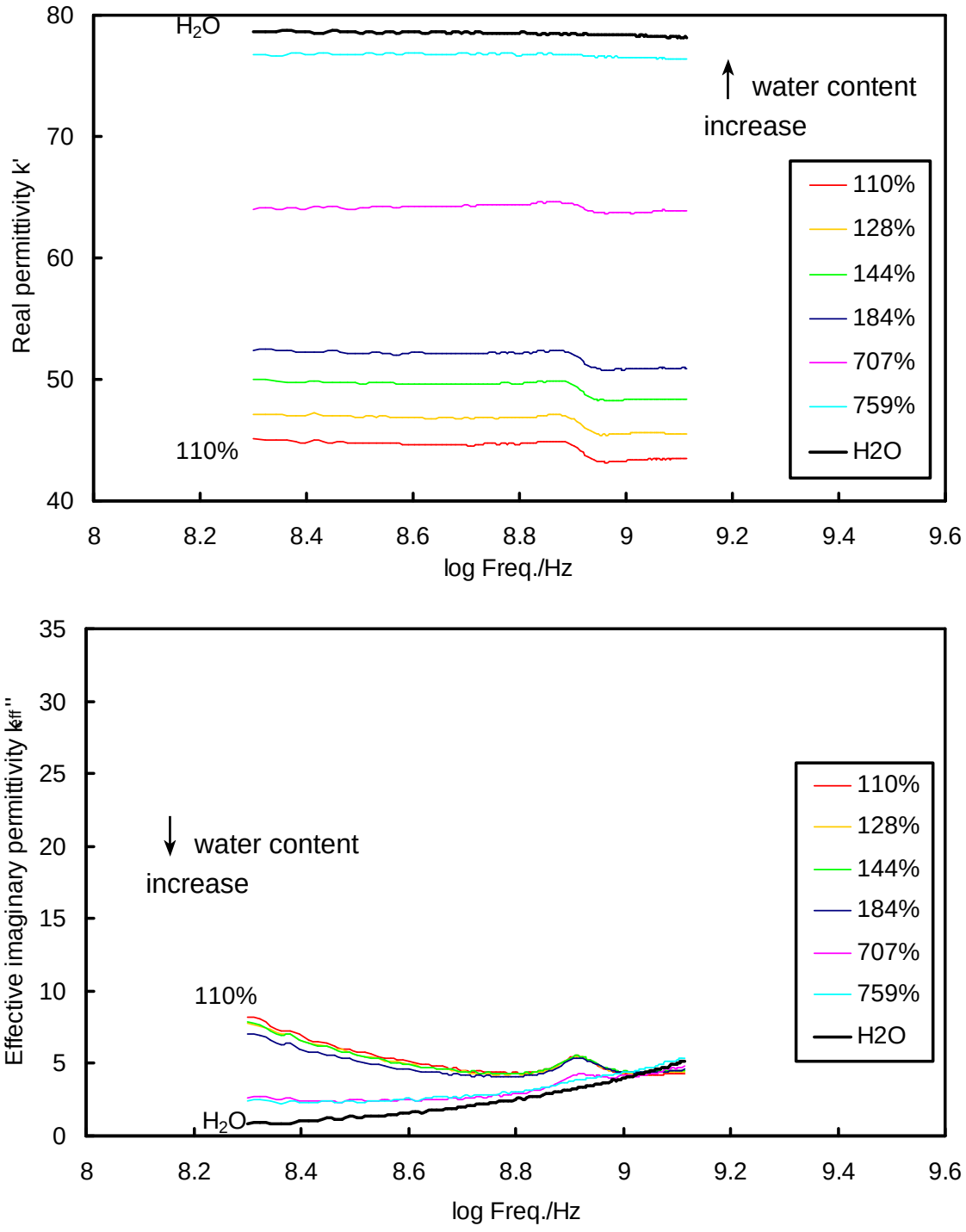

Figure 3-17. Real and effective imaginary permittivity of 100% TBA bentonite.

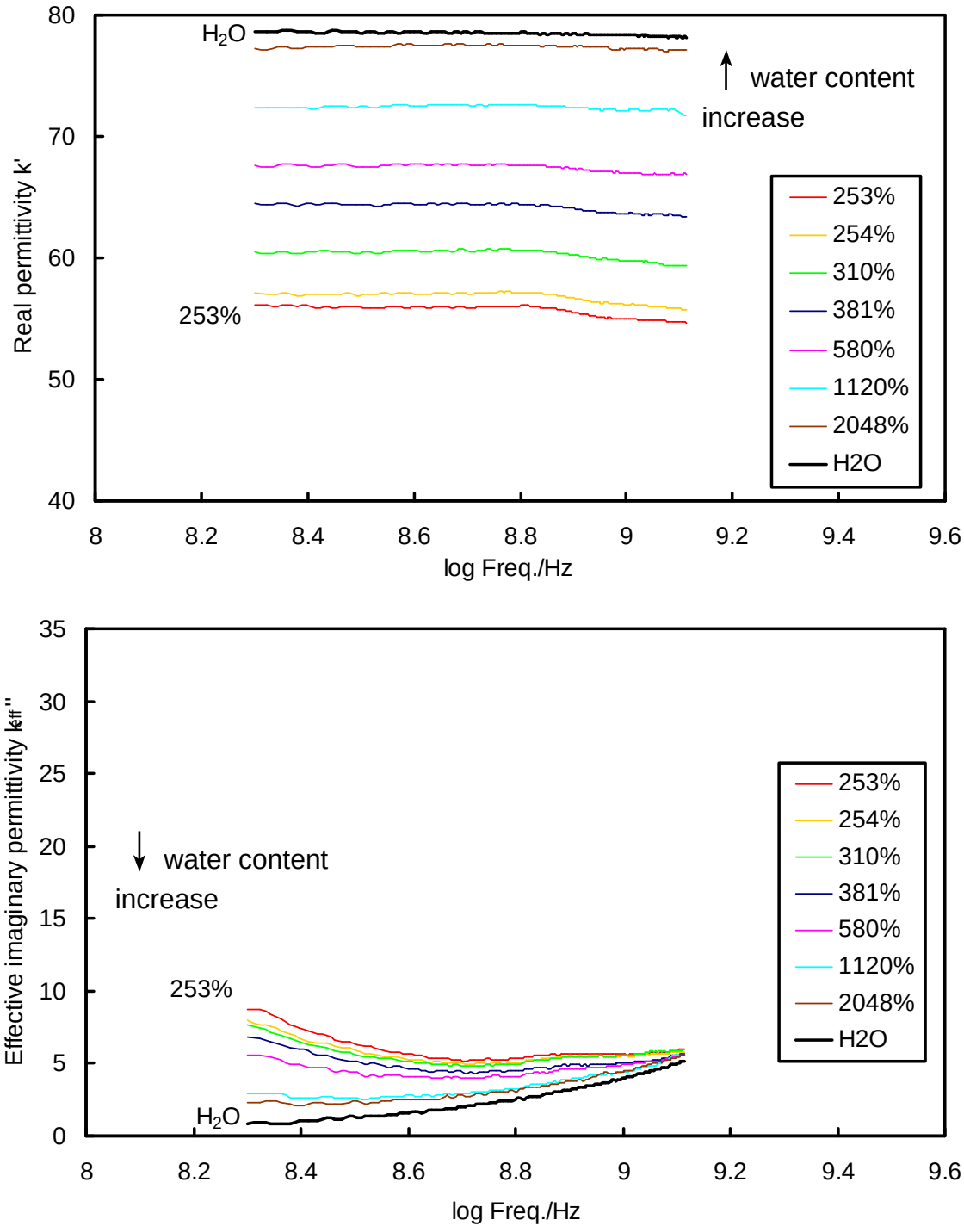

Figure 3-18. Real and effective imaginary permittivity of 100% DTMA bentonite.

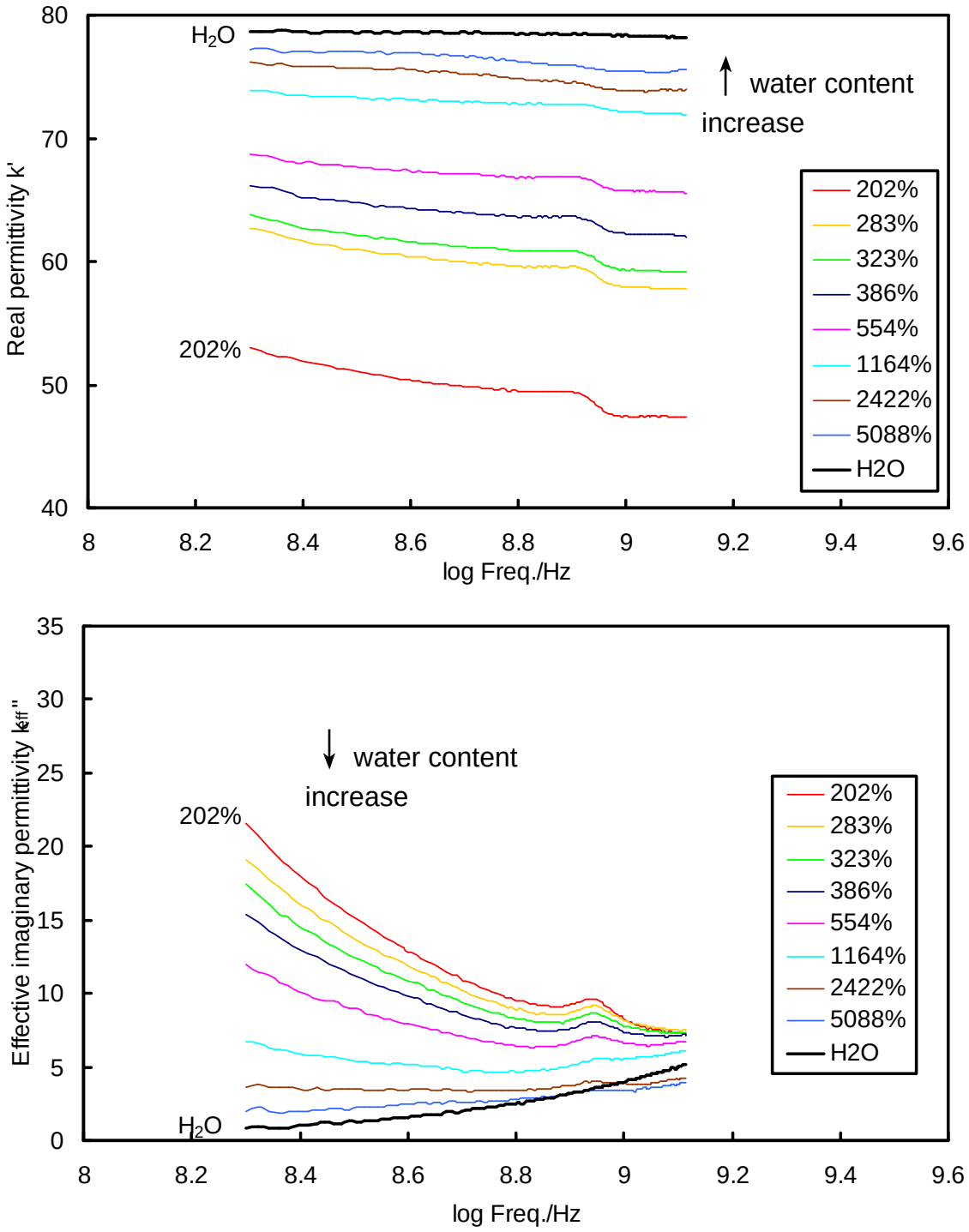

Figure 3-19. Real and effective imaginary permittivity of 30% HDTMA bentonite.

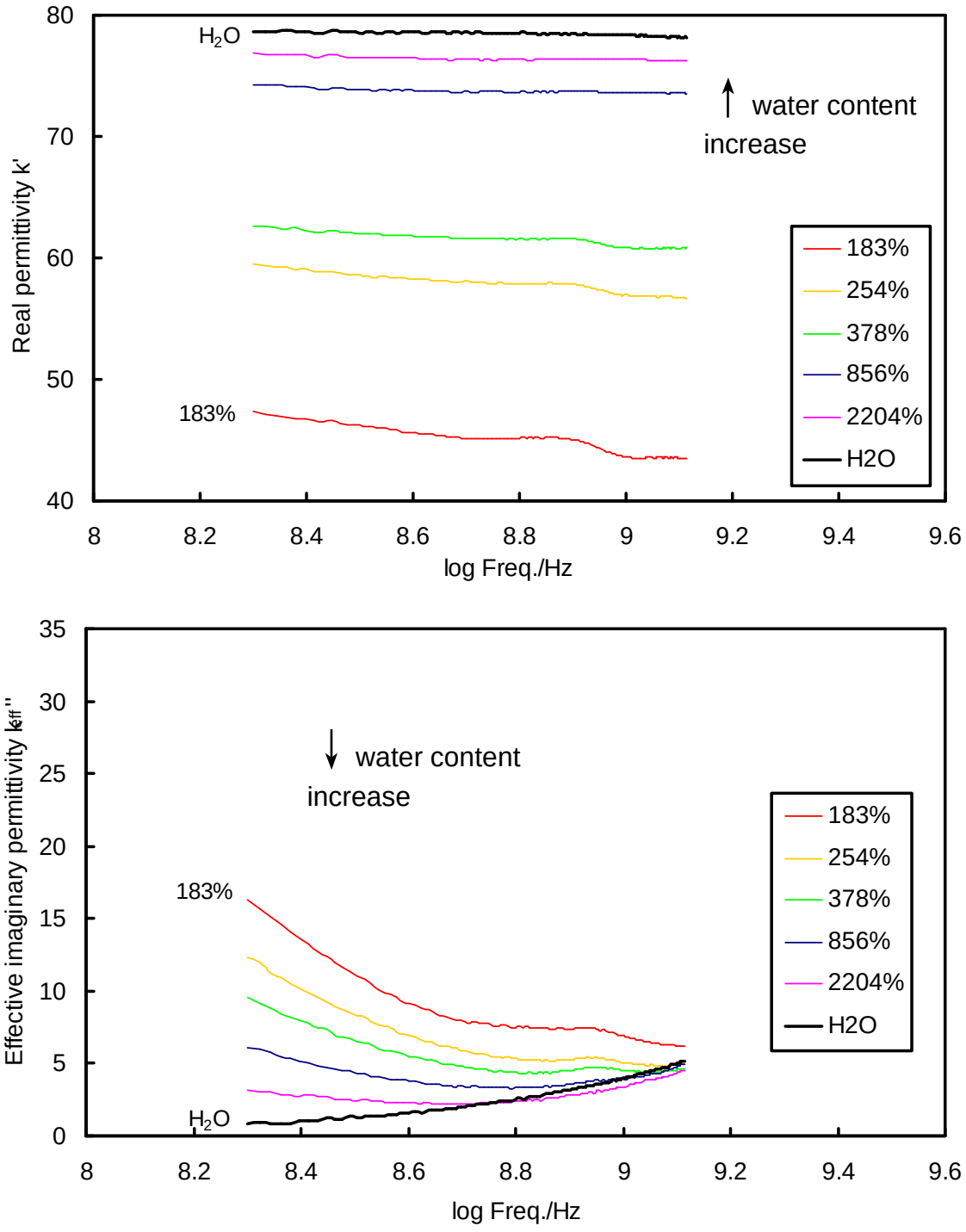

Figure 3-20. Real and effective imaginary permittivity of 60% HDTMA bentonite.

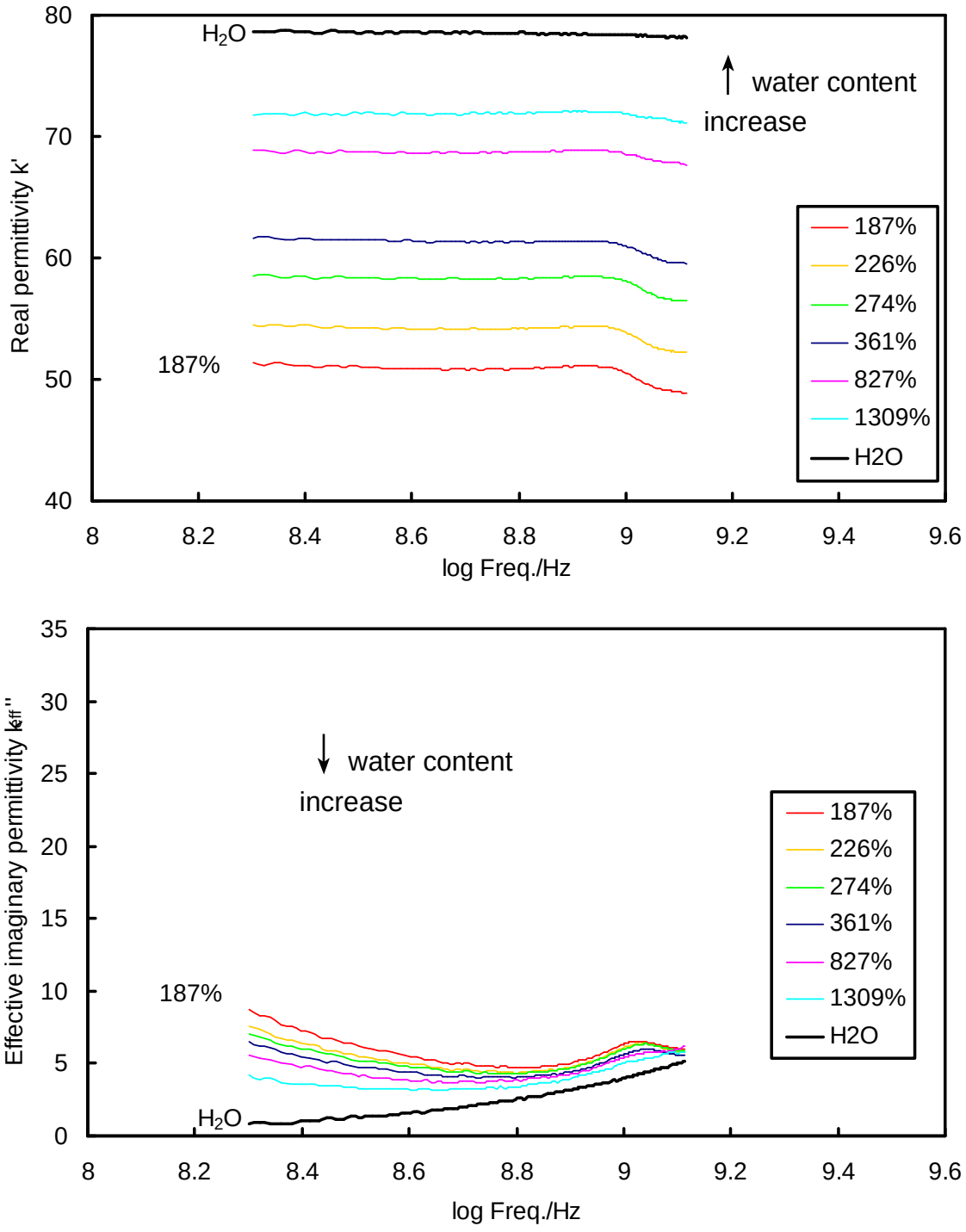

Figure 3-21. Real and effective imaginary permittivity of 100% HDTMA bentonite.

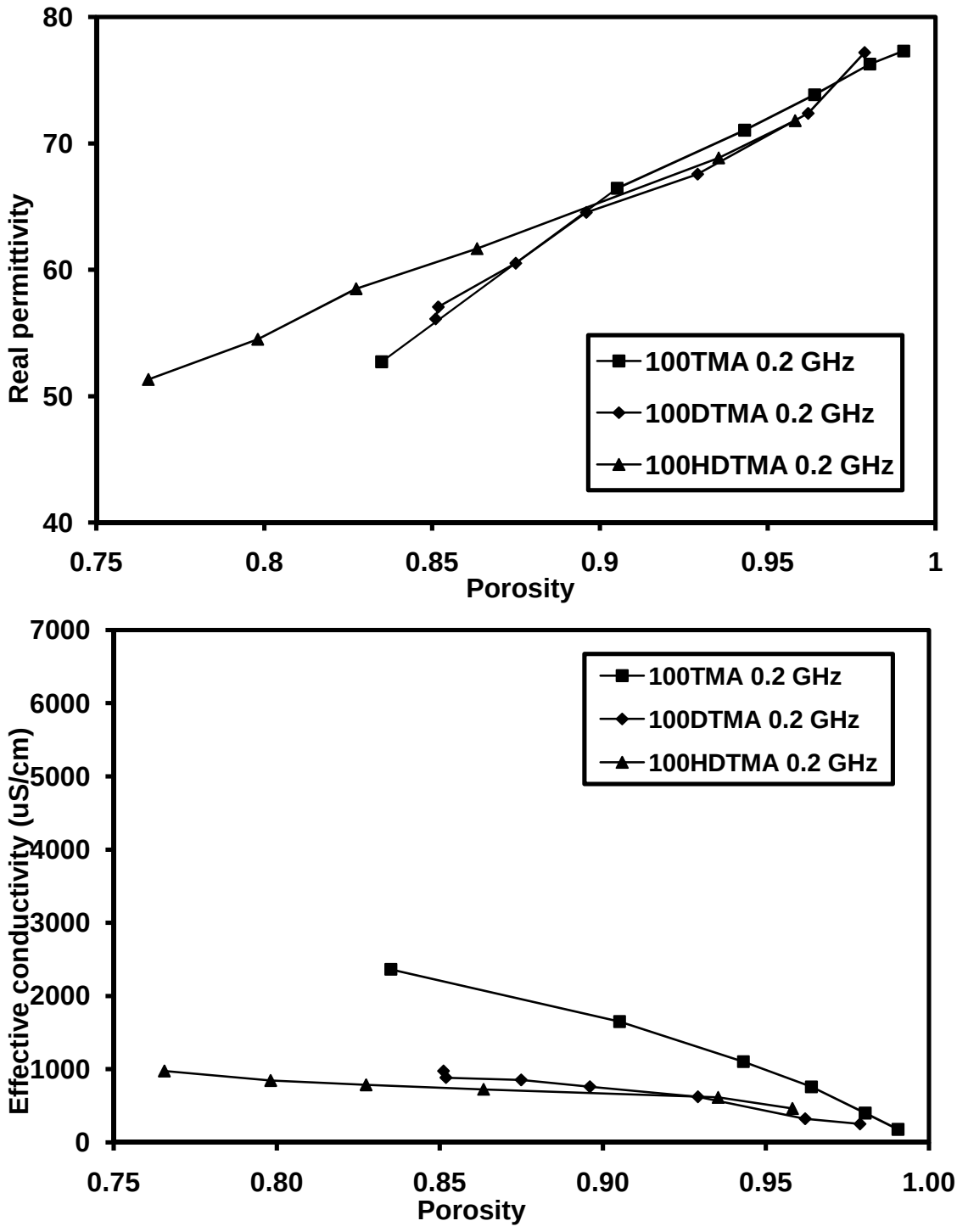

Figure 3-22 Real permittivity and effective conductivity of 100TMA, 100DTMA, and 100HDTMA bentonites versus porosity at 0.2 GHz.

As the size, or the length of four branches, of exchanged organic cations increased from 4C1 (TMA) to 4C2 (TEA) and 4C4 (TBA), the real relative permittivity showed some variation but no clear trend (Figure 3-23). However, as the length of single long C-chain of exchanged organic cations increased from 4C1 (TMA) to 1C10 (DTMA) and 1C16 (HDTMA), the real relative permittivity continuously decreased (Figure 3-24). As the organic loading of TMA cations increased from 30% to 60% and 100% of CEC of bentonite, real permittivity decreased with those of 60% and 100% TMA-bentonite displaying similar values (Figure 3-25). Similarly, as the organic loading of HDTMA cations increased from 30% to 60% and 100% of CEC of bentonite, real permittivity decreased but the values of 30% and 60% HDTMA-bentonite revealed cross over as a function of water content (Figure 3-26). Real relative permittivity showed some variations due to the change of size, length of long C-chain, and organic loading amount, but in general, as the total organic carbon content was increased, the real permittivity decreased, which was driven by the reduction in free water due to the presence of the hydrophobic organic phase on the clay surface. The higher specific surface areas observed at low total organic carbon content corresponded to a higher amount of bound water (Santamarina et al., 2001), which in turn represented a lower percentage of free water. Therefore the amount of free water decreased as the total organic carbon content was increased; the measured specific surface area correlated with the decrease in real relative permittivity values (Figure 2-11).

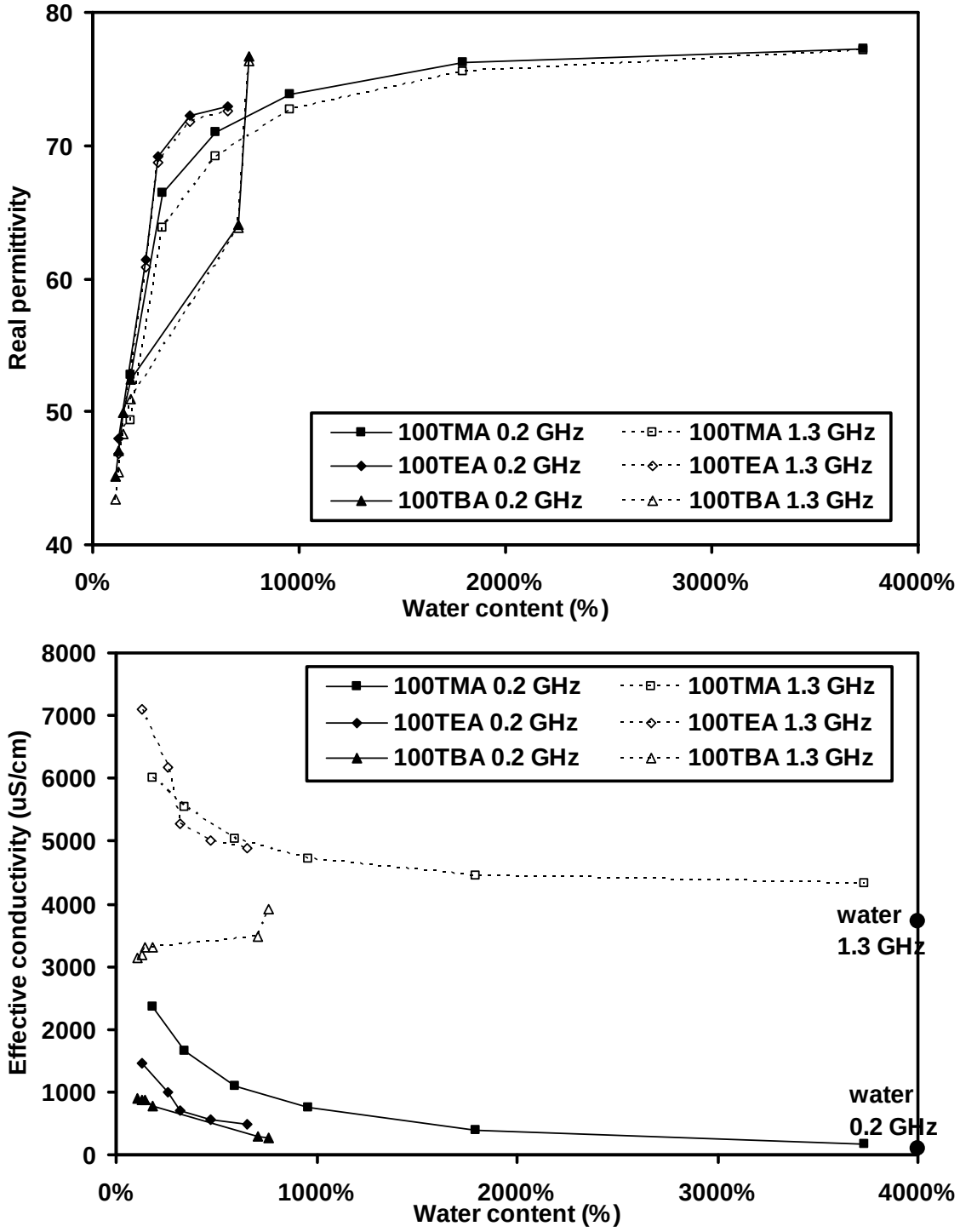

Figure 3-23. (a) Real permittivity and (b) effective conductivity of 100TMA, 100TEA, and 100TBA bentonite at 0.2 GHz and 1.3 GHz.

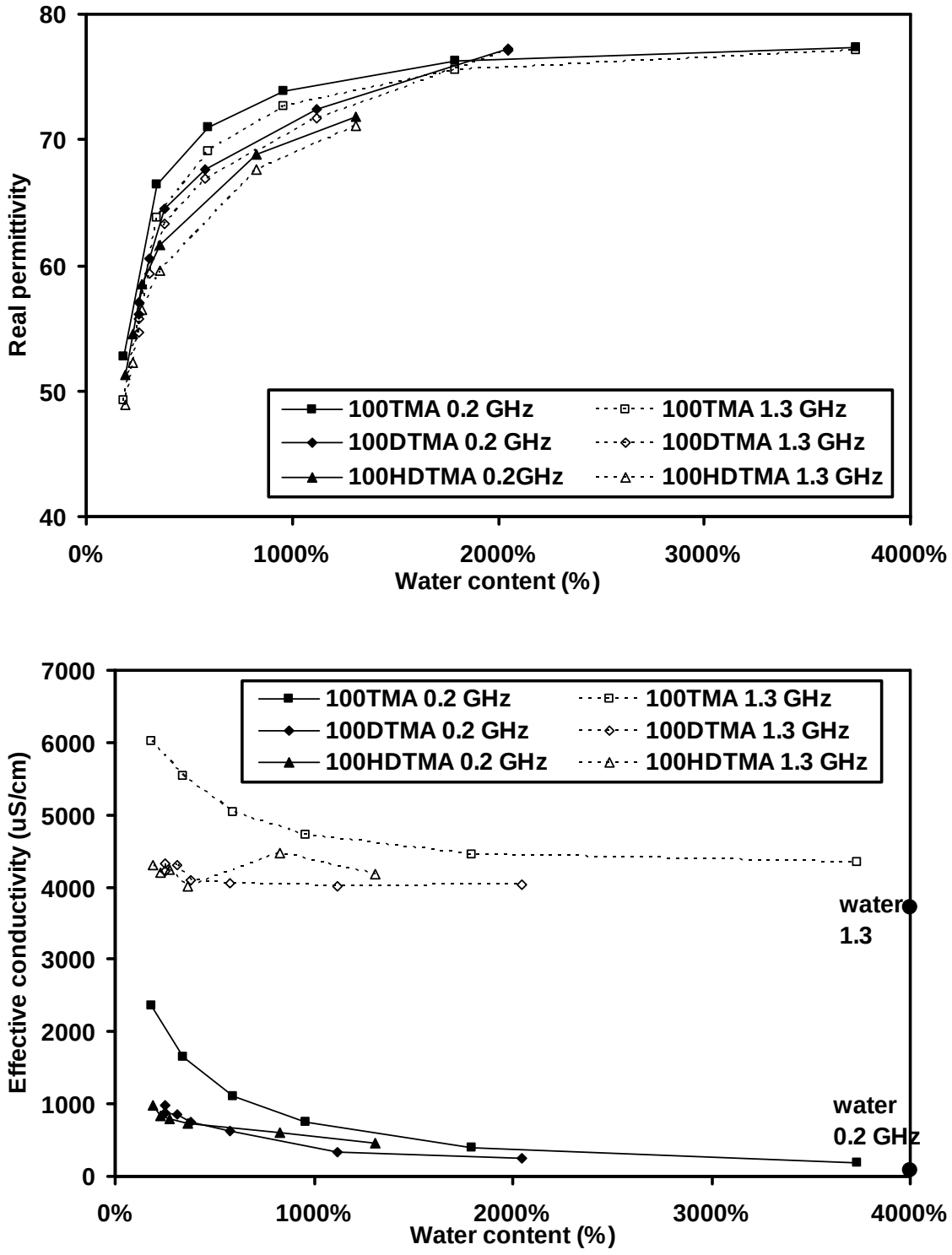

Figure 3-24. (a) Real permittivity and (b) effective conductivity of 100TMA, 100DTMA, and 100HDTMA bentonite at 0.2 GHz and 1.3 GHz.

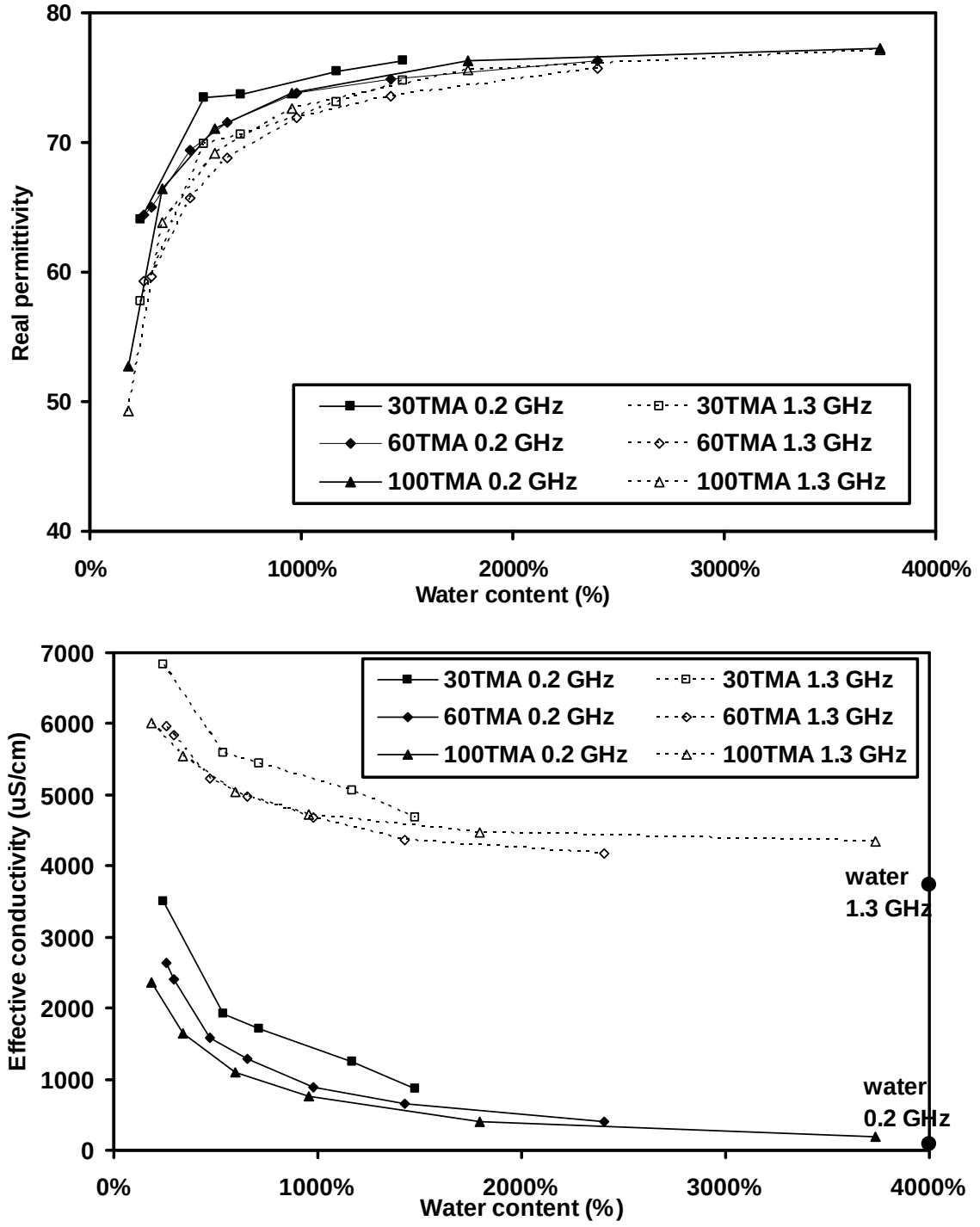

Figure 3-25. (a) Real permittivity and (b) effective conductivity of 30TMA, 60TMA, and 100TMA bentonite at 0.2 GHz and 1.3 GHz.

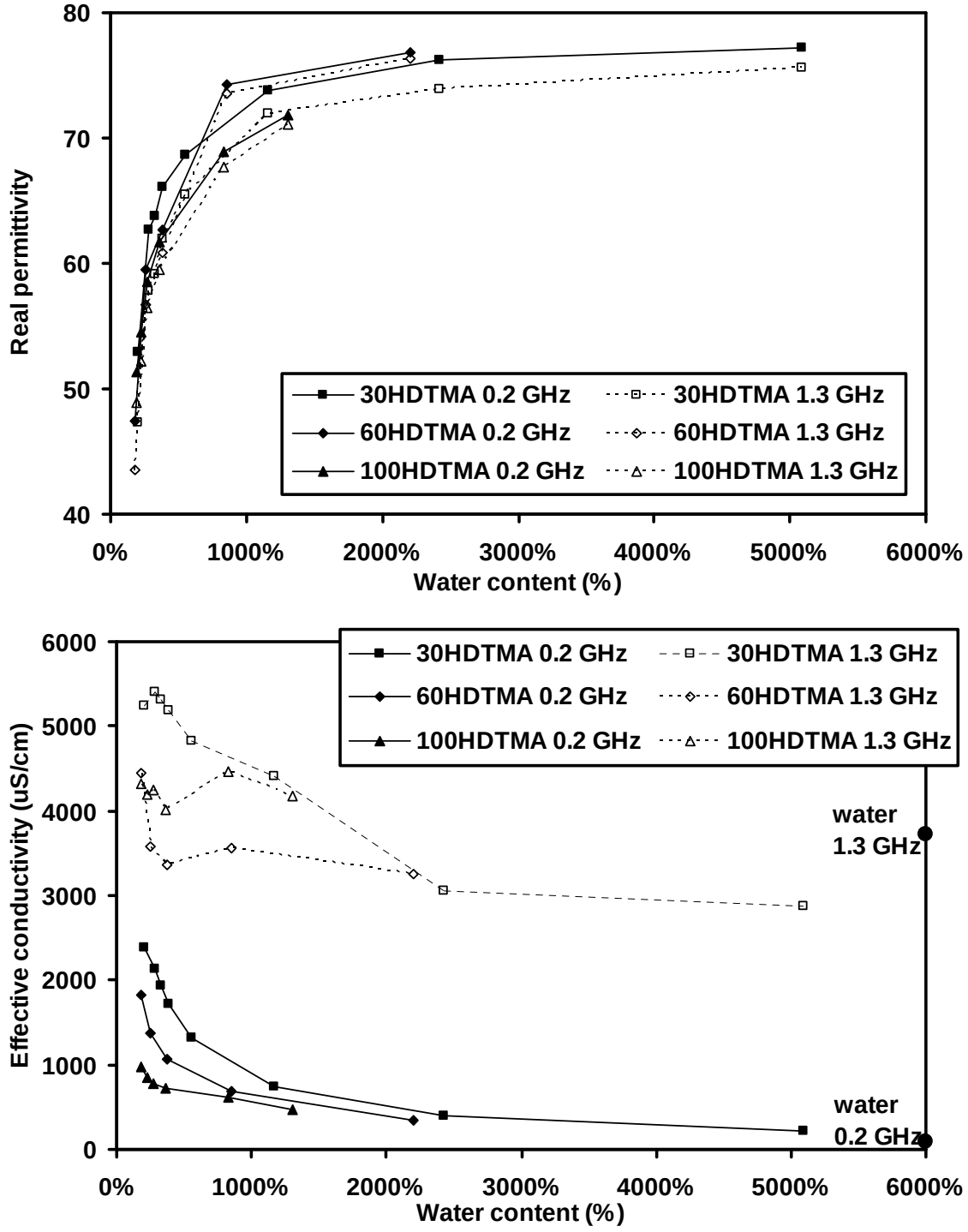

Figure 3-26. (a) Real permittivity and (b) effective conductivity of 30HDTMA, 60HDTMA, and 100HDTMA bentonite at 0.2 GHz and 1.3 GHz.

In general, the effective conductivity of organobentonite suspensions at 0.2 GHz electrical excitement decreased as the size, or the length of the single long C-chain, or the amount of organic loading increased (Figure 3-23 through Figure 3-26). This agreed with the trend of the DC conductivity of organic solutions that the larger the exchanged organic cations, or the longer the length of the single long C-chain of exchanged organic cations, the lower the conductivity (Figure 3-1). Organobentonites also have a bound layer of water molecules at the Stern layer (Liu et al., 2007), have limited mobility of ions in the diffuse double layer, and reduced the amount of free cations due to adsorption on the bentonite surface. Effective conductivity of bentonite suspensions would be higher than that of organobentonites due to the increase of ion mobility in both the diffuse layer and the bulk solutions (Santamarina et al., 2001).

Above mentioned trends for effective conductivity held until the orientational polarization relaxation dominated at higher frequency. Characteristic orientational polarization relaxation frequency was approximately 0.83 GHz (Figure 3-18) for 100DTMA bentonite, 1.07 GHz for 30HDTMA, 60HDTMA, and 100HDTMA bentonites (Figure 3-19 through Figure 3-21), 0.83 GHz (Figure 3-17) for 100TBA bentonite, 1.3 GHz (Figure 3-16) for 100TEA bentonite, and not observed at the tested frequency range, but anticipated to be higher than 1.3 GHz for 100TMA bentonite. As the size or the length of the single long C-chain increased, the characteristic relaxation frequency decreased. The amount of organic loading apparently did not have an effect on the characteristic frequency. When the frequency of electrical excitement reached relaxation frequency, the orientational polarization relaxation mechanism of water molecules were taken into account for the observed effective conductivity. Two

mechanisms for the occurrence of orientational relaxation in organobentonite suspensions were postulated. A freely rotating dipolar molecule also had an orientational polarizability. The center N atom in quaternary ammonium cations (such as TMA, TEA, and TBA) was considered to carry +5 valence, whereas the bonded four C atoms in alkyl branches to carry -1 valence each (Hager and Marvel, 1926). The center N atom, therefore, and the surrounding 4 alkyl branches would likely to form a dipole. When dissolved in aqueous solutions, the orientational polarization did not occur at frequency from 0.2 GHz to 1.3 GHz. However, when adsorbed in bentonite interlayers, orientational polarization took place. The Coulomb attraction between clay surface and organics and the lateral hydrophobic interaction among organic cations changed the characteristic frequency of the orientational polarization of the organic cations. This mechanism was attested by the hierarchy of the characteristic frequencies of TMA, TEA, and TBA (i.e., TMA > TEA > TBA). The larger organic cations indicated longer dipole distance, which in turn would register a lower characteristic relaxation frequency. Another possible orientational relaxation mechanism was that the presence of organic phases in organobentonite suspension changed the orientational mobility and the H bonds structure of water molecules. In turn, the relaxation frequency was shifted. Water occupied the majority portion of the pore fluid phases. The strong inclination of water molecules to form H bonds with each other influences their interaction with non-polar molecules that are incapable of forming H bonds, such as hydrocarbons (Israelachvili, 1991). Water molecules were prone to reorient themselves to form tetrahedral “cages” around the non-polar molecules so that H bonds did break (Israelachvili, 1991). The bigger the non-polar molecules, it was more likely that H bonds would disrupt. As a result, larger organic

cations (TBA) likely depressed the orientational mobility of the water molecules around them more than smaller organic cations (TMA) did. Therefore, the characteristic relaxation frequency of TBA was lower than that of TMA.

Hydraulic conductivity

Literature review

The hydraulic conductivity of organobentonites has been well-documented (Burns et al., 2006b; Li et al., 1996; Lorenzetti et al., 2005; Smith et al., 2003). Lorenzetti et al. (2005) reported that the hydraulic conductivity of geosynthetic clay liners (GCLs) increased when GCLs were amended with two different types of organobentonites: BTEA-bentonite and HDTMA-bentonite. As the content of organobentonites amendment increased from 10% to 90%, increases of three orders of magnitude in hydraulic conductivity were obtained. Lorenzetti et al. (2005) postulated that the increase of hydraulic conductivity was partially due to the fact that the organobentonites were hydrophobic and did not swell as much as untreated bentonites in the presence of water. Less swelling led to larger voids available for flow, which increased the hydraulic conductivity. However, if the permeant was changed to an organic solution, the hydraulic conductivity was not significantly altered due to sorption of organic compounds into the organic matter on the clay surface (Li et al., 1996; Lorenzetti et al., 2005).

Materials and experimental methods

Organoclay (TMA, TEA, TBA, DTMA, and HDTMA) samples were prepared by cation exchange as described in Chapter 2. After cation exchange was completed, the slurry was carefully poured into a stainless steel slurry consolidometer, taking care to avoid entrapment of air. The dimensions of the consolidometer were 10.2 cm (4 inch) in diameter and 45.7 cm (18 inch) in height. Axial load was placed on the slurry in increments of 3.5, 7, 14, 28, 56, and 100 kPa, until consolidation was achieved at each load step. The stress was applied to the slurry using Geotac load trac systems (Geotac, Texas, USA). Once the ultimate preloading stress was achieved, the slurry was unloaded by the same increments, in the reverse order. The duration of each load step was typically 1 day; however, at maximum load, the duration was increased, depending on the observed rate of settlement. P5 filter paper (Fisher Scientific) and a nonwoven geotextile were placed on top and bottom of the samples to facilitate drainage. To maintain the ionic strength of the pore fluid during slurry consolidation, a 0.001M NaCl solution was used to maintain saturation. After the slurry consolidated, the samples were extruded from the consolidation tube, and the specimen was divided into 3 parts for further testing. Samples were trimmed with a soil lathe and wire saw into 3.6 cm (1.4 inch) diameter and 7.6 cm (3 inch) height samples. The final water contents of the slurry consolidated samples ranged between 136% and 228%.

The hydraulic conductivity of TMA, TEA, TBA, DTMA, and HDTMA organobentonites at 100% CEC, and TMA and HDTMA at 30% and 60% CEC was tested according to ASTM D5084-03 (effective confining stress = 100kPa). The inflow and outflow fluids used in sample compression were 0.001M NaCl solution in order to

maintain a background ionic strength for the clay surface and the bulk solution. To prevent corrosion within the panel controls, the salt solution was isolated from the de-aired (Nold deaerator) water by two P620000 bladder accumulators (Trautwein Soil Testing Equipment, Houston, Texas, USA). B values of 0.95 were obtained before testing.

Hydraulic conductivity was measured using falling head rising tail system (Method C of ASTM D5083-03). The equation used to calculate hydraulic conductivity was

$$k = \frac{a_{in} \cdot a_{out} \cdot L}{(a_{in} + a_{out}) \cdot A \cdot \Delta t} \ln\left(\frac{h_1}{h_2}\right) \qquad \textbf{Equation 3-17}$$

where a is the cross-sectional area of the burette containing the inflow (a_{in}) and outflow (a_{out}) fluid; L is the height of soil sample, A is the cross-sectional area of soil sample, h_1 and h_2 are the initial and final total head, Δt is the time of permeation.

Results and discussion

The hydraulic conductivities of TMA and HDTMA-bentonite were measured under 100 kPa effective confining pressure at organic loadings of 30%, 60%, and 100% of CEC (Figure 3-27). As was anticipated, the hydraulic conductivity increased as the organic loading was increased. This trend is attributable to the fact that the organobentonites were hydrophobic and did not exhibit the same swelling characteristics as untreated bentonites in the presence of water (Lorenzetti et al., 2005). At the microscopic level, the electrical repulsive forces between organobentonites particles are lower than those between pure bentonite particles, and the attractive forces are higher due to increased hydrophobic interaction between the organic cations attached to the particle

surfaces. As a result, at a given effective confining stress, organobentonite particles tended to form larger aggregates than did unmodified bentonite particles, leaving larger pore voids, which in turn increased the hydraulic conductivity. Hydrophobicity increased as the size of the organic cations increased (TMA→TEA→TBA). Consequently larger aggregates were formed in TEA and TBA clays than in TMA-bentonite, and the hydraulic conductivity was higher. DTMA and HDTMA had a single long carbon chain, with hydrophobicities even higher than organic cations with short carbon chains., and the resulting conductivity increased Their resulting hydraulic conductivity was higher than that of TMA, TEA, and TBA (Figure 3-28). However, the hydraulic conductivity of DTMA was about an order of magnitude higher than that of HDTMA. This is probably due to the decreased water content of HDTMA (116% at 100 kPa) comparing to that of DTMA (190% at 100 kPa). The hydraulic conductivity of the 30% and 60% exchanged HDTMA bentonite did not increase as significantly when compared with TEA and TBA bentonites at similar levels of organic carbon, indicating that it the number of sites exchanged on the clay surface, as opposed to the quantity of organic carbon, may play the dominant role in hydraulic conductivity.

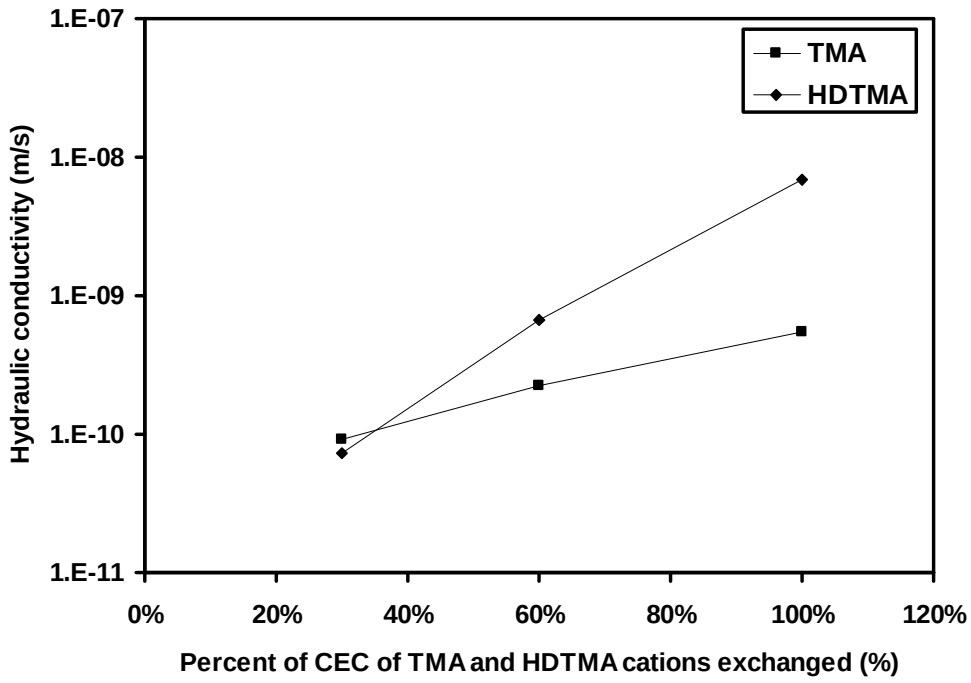

Figure 3-27. Hydraulic conductivity of TMA-bentonite and HDTMA-bentonite as a function of organic loading. .

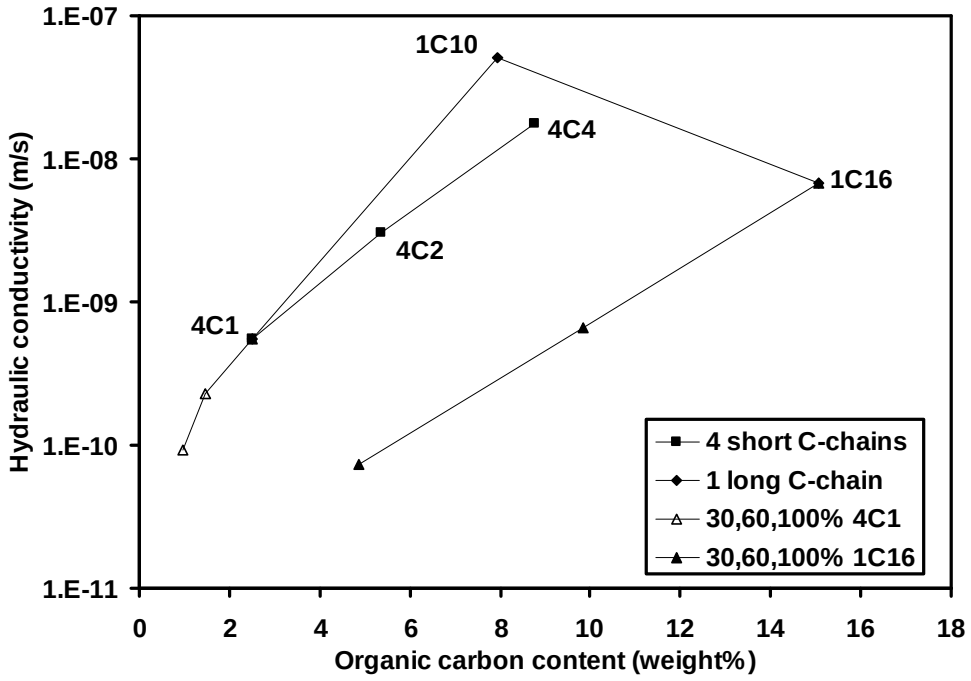

Figure 3-28. Hydraulic conductivity of 100% CEC exchanged organobentonite as a function of length of carbon chain(s) of QACs.

Thermal conductivity

Literature review

Heat flux through geomaterials was often encountered in many engineering applications, including high level nuclear waste isolation, energy piles, thermal ground improvement techniques, and waste containment facilities (Abuel-Naga et al., 2009). Heat transfer mechanisms included conduction, radiation, and convection; however, heat flow through soil and rock was almost entirely by conduction, although radiation may contribute for surface soils, and convection may be important when there was significant water or air flow (Mitchell and Soga, 2005). Thermal conductivity, k_t or λ, was the measurement of the ease with which heat passes through a soil. Soil minerals usually had higher thermal conductivity than water, and water had higher conductivity than air; consequently, heat flow was primarily through the solid phase of the soil, and wet soil transfers heat faster than dry soil. Typical thermal conductivity values of some soil minerals were given in Table 3-5.

Table 3-5. Thermal Conductivities of Selected Geomaterials

Materials	Thermal conductivity, W/m/K
Soil minerals[1]	0.25 – 2.5
Air[1]	0.024
Water[1]	0.60
Dry bentonite[2]	0.4 – 1.1

[1] Mitchell and Soga (2005).

[2] water content 7 – 18%, dry density 1400 – 1800 kg/m^3 (Tang et al., 2008)

Factors that influence thermal conductivity were mineralogy, dry density, pore fluid, saturation, temperature, and gradation (Mitchell and Soga, 2005). Sand and silt usually had higher thermal conductivity than clay (Abuel-Naga et al., 2009). As the saturation or dry density increased, λ increased. Well-graded soil had higher λ than poorly-graded soil, because the contact number increases for well-graded soil. For all crystalline minerals, λ decreased as temperature increased (Abuel-Naga et al., 2009). No study was found that quantified the effect of organic coatings on the thermal conductivity of clay minerals. In this study, the thermal conductivities of seven organobentonites with different types and amount of organic cations exchanged were measured as a function of branch effect and tail length effect.

Materials and experimental methods

The thermal conductivity of 7 organobentonite samples (100TMA, 100TEA, 100TBA, 100DTMA, 30HDTMA, 60HDTMA, and 100HDTMA bentonite) were determined using the needle probe method. The test was based on the infinite line heat source theory as described in (Carslaw, 1959). The thermal conductivity was determined according to Equation 3-15 for heating and Equation 3-16 for cooling (ASTM D5534 – 08):

$$\Delta T \cong \frac{Q}{4\pi\lambda}\ln(t) \quad 0 < t \le t_1 \qquad \textbf{Equation 3-18}$$

$$\Delta T \cong \frac{Q}{4\pi\lambda}\ln\left(\frac{t}{t-t_1}\right) \quad t > t_1 \qquad \textbf{Equation 3-19}$$

where ΔT is temperature rise from time zero (K), Q is the heat input per unit length of heater (W/m), λ is the thermal conductivity (W/m/K), t is time from the beginning of

heating (s), and t_1 is the heating time. The data were plotted as *ln(t)* versus ΔT and as $\ln\left(\frac{t}{t-t_1}\right)$ versus ΔT, and λ was calculated from the slope of each curve and *Q*.

Soil samples were prepared as described in the hydraulic conductivity section, with the maximum one dimensional consolidation pressure equal to 100 kPa. The cylindrical soil sample had a height of 14.2 cm (5.6 inch) and diameter of 7.11 cm (2.8 inch). A small hole was predrilled in the sample prior to inserting the thermal probe; a thin layer of silver grease (Arctic Silver Inc.) was used to reduce the contact resistance and ensure a good contact at the needle-soil interface. A thermal probe (Model no. TC-18, East 30 Sensors) of 60 mm (2.36 in) in height, and 1.27 mm (0.05 in) in diameter was then fully inserted perpendicular to the top plane of the soil cylinder, at the center of the soil sample. The heat was provided by a CR3000 Micrologger (Campbell Scientific), and the heat flux (*Q*), temperature rise (ΔT), ambient temperature were recorded by CR3000 Micrologger data logger. Calibration was performed on 99% glycerine (PTI Process Chemicals). Both the heating and cooling process took 100 seconds. In view of the heat capacity of the needle probe, the data from the first 20 seconds of both the heating and cooling portion were omitted in calculating the slope (ASTM D5534 – 08). The average of both the heating and cooling portion was reported, and a minimum of 5 repeat tests were performed for each soil sample.

Results and discussion

Temperature-time signature of a single measurement on 60% HDTMA bentonite was shown in Figure 3-29(a). The temperature-time signature plot was then plotted in natural log time scale [Figure 3-29(b)], and the slopes of the curves of both heating and

cooling processes were calculated to derive thermal conductivity. The data showed reasonable consistency as shown in the R-square values.

The results of thermal conductivity of organobentonites suggested that as a general trend, thermal conductivity decreased as organic content increased [Figure 3-30(a)]. The smallest QAC, TMA cation ($4C_1$), possessed the highest thermal conductivity of 0.87 W/(K.m), which is higher than that of water (0.60 W/(K.m)). As the size of QACs increased from TMA ($4C_1$) to TEA ($4C_2$) and TBA ($4C_4$), the thermal conductivity decreased from 0.87 to 0.84 and 0.78 W/(K.m), respectively. As the branch size of the organic cation increased, the thermal conductivity decreased, indicating the organic layer acted as an insulator. Similarly, when the length of single C-chain increased from TMA ($4C_1$) to DTMA ($1C_{10}$) and HDTMA ($1C_{16}$), λ decreased from 0.87 to 0.77 and 0.75 W/(K.m). DTMA ($1C_{10}$) with 10 carbon chain had similar effect as TBA ($4C_4$), indicating that total organic carbon content, and not structure of the organics, was controlling the thermal conductivity.

In terms of organic loading on HDTMA ($1C_{16}$), a substantial decrease in thermal conductivity was observed as the surface cover increased from 30% CEC to 60% CEC; however, only a small change was observed from 60% CEC to 100% CEC. This suggested that when more than half of the CEC of bentonite sites were covered with HDTMA cations, direct contact between bentonite face planes was shielded by the organic phases. When the organic coverage was lower than 50% of CEC of bentonite, the organic phase did not cover the complete clay surface, thus allowing more particle to particle contacts and an increase in thermal conductivity.

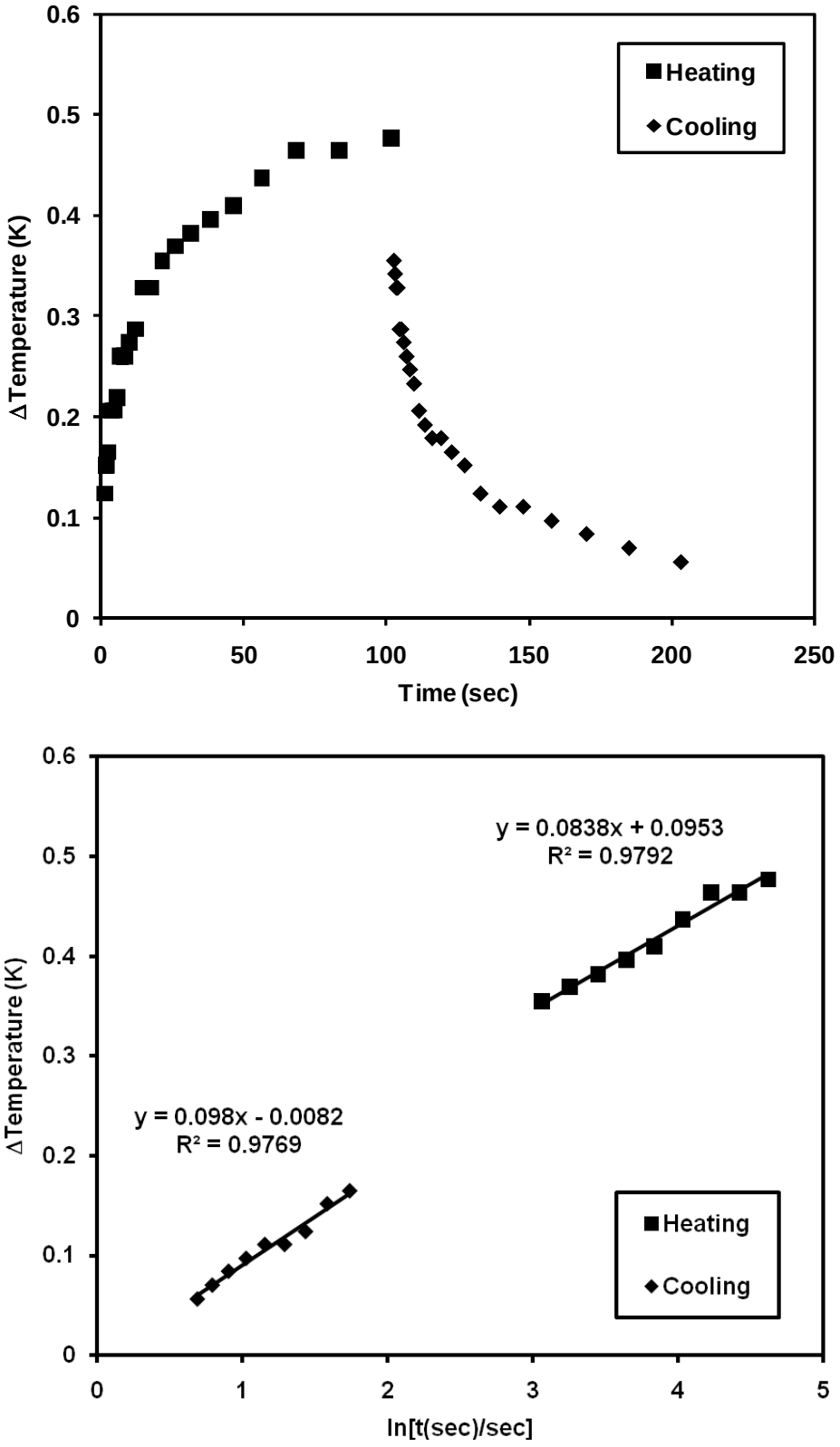

Figure 3-29. (a) Temperature-time signature for a single measurement on 60% HDTMA bentonite. (b) Temperature-ln(t) plot for deriving thermal conductivity.

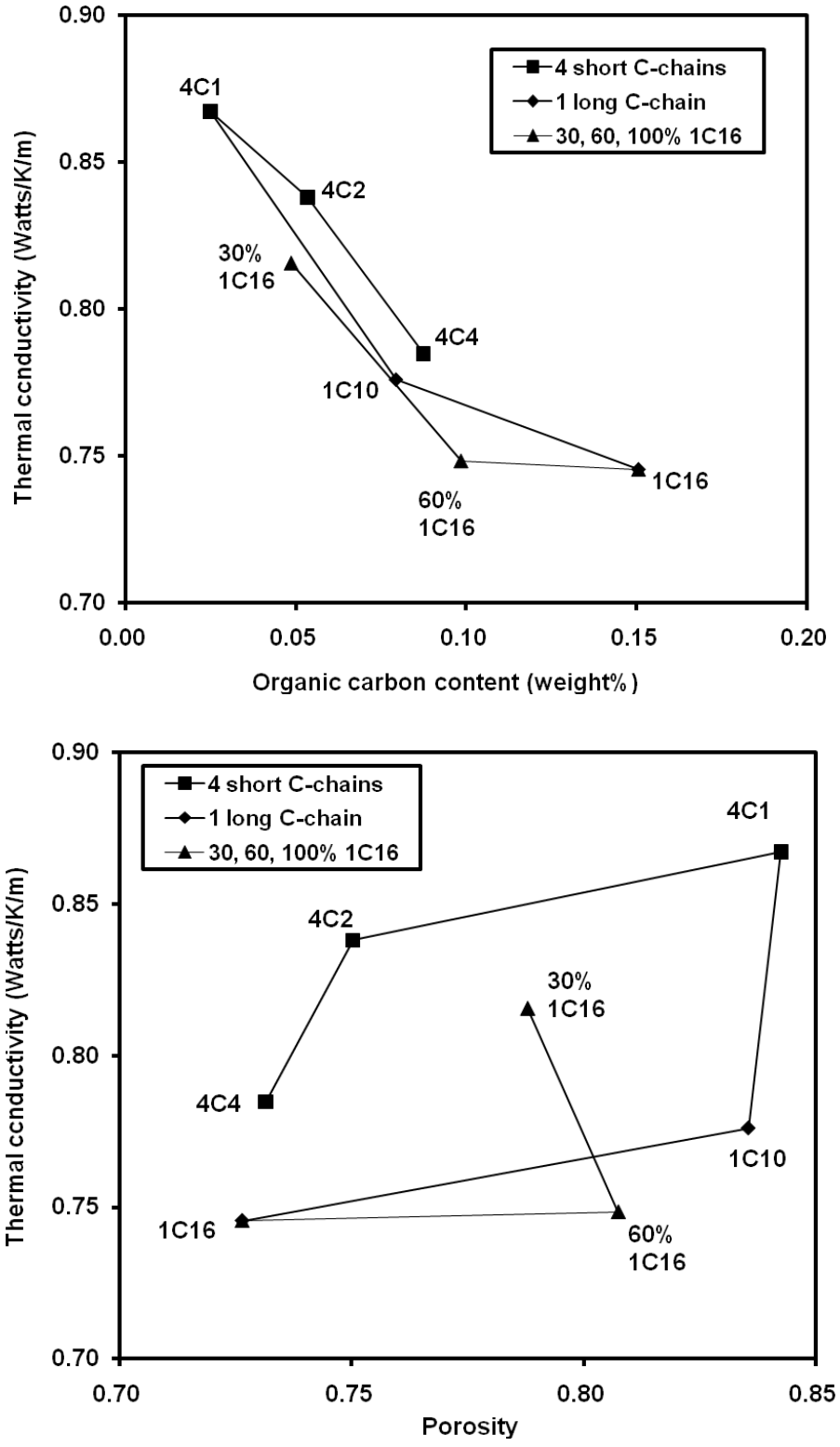

Figure 3-30. Thermal conductivity of organobentonites versus (a) organic loading, and (b) porosity.

Addition of organic coatings to clay surface had two fold of effects on the thermal conductivity. One effect was the decrease of porosity and loss of pore space, and the resulting increase of contacts between particles. Increase in inter-particle contacts, on one hand, lead to more heat transfer paths through particle-particle contacts, and therefore enhanced thermal conduction. On the other hand, increased inter-particle contacts resulted in higher thermal gradient with the surrounding medium, which eventually led to higher heat transfer to the pore space (heat loss) (Yun and Santamarina, 2008). Another effect was on the particle-level heat transport processes. Several heat transfer processes concurred: (1) Conduction along the mineral (2) fluid convection within large pores, (3) conduction along the pore fluid within the pore space (hydrostatic and advecting pore fluid), (4) particle-fluid-particle conduction across the fluid contacts, (5) particle-particle conduction across contacts, and (6) particle-fluid conduction (Cortes et al., 2009). Processes 1 – 3 might be less influenced by the introduction of organics, while processes 4 – 6 were influenced by the organic coating through the interface between particle and fluid or particle. From the measured thermal conductivity results in [Figure 3-30(a)] we found that particle-level heat transfer processes 4 – 6 played an important role in the overall thermal conductivity of organobentonites. In another word, the low thermal conductivity of organic coatings at the particle surface weakened the heat transfer processes through particle to particle and particle to fluid contacts. The porosity change due to the presence of organic cations did not seem to greatly affect the thermal conductivity of organobentonite [Figure 3-30(b)].

Conclusions

In terms of the observed conduction phenomena, the following conclusions can be drawn:

- At a given concentration, the conductivity of quaternary ammonium cations solutions decreased as the cation size increased, due to lower mobility. In addition, the micelle formation of QACs with long C-chain further decreased the mobility of organic cations.
- Critical micelle concentration were identified by the measurements of the DC conductivity test, and agreed with the surface tension results and with those in the literature.
- Polarization loss of water at low concentration (<0.01M) was constant (about 5) for all organic solutions, while higher concentrations (> 0.01M) showed some small variations ($\pm$ 3), but still less significant than the DC conduction. DC conduction contributed to the effective imaginary conductivity primarily, except for very low concentration solutions, where DC conductivity was very low.
- Real permittivities of NaCl, TMA Cl, TEA Br, TBA Br, DTMA Br, DDTMA Br, and HDTMA Br solutions decreased as concentration increased, which held true at all frequencies from 0.1 to 1.3 GHz. Real permittivity decreased because the mobility of water molecules involved in hydrating ions was decreased due to the increased presence of electrolyte ions; however, there were exceptions: at frequencies lower than 0.6 GHz, organic cations with a long C-chain (DTMA, DDTMA, and HDTMA) and concentration higher than approximately 0.02 M, higher concentration led to an increased real permittivity value. Polarization of water molecules alone was not

enough to generate such high values of real permittivities. It is postulated that the spatial relaxation mechanism prevailed at the frequency range from 0.1 to about 0.6 GHz due to the presence of micelles, which would occur in high concentration solutions of organic cations with a long C-chain (DTMA, DDTMA, and HDTMA). The relation between micelles and the relaxation mechanism was not clear.

- Organic phases, having less permittivity than free water, reduced the real permittivity and effective imaginary conductivity of organobentonites in general. The amount of bound water determined the polarizability of the organobentonite suspensions, and the specific surface area determined the amount of bound water molecules. It was also found that specific surface area measurement correlated well with real permittivity.
- Characteristic frequency of the relaxation due to orientational polarization of water was influenced by the presence of organobentonites. For organobentonite suspensions, the characteristic frequencies were 0.83 GHz, 1.3 GHz and larger than 1.3 GHz for TBA, TEA, and TMA bentonites, and were 0.83 GHz and 1.07 GHz for DTMA and HDTMA bentonites. The amount of organic loading did not seem to affect the characteristic frequencies. The relaxation mechanism significantly changed the measurements of real permittivity and effective imaginary conductivity for organobentonite suspensions.
- Hydraulic conductivity of organobentonites increased as the size, the length of a single long C-chain, or the amount of organic loading increased. This trend was attributable to the fact that the organobentonites were hydrophobic and did not exhibit the same swelling characteristics as untreated bentonites in the presence of water (Lorenzetti et al., 2005).

- Thermal conductivity of organobentonites decrease as the size, the length of a single long C-chain, or the amount of organic loading increased. The low thermal conductivity of organic coatings at the particle surface weakened the heat transfer processes through particle to particle and particle to fluid contacts. The porosity change due to the presence of organic cations did not seem to greatly affect the thermal conductivity of organobentonite.

Chapter 4 Effect of Total Organic Carbon Content and Structure on the Electrokinetic Behavior of Organoclay Suspensions

Introduction

In addition to changing the mechanical and hydraulic properties of the clay soil (Burns et al., 2006b), exchanging organic cations on to the clay surface also has significant impacts on the electrokinetic behavior of the mineral. When a charged particle is immersed in water and is subjected to an electric field, it will move relative to the bulk solution. The particle, along with sorbed ions and a sorbed fluid phase, will translate through the bulk fluid; the zeta potential (ζ) represents the electric potential measured at the interface between this slipping plane and the bulk fluid. The measured zeta potential yields insight into the surface charge of the clay mineral and its electrokinetic interactions with the fluid phase.

Previous work has quantified either the electrophoretic mobility or the zeta potential of montmorillonite in NaCl solutions, with measured values of ζ ranging from -60 mV to – 30 mV (Duran et al., 2000; Saka and Guler, 2006; Singh and Sharma, 1997; Tombacz and Szekeres, 2006). The reported differences may be attributed to variation in parameters such as the degree of isomorphic substitution of the montmorillonite or concentration of the background solutions. Additionally, when the bulk solution background electrolyte was changed to a different inorganic cation, the measured zeta potential was altered in part according to the affinity of the clay for the inorganic cation (Galindo-Gonzalez et al., 2005; Gecol et al., 2006; Kaya and Yukselen, 2005; Khaldoun

et al., 2006; Niriella and Carnahan, 2006; Pierre and Ma, 1997; Pierre and Ma, 1999; Saka and Guler, 2006; Singh and Sharma, 1997; Zhuang and Yu, 2002).

Similarly, the addition of an organic cation to the charged clay surface will also influence the resulting zeta potential. A variety of organics can be used to create organic rich clays, including surfactants such as sodium dodecyl sulfate and dodecyltrimethylammonium bromide (Gunister et al., 2004; Kaya and Yukselen, 2005), humic acid and fulvic acid (Ramos-Tejada et al., 2001; Ramos-Tejada et al., 2003; Sondi and Pravdic, 1996), and many types of polymers (Bottero et al., 1988; Gunister et al., 2007; Kaya and Yukselen, 2005; Ramos-Tejada et al., 2006). Zeta potential measurements of these organic rich clays showed that anionic surfactants, such as dodecyl sulfate anion, decrease the zeta potential, while cationic surfactants, such as dodecyltrimethylammonium cation, increase the zeta potential, while charge-neutral organic compounds, including some humic and fulvic acids, have little or no effect on the measured zeta potential. Polymers are more complex than simple organic ions because they often consist of more than one functional group, and the resulting zeta potential can be increased, decreased, or not affected.

This study focused on the behavior of montmorillonite that was modified with six different quaternary ammonium organic cations. For the materials studied in this investigation, the montmorillonite was hydrophilic, and the quaternary ammonium cations had alkyl functional groups with an ammonium head group; therefore, the primary driving forces for interaction at the particle surface were electrostatic interaction and hydrophobic lateral interactions. The organic cations chosen for study were selected to examine the effect of cation size (i.e., increasing the carbon chain length in all four

alkyl positions), as well as the effect of cation chain length (i.e., increasing the carbon chain length in one of four alkyl positions) on the measured zeta potential. Changing the size and chain length of the organic cation altered both the packing on the clay surface as well as the hydrophobicity of the exchanged clay, which in turn altered the measured zeta potential.

Materials and Experimental Methods

Materials.

Six quaternary ammonium cations were chosen for study: tetramethylammonium (TMA, denoted: *4 C_1*) chloride [$(CH_3)_4NCl$], tetraethylammonium (TEA, denoted: *4 C_2*) bromide [$(CH_2CH_3)_4NBr$], tetrabutylammonium (TBA, denoted: *4 C_4*) bromide [$((CH_2)_3(CH_3))_4NBr$], decyltrimethylammonium (DTMA, denoted: *1 C_{10}*) bromide [$(CH_3)_3NC_{10}H_{21}Br$], dodecyltrimethylammonium (DDTMA, denoted: *1 C_{12}*) bromide [$(CH_3)_3NC_{12}H_{25}Br$], and hexadecyltrimethylammonium (HDTMA, denoted: *1 C_{16}*) bromide [$(CH_3)_3NC_{16}H_{33}Br$]. All cations were obtained from Fisher Scientific, and were used as received. Hydrochloric acid (HCl, Fisher Scientific), sodium hydroxide (NaOH, Fisher Scientific), sodium chloride (NaCl, Fisher Scientific), and soda lime (> 4% NaOH, J.T. Baker) were also used as received, and the water used in all experimentation was deionized (Barnstead E-pure). Wyoming bentonite (CG-50, CETCO), composed primarily of sodium montmorillonite, was the base clay for the study and was used as received. The natural-organic carbon content of the material was 0.2% (Huffman Laboratories, Inc., Golden, CO), and its cation exchange capacity (CEC) was 69.1 meq/100g (ammonium acetate saturation, Hazen Research, Inc., Golden, CO).

Experimental Methods

The organobentonites used in this study were synthesized in the laboratory by exposing the particle surfaces of the bentonite to an aqueous solution containing the quaternary ammonium cation at 30%, 60%, and 100% of the cation exchange capacity of the clay. The organic compound was dissolved in 2 liters of deionized water, and 20 grams of the clay were added to the aqueous solution. The resulting suspension was mechanically stirred for 15 minutes and allowed to stand for a minimum of 24 hours to allow gravity separation. The supernatant was then siphoned off, and the solids were rinsed with deionized water to remove any salts or loosely bound cations, and the process was repeated until the conductivity of the supernatant was below 600 $\mu S/cm$. Mineralogical impurities were separated by gravity settling. The suspension was then oven-dried at 105 ^{o}C until the water was completely evaporated. Large clumps of the organoclay were pulverized and further ground to fine powder with a mortar and pestle. The fine-grained portion was separated by sieving through No. 200 sieve and then stored in airtight containers until tested.

The zeta potential was measured using a ZetaPlus zeta potential analyzer (Brookhaven Instruments Corporation, Holtsville, NY, USA). ZetaPlus uses eletrophoretic light scattering and the laser Doppler velocimetry (LDV) method to determine particle velocity or mobility, and the zeta potential was determined from particle mobility using Henry's equation:

$$\mu_e = \frac{\varepsilon_r \varepsilon_o \zeta}{\eta} f(\kappa a) \qquad \textbf{Equation 4-1}$$

where μ_e is the electrophoretic mobility, ε_r is the relative dielectric constant, ε_o is the permitivitty of free space, η is suspension viscosity, a is the radius of the suspended particles, ζ is the zeta potential, and κ is the reciprocal Debye length. The Smoluchowski limit was adopted in the calculations, by assuming the radius of the kinetic unit was far greater than the thickness of the electrical double layer ($\kappa a >> 1$), resulting in:

$$\mu_e = \frac{\varepsilon_r \varepsilon_o \zeta}{\eta} \quad \textbf{Equation 4-2}$$

Sample preparation included mixing 0.12 grams of each organoclay with 200 mL of 0.01 mol/L NaCl solution. The resulting suspensions were then ultrasonically dispersed (Branson 8510, Branson Ultrasonics Corporation, Danbury, CT, USA) for 30 minutes to break clay aggregates. The suspension was then transferred into a nitrogen atmosphere (CO_2-free) within a glove box (Scienceware, Fisher Scientific) to prevent the dissolution of atmospheric CO_2 into the suspension. During the course of the experiments, nitrogen gas was circulated through the glove box to reduce the entry of CO_2 and a granular sodium calcium hydrate (4 – 8 mesh, soda lime, JT Baker) was used as a CO_2 absorber within the glove box.

The zeta potential was measured for each organoclay at acidic pH values between 3.5-4.5, as well as over a range of pH, varying from approximately 3.5 to 10.5. The value of pH was adjusted using either1 mol/L HCl or NaOH solutions. Additionally, the zeta potential of the unmodified bentonite was measured as a function of pH, ranging from pH = 2 to 11. Throughout the course of the experiments, some pH drift was observed, typically within 0.5 – 1.5 pH units. The drift of pH will be discussed later.

Approximately 1.5 mL of the suspension supernatant was extracted to a cuvette for each zeta potential measurement. The suspension was stirred before extraction in order to uniformly distribute particles. Zeta potential measurements were taken in duplicate every 1 to 7 days, until the measured differences of last 10 readings were within 5 mV. Measurements were continued until the readings stabilized, typically between 30 to 76 days. Equipment operation was verified daily by measuring the zeta potential of a reference material of known zeta potential (ZR-3, Brookhaven Instruments).

Results and Discussion

The zeta potential of unmodified montmorillonite (with naturally occurring inorganic cations) was measured over a pH range from 2 to 10.5 (Figure 4-1). The measured zeta potential was approximately -28 mV at pH = 2, becoming more negative as the pH value was increased to pH = 4.5, and then remaining relatively stable at a value of approximately -46 mV up to pH = 10.5. At extreme values of pH, the montmorillonite structure would undergo dissolution, which was generally agreed to occur at the particle edges and progress through the breaking of the bridge oxygen bond (Si-O-Al), releasing aluminum and then silicon atoms into solution (Bickmore et al., 2001; Oelkers, 2001; Rozalen et al., 2008). At low values of pH, the predominant aqueous form of released aluminum was Al^{3+}, which along with H^{+}, exhibited a high affinity for the clay surface. Aluminum displaced the naturally occurring sodium, resided in the bound layer and effectively neutralized more negative surface charge than sodium, which in turn, resulted in a less negative zeta potential. At values of pH in basic conditions, dissolution of the mineral would also occur; however, the predominant aqueous species of aluminum at elevated values of pH was $Al(OH)_4^-$, which was repelled from the negatively charged

particle surface due to electrostatic repulsion. The predominant cation at these high values of pH will again be Na^+, which is weakly bound and results in less positive charge being retained within the shear plane, and a negative zeta potential over pH values in the basic range. Zeta potential of the unmodified montmorillonite in the variable pH solutions was also measured as a function of time (up to 70 days); however, the measured values did not deviate significantly from the initially measured values (<10 mV, data not shown).

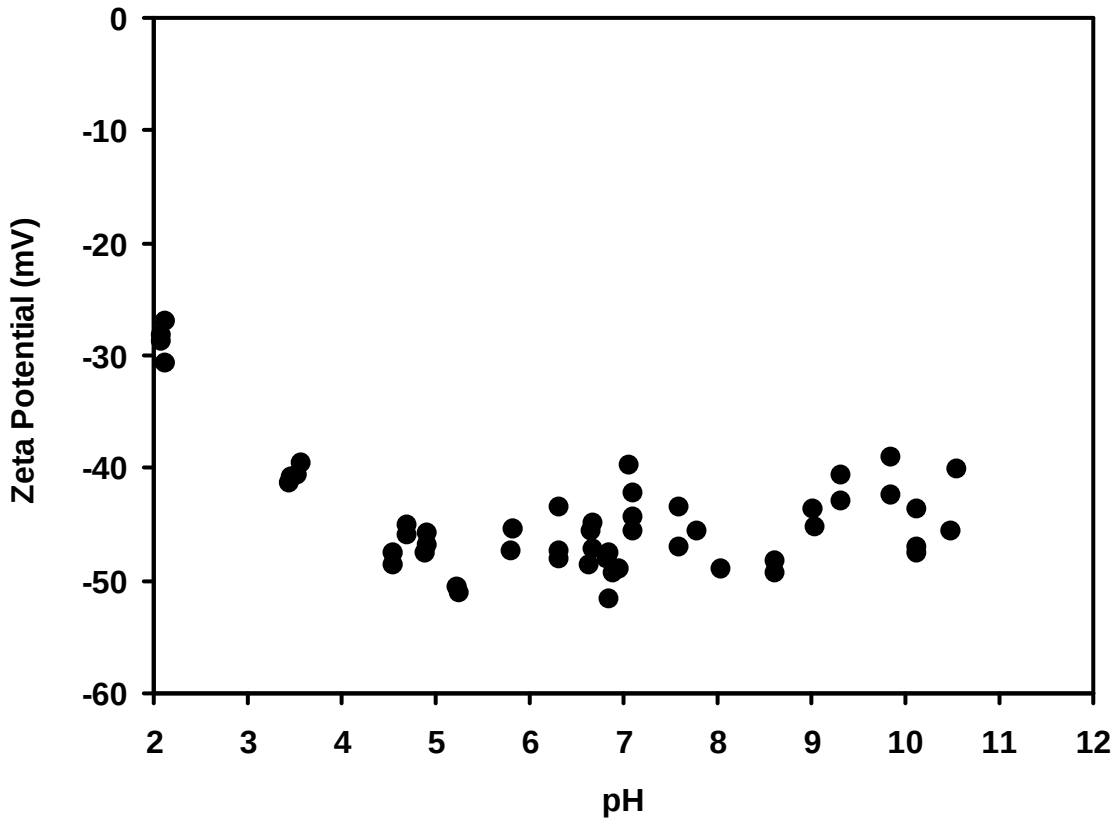

Figure 4-1. Zeta potential as a function of pH for unmodified sodium montmorillonite.

The exchange of the organic quaternary ammonium cations for the clay's naturally occurring inorganic cations had significant influence on the measured zeta

potential (Figure 4-2 and Figure 4-3). The effects of two variables were measured: first, the effect of the length of the carbon chain in one of the quaternary positions (methyl groups in the three remaining positions) and second, the effect of cation size (increasing the length of all four carbon chains). Increasing the length of the chain on one of the four quaternary positions allowed comparison of TMA (*4 C_1*), DTMA (*1 C_{10}*), DDTMA (*1 C_{12}*), and HTMA (*1 C_{16}*) (Figure 4-2), while increasing the length of the chain in all four quaternary positions allowed comparison of TMA (*4 C_1*), TEA (*4 C_2*), and TBA (*4 C_4*) (Figure 4-3).

Increasing the length of one of the carbon chains in the quaternary group resulted in two pronounced effects on the zeta potential of the clay (Figure 4-2). First, at each exchange level (30% CEC, 60% CEC, and 100% CEC), increasing the number of carbons (*1 $C_{\#}$*) in one chain increased the zeta potential of the clay (that is, made it less negative). Over the range of tested organic content, measured values for TMA (*4 C_1*) were between -30 and -35 mV, while the measured values at the same exchanged percentage for HDTMA (*4 C_{16}*) ranged from 0 to -17 mV (Figure 4-2). Increasing the tail length on the carbon chain increased the hydrophobicity of the clay, which increased the hydrophobic lateral interaction between cations. This result was significant because it bonded more positive charge within the shear plane, resulting in a less negative zeta potential. The effect was most pronounced as the number of carbon was increased because longer chains led to stronger lateral interaction (Zhang and Somasundaran, 2006), binding more cation within the shear plane. For example, even at 100% cation exchange capacity for DDTMA clay (*1 C_{12}*), a negative zeta potential was measured (-8 mV), indicating that not all DDTMA cations were held within the shear plane, even when 100%

of the CEC was exchanged with the organic cation; however, for HDTMA (*1 C_{16}*) clay exchanged at 100% of its CEC, the measured zeta potential was essentially equal to zero, indicating that lateral interaction between the cation chains was strong enough to retain most of the HDTMA cations (100% CEC) within the shear plane. Note also that the measured zeta potential increased as the percentage of exchanged organic cation was increased from 30% of the cation exchange capacity to 100% of the CEC (Figure 4-2). It is believed that the addition of the organic cation to the particle surface resulted in a hydrophobic surface phase that tended to force inorganic cations out of the sorbed layer, and into the diffuse double layer, even at low total organic carbon contents. Subsequently, much of the negative surface charge was not compensated within the bound layer, resulting in a net negative zeta potential. The effect diminished as the organic content was increased, because more positive charge was bound within the shear plane in the form of organic cations.

For all clays tested, increasing the total organic carbon content resulted in a less negative zeta potential, indicating that more organic cation was bound within the shear plane as the percentage exchanged was increased (Figure 4-2). In the case of HDTMA, there was an approximately linear increase in zeta potential as the exchanged cation percentage was increased; however, as carbon chain length was reduced to 10 or 12 carbons, the function was nonlinear, and the measured zeta potential values were negative (-10 to -15 mV) at 100% CEC, indicating that some of the cations were not bound within the shear plane, but within the diffuse double layer.

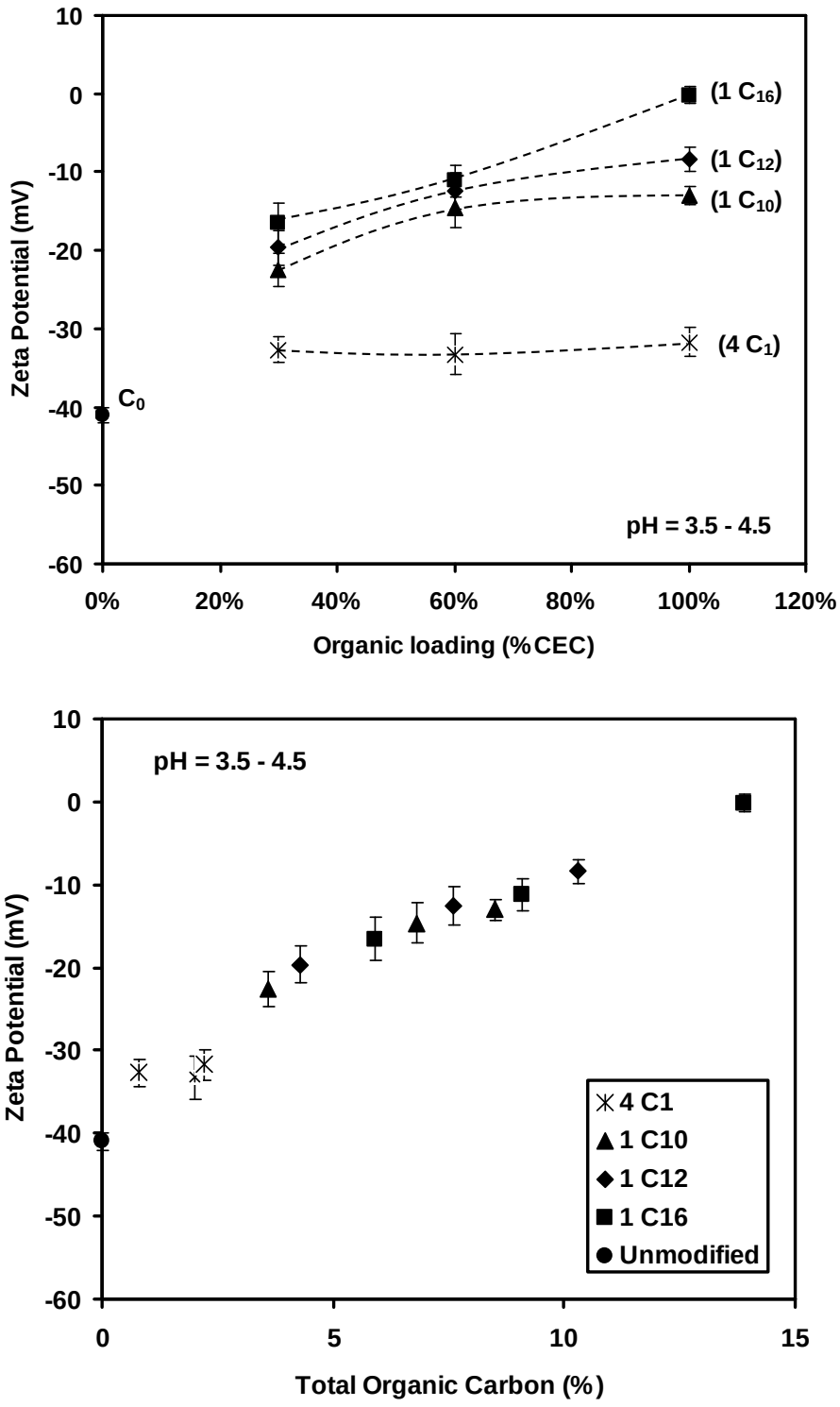

Figure 4-2. Zeta potential as a function of organic loading, varying the length of one carbon chain: a) as a function of percent CEC exchanged; and b) as a function of total organic carbon.

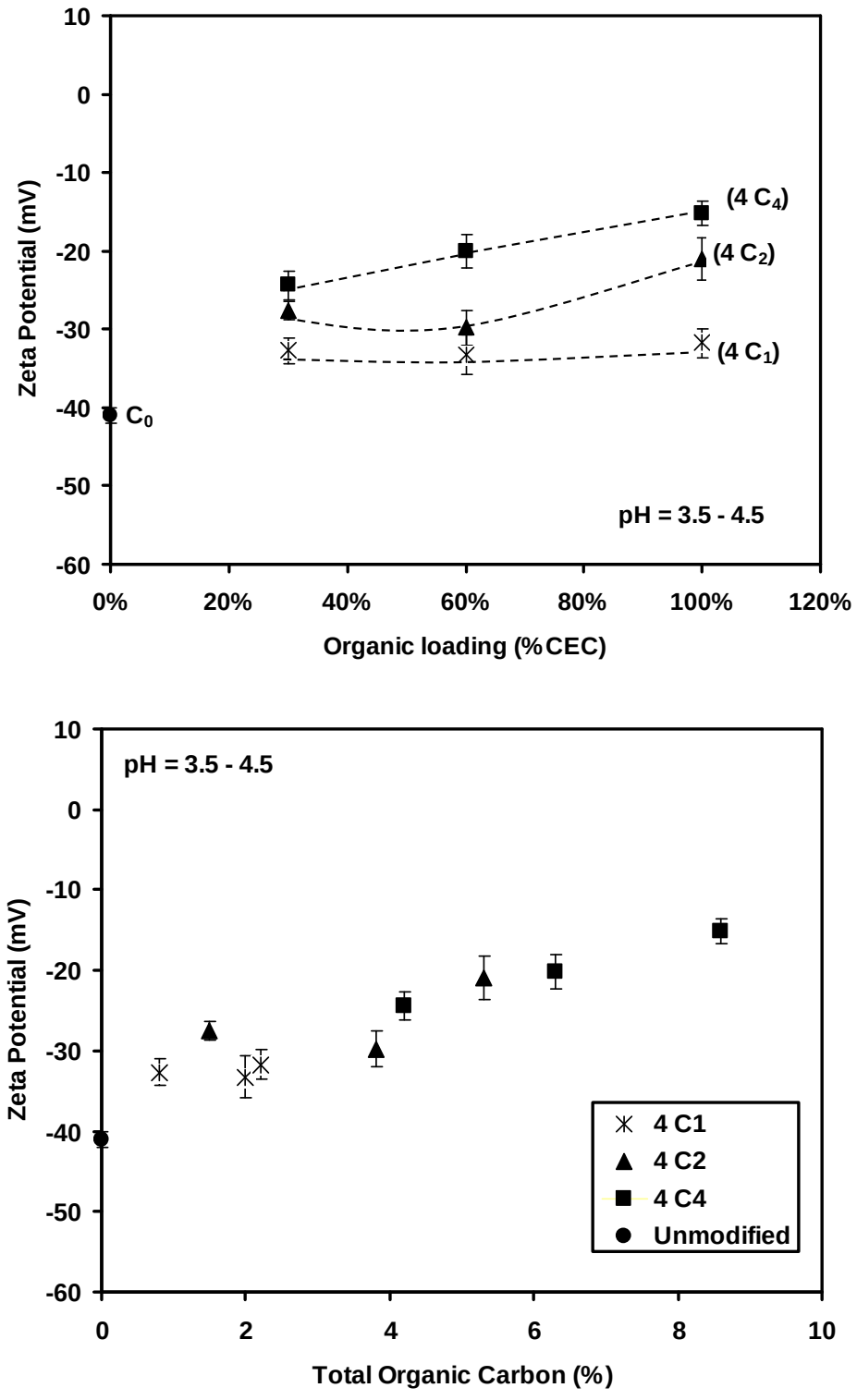

Figure 4-3. Zeta potential as a function of organic loading, varying the size of the organic cation: a) as a function of percent CEC exchanged; and b) as a function of total organic carbon.

The effect of increasing the size of the organic cation by increasing the chain length of all four chains in the quaternary ammonium positions was also studied (Figure 4-3). As the number of carbons on each branch of the quaternary ammonium cation increased from 1 to 2 to 4 (TMA to TEA to TBA), the measured zeta potential became less negative, indicating that more of the organic cation was retained within the shear plane as the size of the cation was increased (Figure 4-3). The effect was most pronounced in the transition from TMA to TEA at high organic carbon contents. Increasing the total number of carbons in the organic cation decreased the solubility of the cation, which increased the attraction of the cation to the particle surface, resulting in more positive charge being bound within the shear plane. However, even at organic loadings as high as 100% CEC, only a portion of the positive charge was bound within the shear plane, resulting in measured zeta potential values that were still less than zero, but which, notably, increased as the total organic carbon sorbed to the clay was increased (Figure 4-3).

Comparing the measured zeta potential values for the organoclays as a function of increasing size (four carbon chains with $4\ C_{\#} \leq 4$) to the values measured as a function of increasing length of only one carbon chain ($1\ C_{\#} \geq 10$), it was found that the longer carbon chain was a more effective method to bind cations within the shear plane (Figure 4-4). Even when the total organic carbon content was similar (e.g., TBA versus DDTMA), the measured zeta potential was measurably less negative for DDTMA, indicating that the structure of the organic cation was of primary consideration, as opposed to the total mass of organic present on the clay surface, in determination of the zeta potential. The increased size of the TBA cation limited its ability to pack tightly on the clay surface,

rendering a lower packing density, and subsequently, decreased exchange when compared to the cations in which only one tail length was increased (e.g. DTMA, DDTMA, and HDTMA). The resulting surface potential for TBA was consequently more negative than that of DDTMA, which was reflected in the more negative measured zeta potential.

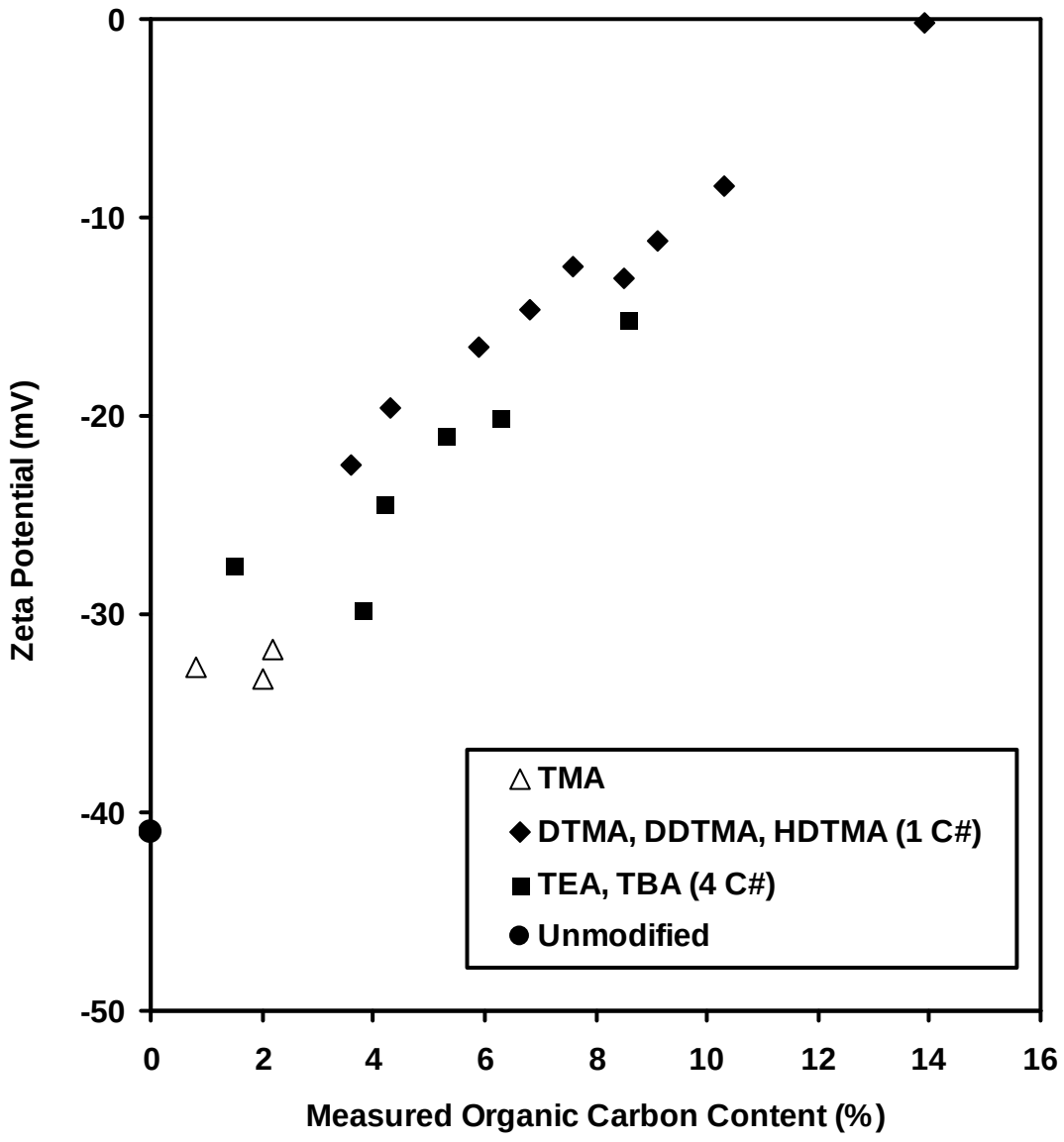

Figure 4-4. Comparison of zeta potential as a function of organic content, chain length, and cation size.

The influence of the organic cations on the zeta potential was measured over a range of pH values, varying between approximately 3.5 – 10.5 (data shown for 100% CEC clays for clarity, trends were similar at other exchanged percentages) (Figure 4-5). For all organoclays at all measured values of pH, the zeta potential of the organoclay was higher than the zeta potential of the unmodified montmorillonite, indicating that the organic cations were retained at a higher percentage inside the shear plane than are the naturally occurring inorganic cations, and that the bonding between organic cations and montmorillonite was stronger than that between sodium cations and montmorillonite. Across the entire pH range tested, the hydrophobicity of the organic cations led to expulsion from the polar aqueous phase, increased lateral interaction between the cation tails (Fuerstenau and Pradip, 2005; Zhang and Somasundaran, 2006), and higher affinity for the charged clay surface than the inorganic cations that had a relative affinity for the polar water phase.

In all cases, the measured zeta potential became more negative as the pH increased, as was observed in the case of unmodified montmorillonite; however, the decrease was slight for the larger sized organic cations (TEA (*4 C_2*) and TBA (*4 C_4*)) (Figure 4-5), and the zeta potential was less sensitive to pH as the total organic carbon was decreased. Additionally, the long chain organoclays also exhibited notable behavior: at low pH, the zeta potential became less negative as the length of the quaternary chain was increased (i.e., HDTMA > DDTMA > DTMA > TMA). Consequently, even at 100% CEC, a negative zeta potential was measured for the shorter chain clays. The effect of the pH on the interaction of the organic phase with the mineral surface is complex, but it is believed that increasing the tail length on the quaternary ammonium cation increased the

specific interaction of organic cation with the negatively charged surface sites on the clay mineral surfaces. In turn, this hydrophobic interaction, which increased as the length of the carbon tail was increased, shielded the negative surface charge, resulting in a net charge within the shear plane that approached zero as the pH was decreased, organic content was increased, and the tail length was increased to 16 (HDTMA, *1* C_{16}). The binding of positive charge on the surface was less efficient as the chain length was decreased, which resulted in less screening of negative surface charge and negative zeta potential. The same trends held for the organic cations that were selected to study increasing size (TMA, TEA, TBA).

Throughout the study, the measured zeta potential values exhibited a time-dependency, increasing from the initially measured value by a magnitude of 5 to 20 mV. Clay minerals typically exhibit minimum solubility at the zero point of charge, pH_{zpc}. Consequently, the rate of dissolution increased as the pH diverged from the point of zero charge (Rozalen et al., 2008), releasing metal cations, such as Si^{4+}, Al^{3+}, and Mg^{2+} (Baron and Shainber.I, 1970; Barshad, 1960; Chernov, 1947). The dissolution was expected to be congruent and stoichiometric at pH < 4 and pH > 10, but was incongruent in the range of pH = 5 - 10, where adsorption/precipitation of Al was expected to occur (Rozalen et al., 2008). The released Al^{3+} from the montmorillonite edges had high relative affinity for basal planes of montmorillonite (Barshad, 1969; Chernov, 1947; Coleman and Craig, 1961); in this study, it is believed that the dissolution of montmorillonite and subsequent release of Al^{3+} liberated higher valence cations that could displace the sorbed monovalent (Na^{+}) cations from the montmorillonite, which in turn partially neutralized surface charge and yielded a less negative zeta potential. At pH < 4.7, Al is present predominantly in the

Al^{3+} form; while at pH = 4.7 - 6.5, the predominant species is $Al(OH)^{2+}$; and at pH = 6.5 – 8 $Al(OH)_3$ predominates. Above pH = 8, the primary species is $Al(OH)_4^-$. The surface reactions will also be influenced by the precipitation of $Al(OH)_{3(am)}$ on the clay surface for zeta potential values that were measured between pH 5.0-10.0 (Tombacz and Szekeres, 2004; Wiese and Healy, 1975). Additionally, Jackson (Jackson, 1960) notes that polymerization of aluminum species begins above pH 5 (general chemical structure $\left[\left(Al(OH)_x H_2O\right)_{6-x}^{(3-x)+}\right]_n$, where n is the average number of Al ions per polymer). Those polymerized units are thought to have higher relative affinity for the particle surface than Al^{3+} (Chernov, 1947; Jackson, 1963; Jenny, 1961). Polymers are thought to be virtually unexchangeable once precipitated onto the surface, and can contribute to the reduction of the cation exchange capacity of soils (Bohn et al., 2001; Sparks, 2003).

Conclusions

The zeta potential of Wyoming montmorillonite clay, and six organically modified clay samples was measured as a function of pH, cation chain length, and cation size. This study presented that compared to the clay's naturally occurring inorganic cations, exchanged quaternary ammonium cations were more likely bound within a particle's shear plane, resulting in a less negative zeta potential for organoclays than that for unmodified bentonite. Zeta potential became less negative as the length of carbon chain was increased (*1 $C_{\#}$*), as the total organic carbon content was increased, and as the pH was decreased. Increasing the length of one carbon tail (*1 $C_{\#}$*) was more effective at binding organic cations within the shear plane than increasing the size of the cation (*4 $C_{\#}$*),

when compared on the basis of total organic carbon content. Increasing the pH of the bulk solution resulted in a decrease in zeta potential for all clays measured.

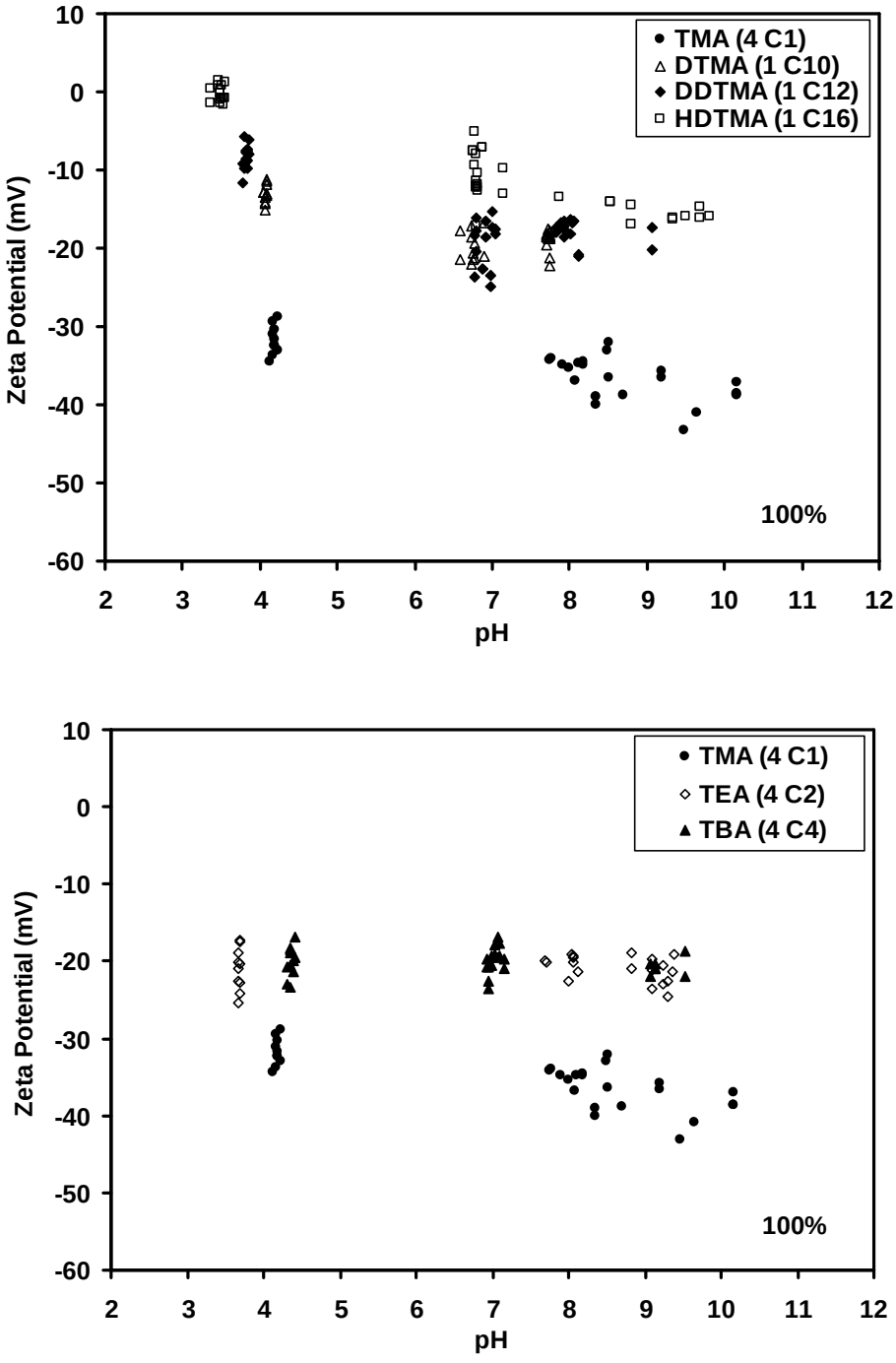

Figure 4-5. Comparison of zeta potential as a function of pH for a) increasing chain length of organoclays (cation with one chain increased); and b) increasing cation size.

Chapter 5 Triaxial Shear Strength Behavior of Bentonite Modified by Quaternary Ammonium Cations

Introduction

Organic materials are ubiquitous in the geologic environment, and can exert significant influence over the interfacial properties of minerals; however, due to the complexity of their structure and interaction with soil solids, their impact has remained relatively unquantified. Natural organic matter (NOM) is generated through the metabolism, death, and breakdown of all types of organic life forms, yielding large concentrations of dissolved or particulate materials that are geochemically reactive with charged inorganic geological materials like soil grains. NOM contents in soils are highly variable, and can range from 0.5% to 5% (by weight) in the surface horizon of soils, to as high as 100% in organic soils (Sparks, 2003). Natural organic matter is of engineering interest because it readily forms organic coatings that can affect the frictional behavior, sensitivity, and hydraulic conductivity/contaminant transport characteristics of a soil deposit. Additionally, organic coatings are an important contributor of nutrients to microbial communities, which in turn create additional organic coatings in the form of biofilms. Natural organic matter occurs in a variety of forms, but can be easily divided into fulvic acids, which are soluble in base and acid, humic acids, which are soluble in base but not acid, and humin, which represents the insoluble portions of organic matter. In addition to naturally occurring organic matter, synthetic organic compounds are also present in a variety of engineered applications in geotechnical engineering, ranging from

applications as lubricants during pipe-jacking, borehole stabilizers, and as components of geosynthetic clay liners and slurry walls to resist highly concentrated chemical solutions. Because the occurrence, weight, and structure of natural organic material is highly heterogeneous and because engineered applications use proprietary undisclosed formulations, it is difficult, if not impossible, to quantify the effects of organic matter on natural geologic materials in a systematic method. Consequently, this work quantifies the frictional interaction of a clay mineral that has been coated with a known, controlled organic phase, with a specified density of coating (both lateral extent and thickness), and structure of the organic cations that were exchanged onto the mineral's surfaces.

Engineered Organic Matter

The organic cations chosen for study were quaternary ammonium cations, which are generated physiologically in living organisms, and produced commercially for a variety of industrial applications. When combined with a mineral of measurable cation exchange capacity, the organic cations will preferentially displace the naturally occurring inorganic cations like Na^{+} and Ca^{2+} and bond electrostatically (at low concentrations, additional drive force were discussed later) to the mineral surface, producing a soil with a base mineral solid phase bonded to a specified organic phase.

In frictional interactions, a regime of particle to particle lubrication dominates when a long-chain carbon surfactant like hexadecyltrimethlyammonium (HDTMA) is loaded onto a particle surface at a high density (Boschkova et al., 2002). For the case of friction measurements at low pressure, the surfactant forms a fluid-like layer which controls particle to particle interaction; that is, the tails of the surfactant chains interact, rather than direct particle to particle contact. However, changing the characteristics or

density of loading of the surfactant can actually change the particle interaction regime from lubrication to increasing friction. Friction can be increased by choosing a surfactant that exhibits disorder at the molecular scale; interactions become governed by energy dissipative mechanisms such as chain entanglement, which becomes more pronounced as the density of surfactant packing on the surface is decreased. Decreasing the density of packing of the surfactant can also lead to changes in the frictional regime because the surfactant monolayer no longer acts as a unified fluid layer, but instead leads to entanglement of the surfactant molecules (Chen and Israelachvili, 1992; Yoshizawa et al., 1993).

The frictional behavior of self-assembled monolayers on particulate materials follows complex interactions according to the packing density and the functional groups that are interacting. Molecular dynamics simulations on the behavior of C_{18} alkyl chains have revealed that the density of packing has a significant influence on the frictional behavior, with tightly packed monolayers exhibiting significantly lower friction than monolayers that are loosely packed (Lee et al., 2000; Mikulski and Harrison, 2001). In loosely packed systems, the sliding causes bond-length fluctuations that cause more energy dissipation (and hence, higher friction) than observed in densely packed systems, where the tightly packed chains are more constrained with respect to movement (Mikulski and Harrison, 2001); surfactant monolayers can exhibit three different phase states as a function of packing density: solid-like, amorphous, and liquid (Yoshizawa et al., 1993).

Although many properties of organobentonites have been studied, such as sorption capacity, swelling, and hydraulic conductivity, little data are available for the

strength of organoclays. Burns et al. (2006) carried out direct shear tests on bentonite that had been exchanged with hexadecyltrimethlyammonium (HDTMA) and benzyltriethylammonium (BTEA) cations, where surface coverage of the organic cation varied from 50% cation exchange capacity (CEC) exchanged to 100% CEC exchanged. The measured direct shear peak friction angle decreased as the surface coverage of HDTMA was increased, as would be expected for a shift from solid/amorphous behavior to amorphous/liquid behavior as the monolayer coverage was increased (Burns et al. 2006). However, BTEA clay showed an increase in strength as the total organic carbon content was increased. It was hypothesized that the degree of disorder in the packing of the benzene ring, in addition to a component of chemical adhesion, was responsible for the increase in measured strength for the BTEA clays. In addition, literature values have reported a measured a direct shear friction angle of 34^{o} for trimenthylammonium (TMA) bentonite exchanged at 85% of CEC (Soule and Burns, 2001).

Xiao et al. (1996) found that the friction between a Si_3N_4 atomic force microscopy tip and mica substrates coated with alkylsilanes [$Me_3Si(CH_2)_nCH_3$] decreased about 1 order of magnitude as the carbon chain length increased from 3 or 6 to 18 (Xiao et al., 1996). In contrast, when the chain length was 3 or 6, the friction was higher than that of uncoated mica. Xiao et al. (1995) attributed van der Waals attractions to the stabilization of long carbon chains to form more compact and rigid layers, so that long chains acted as much better lubricants. The frictional behavior of monolayers with short chains, on the other hand, was dominated by the increased number of energy dissipation modes facilitated by the presence of molecular disorder, such as rotations about the C-C axis and bending.

Naturally Occurring Organic Soils

Although organic soils are typically regarded as highly compressible materials with low frictional strength (Terzaghi, 1996), in many cases, high effective stress friction angles of organic soils, ranging from 25° – 90°, have been reported (den Haan et al., 1995; Hight et al., 1992), with additional detailed summaries (Cheng et al., 2007; den Haan et al., 1995). Cheng et al. (2007) studied the cause of the high friction angle of Dutch OVP organic soils with computed X-ray tomography and electron microscopy. They found that the high friction angles may be attributed to the dense subhorizontal laminae, which contained angular and platy particles of medium silt size, as well as the lens-like structures outside the dense laminae. Hight et al. (1992) measured a friction angle of 34^{o} for Bothkennar clay, which contains a relatively high organic content of 2 – 4 %; however, the high strength was attributed to the dominant angular silt fraction. Additionally, diatoms, residual plant fabrics, and micro-fibers have also been considered to be the causes of high friction angles (Cheng et al., 2007).

Peat, a general category of soil characterized by high organic contents, has also been reported with friction angles of $49 – 53^{o}$, which were measured for two Italian peats (Cola and Cortellazzo, 2005); the authors attributed the high friction angle to the fabric of the soil. Furthermore, it is also well documented that the undrained strength ratios of organic clays are higher than those of inorganic clays (Jamiolkowski et al., 1985; Leroueil et al., 1990).

This study details the results of an experimental investigation designed to measure the shear strength of seven organically modified clays. Five different quaternary ammonium cation structures were studied, with the cations chosen to reflect the influence

of increasing the cation size through equal branching at all four quaternary positions, versus increasing the cation tail length effect, through increasing the cation size at only one quaternary position. Additionally, the effect of cation loading was also studied by synthesizing clays at cation exchange percentages of 30%, 60%, and 100%.

Materials and Experimental Methods

Wyoming bentonite (CG-50, CETCO), composed primarily of sodium montmorillonite, was the base clay for the study and was used as received. The natural-organic carbon content of the material was 0.2% (Huffman Laboratories, Inc., Golden, CO), and its cation exchange capacity (CEC) was 69.1 meq/100g (Hazen Research Inc., Golden, CO). Five quaternary ammonium cations were chosen for study: tetramethylammonium (TMA, denoted: *4 C_1*) chloride [$(CH_3)_4NCl$], tetraethylammonium (TEA, denoted: *4 C_2*) bromide [$(CH_2CH_3)_4NBr$], tetrabutylammonium (TBA, denoted: *4 C_4*) bromide [$((CH_2)_3(CH_3))_4NBr$], decyltrimethylammonium (DTMA, denoted: *1 C_{10}*) bromide [$(CH_3)_3NC_{10}H_{21}Br$], and hexadecyltrimethylammonium (HDTMA, denoted: *1 C_{16}*) bromide [$(CH_3)_3NC_{16}H_{33}Br$] (Figure 2-1). All cations were obtained from Fisher Scientific, and were used as received. The water used in all experimentation was deionized (Barnstead E-pure).

The organobentonites were synthesized using the method described in Chapter 2. After cation exchange was completed, the slurry was carefully poured into a stainless steel slurry consolidometer, taking care to avoid entrapment of air. The dimensions of the consolidometer were 10.2 cm (4 inch) in diameter and 45.7 cm (18 inch) in height. Axial load was placed on the slurry in increments of 3.5, 7, 14, 28, 56, and 100 kPa, until consolidation was achieved at each load step. The stress was applied to the slurry using

Geotac load trac systems (Geotac, Texas, USA). Once the ultimate preloading stress was achieved, the slurry was unloaded by the same increments, in the reverse order. Depending on the type of organobentonite, the duration of each load step ranged from 1 day up to 3 weeks, to ensure 100% completion of primary consolidation. P5 filter paper (Fisher Scientific) and a nonwoven geotextile were placed on top and bottom of the samples to facilitate drainage. To maintain the ionic strength of the pore fluid during slurry consolidation, a 0.001M NaCl solution was used to maintain saturation. After the slurry consolidated, the samples were extruded from the consolidation tube, and the specimen was divided into 3 parts for strength testing. Samples were trimmed with a soil lathe and wire saw into 3.6 cm (1.4 inch) diameter and 7.6 cm (3 inch) height samples. The final water contents of the slurry consolidated samples ranged between 136% and 228%. The measured total organic carbon content in each organoclay agreed well with the calculated values of sorbed carbon (Figure 2-2).

Isotropically consolidated undrained triaxial compression tests were performed using Geotac load trac systems (Geotac, Texas, USA). All shear tests were strain rate controlled tests and were performed in accordance with ASTM D4767-04. Based on the time-deformation readings recorded during slurry consolidation, a strain-rate of 0.5 %/hr was selected for testing. Samples were sheared at effective confining pressures of 50 kPa, 100 kPa, and 200 kPa, with a backpressure of 140 kPa during shear, and all samples recorded a minimum B-value of 0.95 before shearing. Corrections for cross-section area change, membrane stiffness, and friction between loading rod and bushing were accounted for in calculating the stresses from the measurements. The corrected heights and diameters of the samples were used in the shearing test calculation by assuming

deformation of a right circular cylinder. The inflow and outflow fluids used in sample compression and shear tests were 0.001M NaCl solution in order to maintain a background ionic strength for the clay surface and the bulk solution. To prevent corrosion within the panel controls, the salt solution was isolated from the de-aired (Nold deaerator) water by two P620000 bladder accumulators (Trautwein Soil Testing Equipment, Houston, Texas, USA). Water contents of the samples at the end of slurry consolidation and post shear are given in (Table 5-1).

Table 5-1. Water Content of Organobentonites Tested in Triaxial Shear

Organic cations	CEC exchanged (%)	After Slurry Consolidation, before isotropic consolidation (%)	After isotropic consolidation, or after triaxial shearing (undrained) (%)		
			50 kPa	100 kPa	200 kPa
TMA, $4C_1$	30%	164	144	121	105
	60%	162	141	122	101
	100%	184	172	152	126
TEA, $4C_2$	100%	156	136	120	92
TBA, $4C_4$	100%	136	131	107	82
DTMA, $1C_{10}$	100%	228	206	190	146
HDTMA, $1C_{16}$	100%	148	147	116	99

*(Nominal 100 kPa)

Results

The results of the strength tests were analyzed according to changes in four different variables: 1) increasing the cation loading through an increase in the percent of cation exchange capacity that was exchanged, 2) increasing all four quaternary

ammonium branch sizes simultaneously, 3) increasing the length of one branch on the quaternary ammonium center, and 4) increasing the total organic content of the organoclay samples.

Increasing the cation loading on the mineral surface

Results of the CU triaxial tests performed on clays with 30%, 60% and 100% of their inorganic cations exchanged with the organic TMA ($4C_1$) cations displayed peak behavior with positive pore water pressure generation in all cases (Figure 5-1 through Figure 5-3). The pronounced peak behavior was present despite the relatively low levels of overconsolidation (OCR = 1 or 2) to which the specimens were subjected during consolidation and preparation. More interestingly, while the samples exhibited peak behavior, there was no recorded tendency toward dilation, as no negative pore water pressures were recorded. Increasing the exchanged percentage of organic ions onto the clay surface resulted in critical state friction angles that ranged from 26° to 34°, with the maximum friction angle occurring at 60TMA. For all clays tested, substantial differences were recorded between the peak friction angle and the critical state friction angle, and a critical state cohesion was also measured, ranging from approximately 20 – 30 kPa (Figure 5-4).

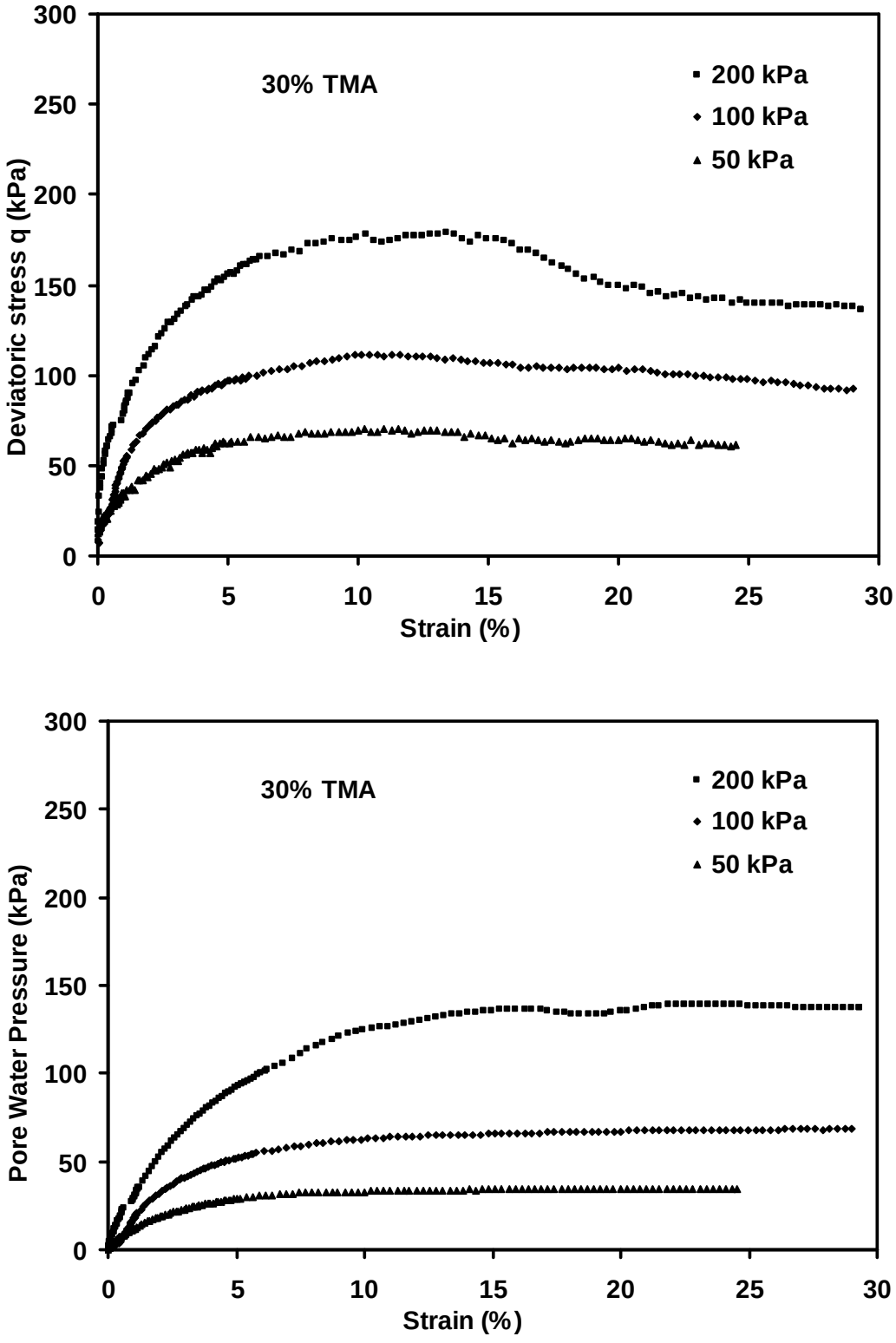

Figure 5-1. CU triaxial strength test results for 30% TMA: a) stress-strain diagrams; b) pore water pressure diagrams.

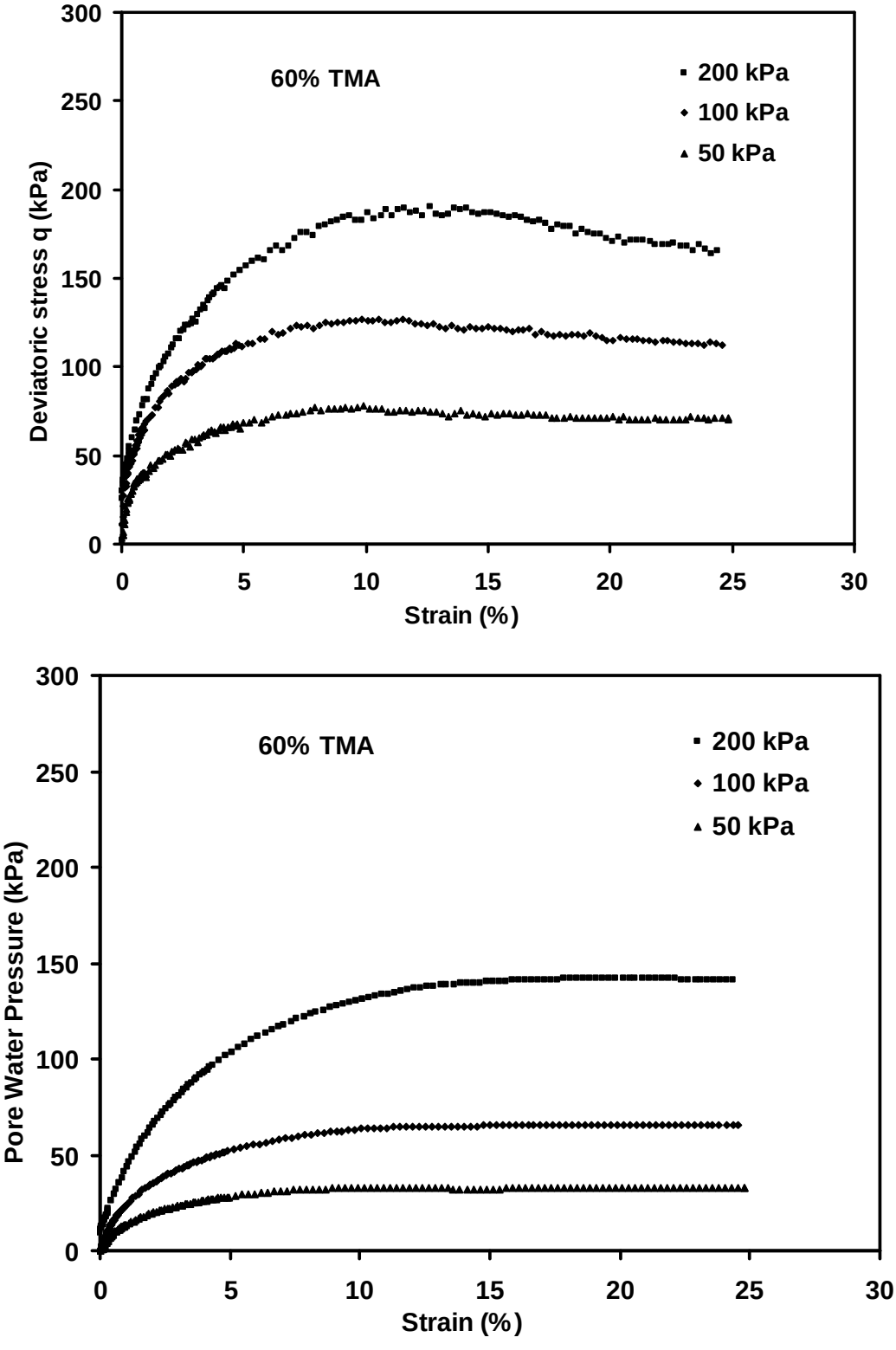

Figure 5-2. CU triaxial strength test results for 60% TMA: a) stress-strain diagrams; b) pore water pressure diagrams.

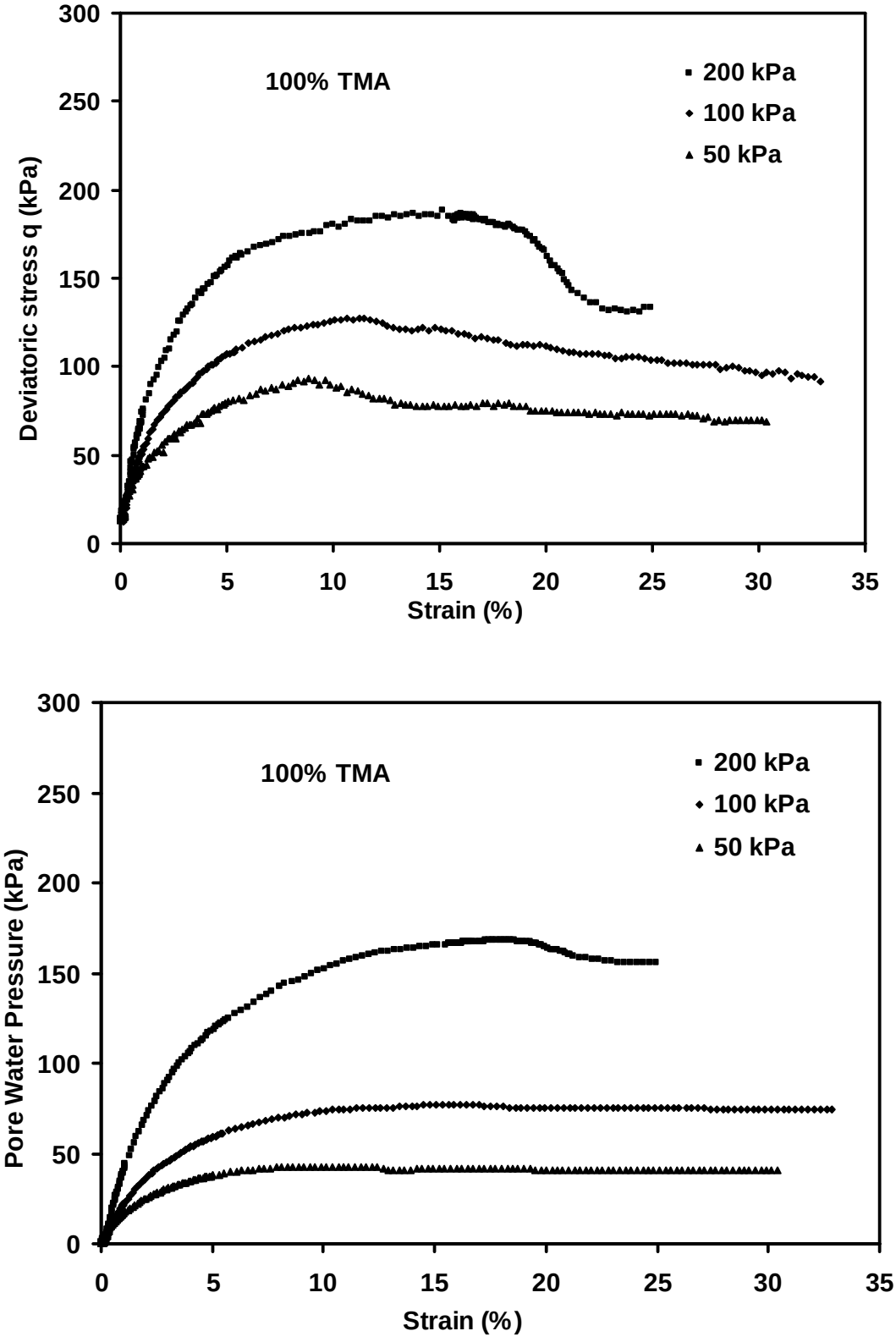

Figure 5-3. CU triaxial strength test results for 100% TMA: a) stress-strain diagrams; b) pore water pressure diagrams.

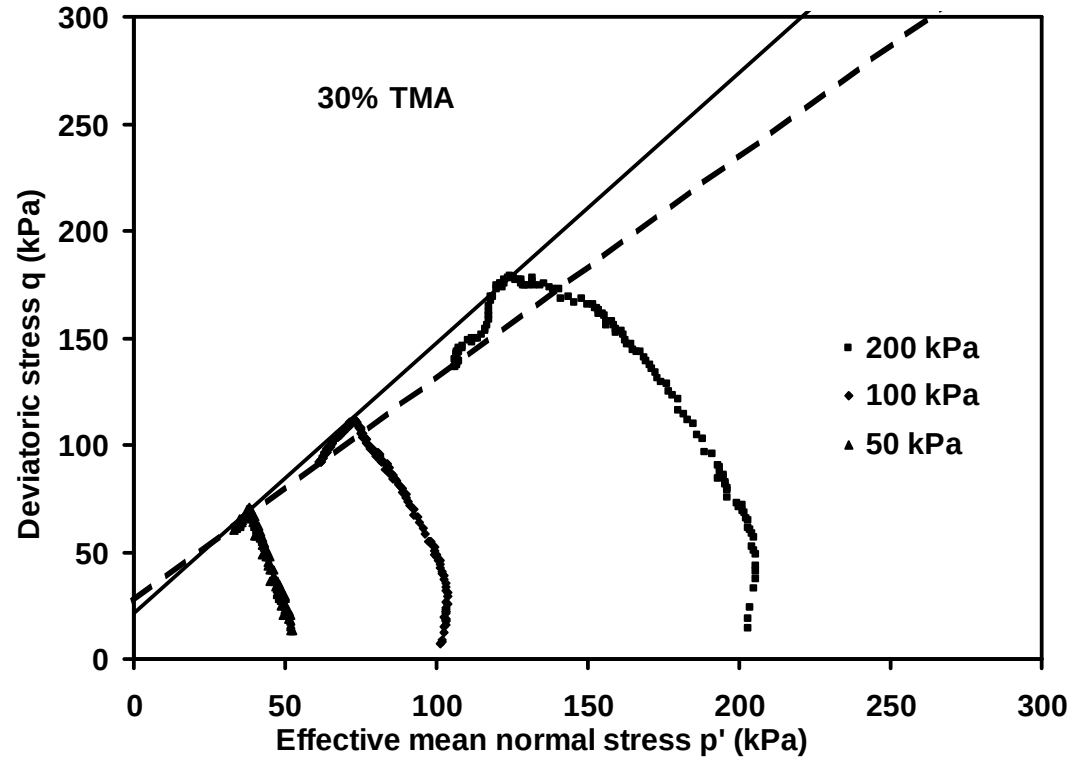

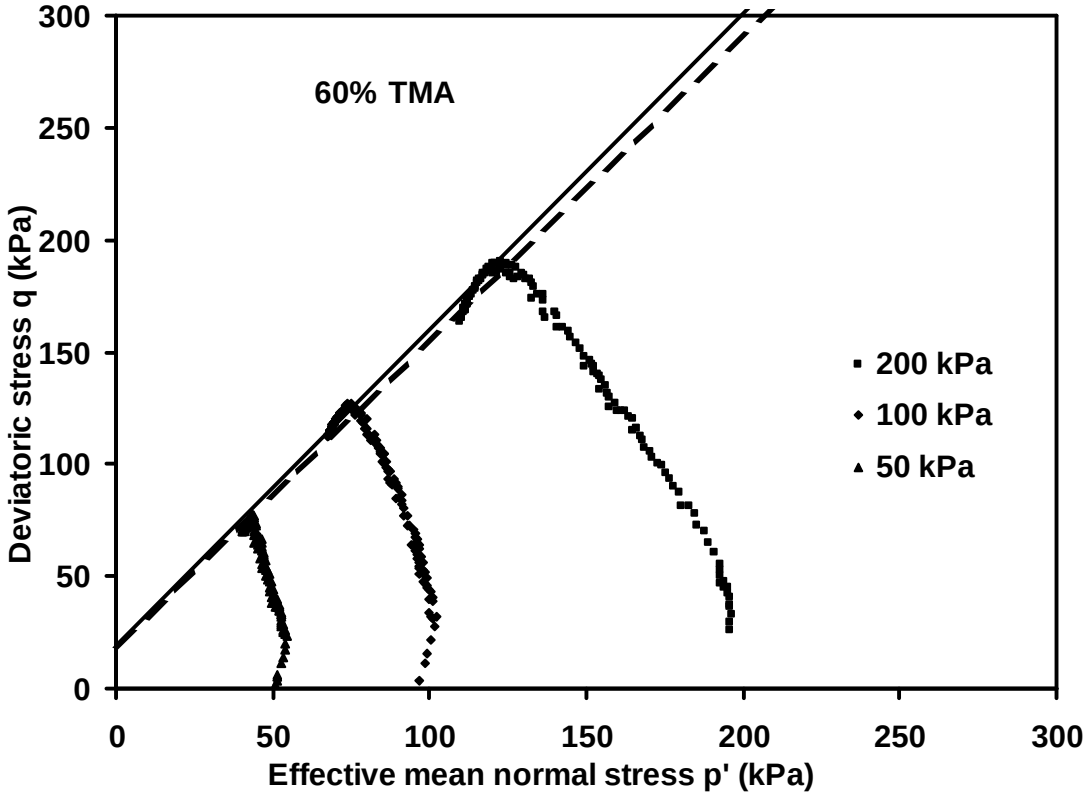

Figure 5-4. q-p' diagrams for TMA clay: a) 30% TMA; b) 60% TMA; c) 100% TMA.

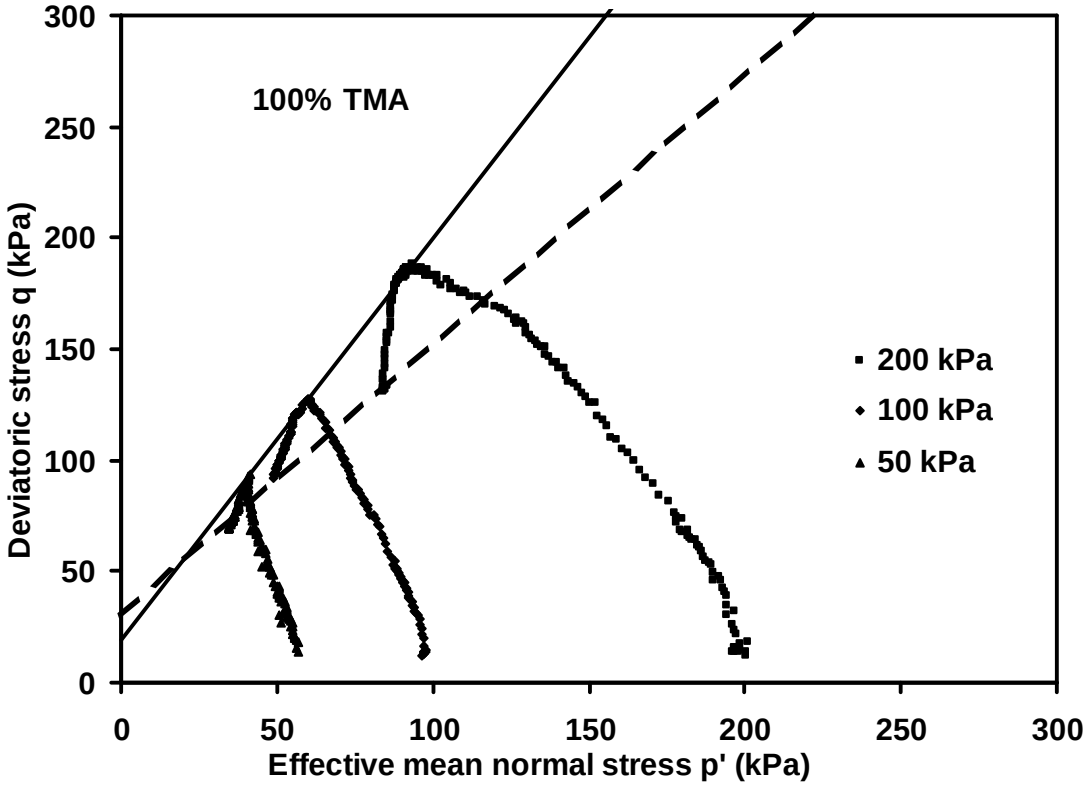

Figure 5-4. q-p' diagrams for TMA clay: a) 30% TMA; b) 60% TMA; c) 100% TMA.

Increasing the size of cation on mineral surface

Results of the CU triaxial tests performed on clays that were synthesized by increasing the chain length on all four branches of the quaternary ammonium position also illustrated peak behavior with positive pore water pressure generation in all cases (Figure 5-3, Figure 5-5 and Figure 5-6). Comparing the data gathered for cations that had 1, 2, and 4 carbon chains in each of the four branches ($4C_1$, $4C_2$, and $4C_4$) resulted in increased critical state friction angle as the size of the cation was increased (Table 5-2 and Figure 5-7). The increase in friction angle that was measured as the branch size was increased was most significant between TMA ($4C_1$) and TEA ($4C_2$), with an increase from 30.4° to 40.7°, while the increase observed from TEA ($4C_2$) to TBA ($4C_4$) was

minor in comparison (40.7° to 41.1°) (Table 5-2). Critical state cohesion was also observed for the TEA and TBA cations, in the ranges of 17-19 kPa.

Increasing the tail length in one quaternary position

Increasing the length of the carbon tail produced pronounced peak behavior with positive pore water pressure, and resulted in the highest observed critical state friction angles in the study, with angles of 44.8° and 53.5° observed for DTMA and HDTMA, respectively (Figure 5-3, Figure 5-8 through Figure 5-10). DTMA also had the highest water content for the soils tested (Table 5-1). Cohesion intercepts of approximately 17 kPa were observed for DTMA and HDTMA.

Table 5-2. Summary of Triaxial Compression Friction Angles

Organic cations	**amount (% CEC)**	**ϕ'_{peak} (degrees)**	**y-intercept (kPa)**	**R^2 (-)**	**ϕ'_{crit} (degrees)**	**y-intercept (kPa)**	**R^2 (-)**
TMA, $4C_1$	30%	31.5	21.06	0.9995	26.3	27.27	0.9995
	60%	34.8	18.85	0.9957	33.9	17.08	0.9963
	100%	44.0	18.91	1.0000	30.4	30.02	0.9905
TEA, $4C_2$	100%	59.0	8.95	0.9946	40.7	16.75	0.9881
TBA, $4C_4$	100%	49.6	16.48	0.9854	41.1	19.29	0.9648
DTMA, $1C_{10}$	100%	59.2	29.96	0.9909	44.8	21.15	0.9933
HDTMA, $1C_{16}$	100%	81.9	3.50	0.9992	53.5	16.83	0.9881

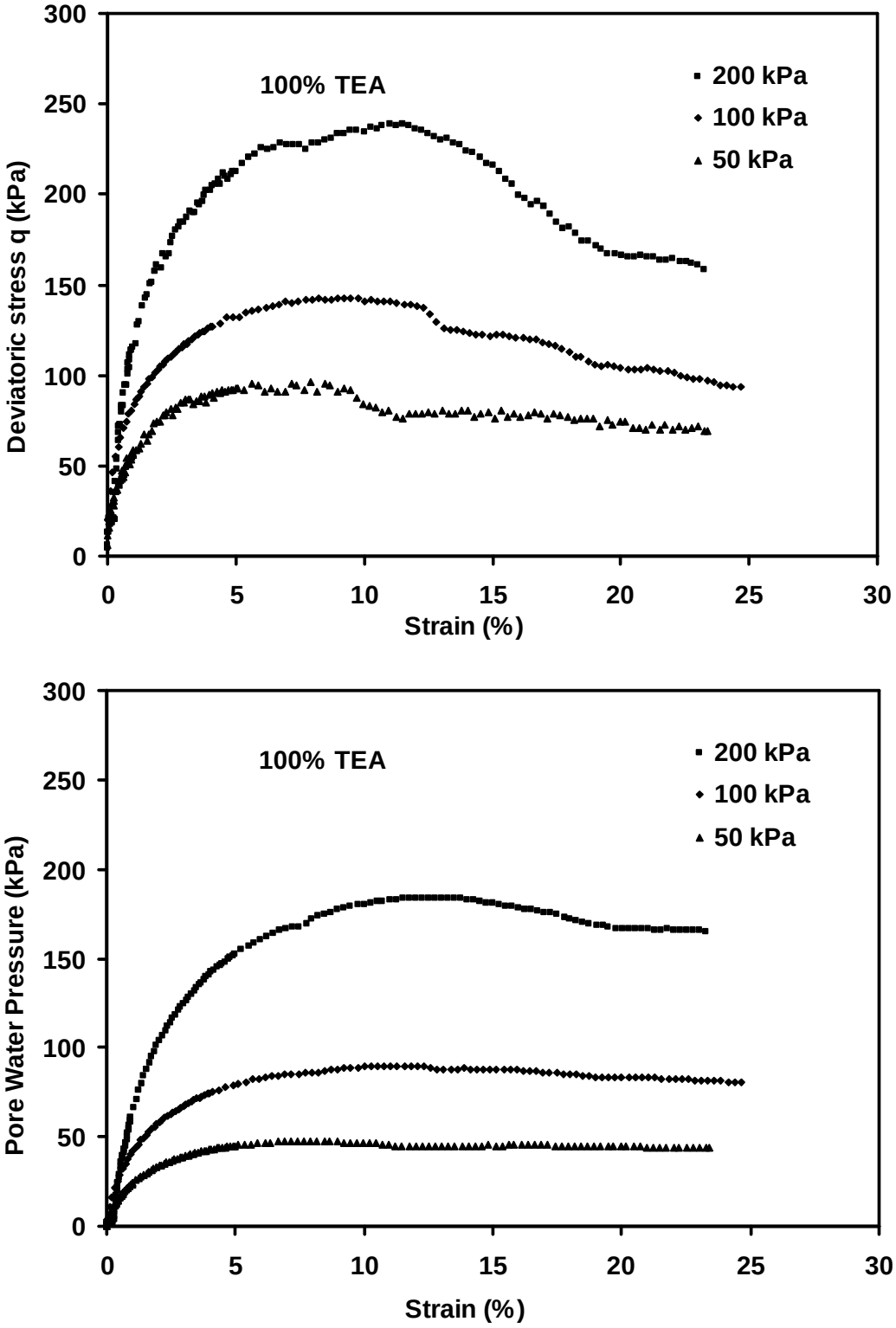

Figure 5-5. CU triaxial strength test results for 100% TEA: a) stress-strain diagrams; b) pore water pressure diagrams.

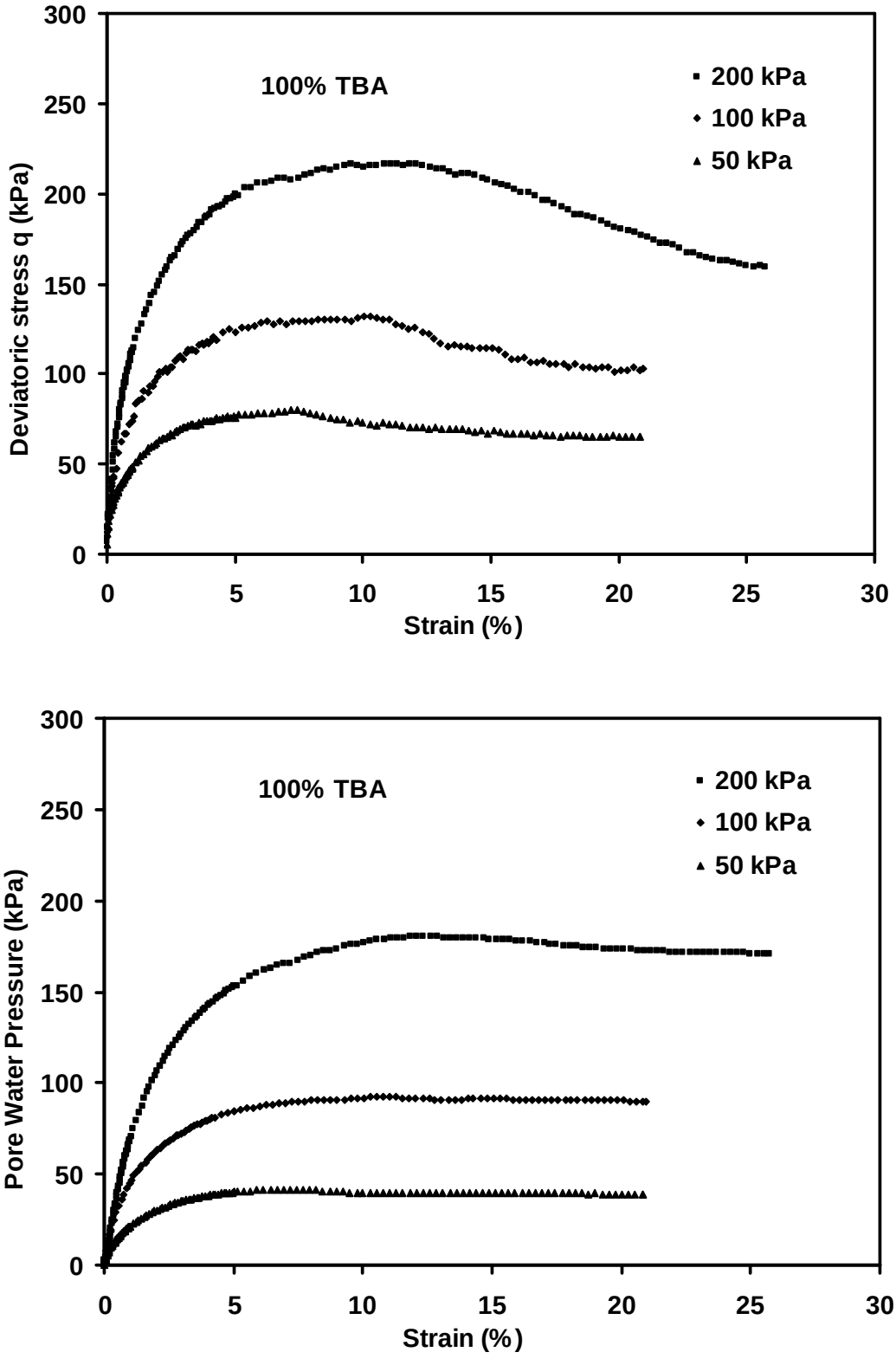

Figure 5-6. CU triaxial strength test results for 100% TBA: a) stress-strain diagrams; b) pore water pressure diagrams.

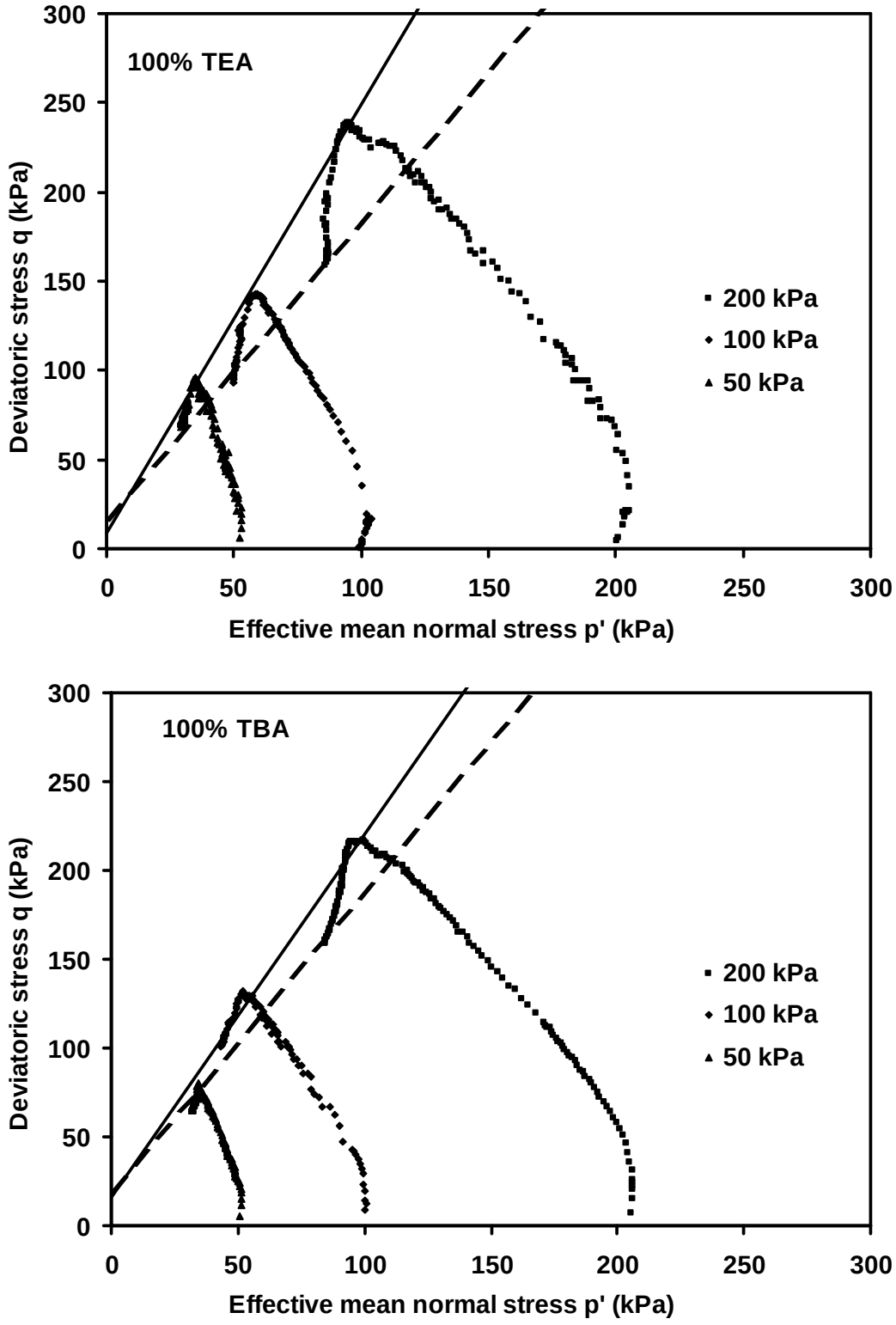

Figure 5-7. q-p' diagrams for TEA and TBA clay: a) 100% TEA; b) 100% TBA.

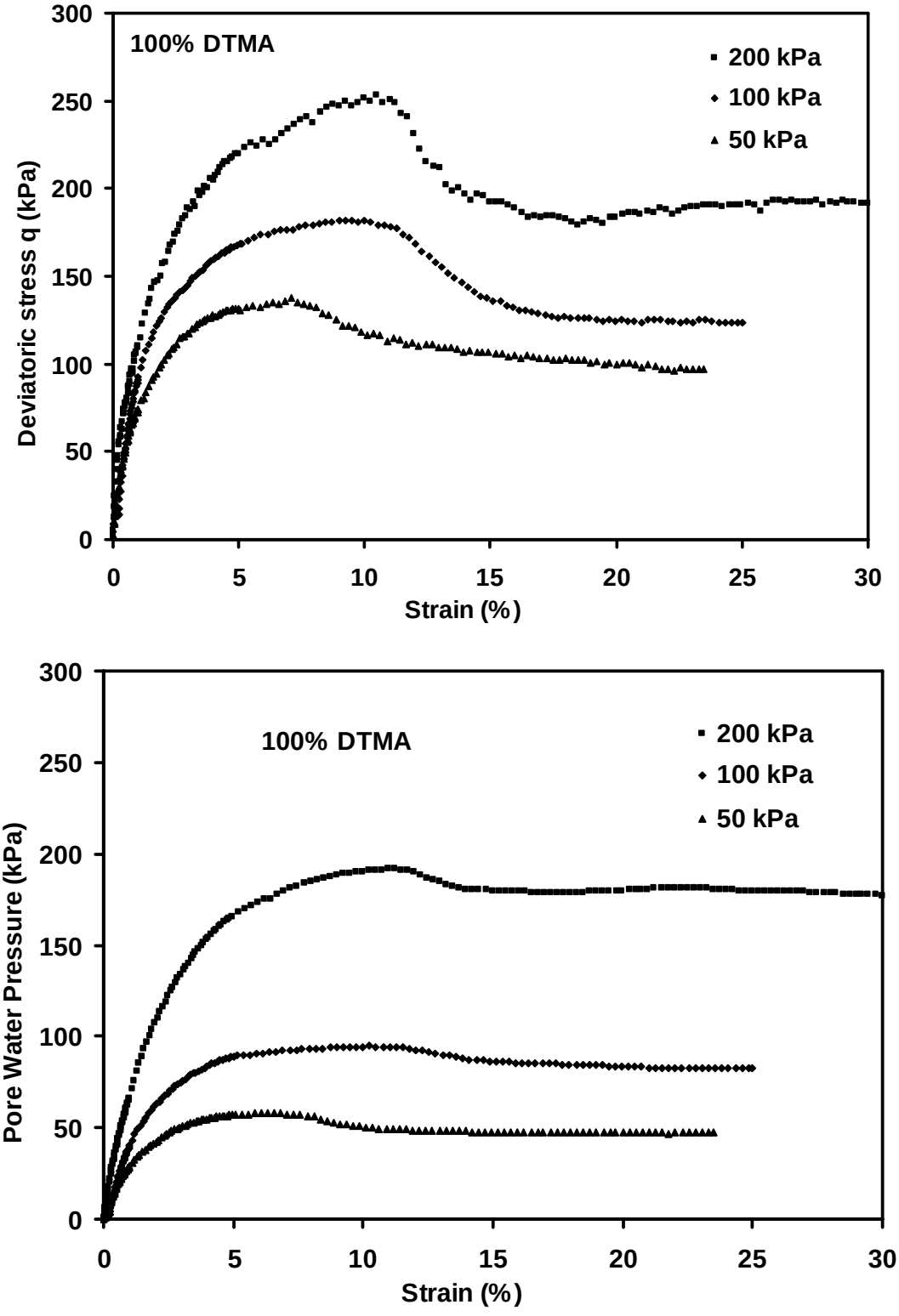

Figure 5-8. CU triaxial strength test results for 100% DTMA: a) stress-strain diagrams; b) pore water pressure diagrams.

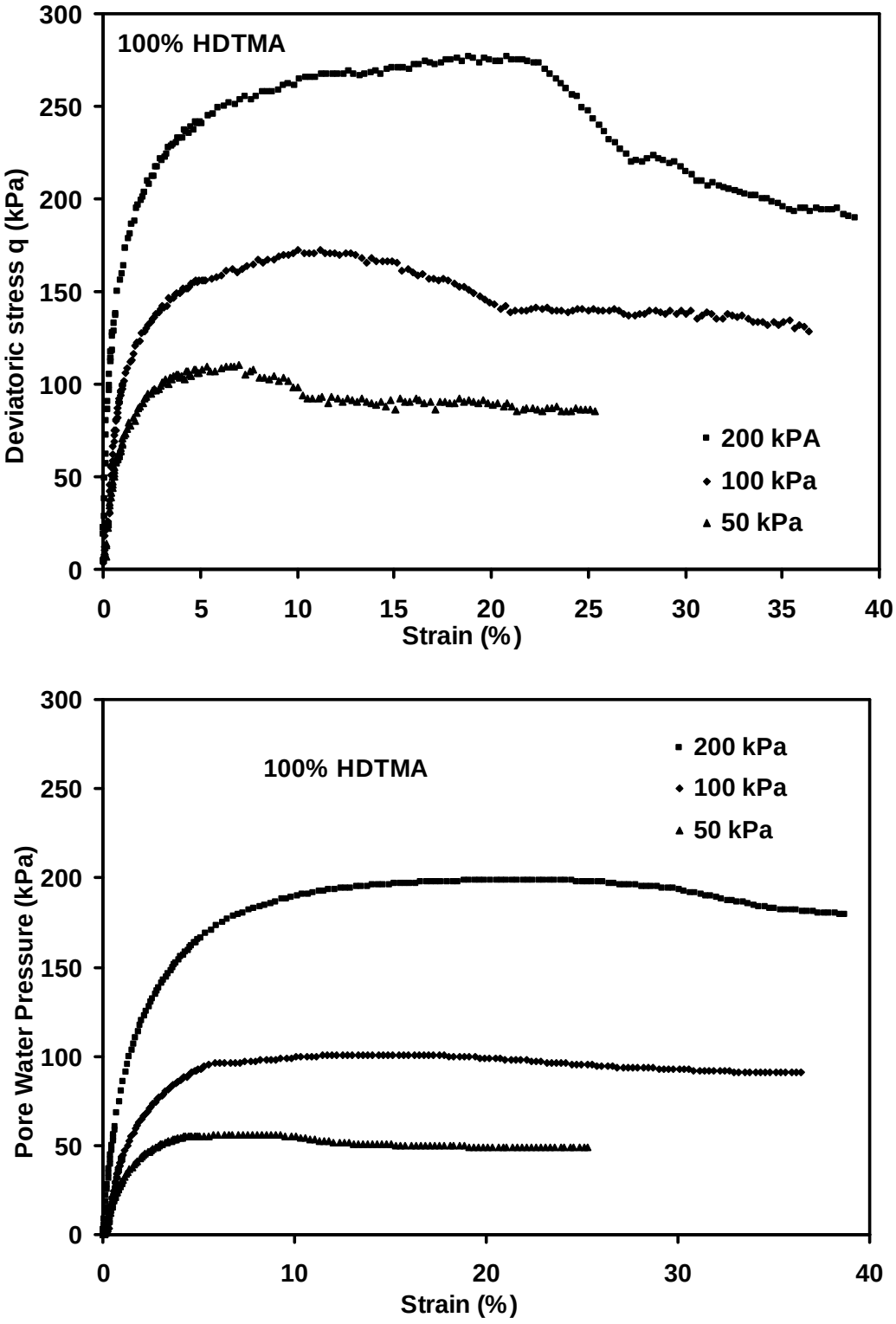

Figure 5-9. CU triaxial strength test results for 100% HDTMA: a) stress-strain diagrams; b) pore water pressure diagrams.

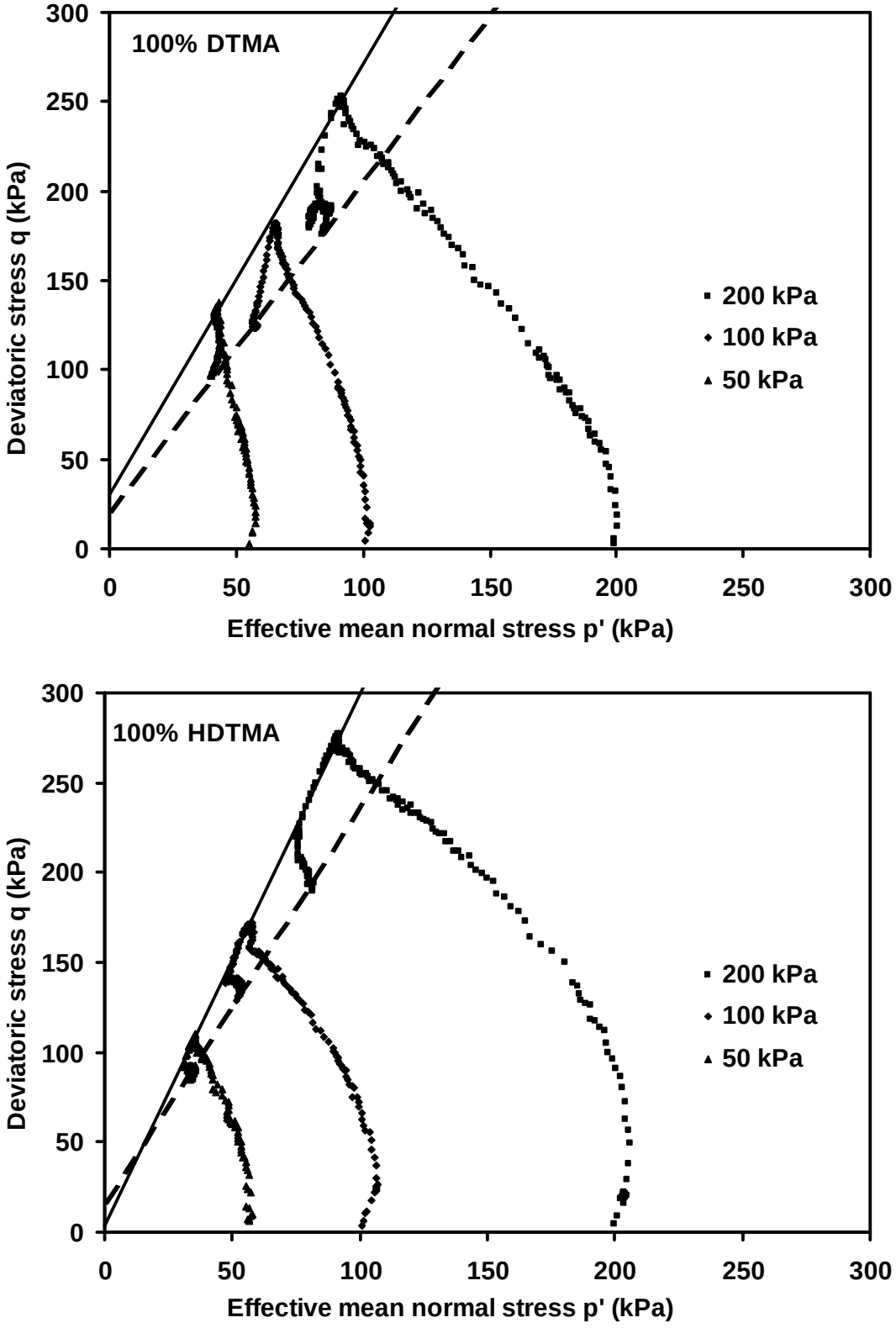

Figure 5-10. q-p' diagrams for DTMA and HDTMA clay: a) 100% DTMA; b) 100% HDTMA.

Normal consolidation line and critical state line

In addition, the normal consolidation line (NCL) and critical state line (CSL) of organobentonites in log p'-e space were plotted in Figure 5-11. Void ratios of organobentonites at different effective confining pressures formed linear normal consolidation lines for most of the organobentonites. Volume properties of different organobentonites were shown to be quite different even at the same confining pressure. Critical state lines were also linear for most of the organobentonites, which was in agreement with the critical state soil mechanics theory.

Increasing total organic carbon content

In all cases, increasing the organic cation loading on the mineral surface resulted in an increase in the effective stress friction angle (Table 5-2, Figure 5-12), with measured critical state friction angles for the nine organoclays tested ranging from 26^o to 54^o. The presence of the organic cation contributed to a strength mechanism that was substantially more significant than that observed for clays with inorganic cations (e.g., Na^+ or Ca^{2+}), where literature values reported for angles of internal friction of calcium and sodium montmorillonite are typically less than 20^o (Mesri and Olson, 1970). Most importantly, the friction angle increased as the total organic carbon sorbed to the mineral surface was increased, a trend which held true for cases of increasing cation size (all four branches), as well as increasing tail length (in one branch only) (Figure 5-13 through Figure 5-15).

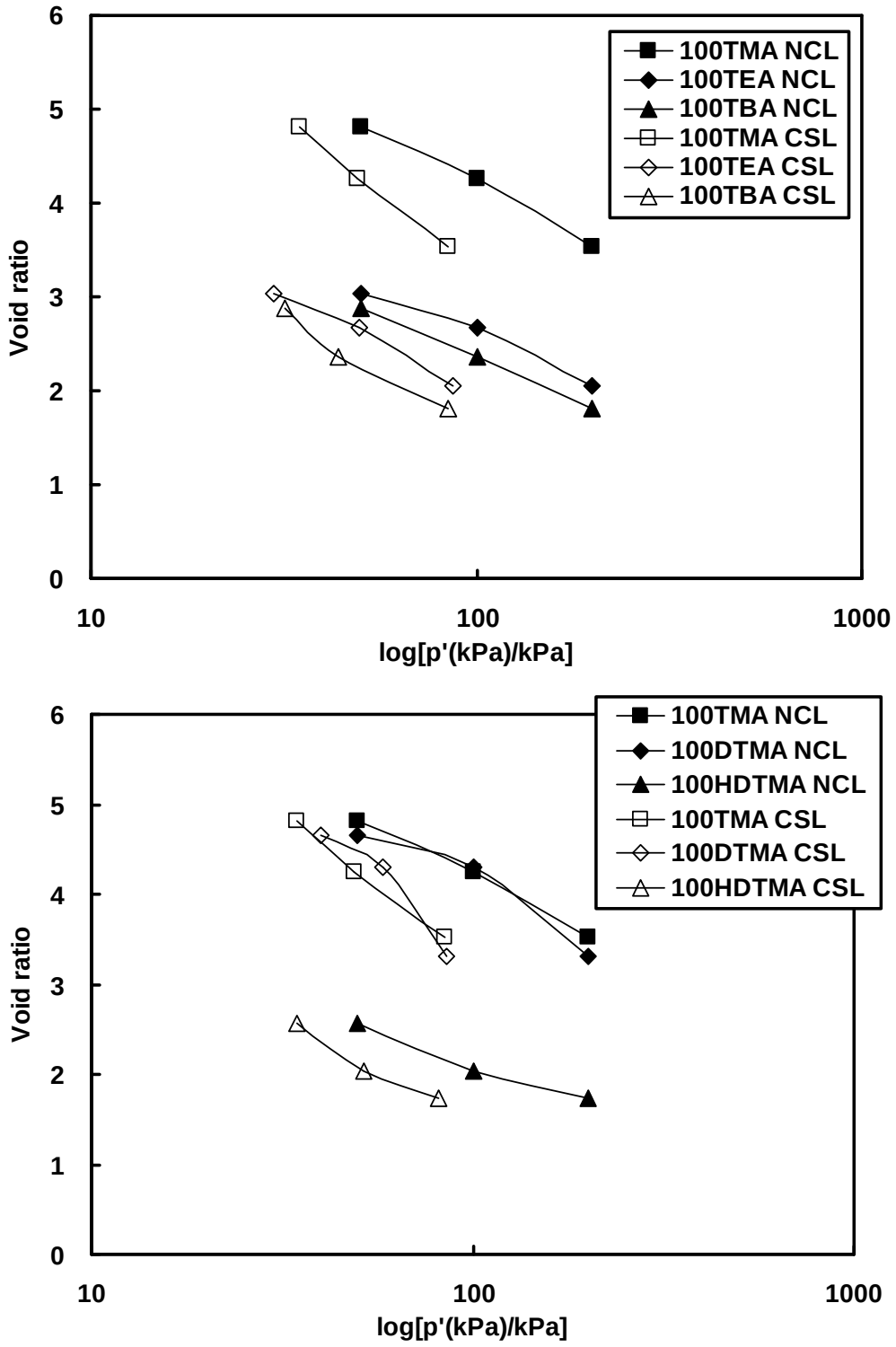

Figure 5-11. Normal consolidation lines (NCLs) and critical state lines (CSLs) for organobentonites.

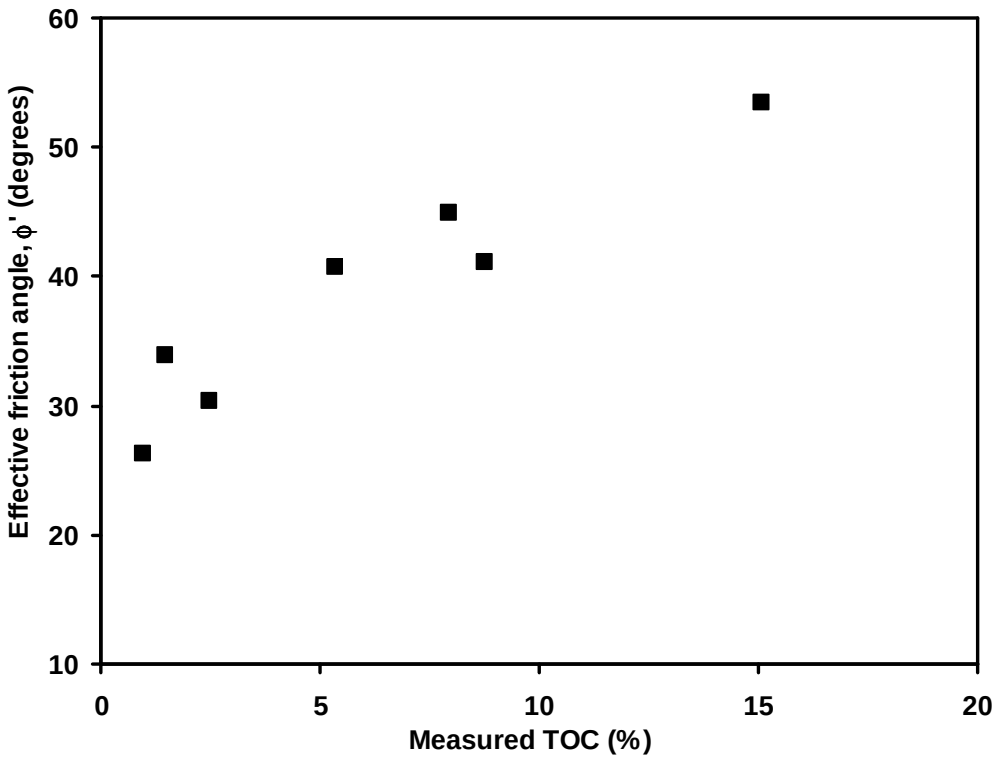

Figure 5-12. Effective stress friction angle for tested organoclays as a function of measured total organic carbon.

The following general conclusions can be drawn regarding the stress strain behavior of the organoclays: 1) All clays tested exhibited peak strength, even though the samples were normally or lightly over-consolidated. Also noted was that the peak was reached faster (i.e., at smaller strains) at low effective confining pressures than at high effective confining pressures; 2) The tests were performed to a minimum of 20% strain so that all tests reached a plateau state in both strength and pore water pressure at large strains (typically larger than 20%) after a peak deviatoric strength. This plateau state was considered to be at or approximate to the critical state of the soil, and the critical state friction angle was determined accordingly; 3) Positive pore water pressure was generated throughout the duration of shearing, and the pore water pressure dropped after the peak

strength in most of the clays, except for 30% and 60% TMA-bentonites; 4) The predominant mode of failure in the testing program was shear banding, with displacement along the failure surface; 5) Also notable was the presence of an intercept in the q-p' diagrams. In all cases, the q-p' diagram had an intercept on the y-axis, indicating either: critical state was not achieved at the strains tested, or bonding between the organic molecules recovered during prolonged shear.

Discussion

In all cases, the peak and critical state friction angles measured for the organic exchanged clays were higher than the friction angle of 16° reported for unmodified montmorillonite in similar effective confining pressure range (Mesri and Olson, 1970). Exchanging organics on to the surface of the clay mineral resulted in alteration of multiple strength mechanisms on the clay surface, including reduction in the water content, alteration of the interfacial electrostatic regime between the clay particles, and physical interaction of the organic molecules that were exchanged onto the clay surface.

It is well known that natural montmorillonite is prone to swelling when soaked in aqueous solutions, due to its relatively high surface charge and the polar nature of water. At typical values of groundwater pH, the particles are negatively charged, and repel each other due to the coulomb electrical force developed in aqueous solutions. The repulsive force is so dominant that the water content of a montmorillonite slurry can easily exceed 1000%. In cases where the pore fluid has a low ionic strength, the thickness of the diffuse electrical double layer of bentonite plates will be large, but will compress as the ionic strength of the pore fluid is increased. Exchange of organic cations into the interlayer space significantly alters the character of the diffuse double layer in the montmorillonite.

Unlike inorganic cations, the organic cations have an uncharged hydrophobic component in addition to the region of positive charge, which is centered on the ammonium head group. The concentration of carbon and hydrogen atoms results in a hydrophobic driving force that leads to preferential attraction to the particle surface, when compared to inorganic cations, due to hydrophobic expulsion from water. This phenomenon is clearly reflected in the measured values of zeta potential, which yielded a less negative zeta potential as the organic content was increased, indicating that more of the positive charge was bound within the shear plane of the particle (Bate and Burns, 2010). Comparison with the measured data from the zeta potential test are useful as zeta potential is a measure of the colloidal stability of a suspension, with a zeta potential close to zero indicating a high tendency to coagulation, and a zeta potential diverging from zero (either positive of negative), indicating a tendency of particles to remain in suspension; consequently, zeta potential can be used as a surrogate for the repulsion between the particles. Ultimately, the strong attraction of the organic cations to the particle surfaces resulted in an interlayer organic matter phase, which reduced the sorbed water in the interlayer of the particle. This reduction was clearly reflected in the water contents of the organoclays which were measured after slurry consolidation at 100 kPa, ranging from 136% to 228%. While these water contents were relatively higher than a natural soil, they were much lower than would be observed for a pure unmodified montmorillonite sample prepared using equivalent methods. While the decreased water content can be used in part to explain the higher strength measured for organoclays than that for unmodified montmorillonite, it is important to note that there was no correlation between the final water content and CS friction angle within the tested organoclays.

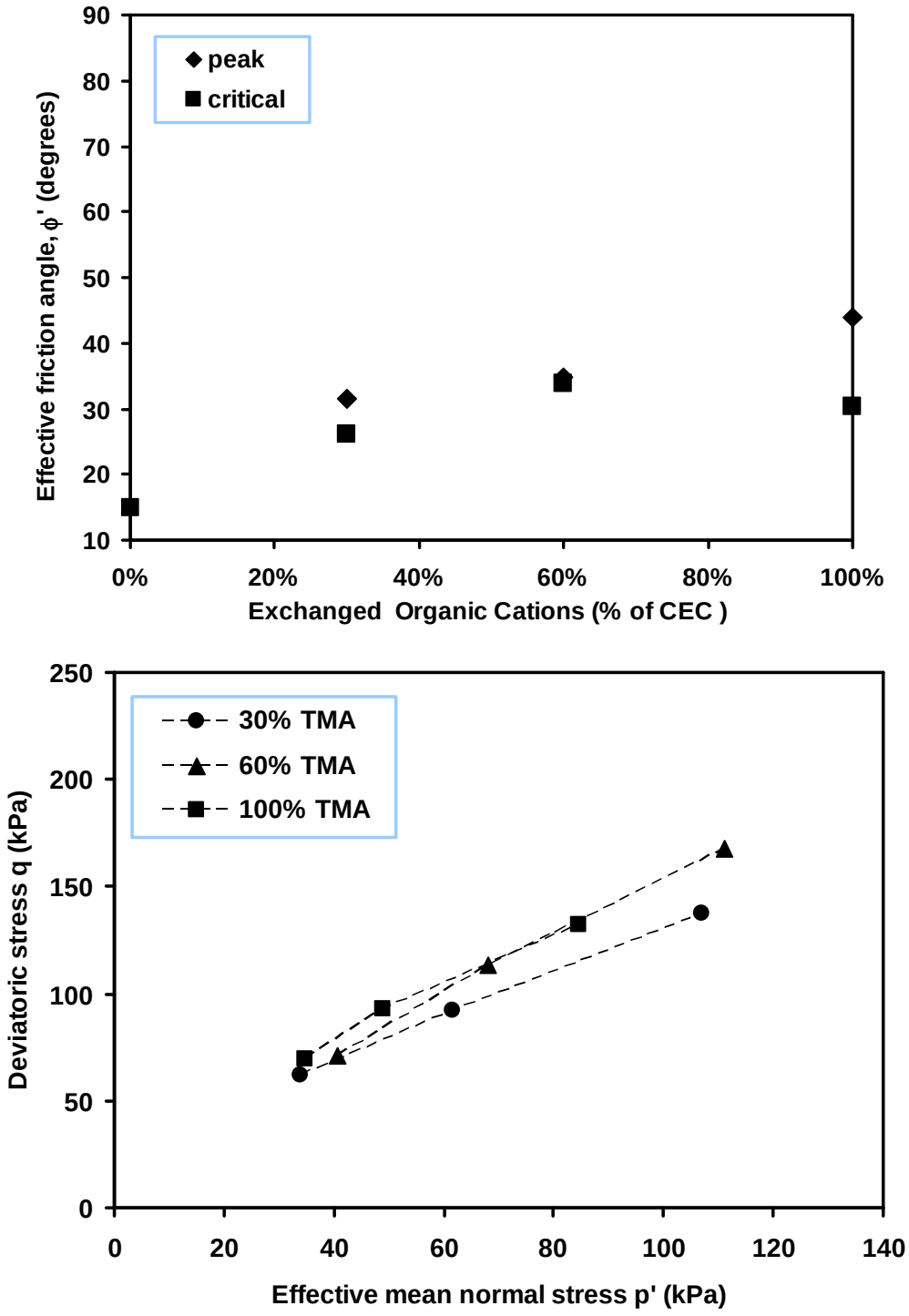

Figure 5-13. Comparison of strength behavior as the density of organic coating was increased for 30% TMA, 60% TMA, and 100% TMA: a) Effective stress friction angle as a function of percent exchanged cations. Data for montmorillonite from Mesri and Olson (1970); b) Deviatoric stress as a function of effective mean normal stress.

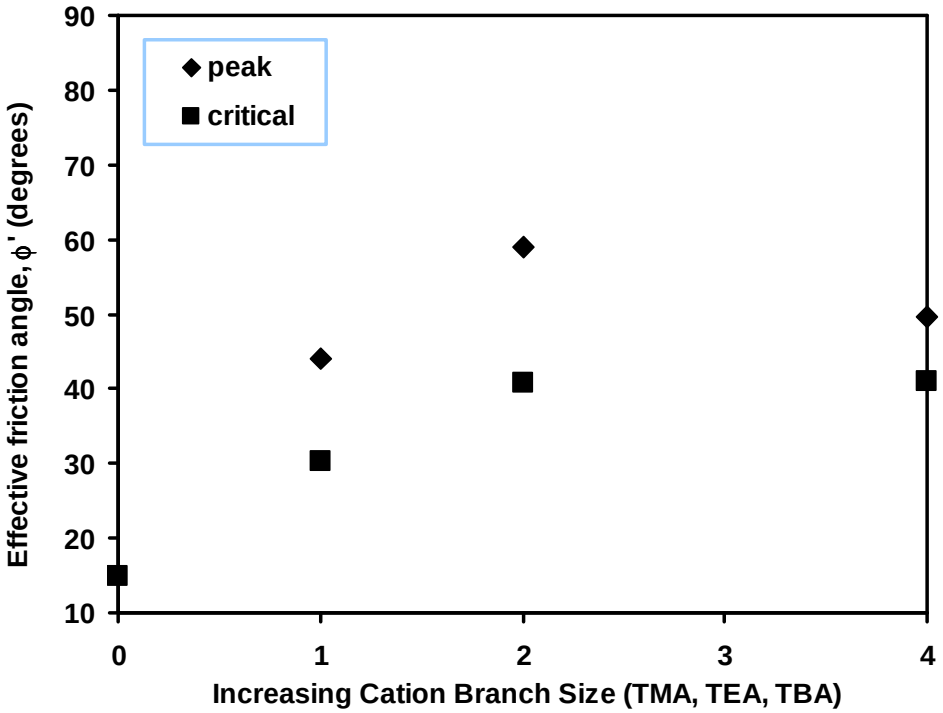

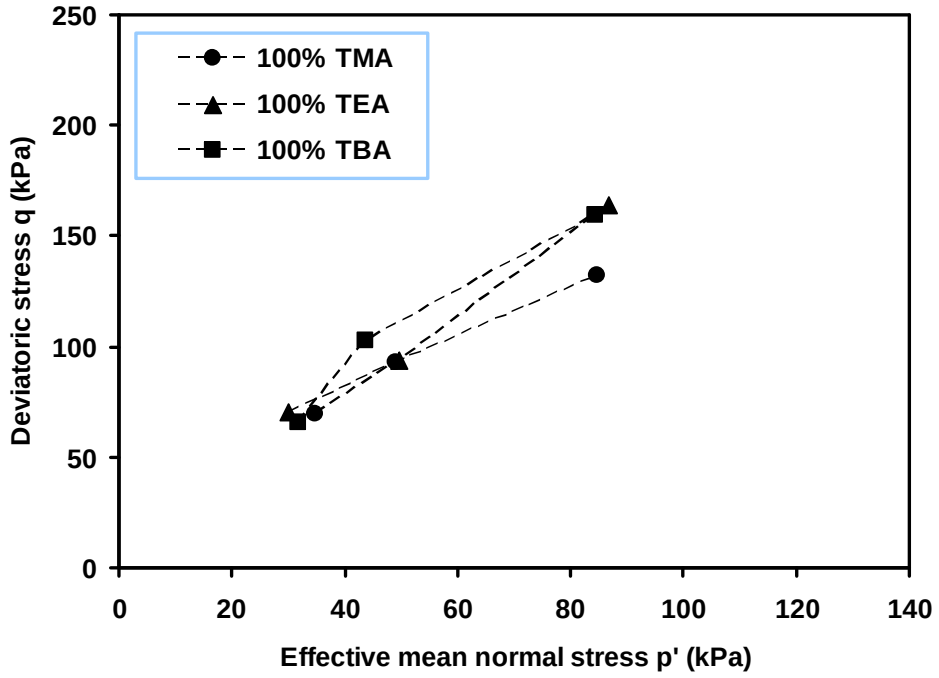

Figure 5-14. Comparison of strength behavior as the branch size of the organic cation was increased for 100% TMA, 100% TEA, and 100% TBA: a) Effective stress friction angle as a function of increasing branch size. Data for montmorillonite from Mesri and Olson (1970); b) Deviatoric stress as a function of effective mean normal stress.

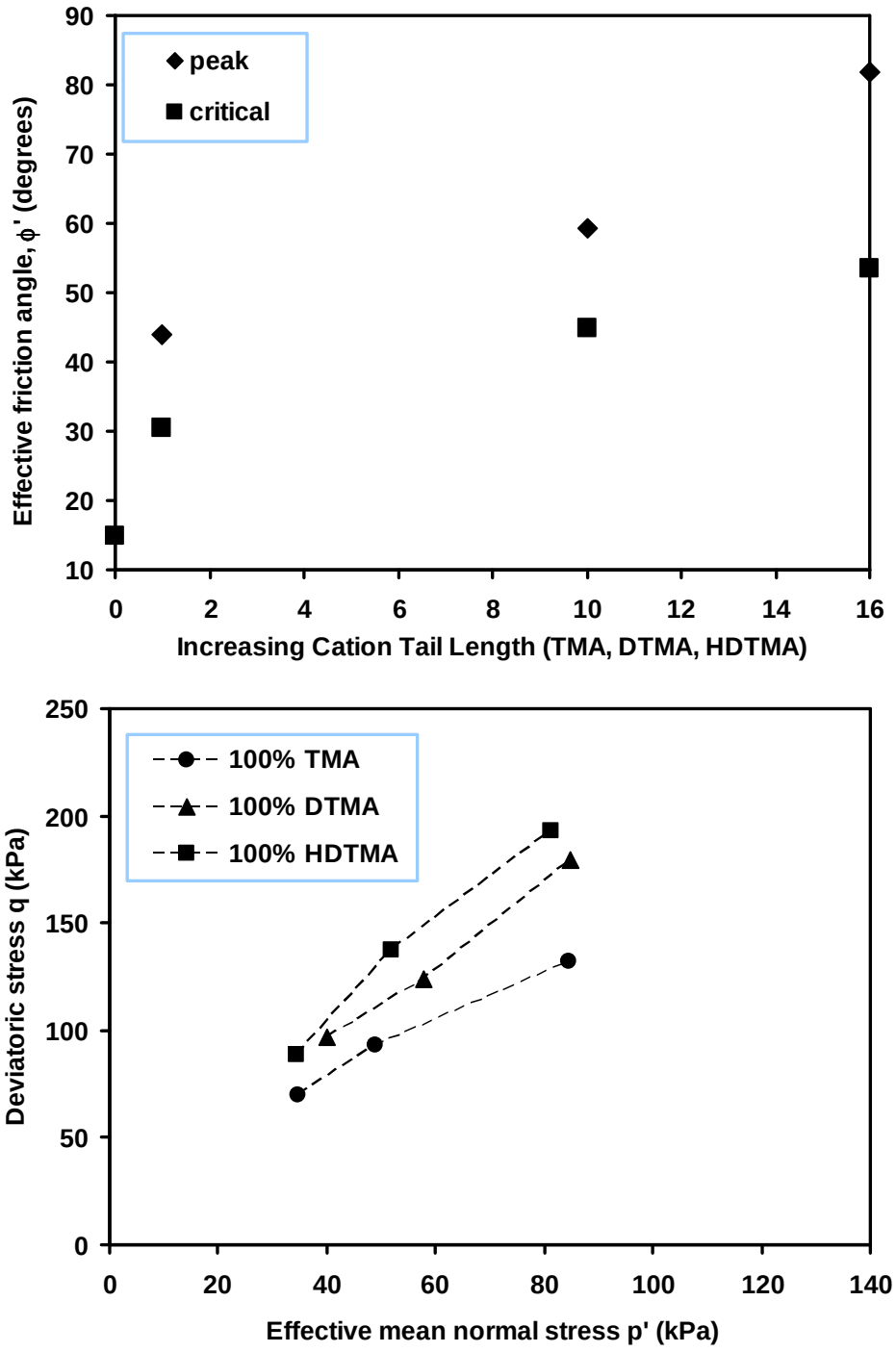

Figure 5-15. Comparison of strength behavior as the tail length of the organic cation was increased for 100% TMA, 100% DTMA, and 100% HDTMA: a) Effective stress friction angle as a function of increasing tail length. Data for montmorillonite from Mesri and Olson (1970); b) Deviatoric stress as a function of effective mean normal stress.

In addition to the lowered water content, the presence of the organic cations on the mineral surfaces resulted in a more effective shielding of the charge on the particle surface. The organic cations were anchored to the particle surfaces, with relatively little mobility (Bate and Burns, 2010), and resulted in less negative net surface charge. Measurement of the zeta potential indicated that the structure of the organic cation was important to the magnitude of the neutralization, with one long chain organic cations (DTMA and HDTMA) more effectively countering the negative surface charge of the particle, when compared to the cations with increased carbon atoms in each of the four chains (TEA and TBA) (Bate and Burns, 2010).

Additionally, the arrangement of the organic cations on the particle surface will also contribute to the measured friction. The size of the organic cations was much larger than the inorganic cations, and yet the measured basal spacing for the modified clays increased only on the order of 50%. Molecular dynamics simulations have suggested that on the particle level, the chains of the organic cations are entangled, leading to a contribution to the friction interaction at the particle surface. Depending on the loading level of the organic cation, the cations will arrange in single, bi layer, or paraffin structure, and the cations will interact laterally through hydrophobic mechanisms.

Conceptually, the previously described mechanisms will contribute to the measured frictional strength in different relative proportions, depending on the concentration and structure of the organic present on the clay surface. The critical state strength measured for TMA modified clay ranged between 26° and 34° degrees, with the maximum strength recorded at 60% CEC (Figure 5-13). The zeta potential data illustrated that the amount of charge bound within the shear plane was relatively insensitive to the

increased exchange percentage for TMA. While the zeta potential measured for 30%TMA, 60%TMA, and 100%TMA was higher than that measured for unmodified montmorillonite (~ -41mV), it was relatively constant with organic content, (~ -32 mV). Essentially, a relatively small and constant number of organic cations were retained within the shear plane of TMA clay, even as the organic loading was increased, resulting in cation interactions on the particle surface that did not change significantly with increasing organic carbon content, as was reflected in both the CS friction angle and the zeta potential.

Increasing the branch size of the exchanged organic cations (TMA to TEA to TBA), resulted in an increase in the critical state friction angle of approximately 10° as the cation was changed from TMA to TEA, but no substantial change as the cation size was increased to TBA (Figure 5-14). Again, measured zeta potential showed a less negative value as the total organic carbon was increased (TMA to TEA to TBA), or as the branch size of each of the four quaternary ammonium chain was increased. However, CS friction angle did not reflect as significant an increase in the transition from TEA to TBA, as was observed in the zeta potential measurements.

Finally, increasing the length of one chain on the quaternary ammonium cation resulted in a significant increase in the critical state friction angle for DTMA (45°) and HDTMA (53°), as compared with TMA (30°) (Figure 5-15). For the long chain organic cations, the interparticle repulsion was at its lowest point (least negative zeta potential), and the global friction angle also reflected the highest measured CS friction angles.

Conclusions

This study investigated the stress-strain behavior of TMA quaternary ammonium cations exchanged bentonite at 30%, 60%, and 100%, and TEA, TBA, DTMA, and HDTMA quaternary ammonium cations exchanged bentonite at 100% of the clay's CEC using consolidated undrained triaxial tests. It was found that: (1) quaternary ammonium cation modified bentonites had higher shear strength than the unmodified bentonite; (2) as the TMA cation loading was increased, the critical state effective friction angle increased; (3) normally to lightly-overconsolidated modified organoclays displayed peak behavior in the stress-strain curves, coupled with positive pore water pressures throughout the duration of shearing; (4) as the size, i.e. the carbon number on all four branches of QACs, was increased, the friction angle increased; and (5) as the length of a carbon chain was increased to 10 (DTMA, $1C_{10}$), the friction angle increased; however, further increase of the carbon chain to 16 (HDTMA, $1C_{16}$) resulted in a decrease in the frictional interaction.

Chapter 6 Dynamic Properties of Organobentonites

Introduction

The dynamic response of soils is an important engineering property, especially for soils with high organic contents because these soils often underlay critical support structures such as highway bridges or levees. Consequently, the initial tangent shear modulus (G_{max}), secant shear modulus ratio (G/G_{max}), and damping ratio (D) are important parameters in evaluating the dynamic soil behavior for soils subjected to earthquake, wind, waves, traffic, and equipment vibration.

Even at very low levels of strain, soil is a nonlinear and inelastic material (Santamarina et al., 2001); at very small strain, the soil stiffness (or the shear modulus) is maximum and is known as the initial tangent shear modulus, G_{max}. G_{max} has been extensively studied for a variety of soils, and the primary influencing soil parameters are void ratio, overconsolidation ratio (OCR), plasticity index, and confining stress (Dobry and Vucetic, 1987; Li et al., 1993). Assuming all other conditions are equal, G_{max} increases with confining stress, OCR, and strain rate, and is inversely related to void ratio and the number of loading cycles (Dobry and Vucetic, 1987).

Under repeated dynamic loading, the stiffness or shear modulus of a soil will decrease, and it is common practice to use the secant shear modulus, G, to characterize the modulus reduction. The ratio of secant shear modulus to initial tangent shear modulus, G/G_{max}, is widely used to quantify the small strain stiffness of geomaterials. The shape of G/G_{max} curve, or shear modulus reduction curve, can depend on plasticity index, confining pressure, void ratio, OCR, number of loading cycles, geologic age, and

cementation (Dobry and Vucetic 1987), with plasticity index being a primary factor (Vucetic and Dobry, 1991). The inelastic behavior of soil can also be measured by the equivalent damping ratio, D, which is a measure of the hysteretic dissipation of energy. Assuming other conditions are equal, damping ratio will increase as cyclic strain is increased, and as confining stress, void ratio, and plasticity index are decreased.

The small strain dynamic soil response can be separated by two threshold cyclic shear strains (Vucetic, 1994). The linear cyclic threshold shear strain γ_t^l corresponds to the onset of shear modulus reduction, and therefore separates linear and non-linear responses. In the very small strain region, $\gamma \leq \gamma_t^l$, the response is linear but inelastic since energy dissipation is observed (Kramer, 1996; Lo Presti et al., 1997). Linear cyclic threshold shear strains for medium plasticity, fine-grained soils is on the order of 10^{-4} (Li et al., 1993; Vucetic, 1994), and it has been observed that increasing natural organic content increases γ_t^l (Kallioglou et al., 2009). The second threshold is the volumetric threshold shear strain γ_t^v, which corresponds to the beginning of irrecoverable volume change in drained condition or excess pore-water pressure in undrained conditions. In the small strain region, $\gamma_t^l < \gamma \leq \gamma_t^v$, the response is both non-linear and inelastic; however, the material properties do not change significantly with increasing shear strain, or with increasing number of loading cycles. The volumetric threshold shear strain for normally consolidated, highly plasticity clays is on the order of 10^{-3} (Vucetic and Dobry, 1991). Microscopically, γ_t^v corresponded to the sliding of the particle contacts and permanent particle reorientation (Kramer, 1996). At intermediate strain region, $\gamma_t^v < \gamma$, irrecoverable microstructural changes will occur (Vucetic, 1994), and the soil properties will decrease

with both cyclic shear strain and the number of loadings. Both γ_t^l and γ_t^v are stress/strain-path and mean effective confining stress dependent. Increasing confining stress leads to increasing both γ_t^l and γ_t^v (Ishihara, 1996).

In recent years, an increasing amount of attention has been given to organic soils. The magnitude of G_{max} for clay type geomaterials varied from 1 kPa for Na-montmorillonite slurry to 10,000 MPa for intact shale (Santagata, 2008). While the magnitude of G_{max} for organic-containing cohesive soils was in the range from 1 to 100 MPa. The organic compounds were in the form of highly fibrous, semidecomposed, or amorphous. It was reported that organic content will decrease the initial tangent shear modulus (Kallioglou et al., 2009; Kishida et al., 2009).

Several fundamental studies on the dynamic response of either peat or high organic content soils include soil beneath a levee in the Sacramento-San Joaquin Delta in California (Boulanger et al., 1998; Wehling et al., 2003), from the undeveloped Mercer Slough in Bellevue, Washington (Kramer, 2000), from Union Bay in Seattle, Washington (Seed and Idriss, 1970), and from the Queensboro Bridge in New York (Stokoe et al., 1994). For the sake of simplicity, the soils investigated in these studies will be referred to as peat, even though in some cases, it may be more technically correct to refer to them as high organic. In examination of earthquake motions recorded at Union Bay in Seattle, Seed and Idriss (Seed and Idriss, 1970) estimated damping ratios for peat that were approximately three times larger than the damping ratios for the clay at the site, and were also more nonlinear than the damping ratios for the clays at the site. Resonant column experiments on the peat specimens from the Queensboro Bridge reported that for the range of cyclic shear amplitudes tested (up to approximately 1%, at confining pressures

ranging from 7 kPa to 303 kPa), the peat exhibited essentially linear behavior with low damping (Stokoe et al., 1994). Resonant column tests on the Mercer Slough peat presented significant nonlinearity at low consolidation stresses, which decreased as the confining pressure was increased (Kramer, 2000). Cyclic triaxial tests on a peat from the Sherman Island levee illustrated that the normalized secant shear modulus and equivalent damping ratio versus cyclic shear strain amplitude were a function of the consolidation stress up to a critical value, demonstrating increasing linearity up to approximately 40 kPa (Boulanger et al., 1998; Wehling et al., 2003).

In this chapter, these dynamic properties of organobentonites were quantified experimentally using resonant column and bender element tests. The results from this study were evaluated in terms of the effect of shear strain, organic content, void ratio, and plasticity index. The organobentonites tested in this study were formed with an organic phase that was controlled in terms of structure and density of loading. While a degree of representativeness is sacrificed in the creation of a controlled organic phase on the soil surface, it was advantageous because it facilitated a controlled study of the effect of the structure and density of organic loading on the dynamic behavior of the soil.

Materials and Methods

Organobentonite specimens were prepared by 1-D slurry consolidation method, as described in Chapter 2. In summary, organobentonite slurry was incrementally loaded in a consolidation cell of 10.2 cm (4 in) in diameter and 45.7 cm (18 in) in height. Filter paper (P5, Fisher Scientific) and a geotextile were used to provide drainage from the top and the bottom of the cell, and the vertical load was applied to the slurry using a Load Trac testing systems (Geotac, Texas, USA). Loading/unloading was applied in the

following sequence: 3.5, 7, 14, 28, 50, 100, 50, 28, 14, 7, and 3.5 kPa, while deformations were recorded by the accompanying software Sigma-ICON (Geotac, Texas, USA). After end of primary consolidation of each loading step, the next loading step was applied. Six organobentonites were prepared for testing in both the resonant column and with bender elements: 100TMA, 100TEA, 100TBA, 100DTMA, 60HDTMA, and 100HDTMA, which were chosen to test the effect of increasing cation size, tail length, and density of coverage. After consolidation was completed, the specimens were extruded, and trimmed to final heights ranging from 13.2-16.5 cm (5.2 in – 6.5 in), with a diameter of 7.1 cm (2.8 in) for the resonant column test, and samples were trimmed to a diameter of 10.25 cm (4 in) and height of 6.14 cm (2.4 in) for the bender element tests.

A Stokoe-type resonant column test device used in this study was described in detail by (Meng, 2003) and (Valdes, 1999) (Figure 6-1). A brief summary of the setup is given below. The RC testing device composed of four major parts, i.e. the drive system, the motion detection device, the pressure chamber, and the vibration reduction platform (Figure 6-1). A cylindrical soil specimen was mounted on the base pedestal of the chamber, and the top cap was placed on top of the soil sample. The bottom of the specimen was assumed to be fixed, and the cap was a free-end. Both the base pedestal and the cap were corrugated, forming non-slip interfaces. A membrane and o-rings were used to seal the specimen. A drive plate (spider) with four arms was bolted to the top cap. At the end of each arm was a magnet, which was excited by the solenoids placed around it. Input signal to the solenoid was generated by the source channel of a Hewlett Packard 3562A dynamic signal analyzer and passed through a voltage-to-current converter. Current-mode source, implemented via this voltage-to-current converter, was capable of

reducing equipment-generated damping by over three orders of magnitude compared to a conventional voltage-mode source (Meng, 2003). A Columbia Research Model 3026 accelerometer was placed on one arm of the spider to detect the motion, and a counter weight was placed on the arm on the opposing side. Model 4102M charge amplifier was used for the accelerometer. The specimen and the drive and detect systems were enclosed in the air-tight pressure chamcber. Additionally, a pressure chamber was placed on the Nano-K^{TM} "BISCUIT" vibration isolator platform (Model No. 150BM-1, Minus K technology, Inc. Inglewood, CA) to minimize the vibrations caused by ambient noise. After placement of the sample, an isotropic air pressure of 50 kPa was applied to the specimen, and a minimum time of 24 hours was allowed for consolidation of the specimen.

Torsional excitations with frequencies ranging from 30 Hz to 100 Hz were applied to the soil specimen, and the response of the soil column was recorded by the accelerometer. Resonant (or maximum response) frequency (f_r) was achieved within the applied range, typically within 20 – 65 Hz for the organobentonites tested in this study. The shear modulus and damping ratio were determined from the resonant response of the specimen. One dimensional wave propagation theory of torsional waves in an infinitely long rod was used (Kramer, 1996):

$$\frac{J}{J_0} = \frac{\omega_r l}{V_s} \tan \frac{\omega_r l}{V_s} \qquad \textbf{Equation 6-1}$$

where J is the mass polar moment of inertia of the specimen, $J = \frac{1}{2} mR^2$, m and R are the mass and radius of the cylinder; J_0 is the mass polar moment of inertia of the drive system, J_0 = 0.003445758 kg.m^2 (Valdes, 1999), l is the length of the specimen, V_s is the

shear wave velocity, and $\omega_r = 2\pi f_r$ is the resonant circular frequency of the specimen and the drive system. By solving implicitly Equation 6-1, the shear wave velocity was calculated, and the shear modulus was then calculated by:

$$G = \rho V_s^2 \qquad \textbf{Equation 6-2}$$

where ρ is the mass density of the specimen.

The damping ratio was calculated using the half-power bandwidth method:

$$D = \frac{f_2 - f_1}{2 f_r} \quad \textbf{Equation 6-3}$$

where f_1, and f_2 are frequencies at the half-power points where $\gamma = 0.707\gamma_{\max}$.

For a solid cylindrical specimen, shear strain varied along the radial direction. An equivalent shear strain, γ_{eq}, was convenient in representing the magnitude of the strain. Equivalent shear strain can be expressed as:

$$\gamma_{eq} = r_{eq} \frac{\theta_{\max}}{l} \quad \textbf{Equation 6-4}$$

where $\theta_{\max}$ is the maximum rotation angle at the top of the specimen, $r_{eq} = 0.79\ r_0$ is the average motion radius, and r_0 is the radius of the specimen (Chen and Stokoe, 1979). The acceleration at the top perimeter of the specimen can be determined from measured acceleration from the accelerometer:

$$\ddot{\theta}_{\max} = a_{pk} \frac{r_0}{r_a} \quad \textbf{Equation 6-5}$$

where a_{pk} is the output of the accelerometer and r_a is the accelerometer motion radius. Then the maximum rotation angle $\theta_{\max}$ was obtained by integrating the acceleration twice:

$$\theta_{\max} = \frac{\ddot{\theta}}{\omega_r^2} \qquad \textbf{Equation 6-6}$$

By substituting Equation 6-6 into Equation 6-4, the equivalent shear strain can be calculated.

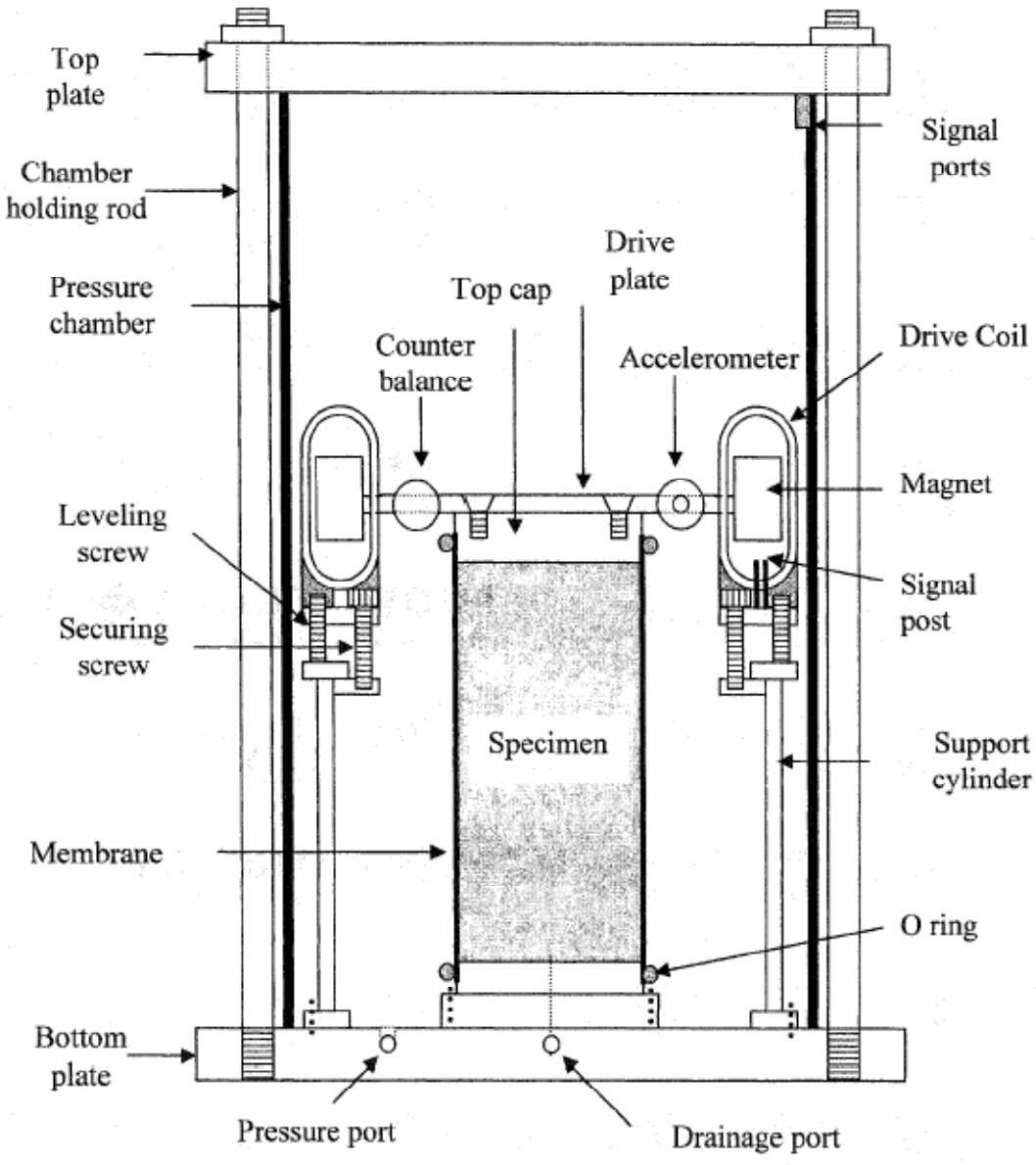

Figure 6-1. Stokoe fix-free type resonant column testing device (from Meng, 2003).

Bender element tests were performed in a modified oedometer cell, similar to that developed by (Lee and Santamarina, 2005), which was used to measure shear wave velocities across the organobentonite samples. Cell dimensions were 102.5 mm (4 in) in diameter and 80.3 mm (3.2 in) in height. BE dimensions were 10 mm (0.4 in) in length, 7 mm (0.28 in) in width, and 0.6 mm (0.02 in) in thickness, with extrusion length of 4 mm (0.16 in) from the cell. Parallel-type BE were used to minimize electronic coupling between source and receiver. The BE were coated with polyurethane, electrically shielded with conductive paint, grounded, anchored into nylon set screws, and connected to coaxial cables. Additional equipment included an Agilent 33210A Function/Arbitrary Wave Form Generator, a Filter/Signal Conditioner, and an Agilent DSO5014A oscilloscope.

Samples used in the bender element testing were prepared using the same one dimensional slurry consolidation procedure as used in the resonant column tests. The samples were trimmed and placed in the cell, and bender elements were installed on top and bottom of the soil samples. The soil sample was reconsolidation to a vertical stress of 100 kPa with a load increment ratio of 1, and the bender element test was performed after reconsolidation was completed.

Because increasing effective confining stress leads to larger soil stiffness, similar effective confining pressure should be selected for evaluation between the results of bender element and resonant column tests. The stress normal to the plane of particle movement and shear wave propagation had negligible effect on shear modulus (Ni, 1987); consequently, the mean effective stress was calculated by:

$$\sigma_m' = \frac{\sigma_v' + K_0 \times \sigma_v'}{2} (kPa) \qquad \textbf{Equation 6-7}$$

where K_0 is coefficient of lateral pressure and $\sigma_v' = 100kPa$. Assuming (Jaky, 1944):

$$K_0 = 1 - \sin\phi' \quad \textbf{Equation 6-8}$$

where ϕ' is the effective friction angle, yielded σ_m' between 57 to 77 kPa, assuming ϕ' = 27^o to 59^o (Table 6-1). Consequently, the resulting stress condition was similar for both testing scenarios.

In addition to the bender element and resonant column tests, results were compared to the secant shear modulus determined from undrained triaxial shear strength tests (Chapter 5), which were converted to G/G_{max} curves using G_{max} from the resonant column results. Two factors were considered when shear modulus results from triaxial tests and from resonant column tests were evaluated together: number of cycles, and loading rate. One factor was the number of cycles, N, at each strain level: N was one for triaxial tests, and five for resonant column tests. (Kim, 1991) and (Lo Presti et al., 1997) found that N had negligible influence on the modulus reduction curve until the strain became larger than the linear threshold strain. Given the small number of cycles for resonant column test (5), it is believed that the effect of number of cycles was minimal in this study. In terms of the loading rate used in the tests, the loading rate for triaxial tests was 0.5%/hr. Lo Presti et al. (1997) proposed an equation to calculate the strain rate of resonant column test:

$$\dot{\gamma} = 4 \times \gamma \times f(\%/s) \quad \textbf{Equation 6-9}$$

where γ is single amplitude strain (unit %, ranging from 2×10^{-5}% - 0.24%), and f is resonant frequency for RC tests (unit Hz, ranging from 20Hz – 65 Hz). Eq. 6.7 yielded strain rate value ranging from 20 – 70000 %/hr. Lo Presti et al. (1997) found that for clay secant shear modulus was very sensitive to strain rate, even at very small strains.

However, from their data, it was observed that below small strain level (~ 0.1%) the strain rate effect was not significant, and the coefficient of strain rate was less than 0.08%. In addition, Kim (1991) reported that the loading rate effect seemed to have no effect on secant modulus. The data in this study, such as those of 100TMA, 100TEA, and 30HDTMA bentonite, also presented a certain level of consistency between RC and triaxial tests. Therefore the results from resonant column tests were comparable to that from triaxial shear tests for most of the strain range (< 0.1%), if not the whole range.

Results and Discussions

Initial tangent shear modulus G_{max}

Resonant column test results of the measured values of the initial tangent shear modulus (G_{max}) for the seven tested organobentonites found that as the length of the single C-chain on one quaternary position increased (*$4C_1$* (TMA) to *$1C_{10}$* (DTMA) to *$1C_{16}$* (HDTMA)) and as the size of the organic cation was increased (*$4C_1$* (TMA) to *$4C_2$* (TEA) to and *$4C_4$* (TBA)), G_{max} increased (Table 6-1 and Figure 6-2). As shown in the zeta potential study (Chapter 4), increasing either the single C-chain length or the size of the organic cation sorbed to the bentonite surface decreased the net surface charge on the bentonite particles. Consequently, the repulsive force between bentonite particles decreased, allowing closer approach of particles and decreased void ratio with increasing organic carbon content, as the organobentonite slurry was formed. Given the same small strain, the increased contacts in the denser soils resulted in an increase in stiffness of the organobentonites (Figure 6-3), which is consistent with results in the literature, i.e. higher void ratio leads to lower G_{max} (Dobry and Vucetic, 1987). Comparing G_{max} as a function

of cation structure and organic carbon content, it is found that increasing a single C-chain length resulted in increased stiffness of organobentonites (e.g. TBA and DTMA have similar values of total organic carbon and stiffness, yet the void ratio of DTMA is almost twice that of TBA). On the other hand, 100% TBA bentonite and 100% HDTMA bentonite have similar void ratio. However the G_{max} of 100% HDTMA bentonite is much higher than that of 100% TBA bentonite (Figure 6-3). It is believed that the hydrophobic lateral interaction among the long tails of the organic cations on the clay surface contribute to the enhanced stiffness of organobentonites.

Table 6-1. Dynamic Properties of Tested Organobentonites

		Resonant Column		**Bender Element**	
Organoclay	**e**	**G_{max} (MPa)**	**V_s (m/s)**	**G_{max} (MPa)**	**V_s (m/s)**
100% TMA	5.4	4.4	58	5.1	61
100% DTMA	5.1	10.7	94	11.3	95
100% HDTMA	2.7	29.3	154	28.5	152
100% TEA	3.0	10.7	91	8.9	83
100% TBA	2.7	12.8	100	21.5	127
30% HDTMA	4.2	11.8	97	--	--
60% HDTMA	3.7	19.8	126	17.1	118

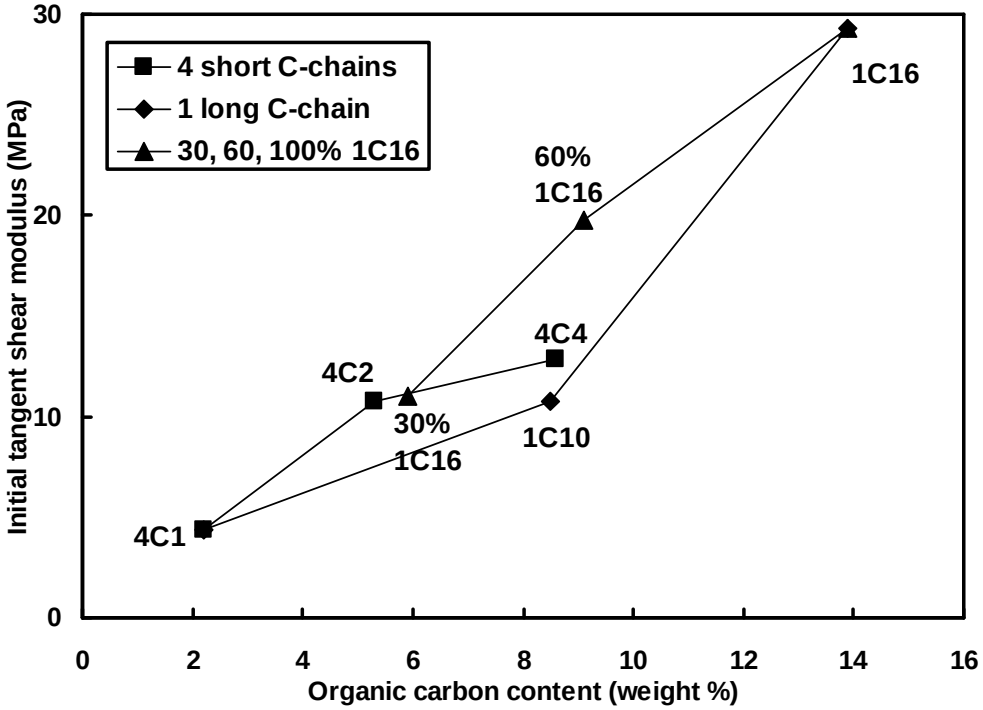

Figure 6-2. Initial tangent shear modulus vs. organic carbon content.

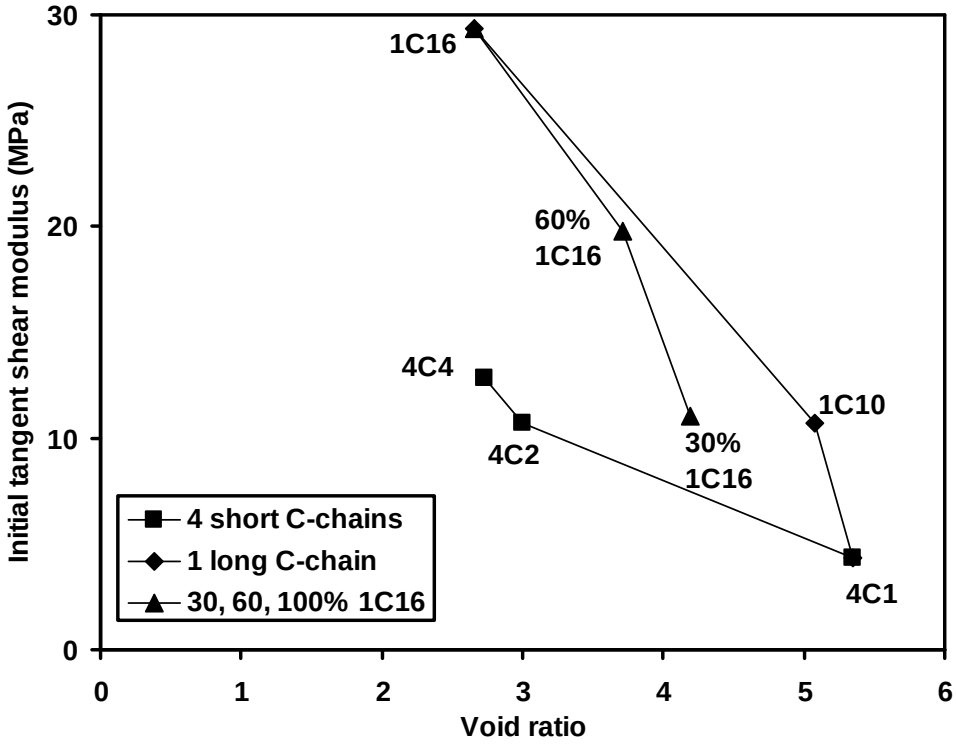

Figure 6-3. Initial tangent shear modulus vs. void ratio.

Another notable trend revealed that increasing the amount of HDTMA loading from 30% to 60% to 100% of the CEC of bentonite resulted in an increase of G_{max} which was almost linear as a function of either void ratio or organic carbon content. The addition of increasing mass of HDTMA cations on the particle surfaces results in cation arrangement that transitions from scattered distribution to more orderly monolayer arrangement of the cation tails on the particle surfaces (Zhang and Somasundaran, 2006). Typically, the organic cations tend to aggregate in clumps on the particle surface, which results in areas of high hydrophobicity mixed with hydrophilic charged portions of the particle surfaces. Because increasing the portions of the particles surfaces that were covered by the organic resulted in an almost linear inverse relationship between total organic carbon content and void ratio, the stiffness increased as the total organic carbon content increased. Simulation from molecular dynamics indicated that the head group of HDTMA cation was about one 3.5 angstrom away in distance from the clay surface (Liu et al., 2009).

In terms of the plasticity index, the value of G_{max} measured for the organobentonites did not show a clear trend (Figure 6-4). This agreed with the conclusion of Dobry and Vucetic (1987) which stated that the initial tangent shear modulus did not change with the plasticity index for normally consolidated soils, as were tested in this study; however, dependence of G_{max} on plasticity index was important for overconsolidated soils.

In addition to the data measured in the resonant column tests, the initial tangent shear modulus and shear wave velocity were also determined from bender element tests (Figure 6-5). For the most part, the results of the two tests agreed well, with the exception

of 100TBA organobentonite, which appeared uncharacteristically high in the bender element measurements. The strain level of the bender element test was approximately 10^{-3} %^{z} (Dyvik and Madshus, 1985), which was less than the linear threshold strain; consequently, the shear modulus from the bender element tests was considered to be the initial tangent shear modulus.

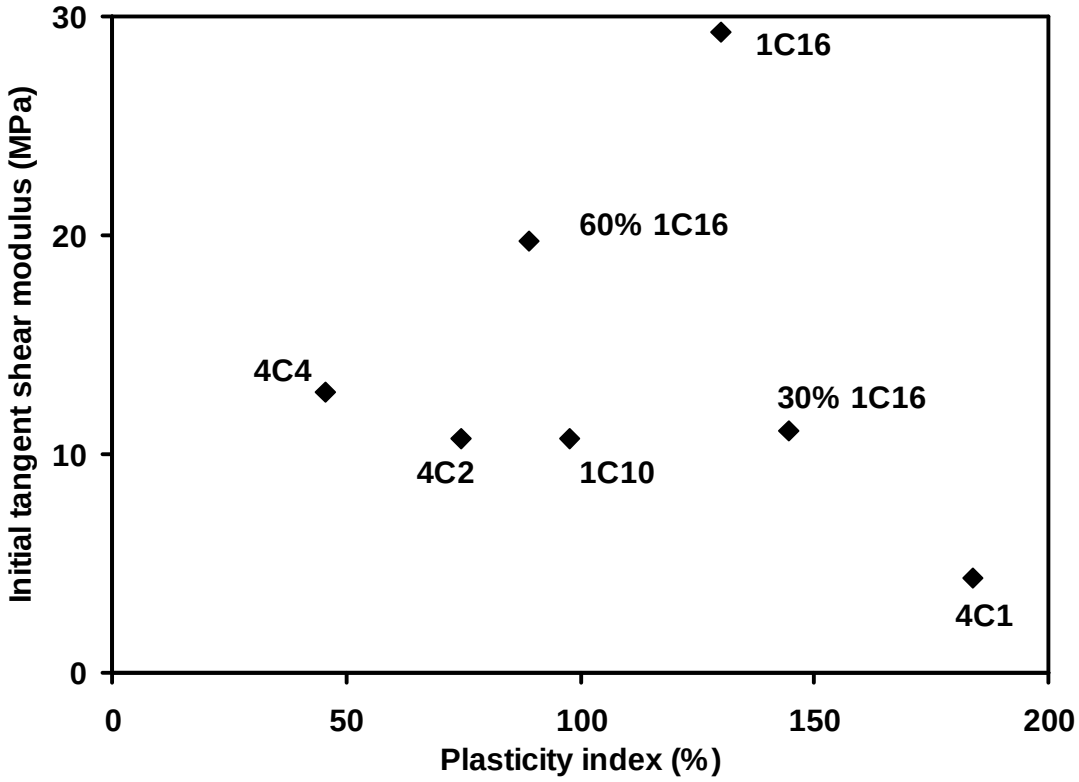

Figure 6-4. Initial tangent shear modulus vs. plasticity index.

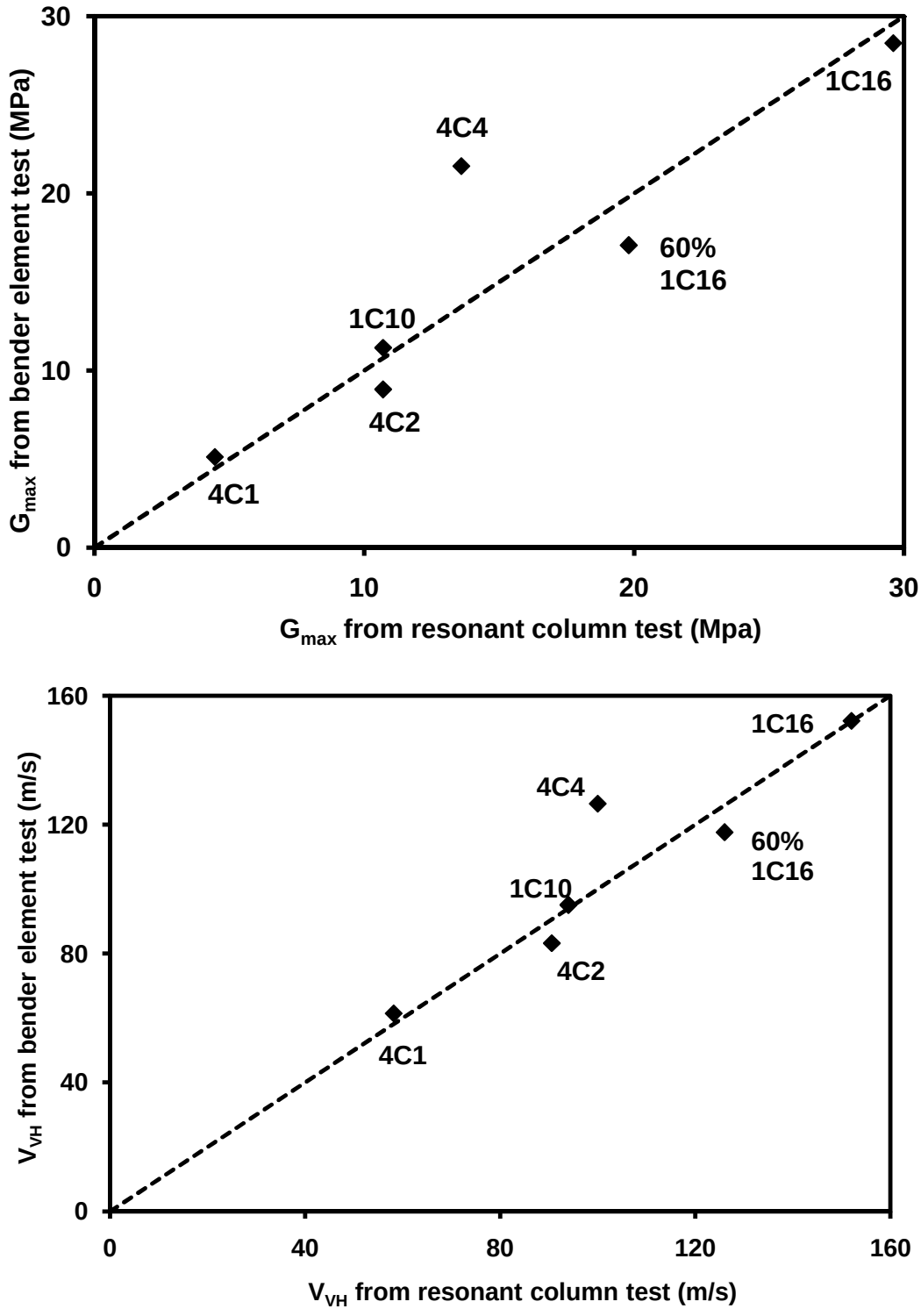

Figure 6-5. (a) Initial tangent shear modulus and (b) shear wave velocity comparison from bender element and resonant column tests.

Secant shear modulus reduction curves

Secant shear modulus reduction curves were obtained from resonant column tests of organobentonites and the results manifested that G/G_{max} decreased as strain increased for organobentonites with low organic carbon contents (T.O.C. < 8.5%, including 100TMA, 100TEA, 30HDTMA, and 100DTMA) (Figure 6-6). All four organobentonites with low organic contents illustrated approximately the same linear threshold strain at 0.024%. The elastic threshold strain for clays is normally approximately 0.01% (Li et al., 1993), demonstrating that the increased organic content increased the linear strain range of organobentonites. For organobentonites with high organic carbon contents (O.C. > 8.5%, including 100TBA, 60HDTMA, and 100HDTMA), reduction of shear modulus was not observed within the strain limit of resonant column device. The strain limit was lower for stiffer soils (soils with higher G_{max}), when equal amount of voltage excitation was applied to the electromagnetic solenoids of the resonant column device. Linear threshold strain for those high organic content organobentonites is expected to be larger than 0.024%.

The shear modulus reduction curves for 100TMA, 100TEA, 100DTMA, and 30HDTMA (low organic content organobentonites) were compared with the curves proposed by Vucetic and Dobry (1991) for soils with plasticity indices between 100 and 200 (Figure 6-6). The plasticity indices of these four soils were between 74 and 184. The shapes of shear modulus reduction curves of organobentonites were in reasonable agreement with non-organic soils that were summarized by Vucetic and Dobry (1991). It is noted that the size of exchanged organic cation had a measureable effect on the

reduction curve. The G/G_{max} curve of the smallest cation, TMA, comparing to larger cation, such as TEA, displayed larger reduction with strain.

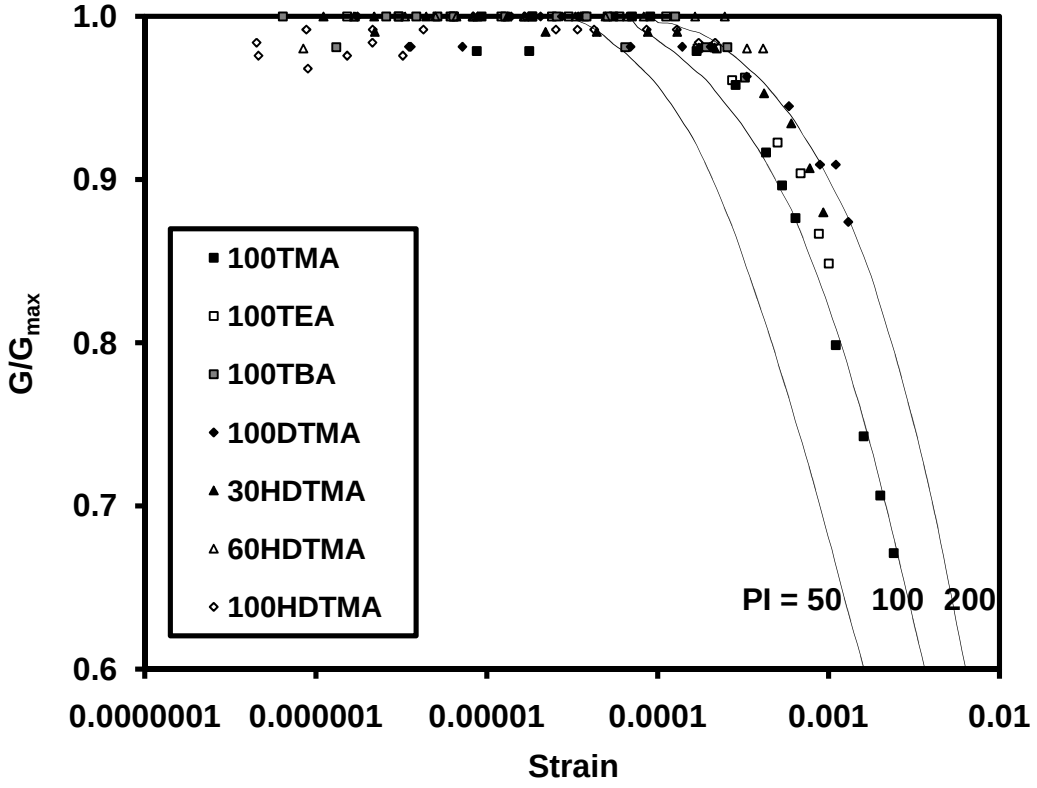

Figure 6-6. Secant shear modulus reduction curves for organobentonites. The curves were from Vucetic and Dobry (1991)

Secant shear modulus reduction curves with data combined from the resonant column and undrained triaxial shear strength tests (from 0.1% to critical state) (Chapter 5) are given in Figure 6-7. In contrast to the behavior at intermediate and large strain, G/G_{max} values were smaller as the organic carbon content increased, whether the increase was due to cation size (i.e., TMA, TEA, and TBA), increasing tail length (i.e., TMA, DTMA, and HDTMA), or increased surface coverage (i.e., 30% HDTMA, 60% HDTMA, or 100% HDTMA). These results indicated that the rate of reduction of secant shear

modulus increased as shear strain was increased and as total organic carbon was increased, regardless of the cation structure and density of loading.

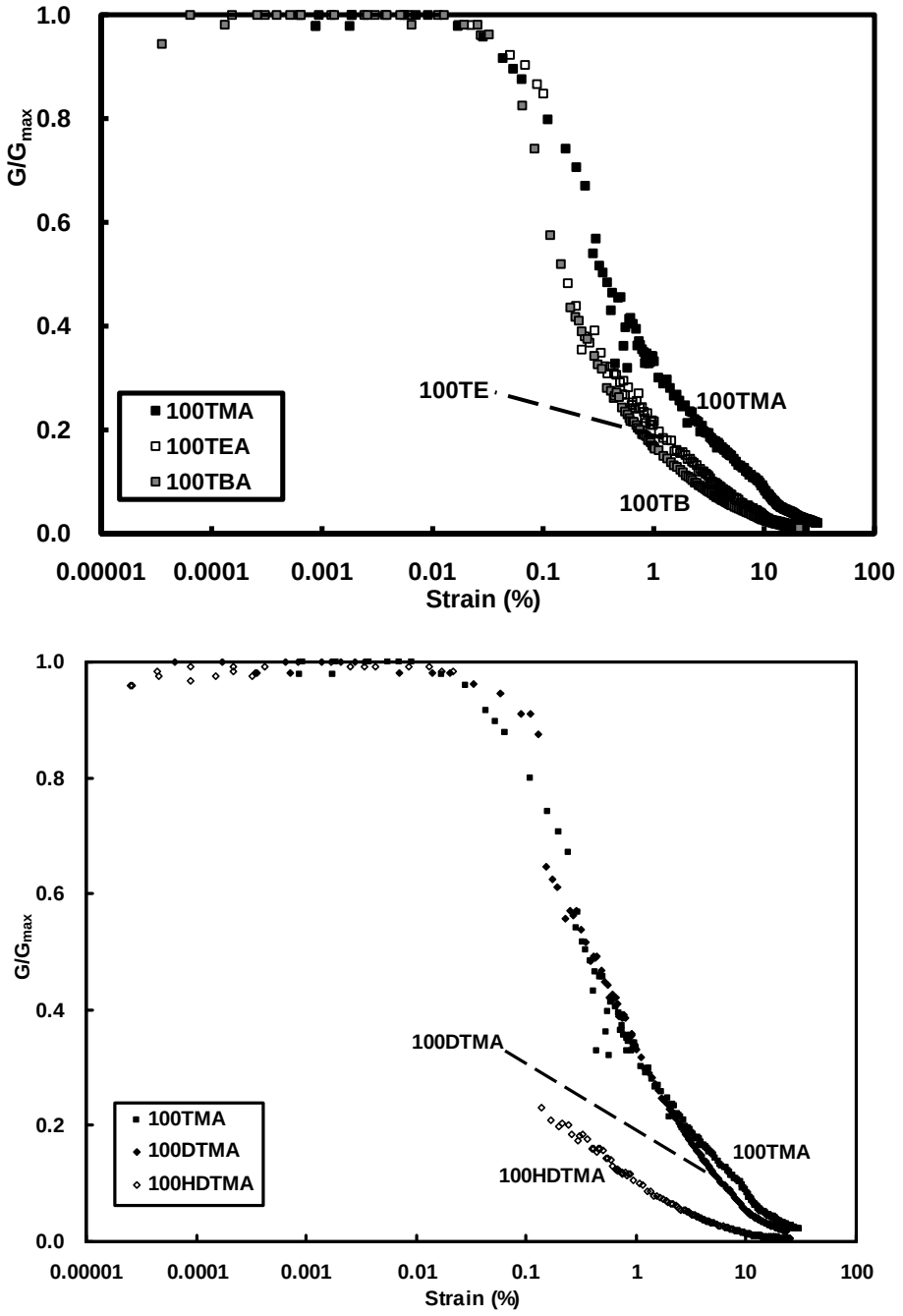

Figure 6-7. Combined secant shear modulus reduction curves from resonant column and triaxial shear tests for organobentonite with (a) 4 short C-chains QACs, (b) 1 long C-chain QACs, and (c) 30%, 60%, and 100% of CEC of HDTMA cations exchanged.

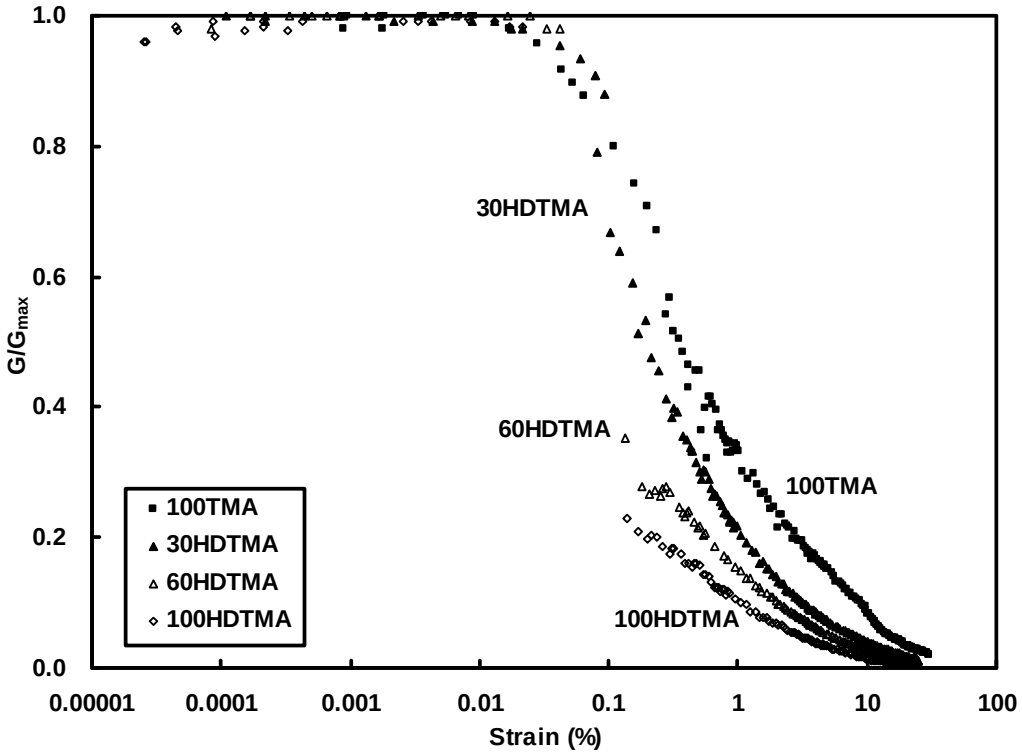

Figure 6-7. Combined secant shear modulus reduction curves from resonant column and triaxial shear tests for organobentonite with (a) 4 short C-chains QACs, (b) 1 long C-chain QACs, and (c) 30%, 60%, and 100% of CEC of HDTMA cations exchanged.

Damping ratio

Data from the resonant column test also allowed analysis of the damping ratio vs. shear strain for the seven organobentonites tested in the study (Figure 6-8). Similarly, the organoclays with low total organic carbon content (T.O.C. < 8.5%, including 100TMA, 100TEA, 30HDTMA, and 100DTMA) possessed significantly different behavior than those clays with total organic carbon contents that were higher than 8.5% (100TBA, 60HDTMA, and 100HDTMA). At low strains, the damping ratios of organobentonites with low carbon content ranged between 0.09% and 1.6%, and increased as strain increased past the linear threshold strain of approximately 0.024%. Damping ratios of

high organic content organobentonites were essentially constant at the tested strain range, with much higher values (2.7%, 3.9%, and 5.5% for 60HDTMA, 100HDTMA, and 100TBA bentonites, respectively) than the low organic content organobentonites at shear strains below threshold strain. Constant damping ratios at tested strain ranges indicated the elastic range of high organic content organobentonites was equal to or higher than 0.024%. However, the damping ratios of high organic content organobentonites were much higher than regular soils, such as proposed by Vucetic and Dobry (1991) (reference curves shown in Figure 6-8). Back electromagnetic force (back-EMF) induced by the counter reaction of solenoids to the motion of the magnets dissipated energy in the system, and resulted in equipment-generated damping ratio. The use of current-mode source, however, reduced equipment generated damping to a negligible level in real time (Meng, 2003). The tested damping ratios for natural clays at resonant frequencies from 20 Hz to 60 Hz were less than 1% (Meng, 2003). The measured damping ratios were similar to those measured for naturally occurring and artificially prepared organic soils (Kallioglou et al., 2009). It was also noted that damping ratio increased as total organic carbon content, except for 100TBA bentonite (Figure 6-9).

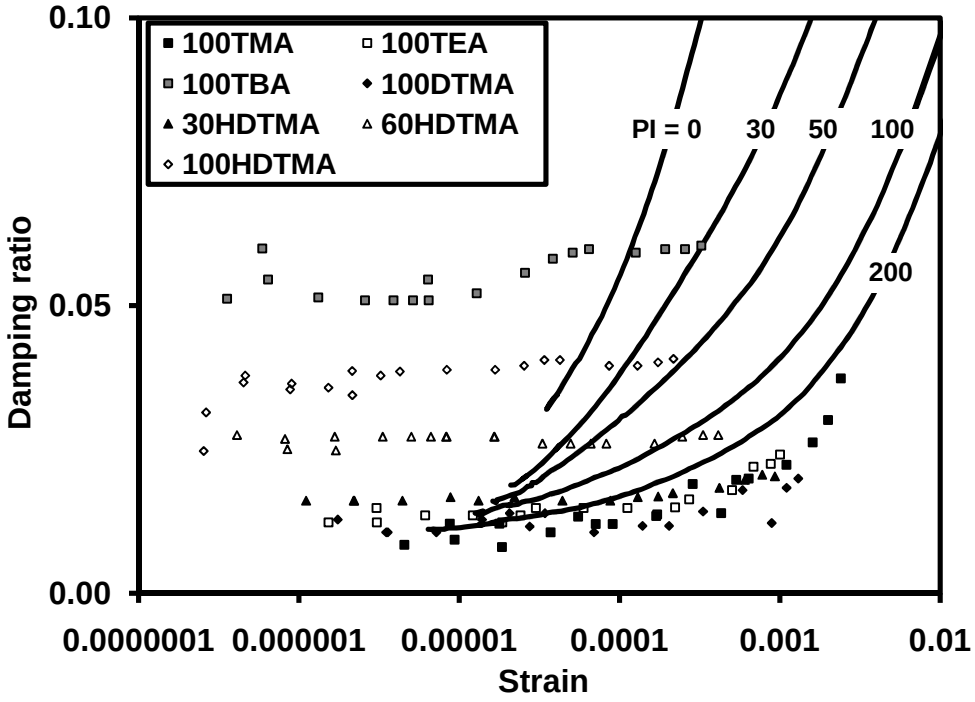

Figure 6-8. Damping ratio vs. shear strain for organobentonites. The curves were from Vucetic and Dobry (1991)

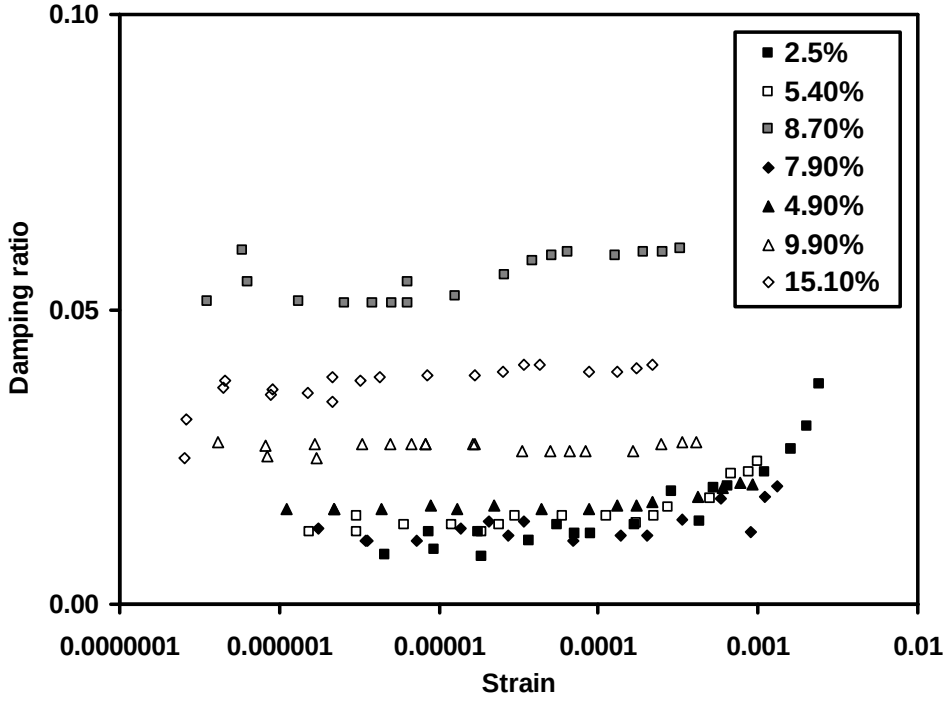

Figure 6-9. Damping ratio vs. shear strain for organobentonites.

Conclusions

The dynamic response of organobentontes was studied with resonant column test and bender element test in this chapter. The following conclusions can be drawn from the study:

- G_{max} increased as the size, the length of a single long C-chain, or the amount of organic loading increased. Increasing the total organic carbon content reduced the net surface charge on the particle, which in turn reduced interparticle repulsion, resulting in a decreasing void ratio as TOC was increased. The increased particle contacts resulted in a higher stiffness soil and a higher value of G_{max}.
- More increase in stiffness was observed when total organic carbon was increased by changing the cation structure with a single increasing tail length, as opposed to increasing cation size, i.e., increasing all four tail lengths.
- For the normally consolidated soils tested in this study, plasticity index did not have an obvious effect on G_{max}.
- G/G_{max} curves for low organic content (O.C. < 8.5%) organobentonite agreed with the model by Vucetic and Dobry (1991), while for high organic content (O.C. > 8.6%) organobentonites, no reduction was observed at the RC experimental strain range.
- The linear threshold strains for low organic content organobentonite were similar (~ 0.024%), which was higher than that of a natural clay (~0.01%). The presence of increasing total organic carbon content increased the linear range of the reduction curve.

- The reduction of the shear modulus curve at intermediate to large strains decreased as the size, the length of long C-chain, or the amount of organic loading increased, which is contrary to the results in the small strain region.
- Damping ratios for low organic content (O.C. < 8.5%) organobentonites showed some consistency with the model proposed by Vucetic and Dobry (1991), while for higher organic content (O.C. > 8.6%) organobentonites, the damping was constant throughout the tested strain region and larger than the model by Vucetic and Dobry (1991).

Chapter 7 Conclusions

This research studied organobentonites that were synthesized with a series of quaternary ammonium cations (QACs). The organoclays were characterized, and the properties of organobentonites were explored in the following areas: electrical, hydraulic and thermal conductivity, high frequency electrical permittivity, electrokinetic potential, triaxial shear strength, and small-strain dynamic properties. The effects of the size (the length of four short carbon chains), the length of long carbon chains, and the amount of organic loading were quantified in each study. Trends observed in the behavior of the organoclays are summarized in Table 7-1.

The laboratory investigation revealed that the presence of the organic cations on the mineral surface resulted in increased hydrophobicity of all clays tested. Conduction studies on the electrical, hydraulic, and thermal properties of the organoclay composites evinced that increasing the total organic carbon content resulted in decreased electrical and thermal conductivity, but increased hydraulic conductivity, due to the reduced swelling of the base clay mineral phase. Electrokinetic properties of the organoclays suggested that compared to the clay's naturally occurring inorganic cations, exchanged quaternary ammonium cations were more likely bound within a particle's shear plane, resulting in a less negative zeta potential for organoclays than for unmodified bentonite. Increasing the length of one carbon tail was more effective at binding organic cations within the shear plane than increasing the size of the cation, when compared on the basis of total organic carbon content.

Table 7-1. Summary of Organoclay Properties and Underlying Mechanisms

Measured Property	Function of Soil/Aqueous Property	As Branch Size ↑	As Tail Length ↑	As %CEC ↑	As TOC ↑	Mechanism
Liquid Limit	Specific area, ionic strength, pore fluid	↓	↓	↔(HDTMA)		Organic content adsorbed on the clay surface, double layer shrinkage, water exclusion.
Surface Tension	Concentration, ion structure, fluid/ fluid properties	↓	↓	n/a	n/a	Accumulation at the air/water interface increases as the hydrophobicity of the cation increases, resulting in decreasing surface tension.
Specific Surface Area	Probe molecule size, surface accessibility	↓	↓	↓	↓	Presence of organic cations limited access to bentonite's interlayer space, primary surface area measured..
Specific Gravity	Density of mineral/ organic phase	↓	↓	↓	↓	Hydrophobic interlayer created by the presence of organic cations excluded disproportionate quantity of water.
Hydraulic Conductivity	Void ratio, permeant, fabric	↑	↑	↑	↑	Organic cations created hydrophobic layer, reduce swelling compared to unmodified clay. Larger aggregates formed, leave larger pore voids.
Thermal Conductivity	Mineralogy, dry density, gradation, water content, temperature	↓	↓	↓	↓	Organic phase created insulating layers, limited heat transfer through mineral and water.
Electrical Conductivity	Concentration, valence, mobility	↓	↓	n/a	n/a	Mobility of organic cations reduced as cation size/tail length increased due to interference with other cations.

Table 7—1 continued. Summary of Organoclay Properties and Underlying Mechanisms

Measured Property	Function of Soil/Aqueous Property	As Branch Size ↑	As Tail Length ↑	As %CEC ↑	As TOC ↑	Mechanism
Aqueous Phase Electrical Permittivity (High Frequency) Real Permittivity	Free water, relaxation	↓	↓	n/a	n/a	Mobility of water molecules involved in hydrating ions was decreased due to the increased presence of electrolyte ions
Aqueous Phase Electrical Permittivity (High Frequency) Effective Conductivity	DC conduction, water polarization, relaxation	↓	↓	n/a	n/a	Mobility of organic cations decreased as size/tail length increased; water polarizability relatively constant.
Solid Phase Electrical Permittivity (High Frequency) Real Permittivity	amount of free water, relaxation, specific surface area	↔	↓	↓	↓	Reduction in free water due to the presence of the hydrophobic organic phase on the clay surface; higher specific surface areas observed at low TOC corresponded to a higher amount of bound water, which reduced the amount of free water.
Solid Phase Electrical Permittivity (High Frequency) Effective Conductivity	Mobility, water polarization, relaxation	↓	↓	↓	↓	Decreased net surface charge decreased the mobility of organobentonites, limited mobility of ions in the diffuse double layer, and reduced the amount of free cations due to adsorption on the bentonite.

Table 7—1 continued. Summary of Organoclay Properties and Underlying Mechanisms

Measured Property	Function of Soil/Aqueous Property	As Branch Size ↑	As Tail Length ↑	As %CEC ↑	As TOC ↑	Mechanism
Zeta Potential	Net surface charge, mobility, viscosity, thickness of double layer, particle size	↑	↑	↑	↑	Increased binding of cations in shear plane as hydrophobicity is increased.
Triaxial Shear Strength	Void ratio, composition, stress history, temperature, strain, strain rate, structure, confining pressure	↑	↑	↑	↑	Sorption of organic cations resulted in decreased water content significantly. Hydrophobic interaction of cation tails may also contribute to increased strength mechanism.
G_{max}	Void ratio, OCR, PI, confining stress, strain rate, number of loadings	↑	↑	↑	↑	Presence of organic cations resulted in decreased void ratio, increased particle contacts at the same confining pressure, resulting in increased stiffness.
G/G_{max} Rate of Decay	cyclic strain, PI, confining pressure, void ratio, OCR, number of loadings, geologic age, cementation	↑	↑	↑	See plot	Observed increase in G_{max} was very large, and dominated the smaller increase in G, resulting in a more rapid decay as size/tail length increased.
Damping	cyclic strain, confining stress, void ratio, PI	↑	↑	↑	See plot	Organic phase on the clay surface resulted in more energy dissipation as the size/tail length of the molecule was increased. Damping increased as size and coverage increased.

Regarding to the large strain strength, the modified organic clays bore increased shear strength, in part due to the reduction in water content due to the presence of the hydrophobic organic layering. Increases in shear strength resulted from increased cation size, although the effect reached a plateau as the cation tail length was increased. In terms of small strain behavior, the shear modulus was shown to be a function of the total organic carbon content, with stiffness increasing as either the size of the cation or the total organic carbon content was increased, due to an increased number of particle contacts. Damping also increased as the organic loading was increased, with the organic phase acting as an energy dissipation mechanism.

This work showed that characterization, conductivity, and electrokinetic studies can provide insight and knowledge to explain the observed behaviors of the engineering properties of soils. This study also illustrated the effects of the size, the length of a single long carbon chain, and the amount of organic loading on many properties of organobentonites. It is recommended that, in the future, the following areas need to be studied further.

- Kinetics study on clay suspensions, including the dissolution/precipitation kinetics of clay mineral, adsorption and desorption of aluminum hydroxide on clay surface, and the subsequent interaction between organic cations and inorganic cations on clay surface.
- Mechanisms of the relaxation frequency shift due to the presence of organobentonites in clay suspension.

- Numerical simulation on the effect of organics on the shear strength behavior using molecular dynamics or programs at the clay particle scale level.
- Both experimental and numerical study on the strength behavior on more organoclays using organics with other functional groups, such as alkenes, alkynes, ketones, aldehydes, and aromatic and carboxylic functional groups, as well as polymers. Further explore the possible recipe for more versatile engineering properties.

References

Abuel-Naga H.M., Bergado D.T., Bouazza A., Pender M.J. (2009) Thermal conductivity of soft Bangkok clay from laboratory and field measurements. Engineering Geology 105:211-219. DOI: 10.1016/j.enggeo.2009.02.008.

Adamson A.W., Gast A.P. (1997) Physical chemistry of surfaces. 6th ed. ed. Wiley, New York :.

Atkins P.W. (1998) Physical chemistry. 6th ed. ed. Freeman, New York :.

Baron P., Shainber.I. (1970) Hydrolysis And Decomposition Of Na-Montmorillonite In Distilled Water. Soil Science 109:241-&.

Barshad I. (1960) Significance Of The Presence Of Exchangeable Magnesium Ions In Acidified Clays. Science 131:988-990.

Barshad I. (1969) Preparation Of H Saturated Montmorillonites. Soil Science 108:38-&.

Bartelt-Hunt S.L., Burns S.E., Smith J.A. (2003) Nonionic organic solute sorption onto two organobentonites as a function of organic-carbon content. Journal of Colloid and Interface Science 266:251-258.

Bartelt-Hunt S.L., Smith J.A., Burns S.E., Rabideau A.J. (2005a) Evaluation of granular activated carbon, shale and two organoclays for use as sorptive amendments in clay landfill liners. Journal of Geotechnical and Geoenvironmental Engineering 131:848-856.

Bartelt-Hunt S.L., Burns S.E., Culver T.B., Smith J.A. (2005b) Optimal design of a compacted soil liner containing sorptive amendments, Geo-Frontiers 2005, January 24, 2005 - January 26, 2005, American Society of Civil Engineers, Austin, TX, United states. pp. 3385-3398.

Bartelt-Hunt S.L., Culver T.B., Smith J.A., Matott L.S., Rabideau A.J. (2006) Optimal design of a compacted soil liner containing sorptive amendments. Journal of Environmental Engineering-Asce 132:769-776. DOI: 10.1061/(asce)0733-9372(2006)132:7(769).

Bate B., Burns S.E. (2010) Effect of total organic carbon content and structure on the electrokinetic behavior of organoclay suspensions. Journal of Colloid and Interface Science 343:58-64.

Bickmore B.R., Bosbach D., M.F. Hochella J., Charlet L., Rufe E. (2001) In situ atomic force microscopy study of hectorite and montronite dissolution: implications for phyllosilicate edge surface structures and dissolution mechanism. Am. Mineral. 86:400-410.

Bohn H.L., McNeal B.L., O'Connor G.A. (2001) Soil Chemistry (Third Edition). Third Edition ed. John Wiley & Sons, INC.

Boschkova K., Kronberg B., Stalgren J.J.R., Persson K., Ratoi Salagean M. (2002) Lubrication in aqueous solutions using cationic surfactants - A study of static and dynamic forces. Langmuir 18:1680.

Bottero J.Y., Bruant M., Cases J.M., Canet D., Fiessinger F. (1988) Adsorption of Nonionic Polyacrylamide on Sodium Montmorillonite: Relation between Adsorption, Zeta Potential, Turbidity, Enthalpy of Adsorption Data and 13C-NMR in Aqueous Solution. Journal of Colloid and Interface Science 124:515-527.

Boulanger R.W., Arulnathan R., Harder L.F., Torres R.A., Driller M.W. (1998) Dynamic Properties of Sherman Island Peat. Journal of Geotechnical and Geoenvironmental Engineering 124:12-20.

Burns S.E., Bartelt-Hunt S.L., Redding A.Z., Smith J.A. (2006a) Coupled Mechanical and Chemical Behavior of Bentonite Engineered with a Controlled Organic Phase. Journal of Geotechnical and Geoenvironmental Engineering.

Burns S.E., Bartelt-Hunt S.L., Smith J.A., Redding A.Z. (2006b) Coupled mechanical and chemical behavior of bentonite engineered with a controlled organic phase. Journal of Geotechnical and Geoenvironmental Engineering 132:1404-1412.

Carslaw H.S. (1959) Conduction of heat in solids. 2d ed. ed. Clarendon Press, Oxford.

Chen A.F.T., Stokoe K.H.I. (1979) Interpretation of Strain Dependent Modulus and Damping from Torsional Soil Tests, U.S. Geological Survey.

Chen N., Maeda N., Tirrell M., Israelachvili J. (2005) Adhesion and friction of polymer surfaces: The effect of chain ends. Macromolecules 38:3491.

Chen Y.-L., Israelachvili J. (1992) Effects of Ambient Conditions on Adsorbed Surfactant and Polymer Monolayers. Journal of Physical Chemistry 96:7752-7760.

Cheng X.H., Ngan-Tillard D.J.M., Den Haan E.J. (2007) The causes of the high friction angle of Dutch organic soils. Engineering Geology 93:31-44. DOI: 10.1016/j.enggeo.2007.03.009.

Chernov V.A. (1947) The Nature of Soil Acidity Press of Acad. Sci. (A translation published by Soil Sci. Soc. America, 1964), U.S.S.R., Moscow.

Cola S., Cortellazzo G. (2005) The shear strength behavior of two peaty soils. Geotechnical and Geological Engineering 23:679-695.

Coleman N.T., Craig D. (1961) The spontaneous alteration of hydrogen clay. Soil Science 91:14-18.

Conway B.E., Verrall R.E., Desnoyer.Je. (1966) Partial Molal Volumes of Tetraalkylammonium Halides and Assignment of Individual Ionic Contributions. Transactions of the Faraday Society 62:2738-&.

Cortes D.D., Martin A.I., Yun T.S., Francisca F.M., Santamarina J.C., Ruppel C. (2009) Thermal conductivity of hydrate-bearing sediments. Journal of Geophysical Research-Solid Earth 114. DOI: B11103:10.1029/2008jb006235.

den Haan E.J., Uriel A.O., Rafnsson E., A. (1995) Theme Report 7: Special problem soils/soft rocks, The interplay between geotechnical engineering and engineering geology: proceedings of the Eleventh European Conference on Soil Mechanics and Foundation Engineering, Copenhagen, Denmark. pp. 139-180.

Dobry R., Vucetic M. (1987) Dynamic properties and seismic response of soft clay deposits, International Symposium on Geotechnical Engineering of Soft soils, Mexico City. pp. 51-87.

Duran J.D.G., Ramos-Tejada M.M., Arroyo F.J., Gonzalez-Caballero F. (2000) Rheological and Electrokinetic Properties of Sodium Montmorillonite

Suspensions I. Rheological Properties and Interparticle Energy of Interaction. Journal of Colloid and Interface Science 229:107-117.

Dyvik R., Madshus C. (1985) Lab Measurements Of Gmax Using Bender Elements, Advances in the Art of Testing Soils Under Cyclic Conditions. Proceedings of a session held in conjunction with the ASCE Convention., ASCE, Detroit, MI, Engl. pp. 186-196.

Fuerstenau D.W. (1971) The adsorption of surfactants at solid/water interfaces, in: M. L. Hair (Ed.), The chemistry of biosurfaces, vol. 1. , Marcel Dekker, New York. pp. 143-176.

Fuerstenau D.W., Pradip. (2005) Zeta potentials in the flotation of oxide and silicate minerals. Advances in Colloid and Interface Science 114-115:9-26.

Galindo-Gonzalez C., de Vicente J., Ramos-Tejada M.M., Lopez-Lopez M.T., Gonzalez-Caballero F., Duran J.D.G. (2005) Preparation and Sedimentation Behavior in Magnetic Fields of Magnetite-Covered Clay Particles. Langmuir 21:4410-4419.

Gao J., Luedtke W.D., Gourdon D., Ruths M., Israelachvili J.N., Landman U. (2004) Frictional forces and Amontons' law: From the molecular to the macroscopic scale. Journal of Physical Chemistry B 108:3410.

Gecol H., Miakatsindila P., Ergican E., Hiibel S.R. (2006) Biopolymer coated clay particles for the adsorption of tungsten from water. Desalination 197:165-178.

Gunister E., Isci S., Alemdar A., Gungor N. (2004) Effect of sodium dodecyl sulfate on flow and electrokinetic properties of Na-activated bentonite dispersions. Bulletin of Material Science 27:317-322.

Gunister E., Pestreli D., Unlu C.H., Atici O., Gungor N. (2007) Synthesis and characterization of chitosan-MMT biocomposite systems. Carbohydrate Polymers 67:358-365.

Hager F.D., Marvel C.S. (1926) The valence of nitrogen in quaternary ammonium compounds. Journal of the American Chemical Society 48:2689-2698.

Hayt W.H., Buck J.A. (2006) Engineering electromagnetics. 7th ed. ed. McGraw-Hill, Boston :.

Hight D.W., Bond A.J., Legge J.D. (1992) Characterization of the Bothkennar clay: An overview. Geotechnique 42:303-347.

Ishihara K. (1996) Soil Behaviour in Earthquake Geotechnics Oxford University Press Inc., New York.

Israelachvili J.N. (1991) Intermolecular and Surface Forces. 2nd ed. Academic Press.

Jackson M.L. (1960) Structural role of hydronium in layer silicates during soil genesis, Trans. Intern. Congr. Soil Sci. 7th Congr. Madison. pp. 445-455.

Jackson M.L. (1963) Aluminum Bonding in Soils: A Unifying Principle in Soil Science. Soil Science Society of American Proceedings 27:1-10.

Jaky J. (1944) The Coefficient of Earth Pressure at Rest. Journal of the Society of Hungarian Architects and Engineers:355-358.

Jamiolkowski M., Ladd C.C., Germaine J.T., Lancelotta R. (1985) New developments in field and laboratory testing of soils, Proceedings of Eleventh International Conference of Soil Mechanics and Foundation Engineering, San Fransisco, USA. pp. 57-153.

Jaynes W.F., Boyd S.A. (1991) Clay mineral type and organic compound sorption by hexadecyltrimethylammonium-exchanged clays. Soil Science Society of America Journal 55:43-48.

Jenny H. (1961) Reflections on the Soil Acidity Merry-go-round. Soil Science Society of American Proceedings 25:428-432.

Kallioglou P., Tika T., Koninis G., Papadopoulos S., Pitilakis K. (2009) Shear modulus and damping ratio of organic soils. Geotechnical and Geological Engineering 27:217-235.

Kandhal P.S., Parker F. (1998) Aggregate tests related to asphalt concrete performance in pavements, National Cooperative Highway Research Program NCHRP Report 405.

Kaya A., Yukselen Y. (2005) Zeta potential of soils with surfactants and its relevance to electrokinetic remediation. Journal of Hazardous Materials B120:119-126.

Khaldoun A., Wegdam G.H., Eiser E., Kerkeb M.L., Duran J.D.G., Gonzalez-Caballero F., Bonn D. (2006) Influence of heavy metals adsorption on the surface-energy properties of fluorinated montmorillonite clays "Rassoul". Colloids and Surfaces A: Physicochem. Eng. Aspects 290:1-6.

Kim D.-S. (1991) Deformational Characteristics of Soils at Small to Intermediate Strains from Cyclic Tests, University of Texas at Austin, Austin, Texas, USA.

Kishida T., Wehling T.M., Boulanger R.W., Driller M.W., Stokoe Ii K.H. (2009) Dynamic properties of highly organic soils from montezuma slough and clifton court. Journal of Geotechnical and Geoenvironmental Engineering 135:525-532.

Kramer S.L. (1996) Geotechnical earthquake engineering Prentice Hall, Upper Saddle River, N.J. :.

Kramer S.L. (2000) Dynamic Response of Mercer Slough Peat. Journal of Geotechnical and Geoenvironmental Engineering 126:504-510.

Lagaly G., Ogawa M., Dekany I. (2006) (Ed.)^(Eds.) Clay mineral organic interactions, Elsevier, Amsterdam. pp. Pages.

Lambe T.W. (1951) Soil testing for engineers Wiley, New York.

Lambe T.W., Whitman R.V. (1969) Soil mechanics Wiley, New York.

Lee J.-S., Santamarina J.C. (2005) Bender elements: Performance and signal interpretation. Journal of Geotechnical and Geoenvironmental Engineering 131:1063-1070.

Lee S., Shon Y.-S., Colorado R., Jr., Guenard R.L., Lee T.R., Perry S.S. (2000) Influence of packing densities and surface order on the frictional properties of alkanethiol self-assembled monolayers (SAMs) on gold: A comparison of SAMs derived from normal and spiroalkanedithiols. Langmuir 16:2220.

Leroueil S., Magnan J.-P., Tavenas F. (1990) Embankments on soft clay Ellis Horwood, New York :.

Li J., Smith J.A., Winquist A.S. (1996) Permeability of earthen liners containing organobentonite to water and two organic liquids. Environmental Science & Technology 30:3089-3093.

Li X.-S., Roblee C.J., Wang G. (1993) Development and evaluation of a prototype tool for in situ determination of high-strain properties of soft to medium-stiff clays Phase I, An interim report to The California Department of Transportation, University of California, Davis, Davis, California.

Lin Q., Meyer E.E., Tadmor M., Israelachvili J.N., Kuhl T.L. (2005) Measurement of the long- and short-range hydrophobic attraction between surfactant-coated surfaces. Langmuir 21:251.

Liu X., Lu X.C., Wang R.C., Zhou H.Q., Xu S.J. (2009) Molecular dynamics insight into the cointercalation of hexadecyltrimethyl-ammonium and acetate ions into smectites. American Mineralogist 94:143-150. DOI: 10.2138/am.2009.2887.

Liu X.D., Lu X.C., Wang R.C., Zhou H.Q., Xu S.J. (2007) Interlayer structure and dynamics of alkylammonium-intercalated smectites with and without water: A molecular dynamics study. Clays and Clay Minerals 55:554-564. DOI: 10.1346/ccmn.2007.0550602.

Lo Presti D.C.F., Jamiolkowski M., Pallara O., Cavallaro A., Pedroni S. (1997) Shear modulus and damping of soils. Geotechnique 47:603-617.

Lorenzetti R.J., Bartelt-Hunt S.L., Burns S.E., Smith J.A. (2005) Hydraulic conductivities and effective diffusion coefficients of geosynthetic clay liners with organobentonite amendments. Geotextiles and Geomembranes 23:385-400.

Meng J. (2003) The influence of loading frequency on dynamic soil properties, School of Civil and Environmental Engineering, Georgia Institute of Technology, Atlanta, Georgia, USA. pp. 174.

Menger F.M., Littau C.A. (1993) Gemini Surfactants: A New Class of Self-Assembling Molecules. Journal of the American Chemical Society 115:10083-10090.

Mesri G., Olson R.E. (1970) Shear Strength of Montmorillonite. Geotechnique 20:261-270.

Mikulski P.T., Harrison J.A. (2001) Packing-Density Effects on the Friction of n-Alkane Monolayers. Journal of the American Chemical Society 123:6873-6881.

Mitchell J.K., Soga K. (2005) Fundamentals of Soil Behavior. Third ed. John Wiley and Sons, Inc., New Jersey.

Ni S.-H. (1987) Dynamic properties of sand under true triaxial stress states from resonant column/torsion shear tests, University of Texas at Austin, Austin, Texas, USA.

Nightingale E.R. (1959) Phenomenological Theory Of Ion Solvation - Effective Radii Of Hydrated Ions. Journal of Physical Chemistry 63:1381-1387.

Niriella D., Carnahan R.P. (2006) Comparison Study of Zeta Potential Values of Bentonite in Salt Solutions. Journal of Dispersion Science and Technology 27:123-131.

Oelkers E.H. (2001) General kinetic description of multioxide silicate mineral and glass dissolution. Geochimica et Cosmochimica Acta 65:3703-3719.

Pierre A.C., Ma K. (1997) Sedimentation behaviour of kaolinite and montmorillonite mixed with iron additives, as a function of their zeta potential. Journal of Materials Science 32:2937-2947.

Pierre A.C., Ma K. (1999) DLVO Theory and Clay Aggregate Architectures Formed with AlCl3. Journal of European Ceramic Society 19:1615-1622.

Polubesova T., Nir S. (1999) Modeling of organic and inorganic cation sorption by illite. Clays and Clay Minerals 47:366-374.

Ramanathan P.S., Krishnan C.V., Friedman H.L. (1972) Models Having the Thermodynamic Properties of Aqueous Solutions of Tetraalkylammonium Halides. Journal of Solution Chemistry 1:237-262.

Ramos-Tejada M.M., de Vicente J., Ontiveros A., Duran J.D.G. (2001) Effect of humic acid adsorption on the rheological properties of sodium montmorillonite suspensions. Journal of Rheology 45:1159-1172.

Ramos-Tejada M.M., Galindo-Gonzalez C., Perea R., Duran J.D.G. (2006) Effect of charged polyelectrolytes on the electrophoretic behavior, stability, and viscoelastic properties of montmorillonite suspensions. Journal of Rheology 50:995-1007.

Ramos-Tejada M.M., Ontiveros A., Plaza R.C., Delgado A.V., Duran J.D.G. (2003) A rheological approach to the stability of humic acid/clay colloidal suspensions. Rheol Acta 42:148-157.

Redding A.Z., Burns S.E., Upson R.T., Anderson E.F. (2002) Organoclay sorption of benzene as a function of total organic carbon content. Journal of Colloid and Interface Science 250:261-264.

Robinson R.A., Stokes R.H. (1965) Electrolyte Solutions: Second revised edition Butterworths, London.

Rosen M.J. (2004) Surfactants and interfacial phenomena. 3rd ed. ed. Wiley-Interscience, Hoboken, N.J. :.

Rozalen M.L., Huertas F.J., Brady P.V., Cama J., Garcia-Palma S., Linares J. (2008) Experimental study of the effect of pH on the kinetics of montmorillonite dissolution at 25 degrees C. Geochimica Et Cosmochimica Acta 72:4224-4253. DOI: 10.1016/j.gca.2008.05.065.

Ruths M., Alcantar N.A., Israelachvili J.N. (2003) Boundary friction of aromatic silane self-assembled monolayers measured with the surface forces apparatus and friction force microscopy. Journal of Physical Chemistry B 107:11149.

Saka E.E., Guler C. (2006) The effects of electrolyte concentration, ion species and pH on the zeta potential and electrokinetic charge density of montmorillonite. Clay Minerals 41:853-861.

Santagata M. (2008) Effects of stress history on the stiffness of a soft clay, in: P. W. M. a. J. C. S. Susan E. Burns (Ed.), The 4th International Symposium on Deformation Characteristics of Geomaterials, IS Atlanta 2008, IOS Press, Atlanta, Georgia, USA. pp. 95-123.

Santamarina J.C., Klein K.A., Fam M.A. (2001) Soils and waves : [particulate materials behavior, characterization and process monitoring] J. Wiley & Sons, Chichester, England ;.

Santamarina J.C., Klein K.A., Wang Y.H., Prencke E. (2002) Specific surface: determination and relevance. Canadian Geotechnical Journal 39:233-241. DOI: 10.1139/t01-077.

Seed H.B., Idriss I.M. (1970) Analyses of ground motions at Union Bay, Seattle during earthquakes and distant nuclear blasts. Bulletin of the Seismological Society of America 60:125-136.

Singh P.K., Sharma V.P. (1997) Effect of Electrolytes on Zeta Potential of Beneficiated Indian Bentonites. Journal of Scientific & Industrial Research 56:281-287.

Smith J.A., Jaffe P.R. (1994) Benzene transport through landfill liners containing organophilic bentonite. Journal of Environmental Engineering 120:1559-1577.

Smith J.A., Galan A. (1995) Nonionic Solute Sorption to Single and Dual Organic Cation Organobentonites from Water. Environmental Science and Technology 29:685-692.

Smith J.A., Li J., Galan A. (1995) Organobentonites as components of earthen landfill liners to minimize contaminant transport, Proceedings of the Specialty Conference on Geotechnical Practice in Waste Disposal. Part 1 (of 2), Febrary 24, 1995 - Febrary 26, 1995, ASCE, New Orleans, LA, USA. pp. 806-814.

Smith J.A., Bartelt-Hunt S.L., Burns S.E. (2003) Sorption and permeability of gasoline hydrocarbons in organobentonite porous media. Journal of Hazardous Materials 96:91-97.

Sondi I., Pravdic V. (1996) Electrokinetics of Natural and Mechanically Modified Ripidolite and Beidellite Clays. Journal of Colloid and Interface Science 181:463-469.

Soule N.M., Burns S.E. (2001) Effects of organic cation structure on behavior of organobentonites. Journal of Geotechnical and Geoenvironmental Engineering 127:363-370.

Sparks D.L. (2003) Environmental Soil Chemistry (Second Edition). Second Edition ed. Academic Press.

Stokoe K.H., Bay J.A., Rosenblad B.L., Huang S.-K., Twede M.R. (1994) In situ seismic and dynamic laboratory measurements of geotechnical materials at Queensboro Bridge and Roosevelt Island, University of Texas, Austin, TX.

Stumm W., Morgan J.J. (1996) Aquatic chemistry : chemical equilibria and rates in natural waters. 3rd ed. ed. Wiley, New York :.

Tang A.-M., Cui Y.-J., Le T.-T. (2008) A study on the thermal conductivity of compacted bentonites. Applied Clay Science 41:181-189.

Terzaghi K. (1996) Soil mechanics in engineering practice. 3rd ed. ed. Wiley, New York :.

Tombacz E., Szekeres M. (2004) Colloidal behavior of aqueous montmorillonite suspensions: the specific role of pH in the presence of indifferent electrolytes. Applied Clay Science 27:75-94. DOI: 10.1016/j.clay.2004.01.001.

Tombacz E., Szekeres M. (2006) Surface charge heterogeneity of kaolinite in aqueous suspension in comparison with montmorillonite. Applied Clay Science 34:105-124.

Valdes J.R. (1999) Simultaneous determination of frequency dependent modulus and damping from resonant column tests, School of Civil and Environmental Engineering, Georgia Institute of Technology, Atlanta, Georgia, USA. pp. 186.

van Olphen H. (1977) An Introduction to Clay Colloid Chemistry. 2nd ed. John Wiley & Sons.

Vucetic M. (1994) Cyclic threshold shear strains in soils. Journal of geotechnical engineering 120:2208-2228.

Vucetic M., Dobry R. (1991) Effect of soil plasticity on cyclic response. Journal of geotechnical engineering 117:89-107.

Wehling T.M., Boulanger R.W., Arulnathan R., Harder L.F., Driller M.W. (2003) Nonlinear Dynamic Properties of a Fibrous Organic Soil. Journal of Geotechnical and Geoenvironmental Engineering 129:929-939.

Wiese G.R., Healy T.W. (1975) Coagulation And Electrokinetic Behavior Of TiO2 And Al2O3 Colloidal Dispersions. Journal of Colloid and Interface Science 51:427-433.

Wong K., Cabane B., Duplessix R., Somasundaran P. (1989) Aggregation Of Silica Using Cationic Surfactant - A Neutron-Scattering Study. Langmuir 5:1346-1350.

www.chemblink.com. June 2010.

www.sigma-aldrich.com. June 2010.

www.usbweb.com. June 2010.

Xiao X.D., Hu J., Charych D.H., Salmeron M. (1996) Chain length dependence of the frictional properties of alkylsilane molecules self-assembled on Mica studied by atomic force microscopy. Langmuir 12:235-237.

Xu S., Boyd S.A. (1995) Cationic Surfactant Adsorption by Swelling and Nonswelling Layer Silicates. Langmuir 11:2508-2514.

Yoshizawa H., Chen Y.L., Israelachvili J. (1993) Fundamental mechanisms of interfacial friction. 1. Relation between adhesion and friction. Journal of Physical Chemistry 97:4128-4140.

Yun T.S., Santamarina J.C. (2008) Fundamental study of thermal conduction in dry soils. Granular Matter 10:197-207. DOI: 10.1007/s10035-007-0051-5.

Zhang R., Somasundaran P. (2006) Advances in adsorption of surfactants and their mixtures at solid/solution interfaces. Advances in Colloid and Interface Science 123:213-229. DOI: 10.1016/j.cis.2006.07.004.

Zhuang J., Yu G.R. (2002) Effects of surface coatings on electrochemical properties and contaminant sorption of clay minerals. Chemosphere 49:619-628.